Mechanism and Kinetics of One-electron Oxidation of Methanesulfinate and Two-electron Oxidation of Thiols and Disulfides

by

Yixuan Yang

A dissertation submitted to the Graduate Faculty of
Auburn University
in partial fulfillment of the
requirements for the Degree of
Doctor of Philosophy

Auburn, Alabama
May 7, 2022

Keywords: Kinetics and mechanisms, Electron-transfer, methanesulfinate oxidation, Thiols, aqueous iodine/iodate, stopped-flow

Approved by

David M. Stanbury, Chair, Professor of Chemistry and Biochemistry
Byron H. Farnum, Associate Professor of Chemistry and Biochemistry
Evert Duin, Professor of Chemistry and Biochemistry
Wei Zhan, Professor of Chemistry and Biochemistry
Angela Calderon, Associate Professor of Harrison School of Pharmacy

ABSTRACT

One-electron oxidation of alkylsulfinic acids has been of great interest for years as the reaction mechanisms are known to be quite elusive. We herein investigate the kinetics and mechanism of oxidation of an alkylsulfinic acid, CH_3SO_2H (MSA) by two types of one-electron oxidants, hexachloroiridate(IV), $[IrCl_6]^{2-}$, and bis(1,4,7-triazacyclononane)nickel(III), $[Ni(tacn)_2]^{3+}$, respectively, in aqueous media at 25 °C under anaerobic conditions, with the aim to provide in-depth knowledge of such reactions. The oxidation of MSA produces $CH_3SO_2^{\bullet}$ as a transient intermediate through outer-sphere electron transfer pathway, and methanesulfonate ($CH_3SO_3^-$) as the final product for both reactions. For the MSA-Ir(IV) reaction, a reactive intermediate of the metal complex is an iridium-bound sulfonyl chloride from the inner-sphere oxidation of $CH_3SO_2^{\bullet}$ by $[IrCl_6]^{2-}$. It undergoes dissociation to form methanesulfonyl chloride, followed by hydrolysis to release $CH_3SO_3^-$. The reaction rate is revealed to be first-order in [MSA] and second-order in [Ir^{IV}]. This reaction is inhibited by strong acid but independent of pH between 3 and 6. Inhibition by the product Ir^{III} is significant. Notably, this work provides the first good evidence of the strong chlorine atom affinity of a sulfonyl radical. The rate law of the overall reaction was determined to be

$$-\frac{d[IrCl_6^{2-}]}{dt} = \frac{2k_1k_2[Ir^{IV}]^2[CH_3SO_2^-]}{k_{-1}[Ir^{III}]+k_2[Ir^{IV}]}$$

With $k_1 = (0.70 \pm 0.01) \times 10^4\ M^{-1}\ s^{-1}$, $k_{-1} = (7.5 \pm 2.5) \times 10^5\ M^{-1}\ s^{-1}$, and $k_2 = (8.0 \pm 2.0) \times 10^7\ M^{-1}\ s^{-1}$ at $\mu = 0.1$ M ($NaClO_4$). The value of k_{-1} was determined from the effect of propiolic acid. For the MSA-Ni(III) reaction, the reaction kinetics is found to have a second-order dependence on [Ni(III)] and first-order on [MSA]. Ni(II) is proved to be a strong inhibitor for the

reaction rate. The trapping of $CH_3SO_2^{\bullet}$ by Ni(III) yields a complex that decomposes slowly to release Ni-tacn, followed by its dissociation to product $[Ni]^{2+}$ ion and the ligand, tacn. The presence of the sulfonyl radical was confirmed by the scavenging competition between PBN and Ni(III). The intermediates that appeared in the system were characterized through NMR and UV-Vis. As a result, the general rate law is formulated as $-\frac{d[Ni^{III}]}{dt} = k'_{obs,2}[Ni(III)]^2$, where $k'_{obs,2}$ is a second-order rate constant expressed as,

$$k'_{obs,2} = \frac{2k_1k_2K_a[MSA]_{total}}{k_{-1}[Ni^{II}](K_a + [H^+])}$$

with $k_1 = (150 \pm 45)\ M^{-1}\ s^{-1}, k_{-1} = 2300\ M^{-1}\ s^{-1},$ and $k_2 = (1.5 \pm 0.3) \times 10^4\ M^{-1}\ s^{-1}$ at $\mu = 0.1$ M (NaCl).

Two-electron oxidation of two thiols (RSH) including 2-mercaptoethansulfonate (MESNA) and β-mercaptoethanol (BME), and several disulfides (RSSR) by iodine/oxy-iodine species are also investigated extensively in this work on account of the biological significance of these species. Iodometric titrations are used to determine the reaction stoichiometry of RSH/iodate reaction, and with excess of IO_3^-, the overall reaction is described as

$$10RSH + 2IO_3^- + 2H^+ \rightarrow 5RSSR + I_2 + 6H_2O$$

The equilibrium and kinetic studies between RSH and iodine/iodate was evaluated through instrumental methods and kinetic fitting to understand the intermediates such as sulfenyl iodide (RSI) and sulfenic acid (RSOH). The ultimate products are characterized by ^{1}H-NMR, UV-Vis, and Mass Spectrometry. This reaction proceeds relatively quickly, depending on the concentration of the reactants, iodide, and pH. The complex reaction dynamics can be interpreted from 2 processes: clock reaction and rapid formation of disulfide. The detailed reaction pathways and relevant kinetic coefficients are elaborated and simulated through a mechanism network of 15 step

reactions. As a follow-up, the reaction between the disulfides of MESNA, BME and 3-mercaptopropionic acid and iodine/triiodide are explored as well. These three disulfides behave differently while reacting with iodine. Rate laws regarding various factors such as [RSSR], [iodide], [iodine], and pH are derived to explain the reaction kinetics and mechanism. The final products of the reactions are identified and found to be thiosulfinate, thiosulfonate and sulfonic acid, respectively.

ACKNOWLEDGEMENTS

I am immensely grateful to many people for their contributions in my research, to this dissertation, and for the time I spent in the graduate school. This dissertation would not have been completed without their invaluable guidance, support, and encouragement.

First, I would like to thank my parents for always encouraging me to pursue higher education. Their strong support and patience made me understand the importance of not giving up. I am very thankful for them for they have always held my head high and motivating me always to be a hard-working person as they are.

On a professional level, it has been an honor to work with Dr. David Stanbury, my program advisor. I cannot express the sheer amount of hard work, determination, and patience he has shown me during my doctoral years. Being intelligent, passionate, and expert in his field, he has motivated me to always push beyond my capabilities. His guidance and mentoring during my graduate life have helped me tremendously. I would also like to thank him for always inviting me to his home for family meals during Thanksgiving holidays. I am truly blessed to have him as my advisor and knowing him, not only professionally, but personally as well.

I am also fortunate to have Dr. Byron Farnum as my co-advisor, Dr. Evert Duin, Dr. Wei Zhan, and Dr. Angela Calderon as my committee members. Thank you all for your assistance and guidance on my research and improving the quality of my work. I would also like to thank Dr. Michael Meadows and Dr. Alvaro Herrera for allowing me to use NMR, Dr. Melissa Boersma for helping me with MS experiments and data interpretation, Dr. Steven Mansoorabadi for allowing

me to use glove box equipment, and Dr. Byron Farnum for allowing me to use their CV instrument. Without their help and advice, I would not have completed my degree.

I would also like to acknowledge the support of ACS Petroleum Research Fund to support my project when I started my program, COSAM of Auburn University, and ACS Auburn Local Section for providing funds to support my conference travel.

My life in Auburn has been filled with many sincere friends, it is their kindness and encouragement that kept me going all these years. I am thankful for my previous lab colleague, Ms. Pradeepa Rajakaruna for her friendship and help. I cannot thank them enough for being there when things got tough, and helping me cross the finish line.

Finally, I would like to thank Auburn Graduate School for providing me the opportunity to let me pursue my dreams and achieve a Ph.D. degree. The research life here at Auburn is an inspiring part that will always help me navigate my life in future.

TABLE OF CONTENTS

LIST OF TABLES

LIST OF FIGURES

1 Introduction

1.1 Chemical Kinetics

The rates of chemical reactions are generally studied to understand the reaction mechanisms. They are expressed as the change in concentration of a reactant or product per unit time. The rate law of an elementary reaction can be determined easily from the stoichiometry of the reaction itself, whereas for a net reaction, we need to identify the individual steps or the elementary reactions to construct the overall mechanism.

Rate laws are used for expressing the relationship between reaction rate and reactant concentrations. Simple rate laws take the form $\text{Rate} = k[\text{X}]^{\text{a}}[\text{Y}]^{\text{b}}$, where k is the rate constant and is generally determined through experiment and calculation. The exponents, a and b, are the orders with respect to the reactant concentration. The sum of the exponents gives the order of the reaction. To measure the rate and solve the rate law, the concentration change of a substrate as a function of time is often recorded. The kinetic data are integrated to obtain the rate constant. Observed kinetics usually depend on the rate-limiting step which is the slowest step of a reaction. Half-time $(\text{t}_{1/2})$ which is the time required for the concentration of a reactant to change by half of its initial concentration, is used for delivering a qualitative idea of the time scale.

The rate of a reaction can be affected by several factors that include temperature, ionic strength, pressure, and diffusion-controlled limit. Descriptions of these factors are provided below.

1.1.1 Temperature

Based on collision theory, the reaction rate increases at a higher temperature due to the fact that a larger fraction of molecules can overcome the activation energy required for the reaction and move faster as temperature increases. According to the Eyring equation which is not related to the collision model,

$$k = \frac{k_B \mathrm{T}}{h} \exp\left(-\frac{\Delta \mathrm{G}^{\neq}}{\mathrm{RT}}\right) \quad \text{Eq. 1-1}$$

Where, k is the rate constant, k_B is Boltzman's constant, h is Plank's constant, R is the gas constant, $\Delta \mathrm{G}^{\neq}$ is the free energy of activation, and T is the absolute temperature, the rise in temperature leads to an increase in the rate constant. This equation can be used for gaseous, condensed, and mixed phase reactions.

1.1.2 Ionic Strength

Ionic strength, μ, is a measure of the concentration of electrically charged species in solution. The effect of μ on reaction rate is from the change in activity of the reacting species with the ionic composition change in the medium. The expression of ionic strength is given as,

$$\mu = \frac{\sum_i c_i Z_i^2}{2} \quad \text{Eq. 1-2}$$

Here, c_i is the concentration of the ion and Z_i is the charge of the ion. The activity coefficients of the species in a solution with $\mu \leq 0.01$ M can be determined by the Debye–Hückel limiting law,

$$\log \gamma_i = -AZ_i^2 \sqrt{\mu} \quad \text{Eq. 1-3}$$

Here, A is a constant for a given solvent. With higher ionic strength ($0.01 \text{ M} \leq \mu \leq 0.1$ M), the equation is further elaborated as,

$$\log \gamma_i = -AZ_i^2 \left(\frac{\sqrt{\mu}}{1 + Ba_i\sqrt{\mu}}\right) \quad \text{Eq. 1-4}$$

Here a_i is the average effective diameter of the ions and B is a constant from solvent properties. Generally, it is necessary to maintain a medium where the ionic composition is a constant. An inert supporting electrolyte such as $NaClO_4$ and $LiClO_4$ can be used for controlling

ionic strength for chemical equilibrium and kinetics studies due to their high solubility and weak reactivity.

1.1.3 Pressure

The rate constant of some reactions can be determined at various applied pressures under certain conditions. A higher pressure leads to an increased reaction rate involving gases. This can be explained by the ideal gas law, $PV = nRT$, where P and V are the pressure and volume of the gas, respectively, n is the number of moles, R is the gas constant, T is the temperature. The increase in pressure will increase the concentration of gas, and therefore ensures more gas molecules frequently collide.

1.1.4 Diffusion-controlled

The maximum rate of the reactants that can diffuse together is restricted, and the upper limit of the reaction rate is known as diffusion-controlled limit. Some reactions can take place at or near diffusion-controlled rates. In aqueous phase, the limit is found to be in the range of 10^9 to 10^{10} M^{-1} s^{-1}. Two types of reactions in water known to occur at diffusion-controlled rate are the protonation reaction of a base and the deprotonation of strong acids. This information can be quite beneficial for estimating the rate of some certain reactions.

In general, the rate data can be obtained by measuring the time dependence of some variable which is proportional to the concentration of the reactant, such as absorbance and NMR peak integral. With the obtained data, the experimental rate law can be established by combining all the kinetic parameters. Next step is to construct the mechanism to justify the rate law mathematically and theoretically. Several methods can be applied to develop the rate law. The most practical one is the steady-state approximation that involves the appearance of one or any number of reactive intermediates in the reaction system. According to the approximation, the

disappearance of the species proceeds as fast as the formation of the species, which leads to negligible concentration change and the rate regarding the intermediate. With this assumption, some terms regarding the concentration of reactants or products can be eliminated from the differential equation, and thus, simplifying the rate law and complex calculations. Another method used to solve the rate law is the rapid equilibrium assumption. This assumes that the reactants are part of a rapid equilibrium, and the equilibrium is always present during the whole process of reaction. So, the total concentration of the reactant is the sum of the valid forms involved in the equilibrium. This information can be very beneficial as it helps to express the concentration of any species in the reaction in terms of the known total concentrations of the reactants appearing in the equilibrium.

1.2 Principle of Detailed Balancing

The principle of detailed balancing states that the equilibrium constant for an elementary reaction equals to the ratio of the forward and reverse rate constants: $K_{eq} = \frac{k_f}{k_r}$. In a simple system, this is very useful as it makes it simple to express one rate constant in terms of the others. However, it can be challenging to follow the rule in a complex system, and the violation of it could generate unreasonable mechanisms. To avoid the negative outcome, valid methods can be applied to check the legality of reaction loops. When one or multiple steps in a reaction set stoichiometrically equals to one or more linear combination of the others, a reaction loop forms. According to Dr. Stanbury [49],[50], there are systematic methods, mostly for closed isothermal homogeneous reaction systems that can be used to detect the validity of the loops to ensure compliance with the principle of detailed balancing.

1.3 Redox Reactions

Redox reactions are of prime importance in human life as they are involved in respiration, cell construction, energy production, storage, and transport process that are closely related to industry and life activities. In the modern world, they are highly connected to metal production, battery design, chemical product synthesis, etc. As a rule, redox reactions are considered as electron-transfer reactions with the change in oxidation state of one or more elements. In biology, the process of effectively controlling and directing the electron migration is considered as the primary regulation mechanism [38]. Therefore, research interest on redox regulation and the movement of signals keeps on increasing. One of the examples is the understanding of how reactive oxygen species (ROS) transduce signals from cell surface to the targeting proteins [38]-[40].

Apart from its biological significance, electron transfer (ET) reactions are mostly studied with respect to their mechanisms as they are fundamental yet most influential. Generally, ET occurs during the collision between the two reactants, and it involves the formation of a short-lived complex. According to the electron transfer pathway, ET process can be categorized into two: inner-sphere electron transfer and outer-sphere electron transfer [41],[42]. In inner-sphere ET reactions, a covalent bond is formed between the oxidant and reductant. Electron transfer happens between two species via a bridging ligand in the first coordination sphere as shown in Figure 1-1.

$$M_{ox}X + M'_{red} \underset{k_{-1}}{\overset{k_1}{\rightleftharpoons}} M_{ox}{-}X{-}M'_{red} \underset{k_{-et}}{\overset{k_{et}}{\rightleftharpoons}} M_{red}{-}X{-}M'_{ox}$$

$$M_{red}{-}X{-}M'_{ox} \xrightarrow{k_2} M_{red} + M'_{ox}X$$

Figure 1-1. Reaction Scheme of inner-sphere ET process.

The bridging ligand can be halide anions, pseudohalide ions, cyanide, thiocyanide, hydroxide ion, thiosulfate, etc. This process can cause a large splitting surface so that a stronger electronic

interaction for the transition state can be achieved. It is more likely to happen if the electron transfer is extremely fast and sensitive to the chemical nature of the bridging group [48].

By contrast, no bridging bonds are broken or formed in outer-sphere electron transfer reaction as the complexes are intact before, during and after the electron transfer process as shown in Figure 1-2.

$$M^{(a)+}{}_{ox}\text{-}L + M'^{b+}{}_{red} \underset{k_{-1}}{\overset{k_1}{\rightleftharpoons}} M^{(a)+}{}_{ox}\text{-}L \cdots M'^{b+}{}_{red}$$

$$M^{(a)+}{}_{ox}\text{-}L \cdots M'^{b+}{}_{red} \underset{k_{-et}}{\overset{k_{et}}{\rightleftharpoons}} M^{(a-1)+}{}_{red}\text{-}L \cdots M'^{(b+1)+}{}_{ox}$$

$$M^{(a-1)+}{}_{red}\text{-}L \cdots M'^{(b+1)+}{}_{ox} \xrightarrow{k_2} M^{(a-1)+}{}_{red}\text{-}L + M'^{(b+1)+}{}_{ox}$$

Figure 1-2. Reaction Scheme of outer-sphere ET process.

An explanation for the behavior is that the coordination of the ligand is restricted by the weak interaction of the two relevant orbitals of the two species [42]. And thus, two separated reactants can be held together through one of the following approaches: Van der Waals force, hydrogen bonding, or electrostatic interactions. Generally, if the reactant is a metal complex that is substitutionally inert, outer-sphere electron transfer mechanism plays the main role.

Electron transfers can be very rapid. According to Frank-Condon principle, it is much faster than nuclear motion so that no effective change of nuclear coordination happens [44]. For an outer-sphere ET, the activation energy required for the process, also known as 'corrected Gibbs free energy', $\Delta G^{\circ\prime}$, can be obtained using Marcus Equation [43]:

$$\Delta G^{\circ\prime} = \Delta G^{\circ} + (z_1 - z_2 - 1)\left(\frac{e^2}{Dr_{12}}\right)\exp(-\chi r_{12}) \qquad \text{Eq. 1-5}$$

Here, ΔG° is the Gibbs free energy, which is the energy difference between separated reactants and products. It can be determined from the standard reduction potential of the reactants through the equation $\Delta G^{\circ} = -nFE^{\circ}$. z_1, z_2 refers to the charge of electron accepter and donor,

respectively. D is the dielectric constant of the media, e is the charge of an electron, χ is the reciprocal Debye radius which is a function of the total ionic strength [46],[47], $r_{12}(= r_2 + r_2)$ is the distance of closest approach of the two spheres.

To calculate the rate constant of an outer-sphere electron transfer reaction in solution, Marcus Cross-Relation (MCR) is used [51]. It defines the relationship between two species, X^- and Y^- that are not related to each other by oxidation and reductions in an electron transfer reaction. The rate constant of this reaction is k_{12}. Associated with that is the self-exchange reactions with rate constant k_{11}, k_{22}, which are used to derive k_{12}.

$$X^- + Y \rightleftharpoons X + Y^- \qquad k_{12}$$

$$X^- + X \rightleftharpoons X + X^- \qquad k_{11}$$

$$Y + Y^- \rightleftharpoons Y^- + Y \qquad k_{22}$$

The simplified MCR is formulated as,

$$k_{12} = (k_{11}k_{22}K_{12}f_{12})^{\frac{1}{2}}W_{12} \qquad \text{Eq. 1-6}$$

where,

$$lnf_{12} = \frac{\left[lnK_{12} + \frac{w_{12} - w_{21}}{RT}\right]^2}{4\left[\ln\left(\frac{k_{11}k_{22}}{Z^2}\right) + (w_{11} + w_{22})/RT\right]} \qquad \text{Eq. 1-7}$$

$$W_{12} = e^{-w_{12}-w_{21}+w_{11}+w_{22}/2RT} \qquad \text{Eq. 1-8}$$

$$w_{ij} = \frac{17.7z_iz_j}{r_{ij}\left(1 + 0.328r_{ij}\mu^{\frac{1}{2}}\right)} \qquad \text{Eq. 1-9}$$

Here, k_{12} is cross reaction rate of X^- and Y, k_{11} and k_{22} are the self-exchange rate constants of X^-/X and Y/Y^- redox couples. 1×10^{11} M^{-1} s^{-1} is used for Z, the collision rate. r is the center-to center distance (in angstroms, A°) between the two reactants. K_{12} is the equilibrium

constant of the cross reaction, w_{ij} are Coulombic work terms associated with all four combinations of the reacting species, z_i and z_j are ionic charges of the reactants.

1.4 Organosulfur Compounds

Organosulfur compounds are sulfur-containing organic compounds which often have significant biological and environmental values. For instance, these substances can be used by bacteria to produce protein and assimilate sulfur since the fully oxidized sulfur is deficient in nature [1]. Some of the species are known for being antioxidants, anti-inflammatory reagents, and their role of reducing blood pressure [2],[3]. In nature, they are present in plants, coal, fossil fuels and natural gas. Several vital amino acids such as cysteine and methionine are organosulfur compounds. As aspect to industrial value, they are widely used as synthetic materials, intermediates, and solvents in the pharmaceutical and biochemical fields. For researchers, many of the compounds are utilized for structural and mechanistic investigations as these species contain an extensive range of sulfur-containing functional groups, and thus display various properties when they are exposed to heat, light, radiation, solvents, and redox reagents [4]. For example, thiols (R-SH) are readily oxidized, and thioesters (R-C(O)-S-R) tend to hydrolyze, whereas disulfides (R-S-S-R) are essential for crosslinking to fold and stabilize proteins. The oxidation state of sulfur in organosulfur compounds varies from -2 to +6 as shown in the figure below.

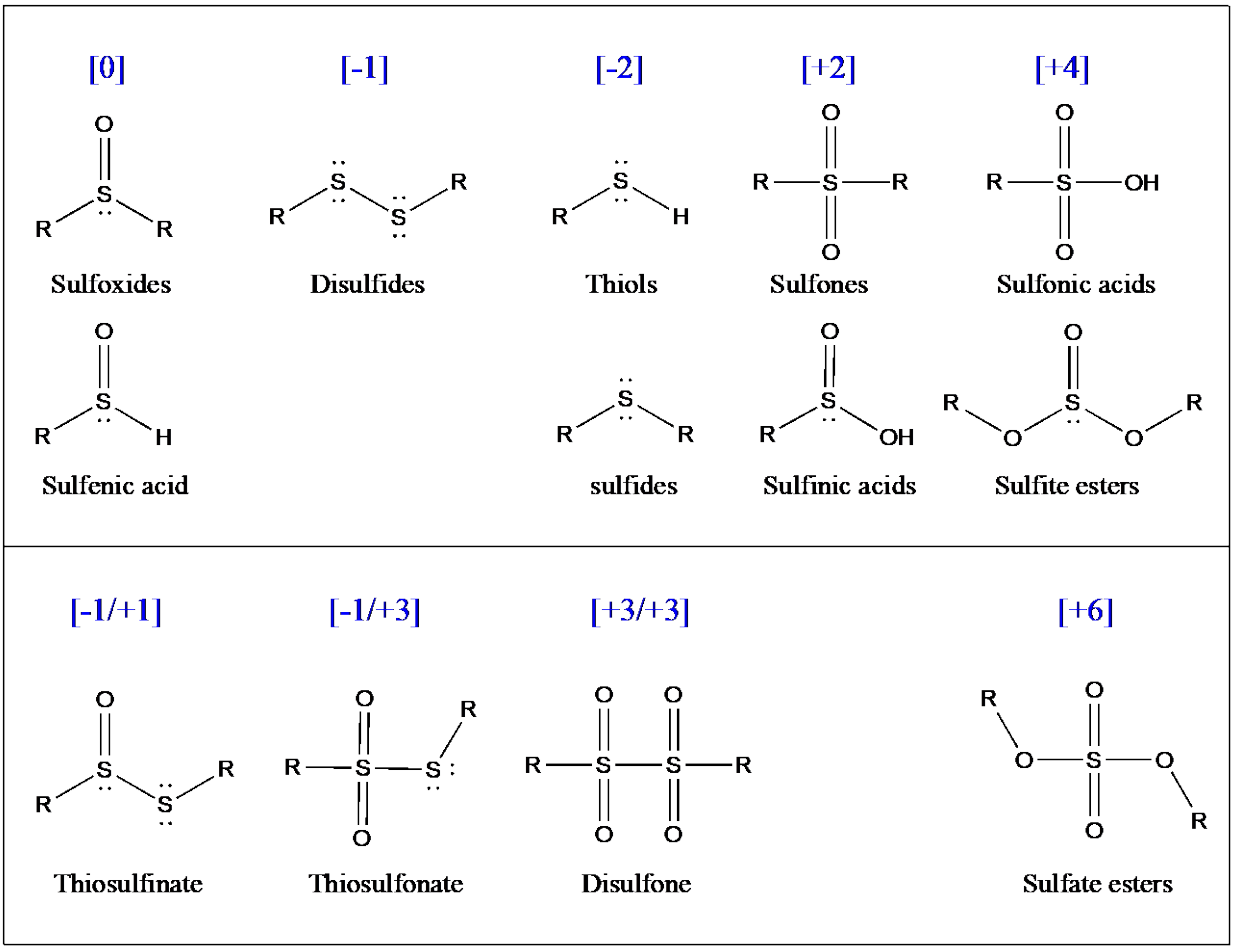

Figure 1-3. Sulfur oxidation states in various organosulfur compounds

Among the enormous number of organosulfur compounds, we herein pick several simple yet prominent substances including alkylsulfinic acids, thiols, and their disulfides as reactants to study the kinetics and underlying mechanisms of the relevant redox reactions in aqueous phase. The knowledge we obtain is expected to provide instructive information for environmental remediation and biochemical application.

1.4.1 Thiols

Thiols (RSH), also known as mercaptans, are the compounds with -SH group. Widely found in living cells, they participate in cell division, growth, and production of mutations, especially in regulatory mechanisms of cellular respiration and work as effective antioxidants and

deoxidants to protect cells from oxidative damage, photolysis, reactive nitrogen species and toxic metal ions [9],[13],[14],[18]. These functions are mostly determined by the activity of the hydrosulfide group of the thiol compounds. -SH groups in proteins are found to be crucial for enzyme activities as they are attached to the side chains of peptides which are used for constructing and maintaining the geometry of the proteins. Aside from that, -SH also works significantly as binding posts between some proteins and prosthetic groups. Some of them such as thioredoxin and glutathione, have great importance for transducing redox signals from cell surface to the nucleus through chain reactions in proteins [15]. Examples of several important thiols are given in Figure 1-4.

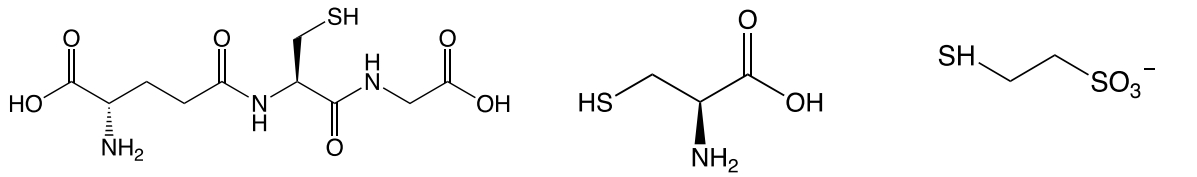

Glutathione L-cysteine Mercaptoethanesulfonate

Figure 1-4. Examples of several thiols.

Generally, thiols are reactive species as they can be oxidized easily. They are capable of reacting with aldehydes, quinones, halogen-containing species and heavy metals. One typical replacement can be the substitution of H in -SH group by a halogen residue. RSH can be oxidized by a variety of agents including oxygen, $NO_2^{\bullet}$, $O_2^{\bullet -}$, H_2O_2, $OH^{\bullet}$, $ClO_2^{\bullet}$, ferricyanide, etc. [7]-[12]. Oxidation of cysteine by oxygen, for example, requires the assistance of a metal catalyst such as copper [21],[52], iron [17], rhodium [53] or manganese [54]. The mechanism of the oxidation pathways involves an electroactive redox mediator of which the catalytical efficiency can be affected by different factors including the structure of the thiols, the intermediate complex, ionic strength, acidity of the system, and in some cases by the addition of other metals. The kinetics of the oxidation of thiols by transition metal complexes such as Ir(IV), $[Fe(bpy)_2(CN)_2]^{+}$, can be

affected by trace amounts of metal ions and inhibited by the resulting products. The ultimate products of the reactions turn out to depend on the amount of oxygen present [6].

Thiols are more acidic with dissociation constants (pK_a) around 8 compared with alcohols with pK_a values close to 16. They behave differently from alcohols upon oxidation. The ionic form of a thiol is a thiolate (RS^-). They are commonly known as better nucleophiles and weaker bases. At a given pH, pK_a values of different thiols can be a key factor to determine whether the species is a mercaptide ion or as its protonated form. The instantaneous ionization of thiols can be expressed from the equation $K_a = \frac{[RS^-][H^+]}{[RSH]}$, from which the ratio of the ion to mercaptan can be regulated by the amount of acid involved.

1.4.2 Disulfides

The coupling of two oxidized thiol groups produces a disulfide (R-S-S-R). A primary process of disulfide formation is from the photolysis [55],

$$RSH + h\nu \rightarrow RS^{\bullet} + H^{\bullet} \qquad \text{Eq. 1-10}$$

$$2RS^{\bullet} \rightarrow RSSR \qquad \text{Eq. 1-11}$$

In this process, thiyl radicals ($RS^{\bullet}$) are often formed as intermediates. As highly reactive species, they appear in different systems including reduction, intramolecular rearrangements, dimerization to release ions, thiols and mostly disulfides as displayed in equations [16],[18].

$$RS^{\bullet} + e^- \rightarrow RS^- \qquad RS^{\bullet} + e^- + H^+ \rightarrow RSH \qquad \text{Eq. 1-12}$$

$$RS^{\bullet} + RS^- \rightarrow RSSR^{\bullet -} \rightarrow RSSR + e^- \qquad \text{Eq. 1-13}$$

Taking glutathione (GSH) as an example: the oxidation of GSH by a biologically generated radical $R^{\bullet}$ gives $GS^{\bullet}$, which combines a thiolate GS^- to produce the disulfide radical anion $GSSG^{\bullet -}$. The anion can be subsequently oxidized by O_2 to release the corresponding disulfide GSSG [19],[20].

1.5 Iodine/Oxy-iodine Species

Iodine is an essential element that has been found in both organic and inorganic forms. In marine plants, animals, and natural water samples, iodine occurs as iodide and iodate. Iodine can also act as a catalyst in the manufacture of antiseptics, germicides, and some aspects of analytical chemistry field. Organic iodine compounds are regarded as secondary metabolites [22], given that they are vital components of the hormones which participate in biosynthesis and metabolism in human tissues [23]. Around 75 percent of the iodine in human body is found in the thyroid gland, and is mainly used by the thyroid gland to produce thyroid hormones thyroxine (T_4) and 3,5,3'-triiodothyronine (T_3). These hormones are regarded as the key for regulating brain development, neuromuscular functioning, energy levels, early body growth and for the maintenance of human reproductive functions [24]. The deficiency of thyroid hormone will cause goiter. This disease commonly results from the lack of iodide ion in the diet and can be prevented by the intake of iodized salt to some extent. Iodine also exists in monoiodotyrosine, diiodotyrosine and 3,3',5'-triiodothyronine (reverse T_3) in human body and mammals, functioning as free T_3 and T_4 through bonding proteins in thyroid and other tissues [25].

Aqueous iodine solution is a complex system which includes many knowns and unknowns. It should be noted that researchers have been trying to understand the elusive iodine equilibria that generate various species, such as I^-, I_3^-, HOI, HIO_2, HIO_3, IO_2^-, I_2OH^-, IO_3^-, OI^-, etc. For example, hypoiodous acid (HOI) has always been of environmental and geochemical interest. Generated by the oxidation of naturally occurring iodide by ozone (O_3), chlorine and chloramine, HOI can react with natural organic matter to produce iodate [26]. The dissection of the process can therefore be of great value as it will deliver important message on determining the fate of iodine in different fields. Normally, equilibria in iodine hydrolysis are strongly governed by H^+ and I^-.

Eigen and Kustin mentioned that the protonation of HOI is predominating below pH 7 in the system [27]. At pH range from 2 to 7, the overall equilibrium is given in the equation [28]. The rapid formation of IO_3^- usually occurs at pH > 7 due to the disproportionation.

$$I_2 + H_2O \rightleftharpoons HOI + I^- + H^+ \ (k_f = \ 2.1\ s^{-1};\ k_r = 3.1 \times 10^{12}\ M^{-2}\ s^{-1}) \qquad \text{Eq. 1-14}$$

$$3HOI \rightarrow IO_3^- + 2I^- + \ 3H^+ \qquad \text{Eq. 1-15}$$

This rate can be greatly affected by pH and the addition of iodide. In solutions with higher acidity, the second-order rate constant was reported by Furrow with a value of 25 $M^{-1}\ s^{-1}$ at 25 °C and found to be independent of pH [27]. Later, the value was confirmed by Schmitz [29] via extending the measurement to a higher perchloric acid media.

Despite the fundamental understanding of the species present in aqueous phase, study of the complicated system involving hydrolysis of iodine/oxy-iodine species along with their dimerization, dissociation, protonation, and deprotonation of the various forms can be still challenging yet intriguing. In particular, some of the parameters regarding equilibrium and rate constants remain open and questionable.

In addition to above, one of the most interesting phenomena involving iodine chemistry is the clock reaction, also known as iodine oscillation [30]. It refers to the coloration and discoloration behavior after an induction time when iodine is mixed and reacting with some reagents. Under some circumstances, addition of reagents can lead to an instant color change and build up a chemical oscillator. Chemical oscillator refers to a complex reaction mixture in which the concentration of one or several components displays a periodic change. Some sulfide ion-based oscillators have been profoundly studied [34]. In addition, sulfur-based oscillators including thiosulfate-chlorite [32], thiocyanate-H_2O_2-Cu(II) [35], thiourea-bromate [36], thiosulfate-hydrogen peroxide-Cu(II) [37] systems are also classical examples.

1.6 Outline

The following part of this dissertation is divided into four parts to report the relevant kinetics and mechanisms of the redox reactions between sulfur-based compounds and several essential oxidants: chapters 2 and 3 are the exploration of the reactions between methanesulfinate and two transition-metal complexes; chapters 4 and 5 are investigations regarding several thiols and disulfides oxidation by iodine/oxy-iodine species. From the results presented in this work, more understanding and insights into the related chemistry field will be contributed, especially on the mechanistical level.

1.7 References

[1] Kertesz, M. A. *FEMS Microbiol. Rev*. **2000**, *24*, 135-175.

[2] Rose, P.; Whiteman, M.; Moore, P. K.; Zhu, Y. Z. *Nat. Prod. Rep.*, **2005**, *22*, 351-368.

[3] Vazquez-Prieto, M. A.; Miatello, R. M. *Molecular aspects of medicine.* **2010**, *31*, 540-545.

[4] Block, E. *Reactions of Organosulfur Compounds: Organic Chemistry: A Series of Monographs*. Academic Press London, **1978**, *37*.

[5] Pethybridge, A. D.; Prue, J. E. *Prog. Inorg. Chem.* **1972**, *17*, 327-390.

[6] Bhattarai, N.; Stanbury, D. M. *Inorg. Chem.* **2012**, *51*, 13303-13311.

[7] Bose, R. N.; Moghaddas, S.; Gelerinter, E. *Inorg. Chem.* **1992**, *31*, 1987.

[8] Everse, J.; Kujundzic, N. *Biochemistry.* **1979**, *18*, 2668.

[9] Ford, E.; Hughes, M. N.; Wardman, P. *Free Radical Biol. Med.* **2002**, *32*, 1314.

[10] Winterbourn, C. C.; Metodiewa, D. *Free Radical Biol. Med.* **1999**, *27*, 322.

[11] Ison, A.; Odeh, I. N.; Margerum, D. W. *Inorg. Chem.* **2006**, *45*, 8768.

[12] Mezyk, S. P. *J. Phys. Chem.* **1996**, *100*, 8861.

[13] Lal, M. *Radiat. Phys. Chem.* **1994**, *43*, 595.

[14] Ercal, N.; Gurer, H.; Aykin, N. *Curr. Top. Med. Chem*. **2001**, *1*, 529.

[15] Sen, C. K. *Current topics in cellular regulation*. **2001**, *36*, 1-30.

[16] Włodek, L. *Pol. J. Pharmacol.* **2002**, *54*, 215.

[17] Taylor, J. E.; Yan, J. F.; Wang, J. L. *J. Am. Chem. Soc.* **1966**, *88*, 1663-1667.

[18] Exner, R.; Wessner, B.; Manhart, N.; Roth, E. *Wien. Klin. Wochenschr.* **2000**, *112*, 610–616.

[19] Sturgeon, B. E.; Sipe, H. J.; Barr, D. P.; Corbett, J. T.; Martinez, J. G.; Mason, R. P. *J. Biol. Chem*. **1998**, *273*, 30116-30121.

[20] Winterbourn, C. C. *Free Radical Biol. Med.* **1993**, *14,* 85–90.

[21] Cavallini, D.; De Marco, C.; Duprè, S.; Rotilio, G. *Arch. Biochem. Biophys*. **1969**, *130*, 354-361.

[22] Edmonds, J. S.; Morita, M. *Pure Appl. Chem*. **1998**, *70*, 1567-1584.

[23] Kohrle, J.; Jakob, F.; Contempré, B.; Dumont, J. E. *Endocr. Rev.* **2005**, *26,* 944-984.

[24] Schomburg, L.; Köhrle, J. *Mol. Nutr. Food Res.* **2008**, *52,* 1235-1246.

[25] Hou, X. *Comprehensive handbook of iodine nutritional, biochemical, pathological and therapeutic aspects*. Academic Press London, **2009**, 139-150.

[26] Bichsel, Y.; Von Gunten, U. *Environ. Sci. Technol.* **1999**, *33*, 4040-4045.

[27] Furrow, S. *J. Phys. Chem.* **1987**, *91*, 2129-2135.

[28] Eigen, M.; Kustin, K. *J. Am. Chem. Soc.* **1962**, 84, 1355.

[29] Schmitz, G. *Int. J. Chem. Kinet.* **2004**, *36*, 480-493.

[30] Briggs, T. S.; Rauscher, W. C. *J. Chem. Educ*. **1973**, *50*, 496.

[31] Rabai, G., Orban, M., Epstein, I. R. *J. Phys. Chem.* **1992**, *96*, 5414.

[32] Orbán, M.; De Kepper, P.; Epstein, I. R. *J. Phys. Chem.* **1982**, *86*, 1431.

[33] Burger, M.; Field, R. J.; *Nature*. **1984**, *307*, 720-721.

[34] Orbán, M.; Epstein, I. R. *J. Am. Chem. Soc.* **1985**, *107*, 2302.

[35] Orbán, M. *J. Am. Chem. Soc.* **1986**, *108*, 6893.

[36] Simoyi, R. H. *J. Phys. Chem*. **1986**, *90*, 2802.

[37] Orbán, M.; Epstein, I. R. *J. Am. Chem. Soc.* **1987**, *109*, 101.

[38] Hurd, T.R.; DeGennaro, M.; Lehmann, R. *Trends Cell Biol.* **2012**, *22*,107-115.

[39] Montell, D. J. *Science.* **2008**, *322*,1502–1505.

[40] Radisky, D. C.; Levy, D. D.; Littlepage, L. E.; Liu, H.; Nelson, C. M.; Fata, J. E.; Leake, D.; Godden, E. L.; Albertson, D. G.; Nieto, M. A.; Werb, Z. *Nature.* **2005**, *436*, 123-127.

[41] Taube, H; Myers, H. *J. Am. Chem. Soc*. **1954**, *76*, 2103.

[42] Taube, H.; Myers, H.; Rich, R. L. *J. Am. Chem. Soc*. **1953**, *75*, 4118-4119.

[43] Marcus, R. A.; Sutin, N. *Biochim. Biophys. Acta.* **1985**, *811*, 265.

[44] Marcus, R. A. *J. Phys. Chem.* **1963**, *67*, 853.

[45] Marcus, R. A.; Eyring, H. *Annu. Rev. Phys. Chem.* **1964**, *15*, 155.

[46] Debye, P. *Trans. Electrochem. Soc.* **1942**, *82*, 265-272.

[47] Eberson, L. E. *Electron Transfer Reactions in Organic Chemistry; Springer: Berlin.* **1987**, *25*.

[48] Jordan, B. R. *Reaction Mechanisms of Inorganic and Organometallic Systems.* Oxford University Press London*.* **1991**, *169*.

[49] Stanbury, D. M.; Hoffman, D. *J. Phys. Chem. A.* **2019**, *123*, 5436−5445.

[50] Stanbury, D. M.; Harshman, J. *J. Phys. Chem. A.* **2019**, *123*, 10240–1024.

[51] Marcus, R. A. *J. Chem. Phys.* **1956**, *24*, 966–978.

[52] Kachur, A.V.; Koch, C. J.; Biaglow, J. E. *Free Radical Res.* **1999**, *31*, 23-34.

[53] Arisawa, M.; Fukumoto, K.; Yamaguchi, M. *ACS Catal.* **2020**, *10*, 15060−15064.

[54] Tan, K.Y. D.; Teng, G. F.; Fan, W. Y. *Organometallics.* **2011**, *30*, 4136–4143.

[55] Weiss, J.; Fishgold, H. *Nature*. **1936**, *137*, 71-72.

2 One-electron Oxidation of Methanesulfinic Acid (MS) by Hexachloroiridate(IV)

2.1 Introduction

One-electron oxidation of alkylsulfinic acids is of great interest currently as the reaction mechanisms are generally complex and elusive. Though it has been reported that the ultimate product of one-electron oxidation of an alkylsulfinic acid is mostly the corresponding sulfonic acid [1]-[4], one might still find it challenging to explain how the process takes place with the limited one-electron oxidants, especially when it comes to elaborating how the intermediates form and convert to the final products. In most cases, the transient S-containing species are sulfonyl radicals ($RSO_2^{\bullet}$) which have been shown in some industrial processes such as sulfoxidation to produce surfactants [5],[13]. Sulfonyl radicals are characterized as σ-type species with a pyramidal center at sulfur through spectroscopy [34]. Despite some may propose that the $RSO_2^{\bullet}$ can go through reduction [3],[4], SO_2 elimination ($RSO_2^{\bullet} \rightleftharpoons R^{\bullet} + SO_2$) [8], radical coupling followed by disproportionation [18], kinetic data involving their formation and conversion are scarce. Plus, the systematic overview and predictive framework of such reactions are not yet established. It is also noteworthy that the behavior can be quite extraordinary when the same oxidant is employed to react with different RSO_2^- because of the distinction in the electronic environment and structure of the sulfinates. As the study on oxidation of cysteinesulfinic acid ($CysSO_2H$) by hexachloroiridate(IV) has been reported lately, it would be interesting to examine the reaction between methanesulfinic acid (MSA, CH_3SO_2H) and the same one-electron oxidant to establish a comparison [3].

The purpose of this investigation is to seek evidence to elucidate the detailed mechanism of oxidation of MSA by hexachloroiridate(IV) and to compare that with other alkylsulfinic acids.

To make it more specific, it is to establish the rate law for the overall reaction. Second being the evaluation of the electron-transfer mechanism and rate-limiting step of the process. In theory, outer-sphere electron transfer is most possibly appearing in $[IrCl_6]^{2-}$ oxidation [6]. A thorough understanding of the pathway might help us predict the actual rate constants using Collision theory and Marcus theory. Other concerns include the pH dependence and Ir(III) effect on the reaction kinetics, which might provide us essential evidence in interpreting the complete mechanism scheme.

Hexachloroiridate(IV) was selected as the oxidant due to its stability as a typical outer-sphere electron-transfer reagent. Compared with some other metal complexes, such as iron(III) complex, $[IrCl_6]^{2-}$ is stable over a wide range of pH [7]. The reduced form $[IrCl_6]^{3-}$ was proved to have no significant acid/base properties as well [6].

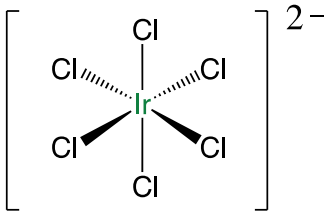

Hexachloroiridate(IV)

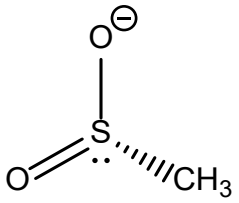

Methanesulfinate

The alkylsulfinic acid employed for this study is methanesulfinate (MSA) with an oxidation number of +2 of sulfur. In aqueous phase, it is regarded as the most significant source of methanesulfonate (the oxidation number of S is +4). MSA is produced from the oxidation of dimethyl sulfide (CH_3SCH_3) in the atmosphere by $OH^{\bullet}$ primarily, which makes it an indispensable intermediate in the global sulfur cycle [9]-[11]. Methanesulfonic acid is present in the atmosphere from the oxidation of MSA by aerosol. The oxidation system as a whole is relevant to climate fluctuation since the processes involve the producing of sulfate particle which is the component of cloud condensation nucleus (aerosol) [10],[12]. MSA can be also found in

dimethylsulfone metabolism from the oxidation of dimethylsulfone by oxygen in the presence of monoxygenase SfnG [25],[26]. The reaction equation is given in Eq. 2-1. Thus, the simplicity of the structure and its importance to environment makes MSA a good candidate for the exploration on organo-sulfur redox reactions.

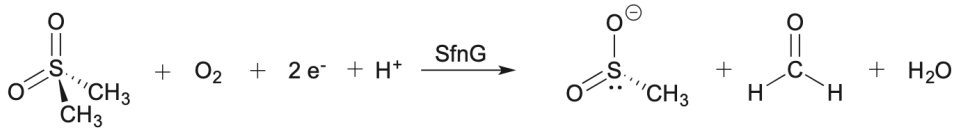

Eq. 2-1

2.2 Experimental Preparations and Methods

2.2.1 Reagents and Solutions

Sodium methanesulfinic acid (MSA, Alfa Aesar), sodium methanesulfonate (Alfa Aesar), ammonium hexachloroiridate (IV) (Aldrich), ammonium hexachloroiridate (III) (Aldrich), NH_4Cl (Fisher), acetic acid (Fisher), HCl (Fisher), $HClO_4$ (Fisher), N-tert-butyl-α-phenylnitrone (PBN, Aldrich), CH_3COONa anhydrous (Sigma), D_2O 99.8% isotopic (Alfa Aesar), 3-(trimethylsilyl)-1-propane sulfonic acid sodium salt (DSS), $NaClO_4$ (Fisher), $MeSO_2Cl$ (Alfa Aesar), $KMnO_4$ (J. T. Baker), $CoCl_2$ hydrate (J. T. Baker), 30% H_2O_2 (Aldrich), ammonium hydroxide (Fisher), CH_2Cl_2 (Alfa Aesar), dimethyl sulfoxide (DMSO) (Alfa Aesar), ethanol (Aldrich), sulfuric acid (Fisher), acrolein, propiolic acid (Alfa Aesar).

$(NH_4)_2IrCl_6$ was recrystallized prior to the experiments by adding saturated NH_4Cl solution to a hot $(NH_4)_2IrCl_6$ solution. After cooling in an ice bath, the mixture was filtered and washed with 20% NH_4Cl, 95% C_2H_5OH, and finally diethyl ether. The recrystallized product has a yield of 79%. The purity of $(NH_4)_2IrCl_6$was examined by UV-Vis spectrophotometer. The molar absorptivity (ε_{eff}) used for this study is $4.14 \times 10^3\ M^{-1}\ cm^{-1}$ ($\varepsilon_{eff}[IrCl_6]^{2-} = 3.98 \times 10^3\ M^{-1}\ cm^{-1}$ at 488 nm [14]). Ir(IV) stock solutions were freshly prepared with pH adjusted to 3 or lower using

$HClO_4$ to minimize its decomposition [15]. All iridium-containing solutions were protected from light due to its photosensitivity.

The purity of MSA was examined through ^{1}H-NMR prior to experiment. MSA stock solutions used for kinetic and stoichiometry studies were titrated by standard $KMnO_4$ solution in the presence of sulfuric acid based on reaction $5CH_3SO_2^- + 2MnO_4^- + 6H^+ \rightarrow 5CH_3SO_3^- + 2Mn^{2+} + 3H_2O$. The final volume of $KMnO_4$ was recorded once the faint pink color appeared. The process was repeated at least 3 times to get the average concentration of MSA.

2.2.2 Instruments and Methods

All the aqueous solutions were freshly prepared using purified de-ionized water with a specific resistivity of 18.2 MΩ cm at 25 °C from an Ultrapure water purification system. UV-Vis spectra were collected at 25 ± 0.1 ℃ using a HP-8453 diode array spectrophotometer equipped with a Brinkman Lauda RM6 thermostatted system to maintain the temperature. The quartz cells for UV measurement are with path length of 1 mm or 1 cm. Kinetic data were collected on a Hi-Tech SF-51 stopped-flow spectrophotometer with 1 cm path length configuration with OLIS 4300 data acquisition and later analyzed by GraphPad PRISM 9. The k_{obs} values reported in this study are averages of at least seven trials. As $(NH_4)_2[IrCl_6]$ has strong absorbance at 488 nm while the Ir-containing products do not, the absorbance loss at this wavelength can thus be monitored to study the kinetic behavior. Ionic strength (μ) was adjusted to 0.1 M with recrystallized $NaClO_4$ unless otherwise indicated.

Acetic acid-acetate buffers were prepared from standard HOAc and NaOAc. pH measurements were performed at room temperature using a Corning 450 pH/ion meter equipped with a Mettler Toledo InLab 421 pH electrode using the relationship $pH = -\log[H^+]$. To prevent the formation and precipitation of $KClO_4$ on the pH probe, the electrode was filled with 3 M NaCl

solution. The pH of each reaction was obtained after mixing the two reactant solutions in a 1:1 ratio. ^{1}H-NMR spectra were obtained on a Bruker AV 500 or 600 MHz spectrometer by dissolving the sample in D_2O with 3-(trimethylsilyl)-1-propanesulfonic acid sodium salt (DSS) as internal standard unless stated. Electrochemical study including cyclic voltammograms (CV) and Osteryoung square-wave voltammograms were performed on a BAS 100B electrochemical analyzer equipped with a BAS C3 cell stand with a purging and stirring system. The working electrode was a glassy carbon electrode, the reference electrode was an Ag/AgCl electrode with 3.0 M NaCl ($E°$ = 0.205 V vs NHE). The auxiliary electrode was a Pt wire.

2.3 Results

2.3.1 Stoichiometry Study

The stoichiometric ratio of MSA and Ir(IV) was determined through spectrophotometric titration under anaerobic conditions. 2.0 ml of 1.126 mM MSA was added into a cuvette and purged with argon for 40 minutes. Later, small aliquots of 4.48 mM Ir(IV) with air excluded were added to the MSA solution in cuvette using a gastight syringe. The absorbance change at 488 nm was recorded until the endpoint was reached. After all MSA was consumed, the absorbance rises linearly due to the excess addition of Ir(IV). The ratio of the consumed Ir^{IV} and MSA was 2.03:1.

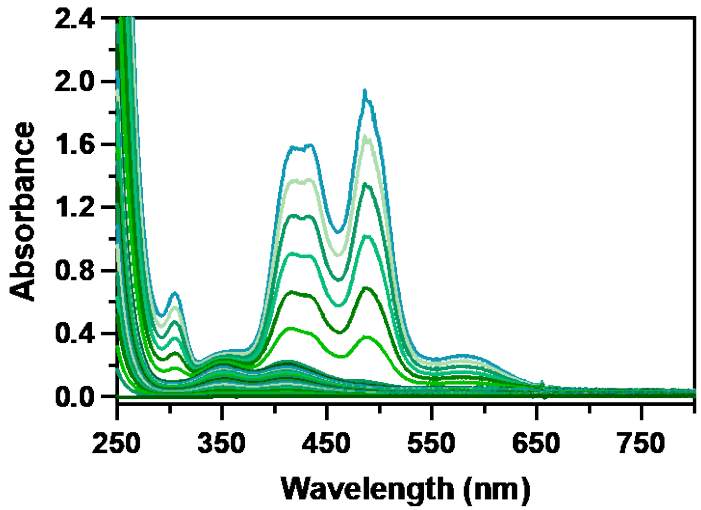

Figure 2-1. UV-vis spectra after each addition.

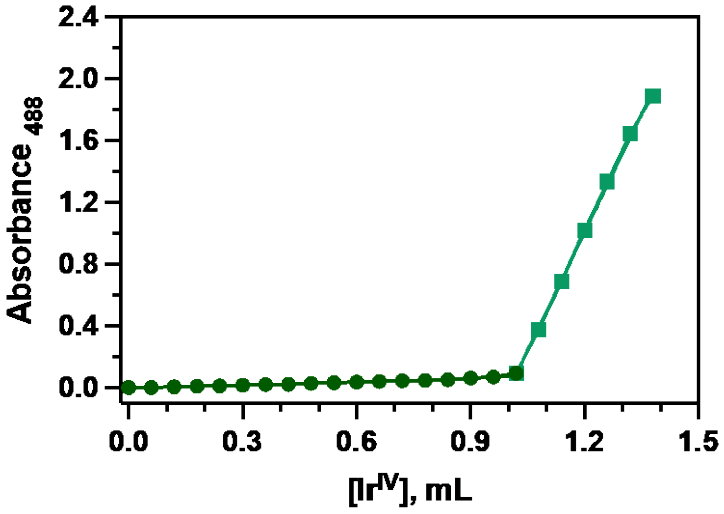

Figure 2-2. Determination of the end point from the titration.

2.3.2 Kinetics of the Reaction between MSA and $[IrCl_6]^{2-}$

The reaction between 1.70 mM MSA and 0.05 mM $(NH_4)_2IrCl_6$ was monitored by stopped-flow instrument at 25 °C, pH 4.6 (acetate buffer), μ = 0.1 M ($NaClO_4$). A loss of absorbance at 488 nm was observed as the consumption of Ir(IV), where the absorbance of products are negligible. The data was collected for at least 12 half-times and plotted into $\log(A_t -$

A_∞) vs time. Given that Ir(IV) is mixed with 34-fold molar excess of MSA, the reaction thus follows pseudo-first order kinetics. The reaction equation is given below.

$$[IrCl_6]^{2-} + CH_3SO_2^- \rightarrow \text{products} \qquad \text{Eq. 2-2}$$

The rate law of the equation is,

$$-\frac{d[Ir^{IV}]}{dt} = k[MSA][Ir^{IV}] \qquad \text{Eq. 2-3}$$

When $[MSA] \gg [Ir^{IV}]$,

$$-\frac{d[Ir^{IV}]}{dt} = k_{obs}[Ir^{IV}] \qquad \text{Eq. 2-4}$$

Where $k_{obs} = k[MSA] = 14.13\ s^{-1}$.

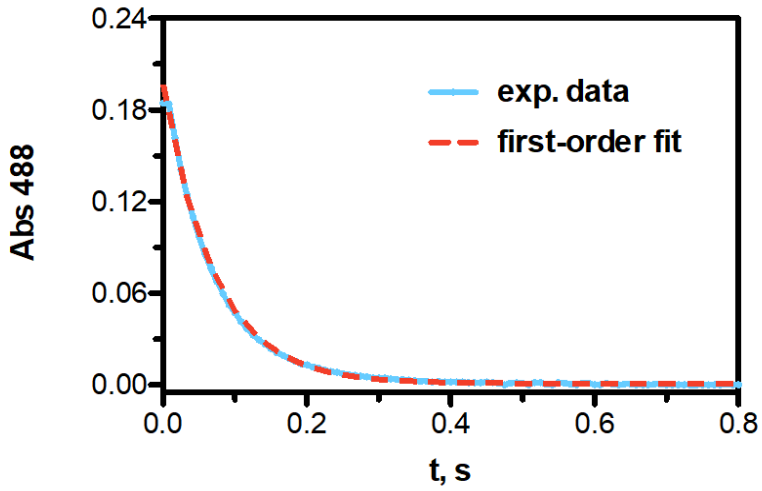

Figure 2-3. Kinetic trace and fit with excess MSA. Conditions: $[MSA]_o = 1.70$ mM, $[Ir^{IV}]_o = 0.05$ mM.

2.3.3 Rate Dependence on [MSA]

A series of reactions with the mixture of 0.078 mM $(NH_4)_2IrCl_6$ and MSA concentration varying from 0.2 mM to 16 mM were performed under anaerobic conditions at 25 °C, pH 3.5 (acetate buffer), μ = 0.1 M ($NaClO_4$). Considering that the fast reactions with [MSA] > 5mM complete within 0.1 second, the mixing process of the stopped-flow is likely to affect the real rate constants. In order to solve the true first-order rate constant, k_r, below equation is used [39].

$$\frac{1}{k_{\text{obs}}} = \frac{1}{k_r} + \frac{1}{k_{\text{mix}}} \qquad \text{Eq. 2-5}$$

In the equation, k_{obs} is the observed rate constant from the fitting of the experimental trace. k_{mix} is a first-order mixing rate constant determined from the instrument with a value of $1540\ \text{s}^{-1}$. The methods for getting this rate constant of our stopped-flow instrument was based on the reaction of $Fe(CN)_6^{4-}$ and $IrCl_6^{2-}$. A series of experiments was performed by varying the concentration of $Fe(CN)_6^{4-}$ and keeping $[IrCl_6^{2-}]$ as constant. The inverse first-order rate constant of the reaction was plotted against 1/ $Fe(CN)_6^{4-}$ as shown in Figure 2-4.

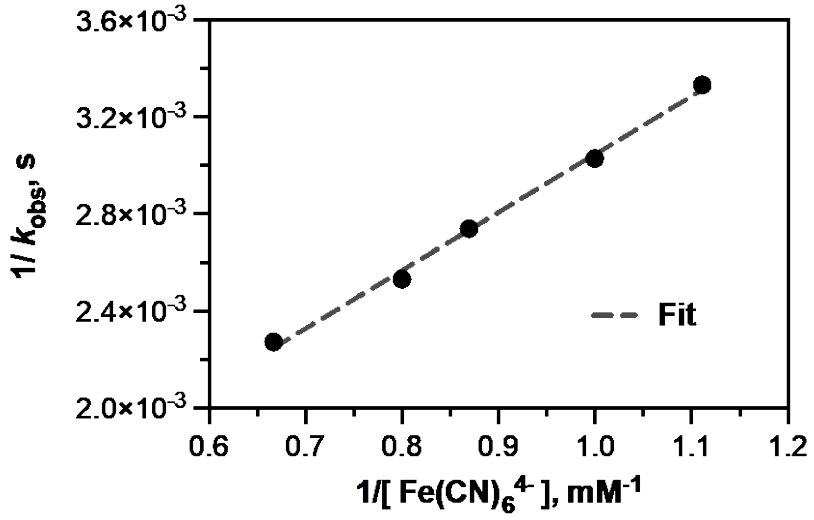

Figure 2-4. Linear fit for determining the mixing rate constant for stopped-flow instrument.

The equation

$$\frac{1}{k_{\text{obs}}} = \frac{1}{k_2[\text{Fe(CN)}_6^{4-}]} + \frac{1}{k_{\text{mix}}}$$

was used to fit the data [39], where k_2 is a second-order rate constant. From the linear fit, k_2 and k_{mix} were determined to be $4.17 \times 10^5\ \text{M}^{-1}\ \text{s}^{-1}$ and $1.54 \times 10^3\ \text{s}^{-1}$, respectively.

With the resolved values, the kinetic dependence on [MSA] is plotted in Figure 2-5, which implies a first-order dependence of k_r on $[\text{MSA}]_0$ from the linear fit with a negligible intercept.

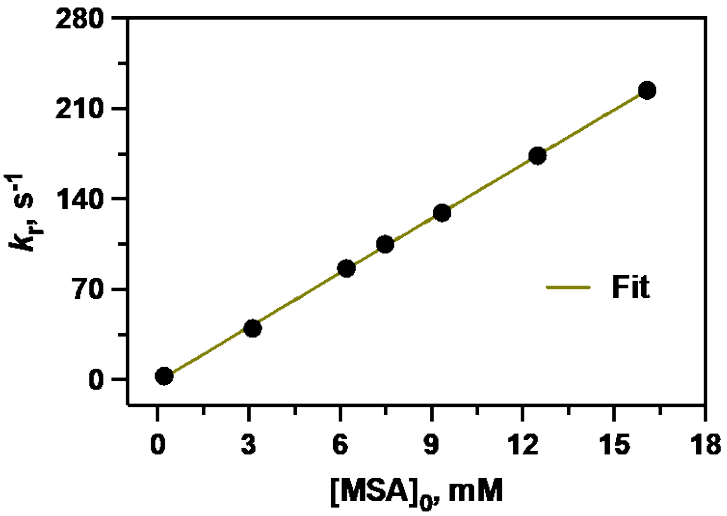

Figure 2-5. Dependence of k_r on [MSA]. Straight line fit with slope $= (1.40 \pm 0.01) \times 10^4\ s^{-1}\ M^{-1}$; Y − intercept $= (-1.3 \pm 1.0)\ s^{-1}$.

Table 2-1. Data table of rate dependence on [MSA].

$[MSA]_0$, mM	k_r, s^{-1}
0.21	2.77
3.12	39.97
6.20	86.27
7.48	105.03
9.34	129.3
12.48	173.6
16.08	224.3

2.3.4 pH Dependence

Excellent pseudo-first order fits can be obtained from pH 1.0 to 6.0, which enables us to evaluate the pH dependence of the reaction rate constant by monitoring the absorbance change at 488 nm with 3.1 mM MSA and 0.08 mM Ir^{IV} under anaerobic conditions at 25°C, μ = 0.1 M ($NaClO_4$). The experiments were performed covering pH range of 1.19 to 5.40 at different media. $HClO_4$ was employed to adjust the reaction at pH 1 to 3.3. The higher pH values were maintained

using acetate buffers. Experiments with pH above 6.0 were not carried out due to the instability of Ir(IV) compounds at high pH. A plot of log(k_{obs}) versus pH in Figure 2-6 shows that as pH increases, significant increase in the values of k_{obs} occurs till a plateau is reached. Both one and two-term rate law were employed to fit the data.

A simple one-term rate law was derived based on the assumption that the sulfinate anion form of MSA participates in the reaction with Ir(IV) primarily whereas the protonated form is least involved,

$$CH_3SO_2H \rightleftharpoons CH_3SO_2^- + H^+;\ pK_a = 2.28 \qquad \text{Eq. 2-6}$$

Here, K_a is the acid dissociation constant of MSA [16].

$$K_a = \frac{[CH_3SO_2^-][H^+]}{[CH_3SO_2H]} \qquad \text{Eq. 2-7}$$

From Eq. 2-2,

$$-\frac{d[Ir^{IV}]}{dt} = k_{obs}[Ir^{IV}] \qquad \text{Eq. 2-8}$$

$$k_{obs} = k[CH_3SO_2^-] \qquad \text{Eq. 2-9}$$

$$[MSA]_{total} = [CH_3SO_2H] + [CH_3SO_2^-] \qquad \text{Eq. 2-10}$$

$$[CH_3SO_2^-] = [MSA]_{total} - [CH_3SO_2H] \qquad \text{Eq. 2-11}$$

$$[CH_3SO_2^-] = [MSA]_{total} - \frac{[CH_3SO_2^-][H^+]}{K_a} \qquad \text{Eq. 2-12}$$

$$[CH_3SO_2^-] + [CH_3SO_2^-]\frac{[H^+]}{K_a} = [MSA]_{total} \qquad \text{Eq. 2-13}$$

$$[CH_3SO_2^-]\left(1 + \frac{[H^+]}{K_a}\right) = [MSA]_{total} \qquad \text{Eq. 2-14}$$

$$[CH_3SO_2^-] = \frac{[MSA]_{total}}{\left(1 + \frac{[H^+]}{K_a}\right)} \qquad \text{Eq. 2-15}$$

$$[CH_3SO_2^-] = \frac{[MSA]_{total}}{\left(\frac{K_a + [H^+]}{K_a}\right)} = \frac{[MSA]_{total} \times K_a}{K_a + [H^+]} \quad \text{Eq. 2-16}$$

$$k_{obs} = k[CH_3SO_2^-] = k\left(\frac{[MSA]_{total} \times K_a}{K_a + [H^+]}\right) \quad \text{Eq. 2-17}$$

$$k_{obs} = \frac{k \times 1.55 \times 10^{-3} \times 5.248 \times 10^{-3}}{(5.248 \times 10^{-3}) + [H^+]} \quad \text{Eq. 2-18}$$

$$k_{obs} = \frac{8.1375 \times 10^{-6} \times k}{(5.248 \times 10^{-3}) + [H^+]} \quad \text{Eq. 2-19}$$

$$\log k_{obs} = \log(8.1375 \times 10^{-6}) + \log k - \log\left((5.248 \times 10^{-3}) + 10^{-pH}\right) \quad \text{Eq. 2-20}$$

Fitting equation can be written as,

$$Y = -5.090 + \log k - \log\left((5.248 \times 10^{-3}) + 10^{-pH}\right) \quad \text{Eq. 2-21}$$

$$k = (1.41 \pm 0.02) \times 10^4\ M^{-1}s^{-1} \quad \text{Eq. 2-22}$$

Two terms fit with the postulation that both protonated form and the sulfinate anion form contribute to the reaction kinetics is provided as,

$$CH_3SO_2H \rightleftharpoons CH_3SO_2^- + H^+ \quad \text{Eq. 2-23}$$

$$K_a = \frac{[CH_3SO_2^-][H^+]}{[CH_3SO_2H]} \quad \text{Eq. 2-24}$$

$$-\frac{d[Ir^{IV}]}{dt} = k_{obs}[Ir^{IV}] \quad \text{Eq. 2-25}$$

$$k_{obs} = k_1[CH_3SO_2^-] + k_2[CH_3SO_2H] \quad \text{Eq. 2-26}$$

Where, k_1 and k_2 stand for the reactivities of CH_3SO_2H and $CH_3SO_2^-$ with Ir(IV).

$$[MSA]_{total} = [CH_3SO_2H] + [CH_3SO_2^-] \quad \text{Eq. 2-27}$$

$$[CH_3SO_2^-] = [MSA]_{total} - [CH_3SO_2H] = [MSA]_{total} - \frac{[CH_3SO_2^-][H^+]}{K_a} \quad \text{Eq. 2-28}$$

$$[CH_3SO_2^-] + [CH_3SO_2^-]\frac{[H^+]}{K_a} = [MSA]_{total} \quad \text{Eq. 2-29}$$

$$[CH_3SO_2^-]\left(1 + \frac{[H^+]}{K_a}\right) = [MSA]_{total} \quad \text{Eq. 2-30}$$

$$[CH_3SO_2^-] = \frac{[MSA]_{total}}{\left(1 + \frac{[H^+]}{K_a}\right)} \quad \text{Eq. 2-31}$$

$$[CH_2SO_2H] = \frac{[CH_3SO_2^-][H^+]}{K_a} = \frac{[MSA]_{total}}{\left(1 + \frac{[H^+]}{K_a}\right)} \times \frac{[H^+]}{K_a} = \frac{[MSA]_{total}[H^+]}{K_a + [H^+]} \quad \text{Eq. 2-32}$$

$$k_{obs} = k_1[CH_3SO_2^-] + k_2[CH_3SO_2H] = k_1\left(\frac{[MSA]_{total}}{\left(1 + \frac{[H^+]}{K_a}\right)}\right) + k_2\left(\frac{[MSA]_{total}[H^+]}{K_a + [H^+]}\right) \quad \text{Eq. 2-33}$$

$$k_{obs} = \frac{k_1[MSA]_{total}}{\frac{K_a + [H^+]}{K_a}} + \frac{k_2[MSA]_{total}[H^+]}{K_a + [H^+]} \quad \text{Eq. 2-34}$$

$$k_{obs} = \frac{k_1K_a[MSA]_{total} + k_2[MSA]_{total}[H^+]}{K_a + [H^+]} \quad \text{Eq. 2-35}$$

$$\log k_{obs} = \log(k_1K_a[MSA]_{total} + k_2[MSA]_{total}[H^+]) - \log(K_a + [H^+]) \quad \text{Eq. 2-36}$$

$$Y = \log(\{k_1 \times 5.248 \times 10^{-3} \times 1.55 \times 10^{-3}\} + \{k_2 \times 1.55 \times 10^{-3} \times 10^{-pH}\}) - \log(5.248 \times 10^{-3} + 10^{-pH}) \quad \text{Eq. 2-37}$$

Fitting equation:

$$Y = \log(k_1 \times 8.134 \times 10^{-6} + k_2 \times 1.55 \times 10^{-3} \times 10^{-X}) - \log(5.248 \times 10^{-3} + 10^{-X}) \quad \text{Eq. 2-38}$$

$$k_1 = (1.40 \pm 0.024) \times 10^4\ M^{-1}\ s^{-1};\ k_2 = (22.5 \pm 55.9)\ M^{-1}\ s^{-1} \quad \text{Eq. 2-39}$$

The two k values yield from the fit indicate that the active form of the reductant for the reaction is $CH_3SO_2^-$ considering the negligible value of k_2 compared with k_1.

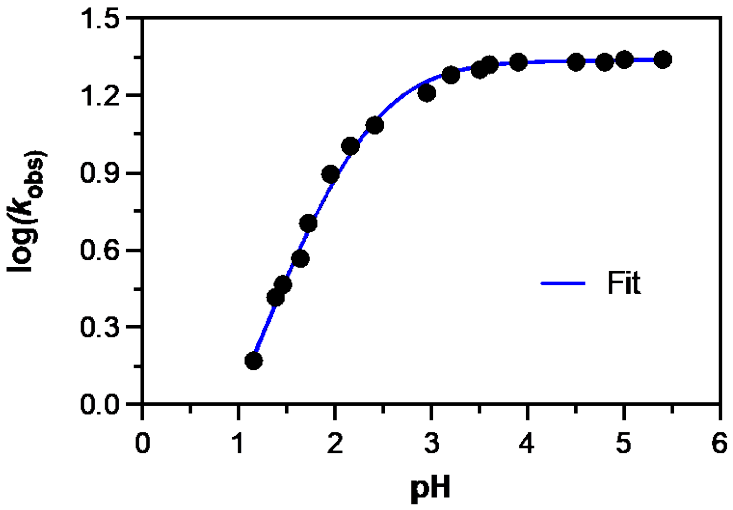

Figure 2-6. Plot of log k_{obs} vs pH. Conditions: $[Ir^{IV}]_0$ = 0.04 mM, $[MSA]_0$ = 1.55 mM.

Table 2-2. Data for determining pH dependence of $k_{obs.}$

pH	log k_{obs}	pH	log k_{obs}
1.16	0.17	2.95	1.28
1.38	0.42	3.20	1.30
1.72	0.70	3.50	1.32
1.46	0.47	3.60	1.33
1.95	0.89	3.90	1.33
1.64	0.57	4.48	1.33
2.16	1.00	4.80	1.33
2.41	1.08	5.00	1.34
2.95	1.21	5.40	1.34

2.3.5 Rate dependence on $[IrCl_6]^{3-}$

Apart from the reactants, effect on the rate dependence can be extended to the product side, particularly Ir(III). Deductions can be made that Ir(III) could inhibit the reaction kinetics because the following equilibrium might establish,

$$\mathrm{Ir(IV)} + \mathrm{CH_3SO_2^-} \rightleftharpoons \mathrm{Ir(III)} + \mathrm{products} \quad \left(k_\mathrm{f}, k_\mathrm{r}, K_{eq}\right) \qquad \text{Eq. 2-40}$$

Such observation is quite usual as it has been shown in other similar reactions, such as the oxidation of SCN^- by Ni(III) [17], $CysSO_2^-$/Ir(IV) reaction [3], etc. One may expect a significant drop of the observed rate constant with the addition of large [Ir(III)] as the equilibrium will shift to the left. Based on the equation given above, the rate law can be thus expressed as,

$$-\frac{\mathrm{d}[\mathrm{Ir^{IV}}]}{\mathrm{dt}} = \frac{k\left(k_f, k_r\right)[\mathrm{Ir^{IV}}][\mathrm{MSA}]}{[\mathrm{Ir^{III}}]} \qquad \text{Eq. 2-41}$$

Where *k* is a function of the forward and reverse rate constants.

To test out our speculation, the effect of Ir(III) was studied by adding extra $(NH_4)_3IrCl_6$ to the reaction mixture. Ir(III) was added to Ir(IV) after bubbling the latter one for 30 mins. The iridium mixture was subsequently saturated with argon for 5 mins. Although the reaction between Ir(IV) and MSA displays excellent pseudo-first order kinetics, deviations appear when Ir(III) is added. The kinetic traces are better fitted with the integrated second-order rate law with the increase in the concentration of Ir^{III}. The pseudo-second -order rate law is described as,

$$A_t = \frac{A_o - A_{final}}{\left(A_o - A_{final}\right)\frac{k_{obs,2}}{\varepsilon_{488} l} t + 1} + A_{final} \qquad \text{Eq. 2-42}$$

Here, A_{final} and A_0 refer to the final and initial absorbance. $k_{obs,2}$ represents the pseudo-second-order rate constant. ε_{488} is the molar absorptivity of $[IrCl_6]^{2-}$ at 488 nm. l is the optical pathlength.

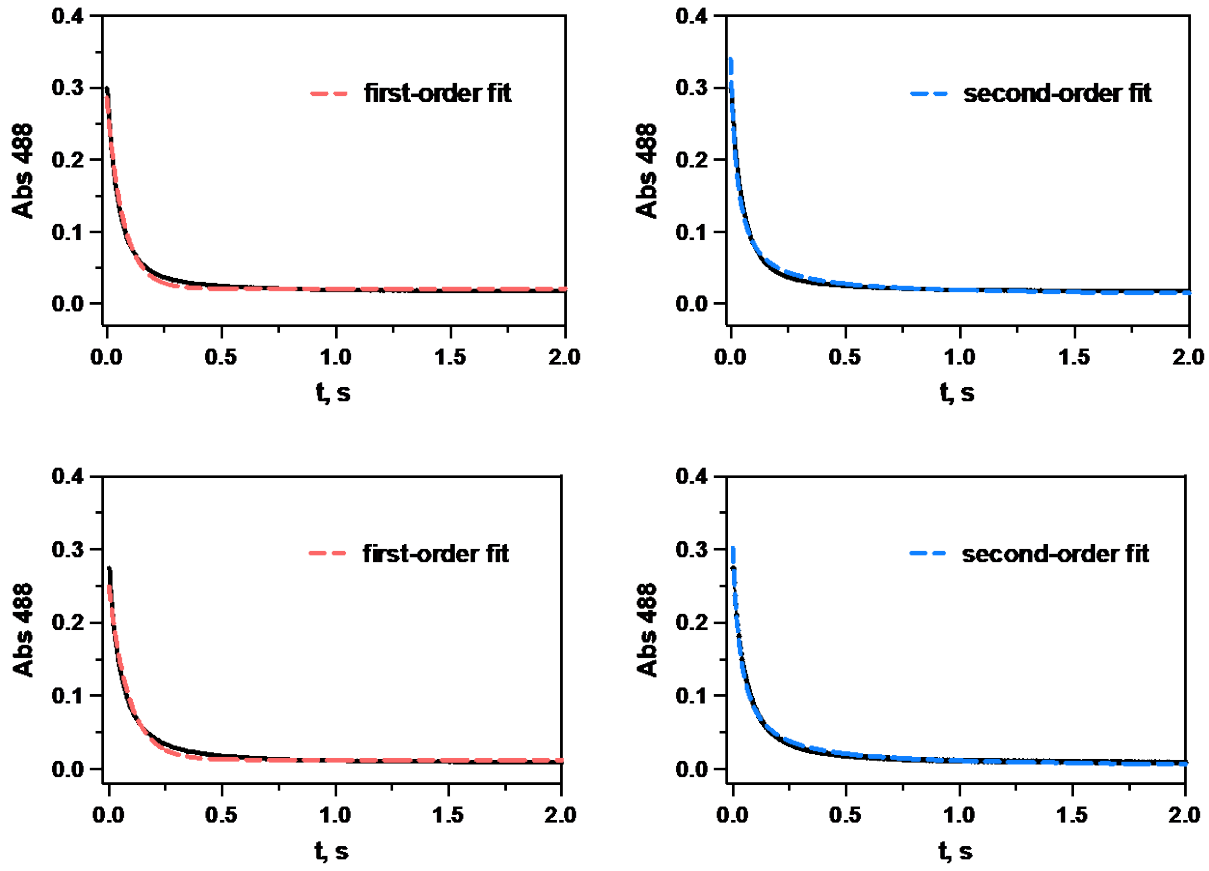

Figure 2-7. Kinetic traces in the presence of Ir^{III}. Left: first-order decay. Right: second-order fit. Conditions: $[Ir^{IV}]_0$ = 0.07 mM, $[MSA]_0$ = 2.75 mM; (top) $[Ir^{III}]_0$ = 0.73 mM (bottom) $[Ir^{III}]_0$ = 1.82 mM; μ = 0.1 M (NaCl), pH = 4.8 (acetate buffer).

A more systematic dependence of [Ir(III)] on $k_{obs,2}$ was studied by keeping $[Ir(IV)]_0$, $[MSA]_0$ constant and varying $[Ir(III)]_0$ from 0 mM to 1.82 mM. It can be observed from the kinetic result that the inhibition from Ir(III) is not very strong.

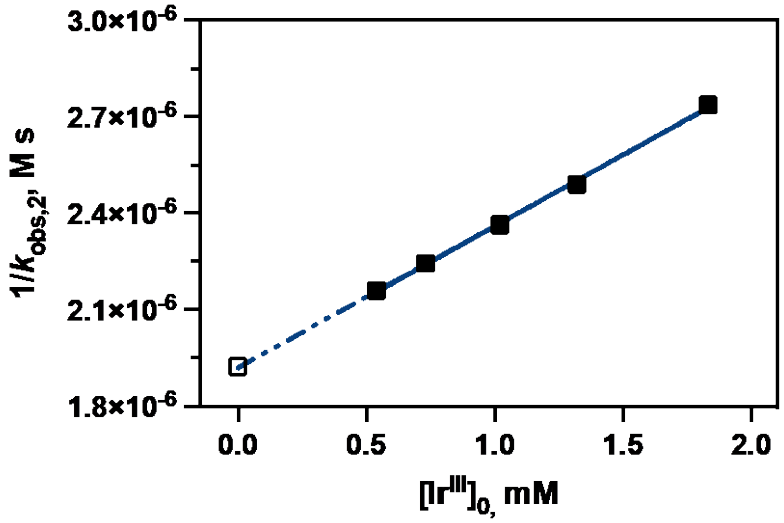

Figure 2-8. Plot of $1/k_{obs,2}$ vs $[Ir^{III}]$ at pH 4.8, acetate buffer. Conditions: $[Ir^{IV}]_0$ = 0.072 mM, $[MSA]_0$ = 1.42 mM. Linear fit with slope = $(4.44 \pm 0.09) \times 10^{-4}$ s, Y-intercept = $(1.9 \pm 0.01) \times 10^{-6}$ M s.

Table 2-3. Effect of Ir(III) on the reaction kinetics.

$[Ir^{III}]_0$, mM	$1/k_{obs,2}$ ($\times 10^6$), M s
0	1.92
0.54	2.16
0.73	2.24
1.02	2.36
1.32	2.49
1.83	2.74

The experimental data was fitted with a linear regression which can be described as,

$$\frac{1}{k_{\mathrm{obs},2}} = \mathrm{A} + k_{\mathrm{i}}[\mathrm{Ir}^{\mathrm{III}}] \qquad \text{Eq. 2-43}$$

Where, $k_i = (4.44 \pm 0.09) \times 10^{-4}$ s.

Here, the factor A is meaningless in this relationship due to the deviation from pseudo-first order to second-order fit with the increasing of [Ir(III)]. The contribution of k_i, however, is not significant enough to affect the reaction rate when $[\mathrm{Ir(III)}]_0 = 0$. The empirical rate law of the reaction with [Ir(III)] = 0 is expressed as,

$$-\frac{\mathrm{d}[\mathrm{Ir^{IV}}]}{\mathrm{dt}} = k_{\mathrm{obs}}[\mathrm{Ir^{IV}}] = k[\mathrm{CH_3SO_2^-}][[\mathrm{Ir^{IV}}] \quad \text{Eq. 2-44}$$

$$-\frac{\mathrm{d}[\mathrm{Ir^{IV}}]}{\mathrm{dt}} = \frac{kK_\mathrm{a}[\mathrm{MSA}]_{\mathrm{Total}}[\mathrm{Ir^{IV}}]}{K_\mathrm{a} + [\mathrm{H^+}]} \quad \text{Eq. 2-45}$$

where k was determined to be $(1.41 \pm 0.02) \times 10^4\ \mathrm{M^{-1}\ s^{-1}}$.

2.3.6 Rate dependence on $[IrCl_6]^{2-}$

The reaction rate dependence on $[\mathrm{IrCl_6}]^{2-}$ was studied by mixing excess MSA with various [Ir(IV)] in the presence of Ir(III). The solutions were prepared with 2.8 mM MSA, 1.26 mM Ir(III) and Ir(IV) concentration varying from 0.034 mM to 0.121 mM at pH 3.5 (acetate buffer). This result shows that the observed rate constant decreases with the increasing of [Ir(IV)].

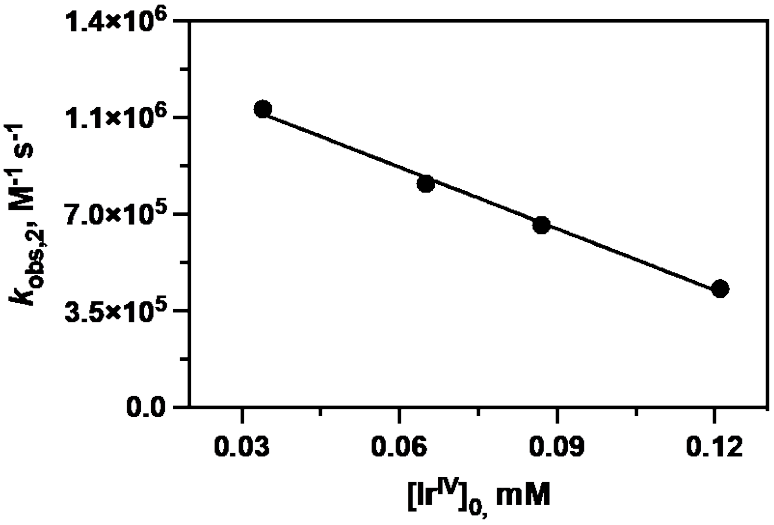

Figure 2-9. Dependence of $k_{\mathrm{obs,2}}$ on [Ir(IV)] in the presence of excess Ir(III).

However, considering that the second-order rate constant should not be determined by the concentration of Ir(IV), a two-phase kinetics including a rapid first-phase reaction, followed by a slower second-phase reaction might be a better description of the kinetic trace. The $\mathrm{t_{1/2}}$ can be thus obtained through the fit of two-phase decay. The plot of the first $\mathrm{t_{1/2}}$ versus [Ir(IV)] is displayed below and the value of $\mathrm{t_{first\ ½}}$ is found to be (0.023 ± 0.003) s.

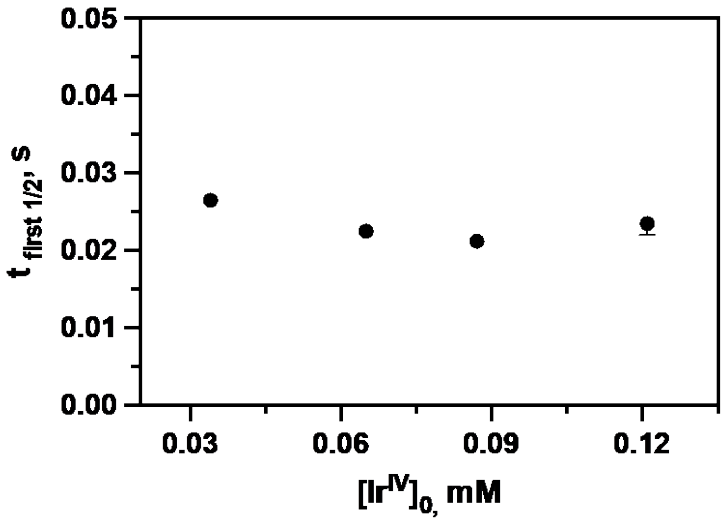

Figure 2-10. The plot of the first half life versus [Ir(IV)].

2.3.7 Spin Trapping Effect

2.3.7.1 PBN Trapping

To capture of the potential radical formed in the reaction, PBN was investigated as a spin trap for $CH_3SO_2^{\bullet}$. UV-vis spectra of Ir(IV) solution and the mixture of Ir(IV) with PBN were collected prior to the kinetic studies to ensure its stability towards the reactant.

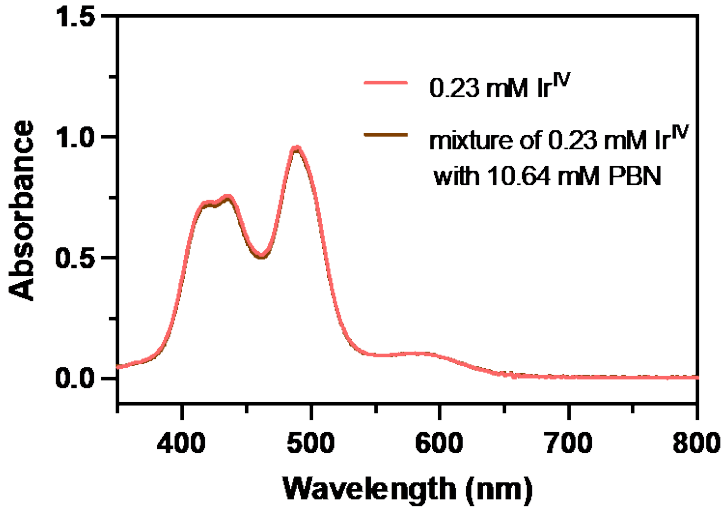

Figure 2-11. UV-vis spectra of Ir^{IV} and the mixture of Ir^{IV} with PBN.

A series of experiments with PBN concentration spanned from 0 mM to 2.0 mM was carried out to determine the effect from the spin trap on the reaction kinetics under anaerobic conditions.

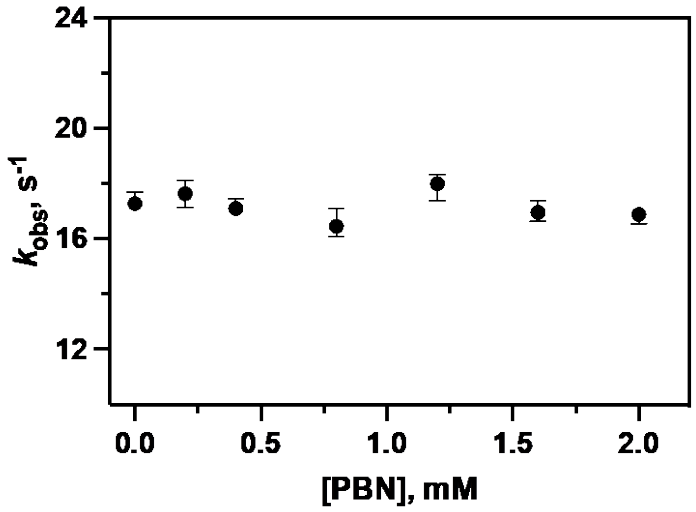

Figure 2-12. PBN effect on the reaction rate. Conditions $[Ir^{IV}]_0$ = 0.077 mM, $[MSA]_0$ = 2.82 mM, μ = 0.1 M ($NaClO_4$), pH 4.8, acetate buffer.

The kinetic data shows undistinguishable effect from the spin trap as the same rate constant can be obtained when PBN is absent. The following two conditions are most likely to be taken as the illustration of what happened when PBN is added to the mixture:

$$Ir^{IV} + CH_3SO_2^- \rightarrow Ir^{III} + CH_3SO_2^{\bullet} \ (k_1) \qquad \text{Eq. 2-46}$$

- $PBN + CH_3SO_2^{\bullet} \rightarrow A$

$Ir^{IV} + A \rightarrow Ir^{III} + A^+$

Rate law: $-\frac{d[Ir^{IV}]}{dt} = 2k_1[Ir^{IV}][CH_3SO_2^-]$

- $Ir^{IV} + CH_3SO_2^{\bullet} \rightarrow Ir^{III} - Cl - O_2SCH_3$

$Ir^{III} - Cl - O_2SCH_3 + H_2O \rightarrow Ir^{III} + CH_3SO_3^-$

Rate law: $-\frac{d[Ir^{IV}]}{dt} = 2k_1[Ir^{IV}][CH_3SO_2^-]$

As both mechanisms share the identical rate law, presence of PBN hence does not affect the reaction kinetics. The result as well confirms that the first step of the reaction with the

formation of Ir(III) is not very reversible, otherwise the rate would be changed by PBN as the backward rate constant will contribute to the overall rate law.

2.3.7.2 Propiolic Acid (POAC) Trapping

With the trapping rate constant of $CH_3SO_2^{\bullet}$ being reported in the literature [34], it might be a promising way to employ propiolic acid as a $CH_3SO_2^{\bullet}$ scanvenger. The competitive kinetics between Ir(IV) and POAC were conducted by adding various amounts of POAC to the reaction mixture of Ir(IV)/MSA in the presence of Ir(III).

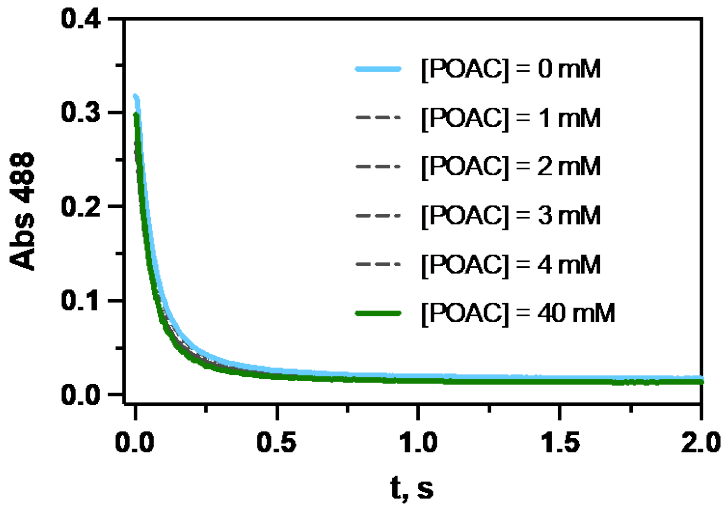

Figure 2-13. Kinetic traces of the reaction with various [POAC]. Conditions: $[Ir^{IV}]_0$ = 0.078 mM, $[MSA]_0$ = 1.2 mM, $[Ir^{III}]_0$ = 1.4 mM, μ = 0.1 M ($NaClO_4$), pH 3.48-3.5, acetate buffer.

The kinetic traces are fitted with a two-phase decay considering that extra Ir(III) was added to the reaction mixture. The first half-life of the rapid reaction is plotted against [POAC].

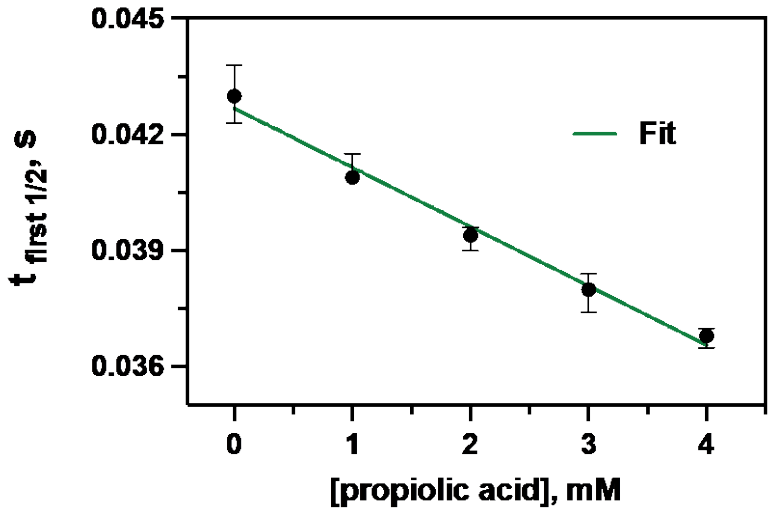

Figure 2-14. POAC effect on the reaction kinetics. Conditions: $[Ir^{IV}]_0$ = 0.078 mM, $[MSA]_0$ = 1.2 mM, $[Ir^{III}]_0$ = 1.4 mM, μ = 0.1 M ($NaClO_4$), pH 3.5, acetate buffer.

When 40 mM of [POAC] was added to the reaction mixture, the second-order fit on the kinetic trace yields a rate constant of $4.34 \times 10^5\ M^{-1}\,s^{-1}$, and the first-order fit gives a rate constant of $14.5\ s^{-1}$.

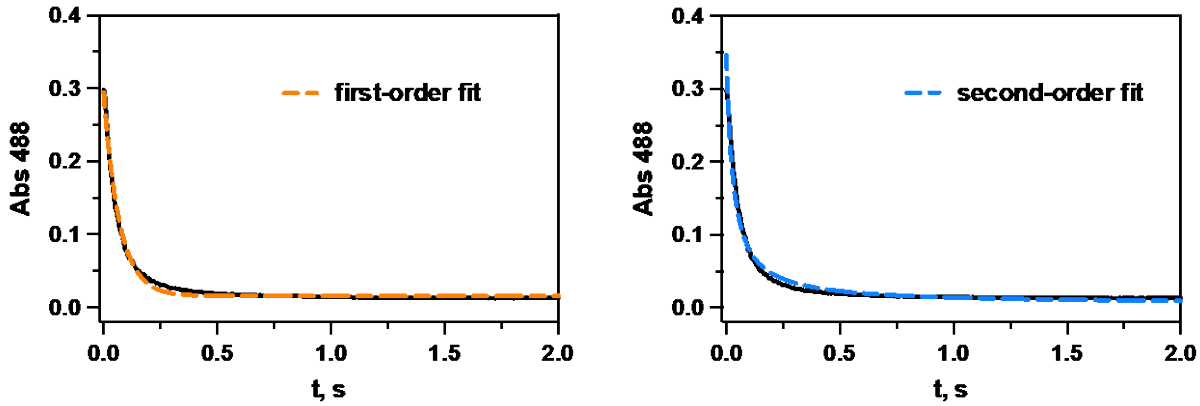

Figure 2-15. Kinetic trace with excess POAC. Conditions: $[POAC]_0$ = 40 mM, $[Ir^{IV}]_0$ = 0.078 mM, $[MSA]_0$ = 1.2 mM, $[Ir^{III}]_0$ = 1.4 mM, pH 3.48, acetate buffer.

2.3.7.3 Acrolein Trapping

Considering that acrolein can also be a potential trapping reagent for the radical, experiments were carried out with [acrolein]= 0 mM − 3.3 mM and maintaining initial [Ir(IV)],

[Ir(III)], and [MSA] concentration as constants. The reactants were purged with argon prior to the addition of acrolein. The plot of the reaction rate constants obtained from the second-order fit versus the concentration of acrolein is shown in Figure 2-16**.** The trend indicates an inhibition of the reaction rate from the radical scavenger, which is very unusual. It might be caused by the fact that oxygen is partially involved in the reaction mixture from acrolein that is not avoidable (purging gas to acrolein will lead to a major loss of the compound). The speculation was later justified by the study on the O_2 effect on the reaction kinetics.

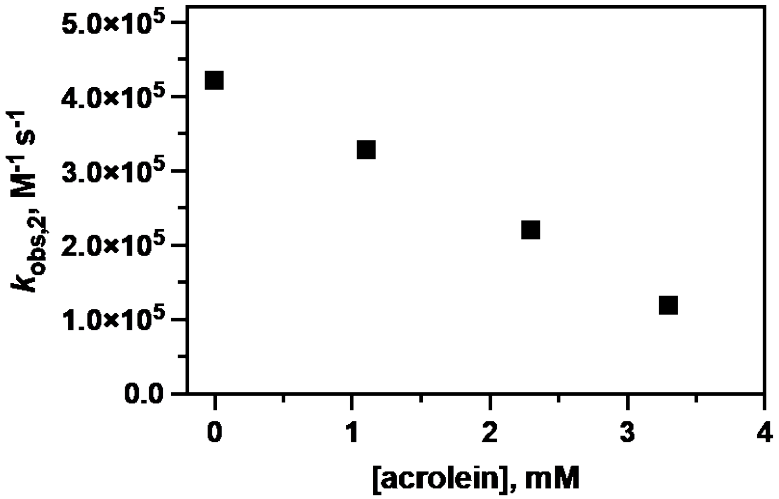

Figure 2-16. Effect of acrolein on the reaction rate. Conditions: $[Ir^{IV}]_0$ = 0.078 mM, $[MSA]_0$ = 1.4 mM, $[Ir^{III}]_0$ = 1.0 mM, μ = 0.1 M ($NaClO_4$), pH 4.5, acetate buffer.

2.3.8 O_2 Effect on the Reaction Kinetics

The effect of O_2 on the reaction kinetics was determined by comparing the k_{obs} values obtained under two conditions: the reaction under argon purged and the experiment with oxygen saturated. Both two kinetic traces were well fitted into first-order rate law with $k_{\text{obs, no } O_2} = 39.1\ s^{-1}$ and $k_{\text{obs, } O_2} = 31.3\ s^{-1}$, implying that the reaction rate is inhibited by O_2. This result therefore can be a fair explanation for the kinetic trend obtained with acrolein included.

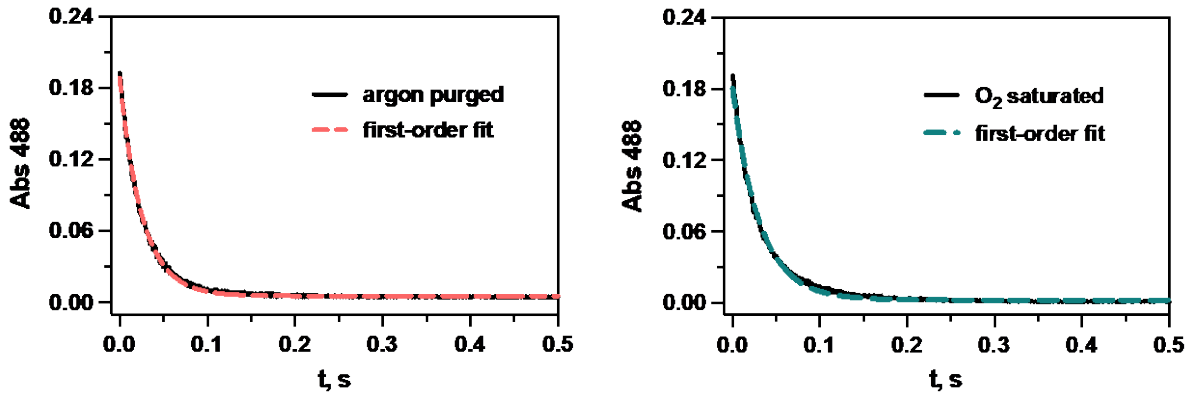

Figure 2-17. O_2 effect on the reaction kinetics. (Left) O_2 absence; (Right) O_2 presence. Conditions: $[Ir^{IV}]_0$ = 0.048 mM, $[MSA]_0$ = 4.7 mM, μ = 0.1 M ($NaClO_4$), pH 3.72, acetate buffer.

2.3.9 Product Analysis

As discussed in the introduction, intermediates of the one-electron oxidation of alkylsulfinic acid are usually the corresponding sulfonyl radicals, whereas the behavior of the radical of this study still needs to be determined. This part of the project enables us to seek evidence upon the presence and conversion of the intermediates to the products, and thus, leading us to the overall reaction equation.

2.3.9.1 ^{1}H-NMR characterization on the reactants and product

NMR spectra of hexachloroiridate (IV), MSA, methanesulfonic acid in D_2O with DSS as reference are displayed below, where the singlets at 2.4 ppm and 2.8 ppm can be identified as arising from MSA and methanesulfonic acid, respectively.

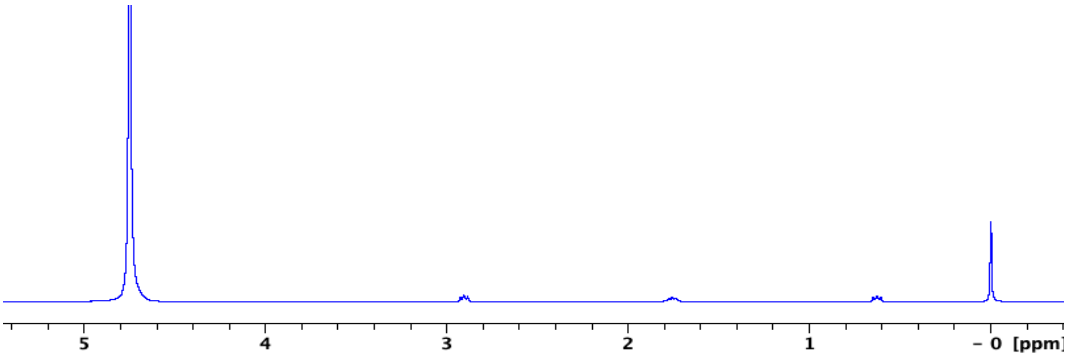

Figure 2-18. ^{1}H-NMR of $(NH_4)_2IrCl_6$ in D_2O with DSS as reference.

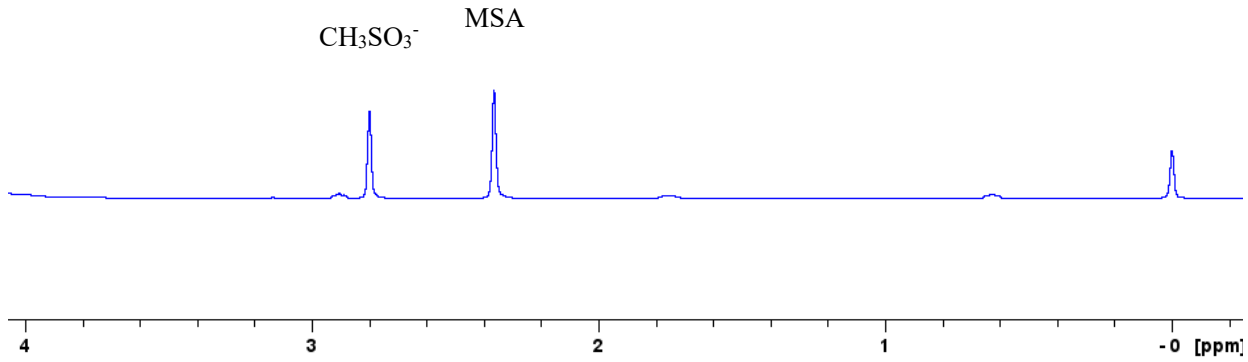

Figure 2-19. ^{1}H-NMR of sodium methanesulfinate (MSA) in D_2O with DSS as reference.

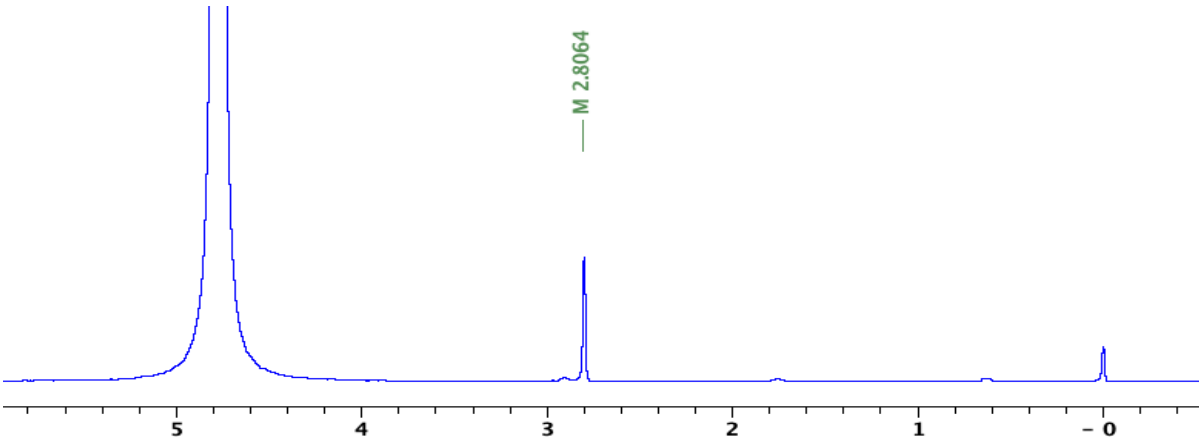

Figure 2-20. ^{1}H-NMR of sodium methanesulfonate ($NaSO_3CH_3$) in D_2O with DSS as reference.

2.3.9.2 ^{1}H-NMR spectra of the Intermediate

A solution consisting of 12.13 mM MSA, 29.0 mM Ir^{IV} in D_2O at pH 3 with DSS as reference was purged with argon for 40 minutes prior to the measurement. The starting MSA concentration was determined from ^{1}H-NMR. The spectral change was obtained at different times to observe the formation of the S-containing products. In the spectra, a singlet at 3.90 ppm decayed slowly and converted to the corresponding sulfonic acid which can be identified from the peak at 2.80 ppm. From Figure 2-21, A yield of 76.8% of initial MSA was obtained from the peak at 3.90 ppm.

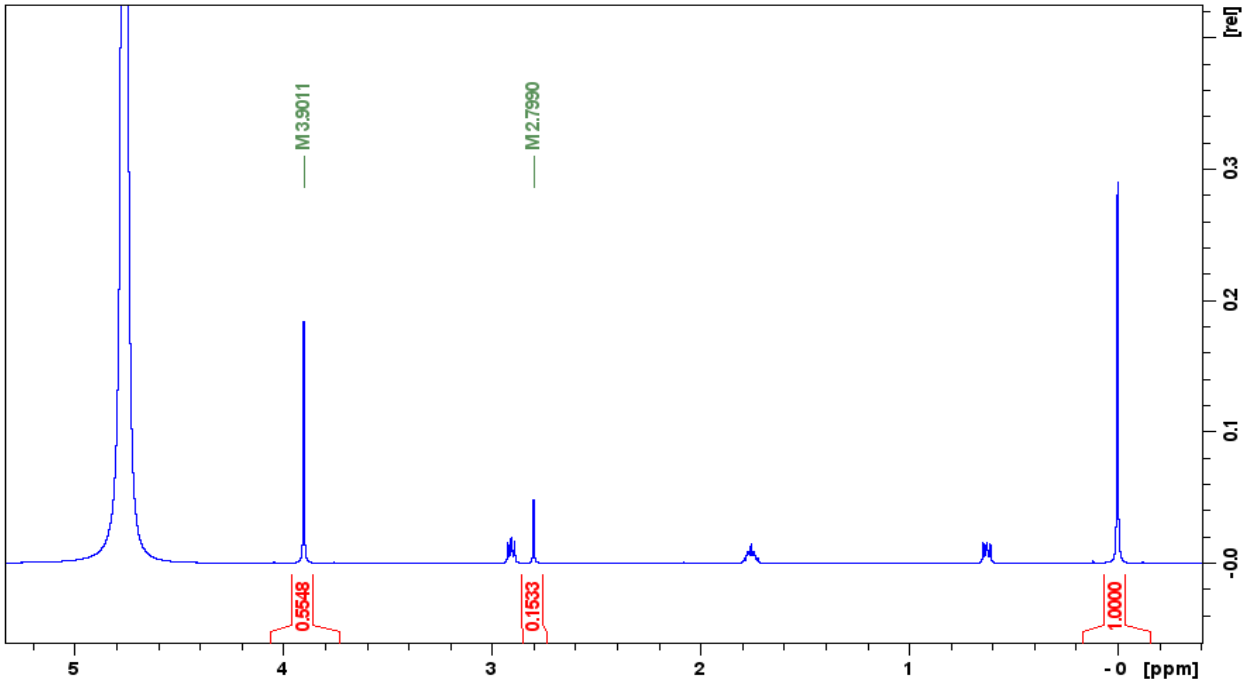

Figure 2-21. ^{1}H-NMR spectrum of the mixture of Ir(IV) with MSA in D_2O after reacting 15 mins with DSS as reference.

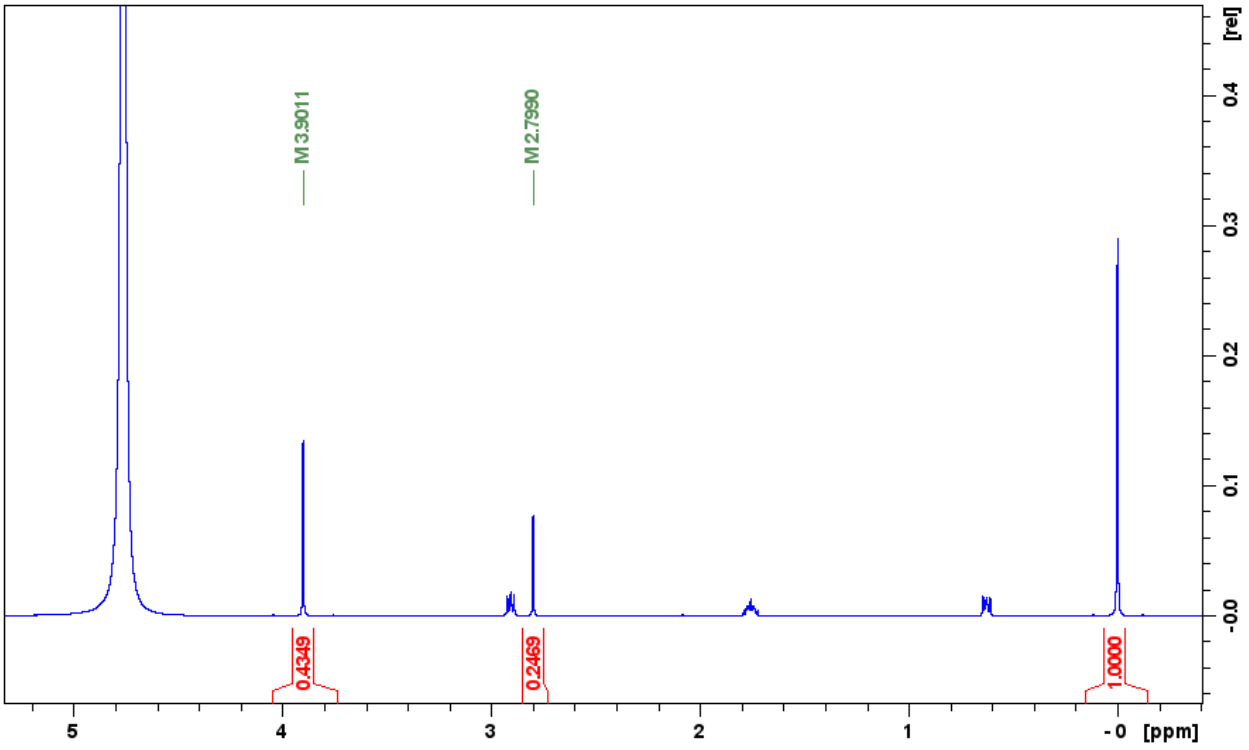

Figure 2-22. ^{1}H-NMR spectrum of mixture of Ir(IV) with MSA in D_2O after reacting 40 mins.

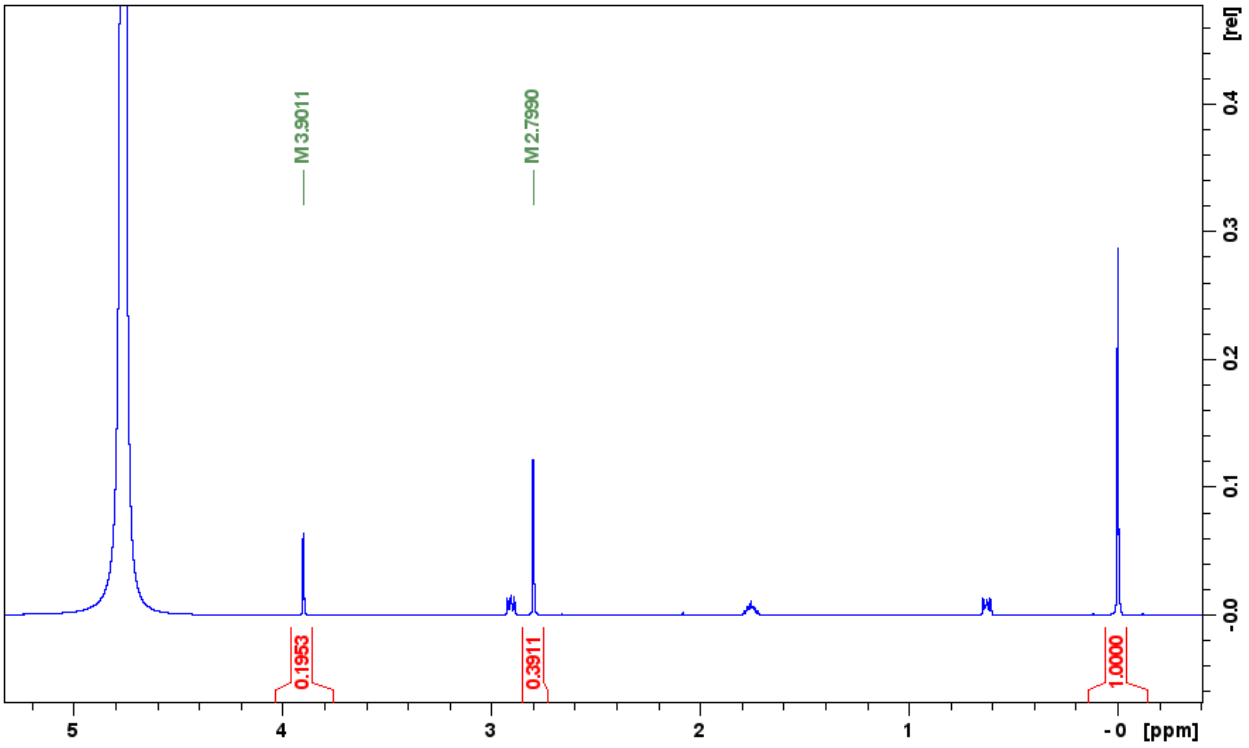

Figure 2-23. ^{1}H-NMR spectrum of mixture of Ir(IV) with MSA in D_2O after reacting 135 mins.

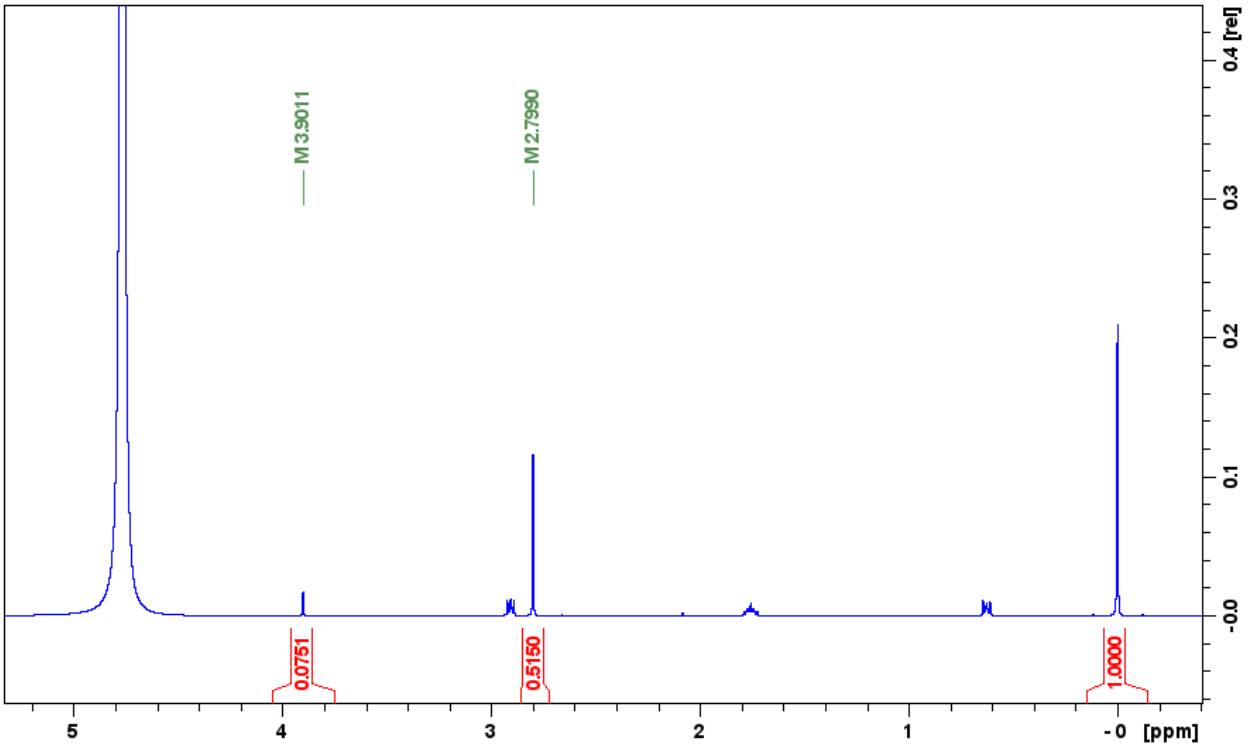

Figure 2-24. ^{1}H-NMR spectrum of mixture of Ir(IV) with MSA in D_2O after reacting 305 mins.

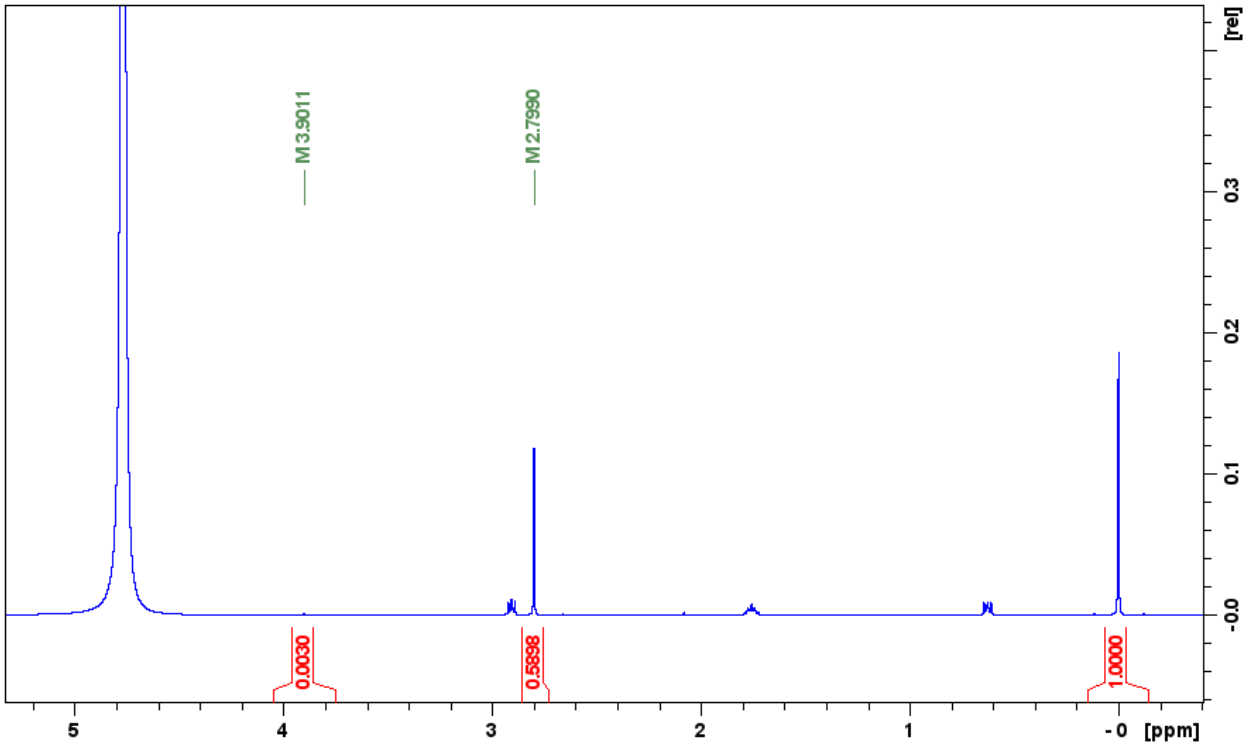

Figure 2-25. ^{1}H-NMR spectrum of mixture of Ir(IV) with MSA in D_2O after reacting 875 mins.

The yield of the major product methanesulfonic acid was calculated to be 98.6% using NMR integrals from the consumed MSA and CH_3SO_3H produced after reaction (initial [MSA] = 12.13 mM; $[CH_3SO_3^-]_{\text{formed}} = 12.11$ mM). This proves a full conversion of MSA to CH_3SO_3H. To further determine the singlet at 3.90 ppm, ^{1}H-NMR spectra of the reaction mixture of Ir(IV) and MSA in D_2O was taken initially. Next, methanesulfonyl chloride was added to the mixture solution. The peak at 3.90 ppm became much intense after the addition, which confirmed the formation of CH_3SO_2Cl as an intermediate.

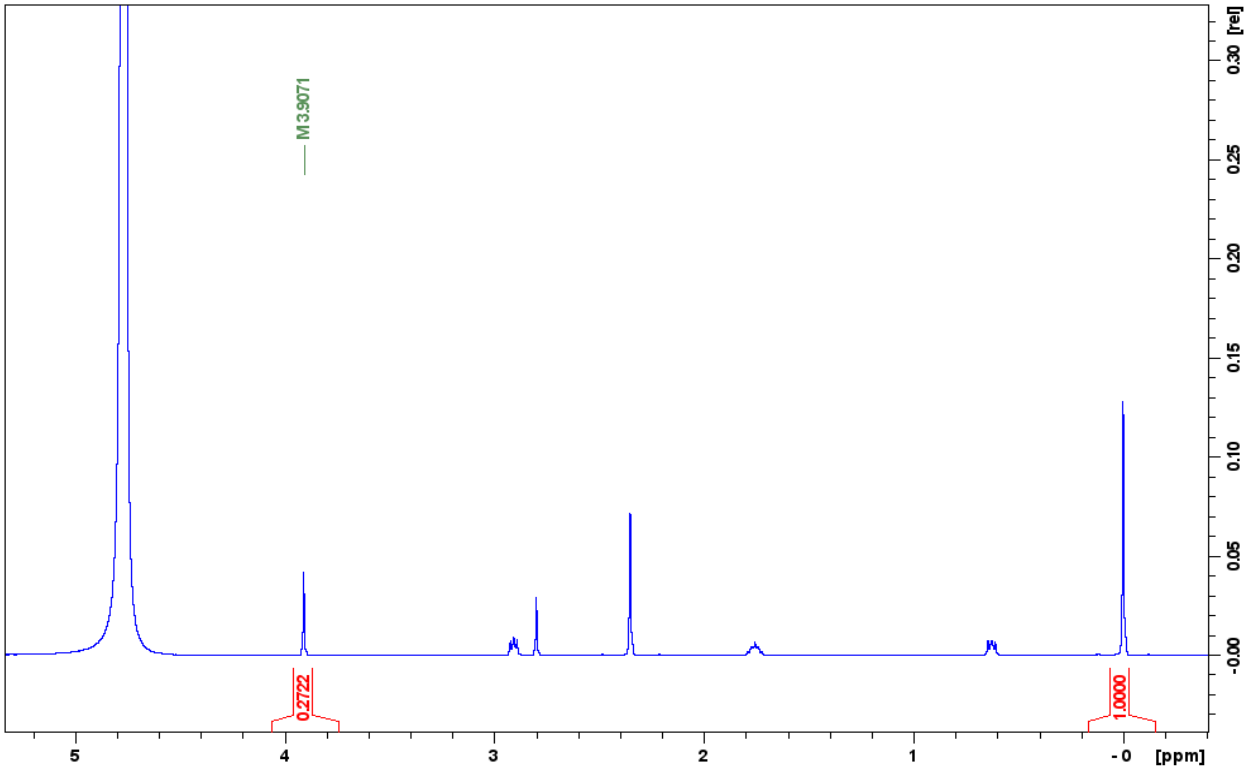

Figure 2-26. ^{1}H-NMR spectrum of the mixture of Ir(IV) with MSA in D_2O before spiking.

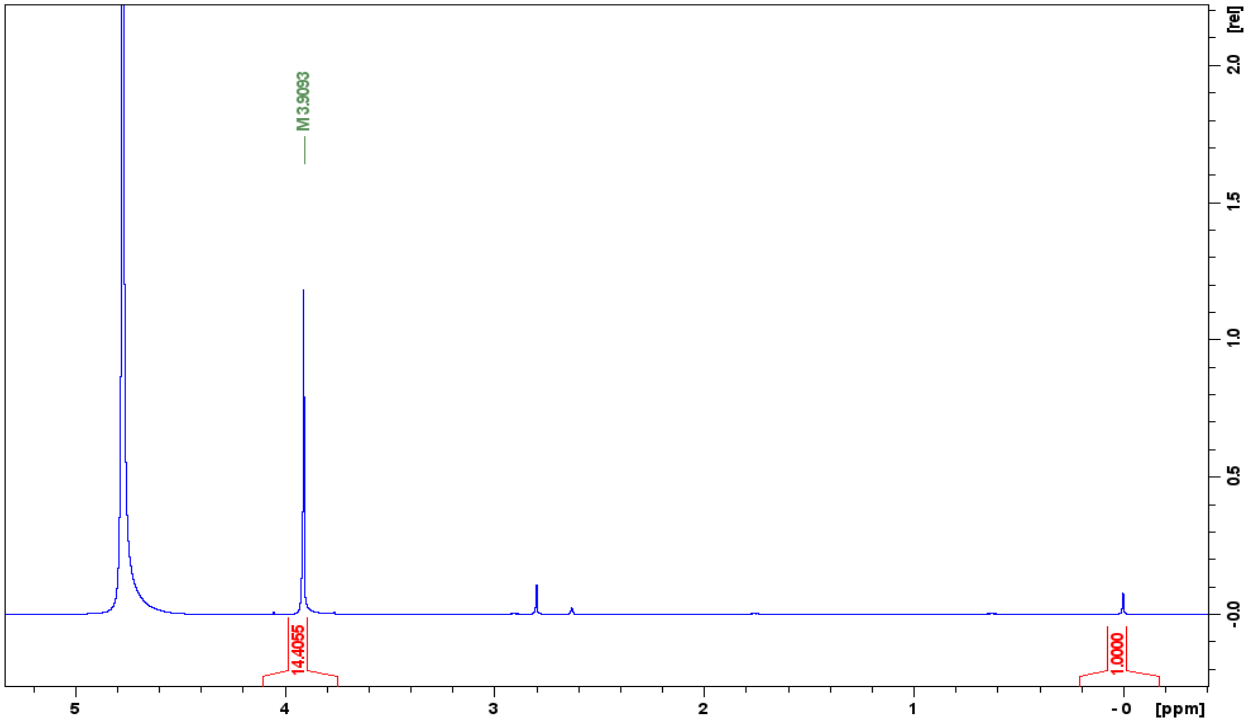

Figure 2-27. ^{1}H-NMR spectrum of the mixture of Ir(IV) with MSA in D_2O, CH_3SO_2Cl spiking.

CH_3SO_2Cl is not very stable in aqueous phase as it undergoes decomposition to yield methanesulfonic acid. The reaction is given below,

$$CH_3SO_2Cl + H_2O \rightarrow CH_3SO_3^- + Cl^- + 2H^+ \qquad \text{Eq. 2-47}$$

The kinetics of CH_3SO_2Cl hydrolysis was investigated by plotting the ^{1}H-NMR integral at 3.90 ppm against time from the reaction mixture of MSA and Ir(IV). A rate constant of $(1.47 \pm 0.14) \times 10^{-4}$ s^{-1} ($t_{1/2} = 4.71 \times 10^3$ s) was obtained from the first-order fit. The result is within the range of the reported values of 1.08×10^{-4} s^{-1} [32] and 2.01×10^{-4} s^{-1} in literature [33] under the similar conditions.

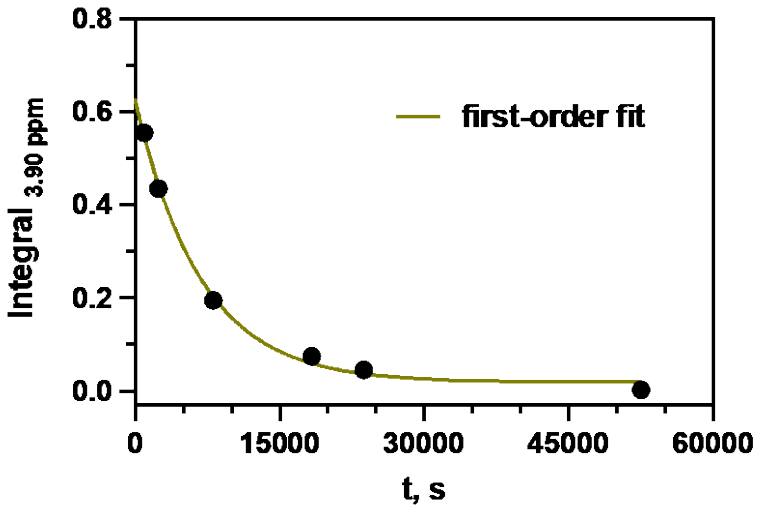

Figure 2-28. ^{1}H-NMR kinetics for determining the rate constant of CH_3SO_2Cl hydrolysis. Conditions: $[MSA]_0$ = 12.14 mM, $[Ir^{IV}]_0$ = 29.0 mM.

2.3.9.3 Synthesis of disulfone via Oxidation of MSA by Co $(H_2O)_6^{3+}$

Given the fact that sulfonyl radicals are capable of dimerizing to form disulfones, which are known for their disproportionation to generate sulfinic acids and sulfonic acids [18], investigation was carried out to test the presence of disulfone as an intermediate of the reaction. Efforts were made to synthesize $CH_3SO_2SO_2CH_3$ by the method described as following.

Hexaminecobalt(III) chloride was prepared initially by oxidizing $CoCl_2$ hydrate with hydrogen peroxide in the presence of NH_4Cl and ammonium. Next, 0.125 M $[Co(H_2O)_6]^{3+}$ solution was prepared by adding 3 g crystalline $[Co(NH_3)_6][Co(CO_3)_3]$ to 60 ml $HClO_4$ following the process from 3.1 to 3.3 described in Wangila & Jordan's 2003 paper [19]. Later, 740 mg of MSA was added to the acidified $[Co(H_2O)_6]^{3+}$ solution and was allowed to react for 2 mins. The mixture was extracted by methylene chloride for 15 times. Removal of the methylene chloride through evaporation gave white solid as the product [20]. The product was found to dissolve well in DMSO and acetonitrile. ^{1}H-NMR Spectra of the synthesized product in DMSO is displayed below.

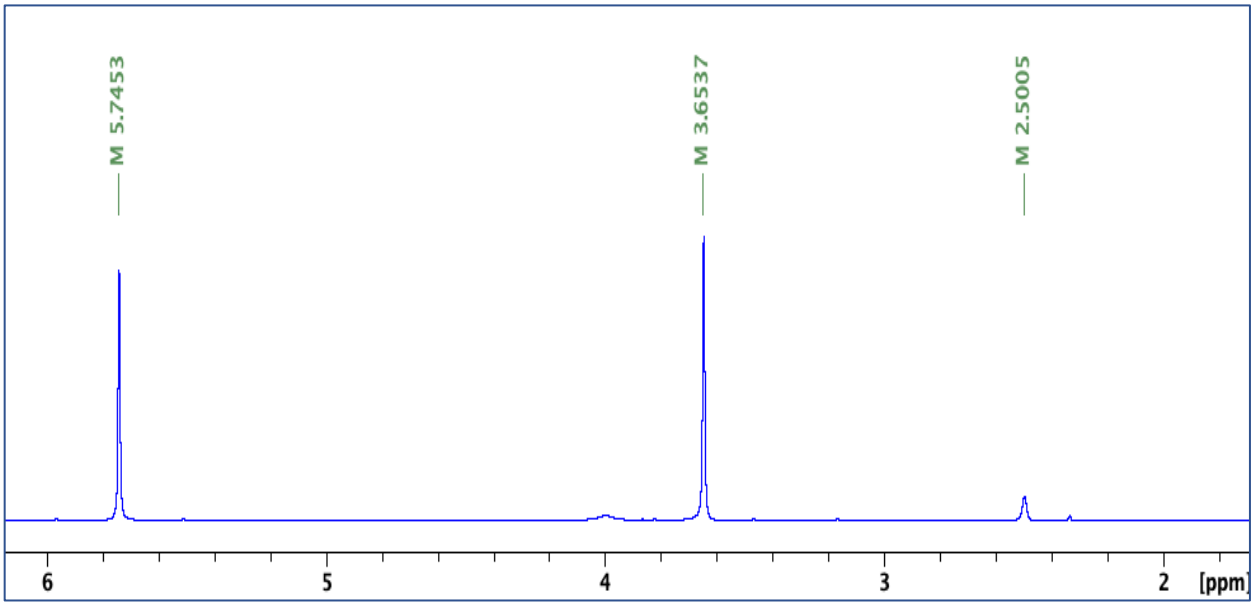

Figure 2-29. ^{1}H-NMR of the synthesized product in DMSO-d_6.

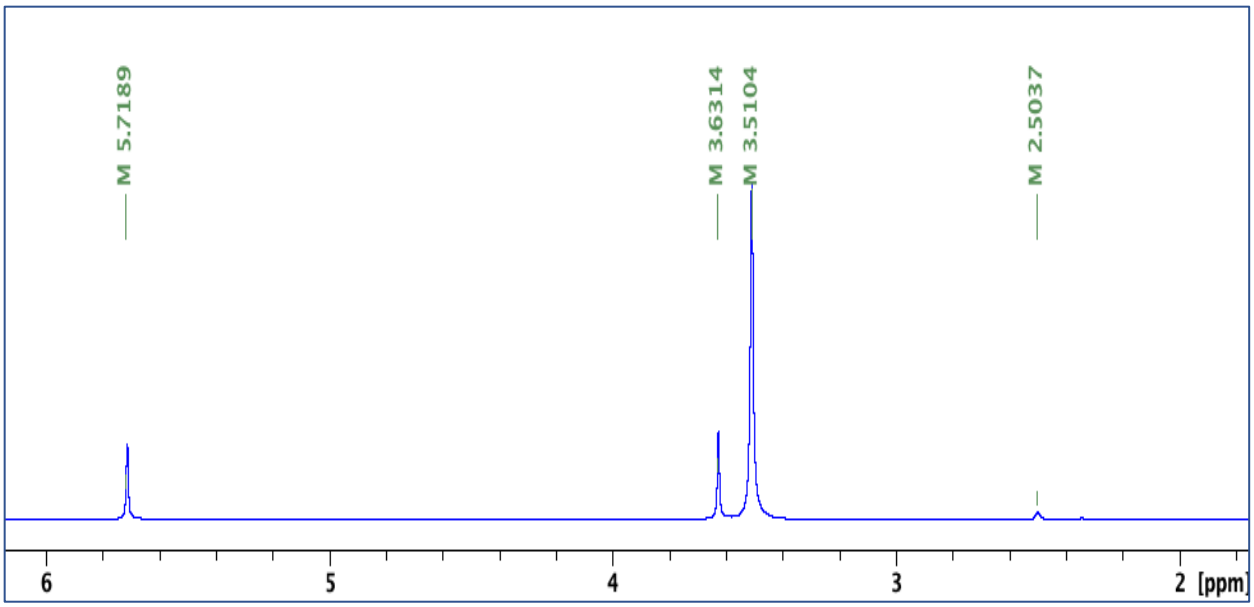

Figure 2-30. ^{1}H-NMR of the synthesized product in DMSO-d_6, H_2O spiking.

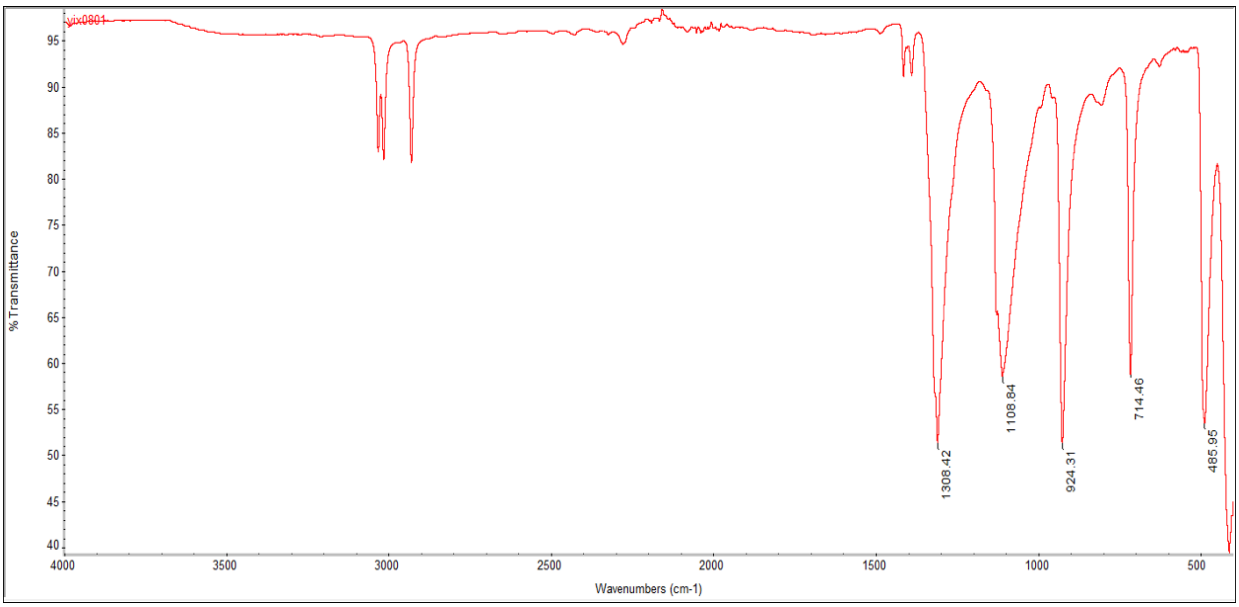

Figure 2-31. Solid state ATR-IR spectrum of the synthesized product.

Strong absorption bands of the synthesized compound are observed at 1308.42 cm^{-1} and 1108.84 cm^{-1} from SO_2 group in ATR-IR spectra. While comparing the ^{1}H-NMR spectra and water solubility of synthesized disulfone with the reaction mixture in Figure 2-21**,** the possibility of disulfone present in the reaction as an intermediate can thus be ruled out.

2.3.9.4 UV-Vis of the Ir-products

To detect the Ir-containing product of the reaction, UV-Vis spectra of 1.82 mM Ir(IV), 1.82 mM $[IrCl_6]^{3-}$ and the reaction mixture of 1.82 mM Ir(IV) and 3.4 mM MSA were obtained. As shown in Figure 2-32, two strong absorbance peaks for the product appear at 350 nm and 410 nm. It can be inferred from the spectra that the product solution consists not only of $[IrCl_6]^{3-}$, but other Ir-containing complex, otherwise the product spectrum will overlap with the spectrum of $[IrCl_6]^{3-}$.

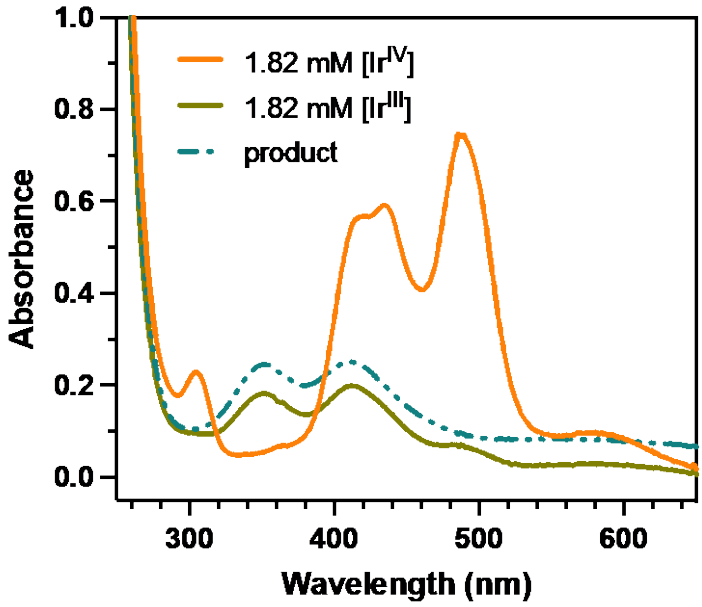

Figure 2-32. UV spectra of 1.82 mM Ir(IV), Ir(III), the reaction mixture of 1.82 mM Ir(IV) and 3.4 mM MSA with 0.1 M $NaClO_4$.

2.3.9.5 Electrochemical study

To further look into the Ir-complexes generated from the reaction, the cyclic voltammogram of Ir^{IV} and the product of the mixture of MSA/Ir^{IV} were preformed respectively. Data below was collected at the room temperature with N_2 purged. The voltammogram of Ir^{IV} shows a reversible CV as it is reduced to Ir^{III} with $E_{1/2} = 0.70$ V vs Ag/AgCl at μ = 0.1 M

($NaClO_4$). The CV of the product mixture in Figure 2-34 implies that two iridium products are formed from the reaction.

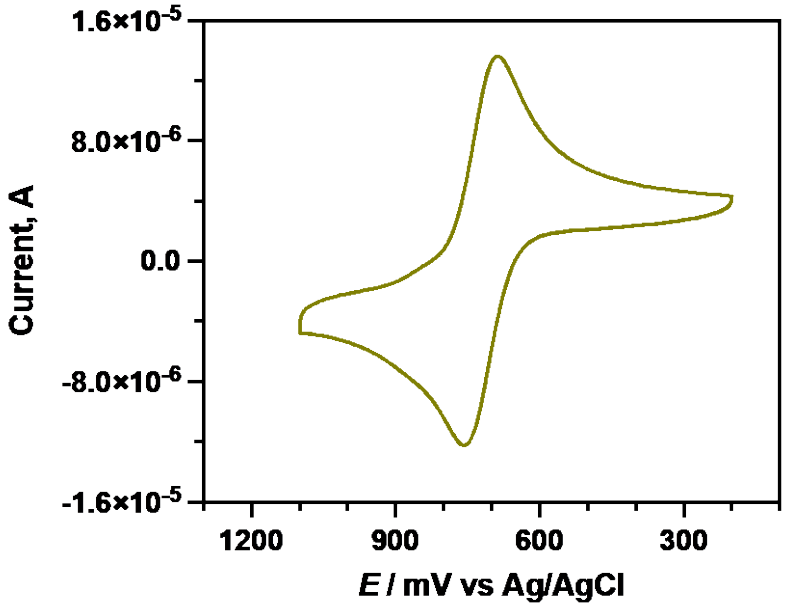

Figure 2-33. The CV of 1.1 mM Ir^{IV} at pH 2.76 ($HClO_4$). Scan rate = 100 mV s^{-1}.

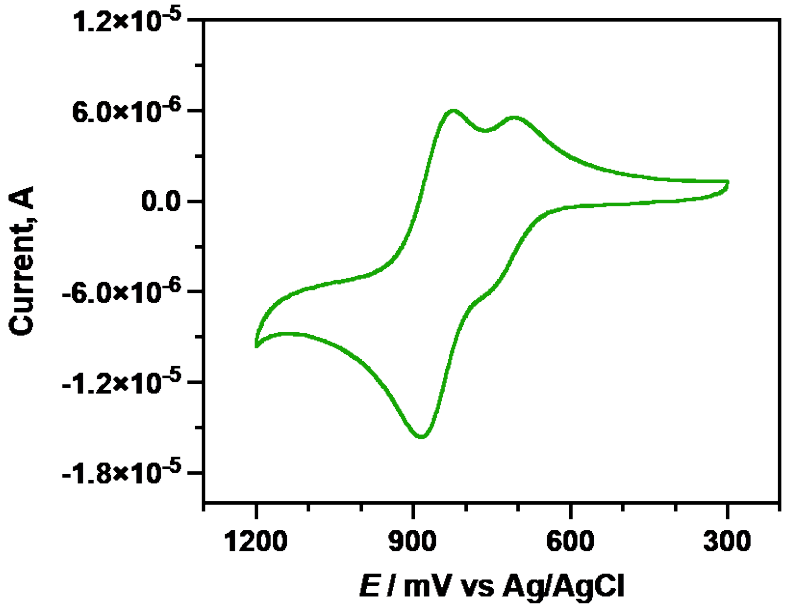

Figure 2-34. The CV of the reaction products between 1.1 mM Ir^{IV} and 1.0 mM MSA at pH 1.76 ($HClO_4$). Scan rate = 100 mV s^{-1}.

The two sets of waves appeared in the CV from the reaction mixture are due to the formation of $IrCl_6^{3-}$ and $Ir(OH_2)Cl_5^{2-}$. The yield of the two iridium complexes was later determined through Osteryoung square-wave voltammetry (OSWV). The decomposition of the species at different pH was primarily studied to get an optimal condition.

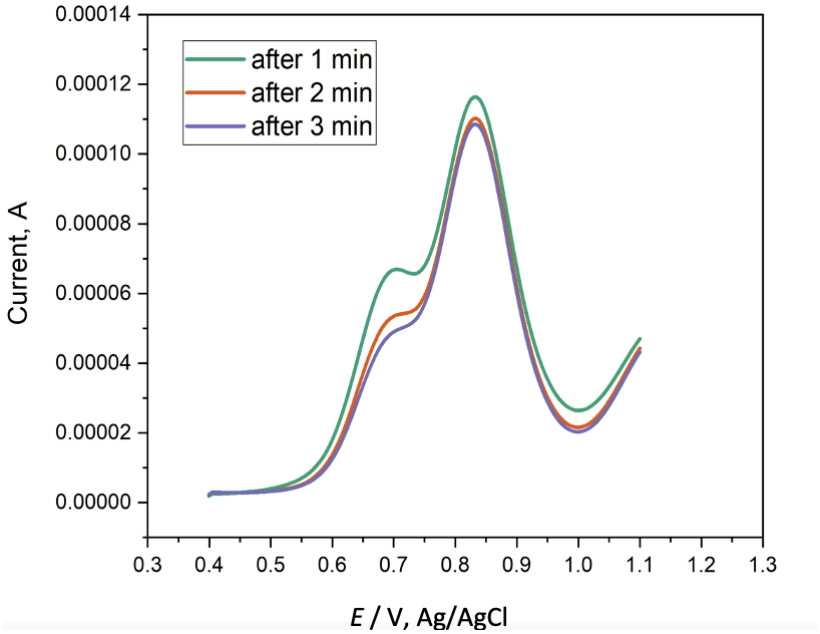

Figure 2-35. OSWV analysis of the reaction products of Ir(IV)/MSA at pH 2.6 ($HClO_4$). Conditions: $[MSA]_0$ = 0.99 mM, $[Ir(IV)]_0$ = 0.91 mM, μ = 0.1 M ($NaClO_4$).

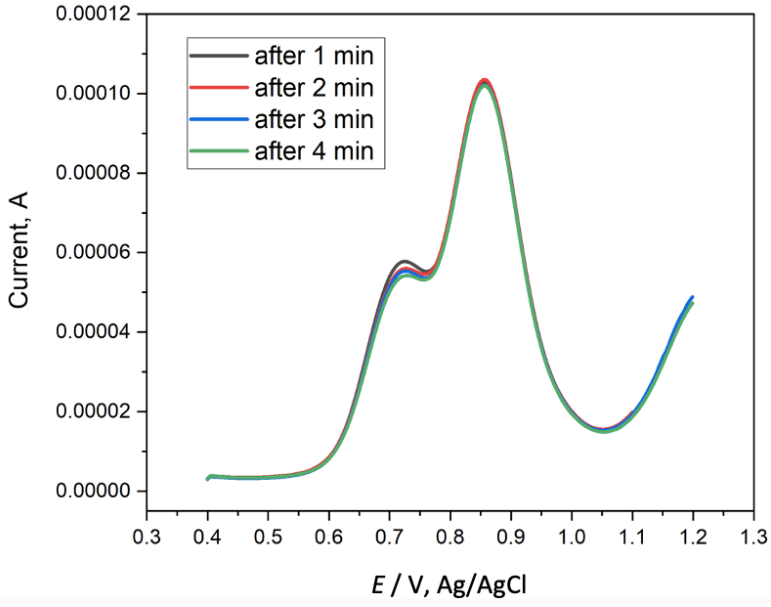

Figure 2-36. OSWV analysis of the reaction products of Ir(IV)/MSA at pH 1.53 ($HClO_4$). Conditions: $[MSA]_0$ = 0.99 mM, $[Ir(IV)]_0$ = 0.91 mM, μ = 0.1 M ($NaClO_4$).

The reaction products were found to be sensitive to pH. An optimized pH of 1.5 was selected for the voltammetry. The yield of $[IrCl]_6^{3-}$, 35.2%, can be calculated from the peak at $E^o = 0.73$ V, and the peak having $E^o = 0.85$ V is assigned to $[Ir(OH_2)Cl]_5^{2-}$ with a yield of 64.8%, based on the known evidence that the derivatives of $[IrCl]_6^{2-}$ have higher E^o values [21].

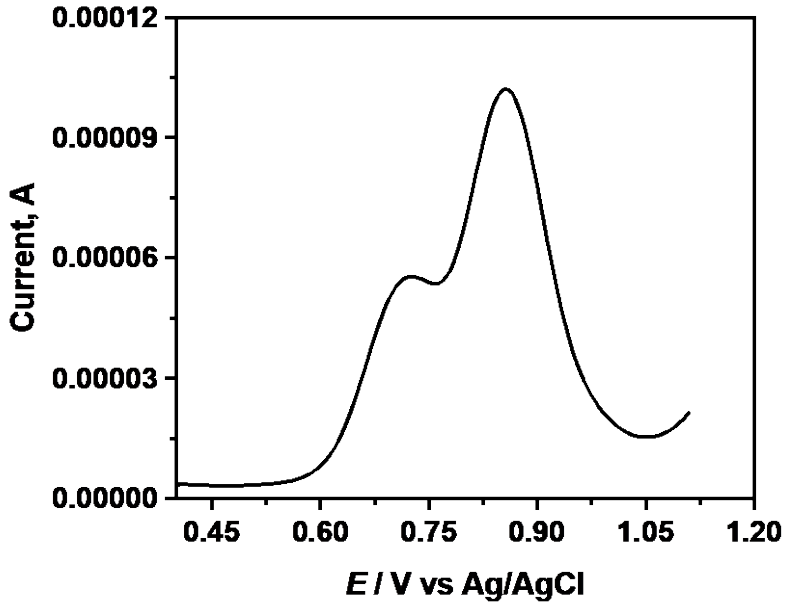

Figure 2-37. OSWV for determining the ratio of the reaction products of Ir(IV)/MSA at pH 1.5 ($HClO_4$).

2.3.9.6 Chlorination of the Ir products

In order to determine the percentage of Ir(III)-containing products of the reaction, Ir(IV) was allowed to react with MSA initially, followed by the chlorination of the iridium-products. 0.23 mM Ir(IV) at pH 2 ($HClO_4$) was prepared in a quartz cuvette and purged with argon for 40 minutes. Next, 0.34 mM MSA with O_2 excluded was added to Ir(IV) solution. The UV spectra of the original Ir(IV) and the solution after the addition of MSA were recorded. Whereafter, sufficient Cl_2 was prepared from the oxidation of HCl by $KMnO_4$ and added to the reaction mixture of Ir/MSA till the absorbance at 488 nm reached to the maximum. The solution was afterwards degassed with N_2

till the UV-vis reading became stable. According to the resulting spectrum after chlorination, the yield of $[IrCl_5(H_2O)]^{2-}$ and $[IrCl_6]^{3-}$ are calculated to be 49% and 51% respectively upon the knowledge that the corresponding Ir(IV) products can be obtained from the chlorination of the derivatives of $[IrCl_6]^{3-}$ and readily distinguished from their UV-Vis spectra [22].

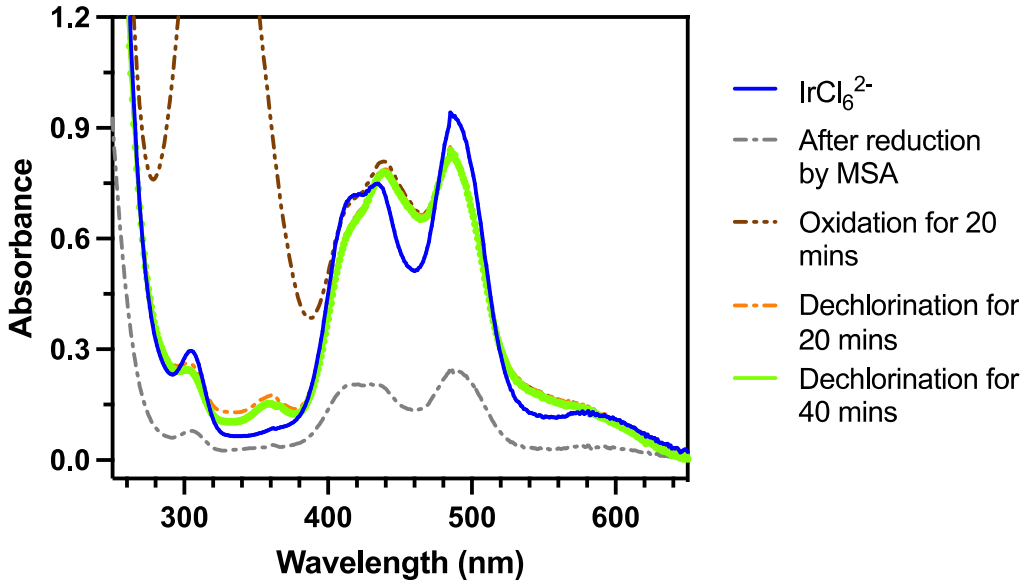

Figure 2-38. UV-Vis spectra of the reaction before and after chlorination.

The studies on stoichiometry, NMR, and chlorination thus lead to the overall reaction:

$$2[IrCl_6]^{2-} + CH_3SO_2H + 2H_2O \rightarrow [IrCl_6]^{3-} + [IrCl_5(H_2O)]^{2-} + CH_3SO_3H + Cl^- + 2H^+ \quad \text{Eq. 2-48}$$

2.4 Discussion

2.4.1 General Mechanism

Methanesulfinic acid has a pK_a value of 2.38 [16]. The deprotonation takes place at the sulfite site. Since this study was performed in a pH range of 1.0-5.6, the presence of MSA should be primarily the monoanionic form, $CH_3SO_2^-$, or at very low pH, its protonated form, CH_3SO_2H. The oxidation of MSA with $[IrCl_6]^{2-}$leads to $[IrCl_6]^{3-}$, $[IrCl_5(H_2O)]^{2-}$ and $CH_3SO_3^-$. All of the observed stoichiometry and kinetic behaviors can be interpreted in the general scheme below, which involves multiple steps: two of which describe the fate of the sulfonyl radical, and the

remaining two being the rapid decomposition of the intermediate to form sulfonyl chloride which will further hydrolyze to release sulfonic acid.

$$[IrCl_6]^{2-} + CH_3SO_2^- \rightleftharpoons [IrCl_6]^{3-} + CH_3SO_2^{\bullet} \mid k_1; k_{-1} \quad \text{Eq. 2-49}$$

$$[IrCl_6]^{2-} + CH_3SO_2^{\bullet} \rightarrow [Cl_5 - Ir^{III} - Cl - O_2SCH_3]^{2-} \mid k_2 \quad \text{Eq. 2-50}$$

$$[Cl_5 - Ir^{III} - Cl - O_2SCH_3]^{2-} + H_2O \rightarrow [IrCl_5(H_2O)]^{2-} + CH_3SO_2Cl \mid k_3 \quad \text{Eq. 2-51}$$

$$CH_3SO_2Cl + H_2O \rightarrow CH_3SO_3^- + Cl^- + 2H^+ \mid k_4 \quad \text{Eq. 2-52}$$

When the steady-state approximation is applied to the radical,

$$\frac{d[CH_3SO_2^{\bullet}]}{dt} = k_1[IrCl_6]^{2-}[CH_3SO_2^-] - k_{-1}[IrCl_6]^{3-}[CH_3SO_2^{\bullet}]_{ss} - k_2[IrCl_6]^{2-}[CH_3SO_2^{\bullet}]_{ss} \quad \text{Eq. 2-53}$$

$$\frac{d[CH_3SO_2^{\bullet}]}{dt} = 0 \qquad ([CH_3SO_2^{\bullet}] \approx 0) \quad \text{Eq. 2-54}$$

$$k_1[IrCl_6]^{2-}[CH_3SO_2^-] = k_{-1}[IrCl_6]^{3-}[CH_3SO_2\cdot]_{ss} + k_2[IrCl_6]^{2-}[CH_3SO_2^{\bullet}]_{ss} \quad \text{Eq. 2-55}$$

$$k_1[IrCl_6]^{2-}[CH_3SO_2^-] = [CH_3SO_2^{\bullet}]_{ss}(k_{-1}[IrCl_6]^{3-} + k_2[IrCl_6]^{2-}) \quad \text{Eq. 2-56}$$

$$[CH_3SO_2^{\bullet}]_{ss} = \frac{k_1[IrCl_6]^{2-}[CH_3SO_2^-]}{k_{-1}[IrCl_6]^{3-} + k_2[IrCl_6]^{2-}} \quad \text{Eq. 2-57}$$

$$[CH_3SO_2^-] = \frac{K_a[MSA]_{total}}{K_a + [H^+]} \quad \text{Eq. 2-58}$$

The rate law can be expressed as,

$$-\frac{d[IrCl_6^{2-}]}{dt} = k_1[Ir^{IV}][CH_3SO_2^-] - k_{-1}[Ir^{III}][CH_3SO_2^{\bullet}] + k_2[Ir^{IV}][CH_3SO_2^{\bullet}] \quad \text{Eq. 2-59}$$

$$-\frac{d[IrCl_6^{2-}]}{dt} = k_1[Ir^{IV}][CH_3SO_2^-] - k_{-1}[Ir^{III}]\frac{k_1[Ir^{IV}][CH_3SO_2^-]}{k_{-1}[Ir^{III}] + k_2[Ir^{IV}]} + k_2[Ir^{IV}]\frac{k_1[Ir^{IV}][CH_3SO_2^-]}{k_{-1}[Ir^{III}] + k_2[Ir^{IV}]} \quad \text{Eq. 2-60}$$

$$= \frac{k_1k_{-1}[Ir^{III}][Ir^{IV}][CH_3SO_2^-] + k_1k_2[Ir^{IV}]^2[CH_3SO_2^-] - k_{-1}k_1[Ir^{III}][Ir^{IV}][CH_3SO_2^-] + k_1k_2[Ir^{IV}]^2[CH_3SO_2^-]}{k_{-1}[Ir^{III}] + k_2[Ir^{IV}]} \quad \text{Eq. 2-61}$$

$$-\frac{d[IrCl_6^{2-}]}{dt} = \frac{2k_1k_2[Ir^{IV}]^2[CH_3SO_2^-]}{k_{-1}[Ir^{III}] + k_2[Ir^{IV}]} \quad \text{Eq. 2-62}$$

When $[CH_3SO_2^-] \gg [Ir^{IV}]$ and $[Ir^{III}] \gg [Ir^{IV}]$

$$k_{obs,2} = \frac{2k_1k_2[\mathrm{CH_3SO_2^-}]}{k_{-1}[\mathrm{Ir^{III}}]} \quad \text{Eq. 2-63}$$

$$1/k_{obs,2} = \frac{k_{-1}[\mathrm{Ir^{III}}]}{2k_1k_2[\mathrm{CH_3SO_2^-}]} \quad \text{Eq. 2-64}$$

Comparing Eq. 2-64 to Eq. 2-43 obtained from the result of Ir(III) dependence, the following equation is available.

$$\frac{k_{-1}}{2k_1k_2[\mathrm{CH_3SO_2^-}]} = k_i = (4.44 \pm 0.09) \times 10^{-4}\ \mathrm{s} \quad \text{Eq. 2-65}$$

$$\frac{k_{-1}}{\frac{2k_1k_2K_a[\mathrm{MSA}]_{\mathrm{total}}}{K_a + [\mathrm{H^+}]}} = \frac{k_{-1}(K_a + [\mathrm{H^+}])}{2k_1k_2K_a[\mathrm{MSA}]_{\mathrm{total}}} = k_i \quad \text{Eq. 2-66}$$

Due to the high reactivity and large favorable free energy of $\mathrm{CH_3SO_2^\bullet}$ ($\Delta_f G^0 = -170.5\ \mathrm{KJ\ mol^{-1}}$ [38], it is reasonable to believe that the second step is quite rapid. The scavenging of the sulfonyl radical by excess Ir(IV) to form the Cl-bridged adduct is very fast, occurring before $\mathrm{CH_3SO_2^\bullet}$ can react with $[\mathrm{IrCl_6}]^{3-}$. This could also account for the observation of mild Ir(III) dependence on the reaction. Thus, with the assumption of $k_2[\mathrm{Ir^{IV}}] \gg k_{-1}[\mathrm{Ir^{III}}]$, the rate law above can be reduced as,

$$-\frac{\mathrm{d}[\mathrm{IrCl_6^{2-}}]}{\mathrm{dt}} = \frac{2k_1k_2[\mathrm{Ir^{IV}}]^2[\mathrm{CH_3SO_2^-}]}{k_2[\mathrm{Ir^{IV}}]} = 2k_1[\mathrm{Ir^{IV}}][\mathrm{CH_3SO_2^-}] \quad \text{Eq. 2-67}$$

$$-\frac{\mathrm{d}[\mathrm{IrCl_6^{2-}}]}{\mathrm{dt}} = \frac{2k_1K_\mathrm{a}[\mathrm{Ir^{IV}}][\mathrm{MSA}]_{\mathrm{total}}}{K_\mathrm{a} + [\mathrm{H^+}]} \quad \text{Eq. 2-68}$$

Comparing Eq. 2-68 with Eq. 2-45, $k_1 = \frac{k}{2} = (0.70 \pm 0.01) \times 10^4\ \mathrm{M^{-1}\ s^{-1}}$.

With k_1, K_a, $[\mathrm{H^+}]$ and $[\mathrm{MSA}]_{\mathrm{total}}$ known for Eq. 2-66, the ratio of $\frac{k_{-1}}{k_2}$ is thus calculated to be $(1.70 \pm 0.04) \times 10^{-2}$. Given that the reaction is not exactly following the second-order kinetics in the presence of excess Ir(III), this ratio might be better used as an estimation.

2.4.2 Quasi-inner sphere pathway for the radical

A hypothesis with respect to $CH_3SO_2^{\bullet}$ could be the dimerization to yield the corresponding disulfone which later undergoes disproportionation to release sulfonic acid,

$$2CH_3SO_2^{\bullet} \rightarrow CH_3SO_2SO_2CH_3 \quad \text{Eq. 2-69}$$

$$2CH_3SO_2SO_2CH_3 + H_2O \rightleftharpoons CH_3SO_2^- + CH_3SO_3^- + 2H^+ \quad \text{Eq. 2-70}$$

The overall reaction is given as,

$$2[IrCl_6]^{2-} + CH_3SO_2^- + H_2O \rightleftharpoons 2[IrCl_6]^{3-} + CH_3SO_3^- + 2H^+ \quad \text{Eq. 2-71}$$

Here, an inversed second-order dependence of [Ir(III)] on the reaction rate should be observed. However, the linear fit of $k_{obs,2}$ on [Ir(III)] is not favorable of this postulate.

A more promising description of the second step is a one-electron transfer process with chloride bound to iridium serving as a bridging ligand. This is likely to happen as the analogous bond between chloride and the dimethylsulfide radical was detected [24]. Though whether the chlorine is transferred to the reductant or retained by the one-electron oxidant $[IrCl_6]^{2-}$ has been queried in years, evidence was provided to support the feasibility of chlorine abstraction from $[IrCl_6]^{2-}$ to generate alkyl chloride from the reaction between hexachloroiridate(IV) and alkyl radicals such as $CH_3^{\bullet}$, $CH_3CO_2^{\bullet}$, $ClCH_2^{\bullet}$, and the rate constants were reported to be in the range of $10^7 - 10^{10}\ M^{-1}\ s^{-1}$ [29-31]. The inner-sphere path with the formation of a Cl-bonded intermediate was extensively studied as well. For instance, the oxidation of cyclohexanone by hexachloroiridate (IV) occurred through the outer-sphere one-equivalent oxidation of the enol of cyclohexanone by Ir(IV) and followed by the further inner-sphere mechanism to yield $[IrCl_5(H_2O)]^{2-}$ [21]. Some of the long-lived Cl-bridged binuclear intermediates were isolated, characterized and were mostly found to undergo a first-order dissociation to yield the final products [27],[28]. The dissociation took place through the abstraction of a Cl atom followed by

the process where water occupies the vacant coordination site in the pentachloroiridate (III) complexes. Besides, the releasing of methane sulfonyl chloride obtained from NMR evidence also corroborates the presence of the iridium-bound sulfonyl chloride.

The second step is believed to be rate-limiting based on the fact that $CH_3SO_2^{\bullet}$ is a stronger oxidant compared with Ir(IV), since $E^0(\mathrm{Ir(IV)/Ir(III)} < E^0(CH_3SO_2^-/\ CH_3SO_2^{\bullet})$. It is difficult to determine the value of k_2 directly from the experiment since the intermediate is transient, in addition to no strong UV-Vis feature was observed from it. However, it might be helpful to estimate the value through competitive kinetics. Sulfonyl radicals are known for their role of adding reversibility to C-C double and triple bonds [34]. The rate constants of the addition are generally predicted with a limit of diffusion-control ($1 \times 10^{10}\ \mathrm{M^{-1}\ s^{-1}}$), for example, a value of $k = 1 \times 10^9\ \mathrm{M^{-1}\ s^{-1}}$ of the oxidation of $CH_3SO_2^{\bullet}$ by hexane in acetonitrile [35],[36] was reported. Moreover, justified values of the rate constants of trapping $CH_3SO_2^{\bullet}$ were provided through pulse radiolysis with acrolein and propiolic acid, POAC, as radical scavengers in Timokhin's work [34]. The equations are given as

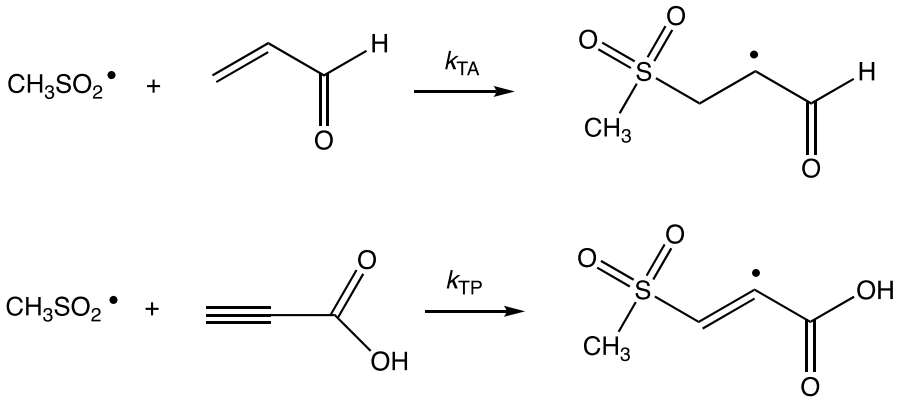

The rate constants of the two reactions were calculated to be $k_{TP} = (5.9 \pm 0.8) \times 10^7\ \mathrm{M^{-1}\ s^{-1}}$ and $k_{TA} = (4.9 \pm 0.1) \times 10^9\ \mathrm{M^{-1}\ s^{-1}}$.

Considering that the first step reaction of Ir(IV)/MSA can be reversible in the presence of extra Ir(III), the reaction scheme includes two radical scavengers, POAC and acrolein, is expressed as,

$$\mathrm{Ir^{IV}} + \mathrm{CH_3SO_2^-} \rightleftharpoons \mathrm{Ir^{III}} + \mathrm{CH_3SO_2^{\bullet}} \quad k_1, k_{-1} \qquad \text{Eq. 2-72}$$

$$\mathrm{POAC/acrolein} + \mathrm{CH_3SO_2^{\bullet}} \rightarrow \mathrm{P_T^{\bullet}} \quad k_{PT} \qquad \text{Eq. 2-73}$$

$$\mathrm{Ir^{IV}} + \mathrm{P_T^{\bullet}} \rightarrow \mathrm{Ir^{III}} + \mathrm{P_T^{+}} \quad k_{3T} \qquad \text{Eq. 2-74}$$

For POAC or acrolein to be an effective trapping reagent, an increased reaction rate would be expected when the scavenging rate k_{PT} or k_{AT} is larger than the rate of Ir(IV) reacting with radical. A reasonable value of $1 \times 10^8\ \mathrm{M^{-1}\ s^{-1}}$ is suggested from the experimental result that the enhanced rate is evident from the addition of POAC. The overall reaction is,

$$\mathrm{Ir^{IV}} + \mathrm{CH_3SO_2^-} + \mathrm{POAc} \rightarrow \mathrm{Ir^{III}} + \mathrm{CH_3SO_2POAc} \qquad \text{Eq. 2-75}$$

The mechanism of the reaction involving spin trap at pH 3 to 4.7 thus lead to the rate law,

$$-\frac{\mathrm{d[Ir^{IV}]}}{\mathrm{dt}} = \frac{2k_T[\mathrm{Ir^{IV}}]^2[\mathrm{CH_3SO_2^-}]}{[\mathrm{Ir^{III}}]} \qquad \text{Eq. 2-76}$$

Where $k_{obs,2} = \frac{2k_T[\mathrm{CH_3SO_2^-}]}{[\mathrm{Ir^{III}}]}$.

When the steady-state approximation is applied to the radical and the intermediate $\mathrm{P_T}$,

$$\frac{\mathrm{d[CH_3SO_2^{\bullet}]}}{\mathrm{dt}} = k_1[\mathrm{Ir^{IV}}][\mathrm{CH_3SO_2^-}] - k_{-1}[\mathrm{Ir^{III}}][\mathrm{CH_3SO_2^{\bullet}}]_{\mathrm{ss}} - k_{PT}[\mathrm{POAC}][\mathrm{CH_3SO_2^{\bullet}}]_{\mathrm{ss}} = 0 \qquad \text{Eq. 2-77}$$

$$k_1[\mathrm{Ir^{IV}}][\mathrm{CH_3SO_2^-}] = k_{-1}[\mathrm{Ir^{III}}][\mathrm{CH_3SO_2^{\bullet}}]_{\mathrm{ss}} + k_{PT}[\mathrm{POAC}][\mathrm{CH_3SO_2^{\bullet}}]_{\mathrm{ss}} \qquad \text{Eq. 2-78}$$

$$[\mathrm{CH_3SO_2\cdot}]_{\mathrm{ss}} = \frac{k_1[\mathrm{Ir^{IV}}][\mathrm{CH_3SO_2^-}]}{k_{-1}[\mathrm{Ir^{III}}] + k_{PT}[\mathrm{POAC}]} \qquad \text{Eq. 2-79}$$

$$\frac{\mathrm{d[P_T]}}{\mathrm{dt}} = k_{PT}[\mathrm{POAC}]\mathrm{CH_3SO_2^{\bullet}}_{\mathrm{ss}} + k_{3\mathrm{T}}[\mathrm{Ir^{IV}}][\mathrm{P_T}] = 0 \qquad \text{Eq. 2-80}$$

$$[\mathrm{P_T}] = \frac{-k_{3\mathrm{T}}[\mathrm{Ir^{IV}}]}{k_{PT}[\mathrm{POAC}][\mathrm{CH_3SO_2^{\bullet}}]_{\mathrm{ss}}} = \frac{-k_{3\mathrm{T}}[\mathrm{Ir^{IV}}]}{k_{PT}[\mathrm{POAC}]\dfrac{k_1[\mathrm{Ir^{IV}}][\mathrm{CH_3SO_2^-}]}{k_{-1}[\mathrm{Ir^{III}}] + k_{PT}[\mathrm{POAC}]}} \qquad \text{Eq. 2-81}$$

With the assumption of $k_{PT}[\mathrm{POAC}]] \gg k_{-1}[\mathrm{Ir^{III}}]$,

$$[\mathrm{P_T}] = \frac{-k_{3\mathrm{T}}[\mathrm{Ir^{IV}}]}{k_{PT}[\mathrm{POAC}]\dfrac{k_1[\mathrm{Ir^{IV}}][\mathrm{CH_3SO_2^-}]}{k_{PT}[\mathrm{POAC}]}} = \frac{-k_{3\mathrm{T}}[\mathrm{Ir^{IV}}]}{k_1[\mathrm{Ir^{IV}}][\mathrm{CH_3SO_2^-}]} \qquad \text{Eq. 2-82}$$

The general rate law of the rate law can be described as,

$$-\frac{\mathrm{d}[\mathrm{Ir^{IV}}]}{\mathrm{dt}} = k_1[\mathrm{Ir^{IV}}][\mathrm{CH_3SO_2^-}] - k_{-1}[\mathrm{Ir^{III}}][\mathrm{CH_3SO_2^{\bullet}}] + k_{3\mathrm{T}}[\mathrm{Ir^{IV}}][[\mathrm{P_T}]$$

$$= k_1[\mathrm{Ir^{IV}}][\mathrm{CH_3SO_2^-}] - k_{-1}[\mathrm{Ir^{III}}]\frac{k_1[\mathrm{Ir^{IV}}][\mathrm{CH_3SO_2^-}]}{k_{PT}[\mathrm{POAC}]} + \qquad \text{Eq. 2-83}$$

$$k_{3\mathrm{T}}[\mathrm{Ir^{IV}}]\ \frac{-k_{3\mathrm{T}}[\mathrm{Ir^{IV}}]}{k_1[\mathrm{Ir^{IV}}][\mathrm{CH_3SO_2^-}]}$$

This complicated rate law was turned out to be not applicable for solving the unknown rate constants. We thus employed kinetic modeling methods to determine the unsolved rate constants including k_{-1} and k_2. The following simulations were preformed using COPASI to testify the validity of the proposed mechanism and to determine the kinetic parameters based on the experimental and theoretical information we obtained in this research. With the effective radical scavenger included, a comprehensive mechanism is proposed in the scheme below.

Table 2-4. Proposed mechanism of MSA-Ir(IV) reaction.

Step	Reaction	Rate Constants
1	$[\mathrm{IrCl_6}]^{2-} + \mathrm{CH_3SO_2^-} \rightleftharpoons [\mathrm{IrCl_6}]^{3-} + \mathrm{CH_3SO_2^{\bullet}}$ $\boldsymbol{k_1; k_{-1}}$	7000; -
2	$[\mathrm{IrCl_6}]^{2-} + \mathrm{CH_3SO_2^{\bullet}} \rightarrow [\mathrm{Cl_5 - Ir^{III} - Cl - O_2SCH_3}]^{2-}$ $\boldsymbol{k_2}$	-
3	$\mathrm{POAC} + \mathrm{CH_3SO_2^{\bullet}} \rightarrow \mathrm{POAC - CH_3SO_2}$ $\boldsymbol{k_3}$	5.9×10^7
4	$[\mathrm{IrCl_6}]^{2-} + \mathrm{POAC - CH_3SO_2} \rightarrow [\mathrm{IrCl_6}]^{3-} + \mathrm{P_1}$ $\boldsymbol{k_4}$	1×10^{10}
5	$[\mathrm{Cl_5 - Ir^{III} - Cl - O_2SCH_3}]^{2-} + \mathrm{H_2O} \rightarrow [\mathrm{IrCl_5(H_2O)}]^{2-} + \mathrm{CH_3SO_2Cl}$ $\boldsymbol{k_5}$	110
6	$\mathrm{CH_3SO_2Cl} + \mathrm{H_2O} \rightarrow \mathrm{P_2}$ $\boldsymbol{k_6}$	1.5×10^{-4}

To get a good fit from the mechanism, various k_{-1} and k_2 values were used to model the kinetics. As a result, the optimized values were found to be $k_{-1} = (7.5 \pm 2.5) \times 10^5\ \mathrm{M^{-1}\ s^{-1}}$ and $k_2 = (8.0 \pm 2.0) \times 10^7\ \mathrm{M^{-1}\ s^{-1}}$. The half-time obtained from the simulated trace of [POAC] dependence is plotted against the concentration of the trapping reagent as displayed below. The effect of [POAC] from the simulation is identical to the experimental result.

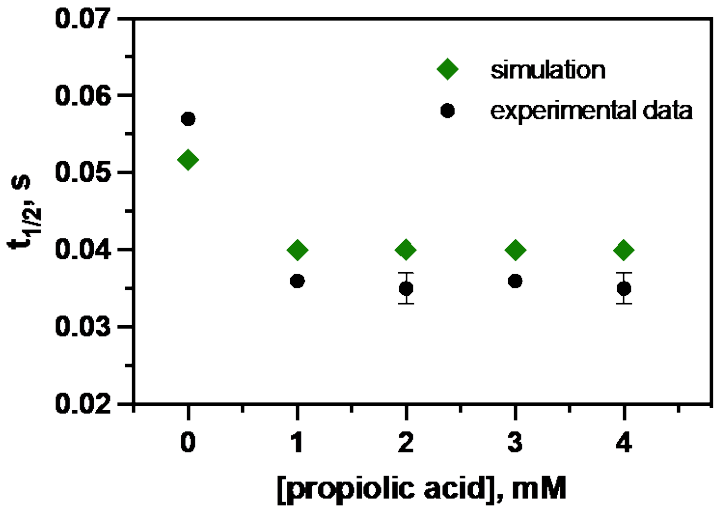

Figure 2-39. Simulated traces of [POAC] dependence.

Using the mechanism and rate constants obtained above, kinetic dependence on [Ir(IV)] was modeled. The first $t_{1/2}$ based on the simulation was determined to be 0.018 s, which is comparable to the value (0.02 s) calculated from the experimental fitting.

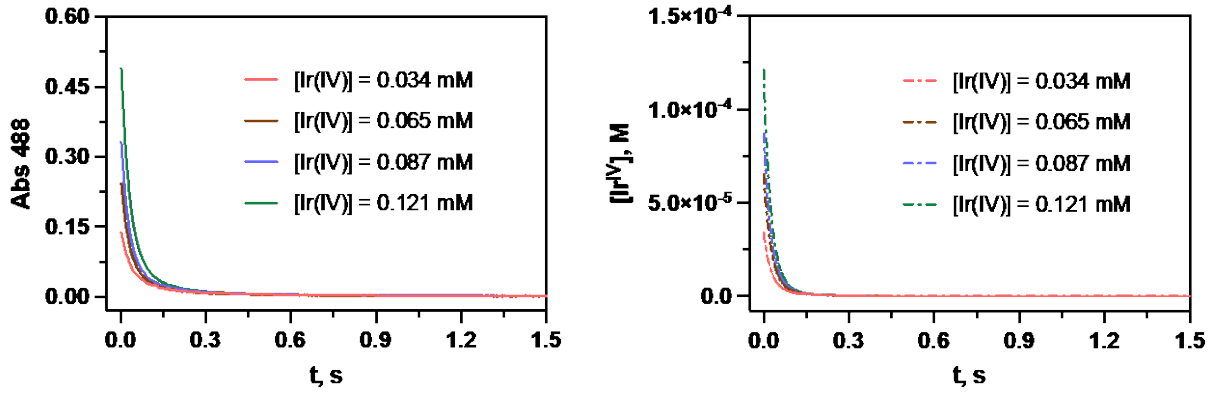

Figure 2-40. Kinetic traces for determining [Ir(IV)] dependence. (Left) Experimental data; (Right) Simulation data.

Given that the decay of the reactant is better described as a two-phase process instead of a second-order kinetics in the present of excess Ir(III), the rate dependence on [Ir(III)] is therefore evaluated by plotting the first half-life against Ir(III) concentration.

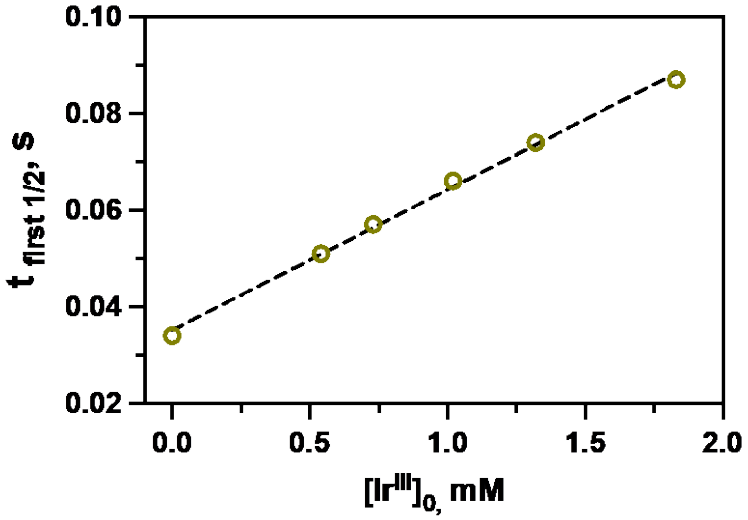

Figure 2-41. Simulated result of [Ir(III)] dependence.

The modeling result indicates that the reaction rate is inhibited by Ir(III), which can be evident from the increased half time as [Ir(III)] become larger. The following graph shows the kinetic dependence on [MSA]. Two set of data are displayed including a plot of the first-order rate constant obtained from the kinetic modeling versus [MSA], and the data obtained from the experimental fit.

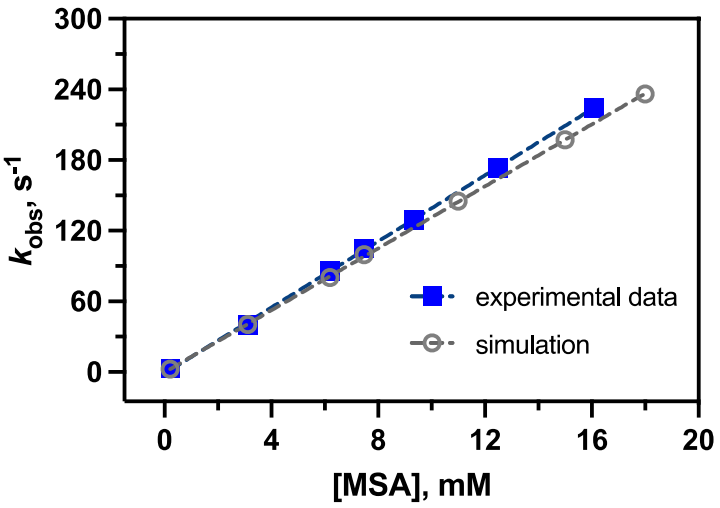

Figure 2-42. Plot of the first-order rate constant vs [MSA] from experimental and simulation data.

The plot from the simulation reveals a linear relationship between [MSA] and k_{obs} with slope $= (1.34 \pm 0.03) \times 10^4\ \text{s}^{-1}\ \text{M}^{-1}$. This result is identical to the straight line fit from the experimental data with slope value of $(1.32 \pm 0.01) \times 10^4\ \text{s}^{-1}\ \text{M}^{-1}$.

2.4.3 Marcus Theory for the k_1 path

The first step of the reaction is likely to be an outer-sphere type, and it is possible to calculate the rate of electron transfer accordingly by Marcus theory using cross relation as below [37],[41].

$$k_{12} = (k_{11}k_{22}K_{12}f)^{\frac{1}{2}}W_{12} \qquad \text{Eq. 2-84}$$

$$lnf_{12} = \frac{\left[lnK_{12} + \frac{w_{12} - w_{21}}{RT}\right]^2}{4\left[\ln\left(\frac{k_{11}k_{22}}{Z^2}\right) + (w_{11} + w_{22})/RT\right]} \qquad \text{Eq. 2-85}$$

$$W_{12} = \text{e}^{\frac{-w_{12}-w_{21}+w_{11}+w_{22}}{2RT}} \qquad \text{Eq. 2-86}$$

$$w_{ij} = \frac{17.7 z_i z_j}{r_{ij}\left(1 + 0.328 r_{ij}\mu^{\frac{1}{2}}\right)} \qquad \text{Eq. 2-87}$$

Here, k_{12} is cross reaction rate of Ir(IV) and MSA, k_{11} and k_{22} are the self-exchange rate constants of Ir(IV)/Ir(III) and $CH_3SO_2^-$ / $CH_3SO_2^{\bullet}$ redox couples. The value for k_{11} of $2 \times 10^5\ M^{-1}\ s^{-1}$ is known [23]. $1 \times 10^{11}\ M^{-1}\ s^{-1}$ is used for *Z*, the collision rate. r is the center-to center distance (in angstroms, A°) between the two reactants. The radii of $[IrCl_6]^{2-}$ and $CH_3SO_2^-$ are 4.1 A° and 2.42 A°, respectively [40]. z_i and z_j are ionic charges of the reactants. With k_{-1} value obtained from the simulation in section 2.4.2, the equilibrium constant of Ir(IV)/MSA can be calculated as,

$$K_1 = \frac{k_1}{k_{-1}} = (9.3 \pm 3.1) \times 10^{-3} \quad \text{Eq. 2-88}$$

This constant is the equilibrium constant of the cross reaction, K_{12}. Based on equations below, and the value of $E^0(\text{Ir(IV)/Ir(III)}) = 0.89$ V,

$$\Delta G^0 = -RT\ln K_{12} = -8.314\ \text{J mol}^{-1}\text{K}^{-1} \times 298.15\ \text{K} \times \ln\{(9.3 \pm 3.1) \times 10^{-3}\} = (1.16 \pm 0.08) \times 10^4\ \text{J mol}^{-1} \quad \text{Eq. 2-89}$$

$$\Delta E^0 = \frac{\Delta G^0}{-nF} = \frac{(1.16 \pm 0.08) \times 10^4\ \text{J mol}^{-1}}{-1 \times 96485\ \text{C mol}^{-1}} = -(0.120 \pm 0.008)\ \text{V} \quad \text{Eq. 2-90}$$

The redox potential of $CH_3SO_2^-/CH_3SO_2^{\bullet}$ is calculated as,

$$\Delta E^0_{(CH_3SO_2^-/CH_3SO_2^{\bullet})} = \Delta E^0_{(\text{Ir(IV)/Ir(III)})} - \Delta E^0 \quad \text{Eq. 2-91}$$

$$= 0.89\ \text{V} - \big(-(0.120 \pm 0.008)\big) = (1.010 \pm 0.008)\ \text{V} \quad \text{Eq. 2-92}$$

For $[IrCl_6]^{2-}/CH_3SO_2^-$,

$$w_{12} = \frac{17.7 \times (-2) \times (-1)}{(4.1 + 2.42)\left(1 + 0.328 \times (4.1 + 2.42) \times 0.1^{\frac{1}{2}}\right)} = 3.239\ \text{KJ mol}^{-1} \quad \text{Eq. 2-93}$$

For $[IrCl_6]^{3-}/CH_3SO_2^{\bullet}$,

$$w_{21} = \frac{17.7 \times (-3) \times 0}{(4.1 + 2.42)\left(1 + 0.328 \times (4.1 + 2.42) \times 0.1^{\frac{1}{2}}\right)} = 0 \text{ KJ mol}^{-1} \quad \text{Eq. 2-94}$$

$$w_{11} = \frac{17.7 \times (-2) \times (-3)}{(4.1 + 4.1)\left(1 + 0.328 \times (4.1 + 4.1) \times 0.1^{\frac{1}{2}}\right)} = 7.0 \text{ KJ mol}^{-1} \quad \text{Eq. 2-95}$$

$$w_{22} = \frac{17.7 \times (-1) \times 0}{(2.42 + 2.42)\left(1 + 0.328 \times (2.42 + 2.42) \times 0.1^{\frac{1}{2}}\right)} = 0 \text{ KJ mol}^{-1} \quad \text{Eq. 2-96}$$

To get W_{12}, R value of 8.314×10^{-3} KJ mol^{-1}K^{-1} is used.

$$W_{12} = \mathrm{e}^{\frac{-w_{12}-w_{21}+w_{11}+w_{22}}{2RT}} = \mathrm{e}^{\frac{(-3.239+7.0) \text{ KJ mol}^{-1}}{2\times 8.314\times 10^{-3} \text{ KJ mol}^{-1}\text{K}^{-1}\times 298.15 \text{ K}}} = 2.13 \quad \text{Eq. 2-97}$$

$$lnf_{12} = \frac{\left(\text{In}\{(9.3 \pm 3.1) \times 10^{-3}\} + n\frac{3.239 \text{ KJ mol}^{-1}}{8.314 \times 10^{-3}\text{KJ mol}^{-1}\text{K}^{-1} \times 298.15 \text{ K}}\right)^2}{4\left[\ln\left(\frac{2 \times 10^5 \text{M}^{-1}\text{s}^{-1} \times k_{22}}{(1 \times 10^{11}\text{M}^{-1}\text{s}^{-1})^2}\right) + \frac{7.0 \text{ KJ mol}^{-1}}{8.314 \times 10^{-3}\text{KJ mol}^{-1}\text{K}^{-1} \times 298.15 \text{ K}}\right]} \quad \text{Eq. 2-98}$$

$$lnf_{12} = \frac{(\text{In}\{(9.3 \pm 3.1) \times 10^{-3}\} + 1.307)^2}{-150.979 + 4\ln k_{22}} \quad \text{Eq. 2-99}$$

$$lnf_{12} = \frac{11.362 \pm 2.247}{-150.979 + 4\ln k_{22}} \quad \text{Eq. 2-100}$$

$$k_{12} = \left(2 \times 10^5 \times k_{22} \times (9.3 \pm 3.1) \times 10^{-3} \times e^{\frac{11.362\pm 2.247}{-150.979+4\ln k_{22}}}\right)^{\frac{1}{2}} \times 2.13 = (0.70 \pm 0.01) \times 10^4 \quad \text{Eq. 2-101}$$

$$k_{22} \times e^{\frac{11.362\pm 2.247}{-150.979+4\ln k_{22}}} = (5.81 \pm 1.94) \times 10^3 \quad \text{Eq. 2-102}$$

$$\ln\left(k_{22} \times e^{\frac{11.362\pm 2.247}{-150.979+4\ln k_{22}}}\right) = \ln\left((5.81 \pm 1.94) \times 10^3\right) \quad \text{Eq. 2-103}$$

$$\ln k_{22} + \ln e^{\frac{11.362\pm 2.247}{-150.979+4\ln k_{22}}} = 8.67 \pm 0.33 \quad \text{Eq. 2-104}$$

$$\ln k_{22} + \frac{11.362 \pm 2.247}{-150.979 + 4\ln k_{22}} = 8.67 \pm 0.33 \quad \text{Eq. 2-105}$$

$$-(1319.86 \pm 50.56) = 4(\ln k_{22})^2 - (186.78 + 2.0)\ln k_{22} \quad \text{Eq. 2-106}$$

$$\ln k_{22} = \frac{(186.78 + 2.0) - \sqrt{(186.78 + 2.0)^2 - 4 \times 4 \times (1364.62 \pm 75.58)}}{2 \times 4} = 8.76 \pm 0.45 \qquad \text{Eq. 2-107}$$

2.5 Conclusions

In this work, we proposed a solid mechanism scheme for the oxidation of methanesulfinate by hexachloroiridate(IV) in aqueous media. The one-electron oxidant $[IrCl_6]^{2-}$ makes the 2-electron transfer process of $CH_3SO_2^-$ to $CH_3SO_3^-$ occur through a rapid and reversible outer-sphere oxidation between Ir(IV) and $CH_3SO_2^-$ to produce Ir(III) and $CH_3SO_2^{\bullet}$, followed by the quasi-inner sphere oxidation of the radical by Ir(IV). The strong chlorine atom affinity of a sulfonyl radical as a reactive intermediate for the reaction was initially proved by the fact that it hydrolyzes and releases a CH_3SO_2Cl. Formation of CH_3SO_3H as final product is confirmed from the hydrolysis of the sulfonyl chloride. To our knowledge, there was no redox potential of any sulfonyl radical reported previously, which makes our measurement and calculation of the redox potential of $CH_3SO_2^-/CH_3SO_2^{\bullet}$ couples with a value of (1.010 ± 0.008) V the first work. Given that such redox conversion takes places mostly in biological environment and living cells, this value will provide essential insights and useful information for estimating and understanding the reactivity of other sulfur species towards various oxidants.

2.6 References

[1] Darkwa, J.; Olojo, R.; Chikwana, E.; Simoyi, R. H. *J. Phys. Chem. A* **2004**, *108*, 5576−5587.

[2] Zhu, L.; Nicovich, J. M.; Wine, P. H. *J. Phys. Chem. A* **2005,** *109*, 3903−3911.

[3] Bhattarai, N.; Stanbury, D. M. *J. Phys. Chem. B* **2014,** *119*, 1097.

[4] Flyunt, R.; Makogon, O.; Schuchmann, M. N.; Asmus, K.-D.; Von Sonntag, C. *J. Chem. Soc., Perkin Trans.* **2001**, *2*, 787−792.

[5] Razskazovskii, Y.; Sevilla, M. D. *J. Phys. Chem.* **1996**, *100*, 4090−4096.

[6] Song, N.; Stanbury, D. M. *Inorg. Chem.* **2012**, *51*, 4909–4911.

[7] Cecil, R.; Littler, J. S.; Easton, G. *J. Chem. Soc. B* **1970**, 626−631.

[8] Thoi, H. H.; Iino, M.; Matsuda, M. *J. Org. Chem.* **1980**, *45*, 3626–3630.

[9] Zhu, L.; Nenes, A.; Wine, P. H.; Nicovich, J. M. *J. Geophys. Res.* **2006**, *111*, D05316.

[10] Yin, F. d.; Grosjean, D.; Flagan, R. C.; Seinfeld, J. H. *J. Atmos. Chem*. **1990**, *11*, 365–399.

[11] Arsene, C.; Barnes, I.; Becker, K. H.; Schneider, W. F.; Wallington, T. T.; Mihalopoulos, N.; Patroescu-Klotz, I. V. *Environ. Sci. Technol.* **2002**, *36*, 5155–5163.

[12] Kukui, A.; Borissenko, D.; Laverdet, G.; Le Bras, G. *J. Phys. Chem. A* **2003**, *107*, 5732–5742.

[13] Griesser, M.; Chauvin J. R.; Pratt, D. A. *Chem. Sci.* **2018**, *9*, 7218.

[14] Bhattarai, N.; Stanbury, D. M. *Inorg. Chem.* **2012**, *51*, 13303−13311.

[15] Fine, D. A. *Inorg. Chem.* **1969**, *8*, 1016.

[16] Wudl, F.; Lightner, D. A.; Cram, D. J. *J. Am. Chem. Soc.* **1967**, *89*, 4099–4101.

[17] Hung, M.-L.; Stanbury, D. M. *Inorg. Chem.* **1994**, *33*, 4062–4069.

[18] Patai, S.; Rappoport, Z., *Sulphonic Acids, Esters and their Derivatives (1991)*, 1st ed.; John Wiley & Sons, Ltd: Chichester, UK, **1991**, pp 2–3.

[19] Jordan, R. B.; Wangila, G. *Inorg. Chim. Acta.* **2003,** *343*, 347-350

[20] Farng, L.; Kice, J. L. *J. Am. Chem. Soc.* **1981**, *103*, 1137–1145

[21] Cecil, R.; Littler, J. S.; Easton, G. J. *Chem. Soc. B* **1970**, 626−631.

[22] Poulsen, I. A.; Garner, C. S. *J. Am. Chem. Soc.* **1962**, *84*, 2032−2037.

[23] Hurwitz, P.; Kustin, K. *Trans. Faraday Soc.* **1966**, *62*, 427.

[24] Bonifacic, M.; Asmus, K.-D. *J. Chem. Soc., Perkin Trans. 2* **1980**, 758-762.

[25] Borodina, E.; Kelly, D. P.; Rainey, F. A.; Ward-Rainey, N. L.; Wood, A. P. *Arch. Microbiol*. **2000**, *173*, 425-437.

[26] Wicht, D. K. *Arch. Biochem. Biophys.* **2016**, *604*, 159-166.

[27] Sykes, A. G.; Thorneley, R. N. F. *J. Chem. Soc. A* **1970,** 232-238.

[28] Grossman, B.; Haim, A. *J. Am. Chem. Soc.* **1970**, *92*, 4835-4840.

[29] Gardner, H. C.; Kochi, J. K. *J. Am. Chem. Soc.* **1975**, *97*, 1855-1865.

[30] Chen, J. Y.; Gardner, H. C.; Kochi, J. K. *J. Am. Chem. Soc.* **1976**, *98*, 6150-6159.

[31] Steenken, S.; Neta, P. *J. Am. Chem. Soc.* **1982**, *104*, 1244-1248.

[32] Robertson, R. E.; Rossall, B.; Sugamori, S. E.; Treindl, L. *Can. J. Chem.* **1969**, *47*, 4199-4206.

[33] King, J. F.; Lam, J. Y. L.; Skonieczny, S. *J. Am. Chem. Soc.* **1992**, *114*, 1743-1749.

[34] Chatgilialoglu, C.; Mozziconacci, O.; Tamba, M.; Bobrowski, K.; Kciuk, G.; Bertrand, M.P.; Gastaldi, S.; Timokhin, V. I.; *J. Phys. Chem. A* **2012**, *116*, 7623−7628.

[35] Gozdz, A. S.; Maslak, P. *J. Org. Chem.* **1991**, *56*, 2179−2189.

[36] Mortensen, A.; Skibsted, L. H.; Sampson, J.; Rice-Evans, C.; Everett, S. A. *FEBS Lett.* **1997**, *418*, 91−97.

[37] Marcus, R. A.; Sutin, N. *Biochim. Biophys. Acta* **1985**, *811*, 277.

[38] Rajakaruna, P. R. *Reaction Mechanisms of One- and Two-Electron Oxidations of Alkanesulfinates in Aqueous Media*. **2021**. Dissertation, Auburn University, Auburn, AL.

[39] Dickson, P. N.; Margerum, D. W. *Anal. Chem.* **1986**, *58*, 3154.

[40] Sun, J. F.; Stanbury, D. M. *J. Chem. Soc., Dalton Trans.* **2002**, 785.

[41] Song, N.; Stanbury, D. M. *Inorg. Chem.* **2011**, *50*, 12771.

3 Oxidation of Methanesulfinate by Bis(1,4,7- triazacyclononane)nickel(III))

3.1 Introduction

Nickel is an earth abundant element and readily available to organisms [1]. The most enriched form of the element is nickel(II) ions. It has been discovered and isolated in some enzymes from plants and bacteria. For instance, methanogenic bacteria are found to require nickel for their growth and the synthesis of Factor 430 (F430, a tightly bound nickel porphinoid) [2]-[4]. Nickel(II) and nickel(III) complexes are known for their stability in acidic media [1], due to which they have been extensively studied and developed for the use as an one-electron redox couple. 1,4,7-triazacyclononane (tacn) is one of the most common ligands for preparing Ni(II) and Ni(III) complex. The coordinated species are sufficiently long-lived to enable the kinetic studies to proceed at pH < 3. In basic media, N-H protons of the tacn ligand tend to deprotonate ($pK_a = 10$) [12]. Given that tacn ligand has no potential binding sites, plus the metal complexes are strictly coordination saturated, outer-sphere electron transfer pathway is expected from the substitution-inert property of the metal complexes [5]-[7].

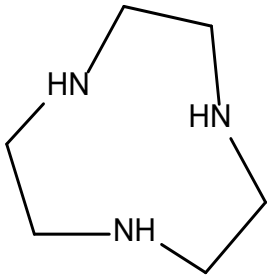

1,4,7-triazacyclononane (tacn)

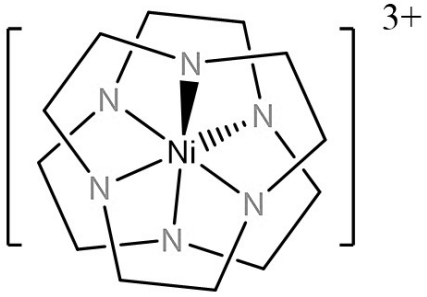

Bis(1,4,7-tacn)nickel(III)

In this project, methanesulfinate ($CH_3SO_2^-$) is selected as the reductant, of which the features and significance have been discussed in chapter 1. $[Ni(tacn)_2](ClO_4)_3$ is a cationic oxidant. $[Ni(tacn)_2]^{3+}/[Ni(tacn)_2]^{2+}$redox couple has a reduction potential of $+0.94$ V [8]. An

advantage of studying this redox couple is that it has a relatively low self-exchange rate constant ($6 \times 10^3\ M^{-1}\ s^{-1}$), which makes the cross-reaction rate constants highly sensitive to the $CH_3SO_2^-$/ $CH_3SO_2^{\bullet}$ redox partner that is investigated in this chapter [9],[10].

Kinetic dependence of this reaction was studied by our previous group member [11]. However, due to the complexity of this reaction, there are problems remaining unsolved regarding the identification of the reaction intermediates, products and the detailed mechanism. In this chapter, important results based on a further study on the oxidation of methanesulfinate (MSA) by bis(1,4,7-triazacyclononane)nickel(III) in aqueous phase are presented including the reaction kinetics, stoichiometry, product identification, and detailed mechanism.

3.2 Experimental Preparation and Methods

3.2.1 Reagents and Solutions

Sodium methanesulfinate MSA, Alfa Aesar), sodium methanesulfonate (Alfa Aesar), $Ni(ClO_4)_2.6H_2O$ (Alfa Aesar), 1,4,7-triazacyclononane trihydrochloride (TCI), HCl (Fisher), $Na_2S_2O_8$, methanol (Aldrich), ethanol (Aldrich), CH_3COONa (Sigma), glacial acetic acid (Fisher), NaOH pellets, NaCl, $HClO_4$ (Fisher), N-tert-butyl-α-phenylnitrone (PBN, Aldrich), D_2O 99.8% isotopic (Alfa Aesar), 3-(trimethylsilyl)-1-propane sulfonic acid sodium salt (DSS), sodium cyanide (Fisher), $NaClO_4$ (Fisher), $KMnO_4$ (J. T. Baker), sulfuric acid (Fisher), diethyl ether (J. T. Baker).

Bis(1,4,7-triazacyclononane)nickel(II)/nicke(III) perchlorate were prepared according to the described methods in literature [9],[10]. 1,4,7-triazacylcononane (tacn) in 1 M NaOH and $Ni(ClO_4)_2 \cdot 6H_2O$ in methanol were prepared initially and then mixed under a steam bath. Later, the pH of the mixture was adjusted to 5 with $HClO_4$ and cooled at 0 ℃. Mauve-pink crystals were

formed overnight. Then $[Ni(tacn)_2](ClO_4)_2$ crystals were collected by filtration and washed with diethyl ether.

To prepare $[Ni(tacn)_2](ClO_4)_3$, $[Ni(tacn)_2](ClO_4)_2$ crystals were dissolved in a minimum volume of 1 M $HClO_4$ and then oxidized by a saturated peroxydisulfate ($Na_2S_2O_8$) solution. A ratio of Ni(II)/$Na_2S_2O_8$ = 1:0.6 was used to obtain the yellow-brown solution, followed by the drop-wise addition of saturated $NaClO_4$ to form the dark brown precipitate. After that, the solution was cooled at 0 ℃ overnight to crystallize. The resulting product was filtered and washed with ethanol and diethyl ether.

3.2.2 Instruments and Methods

All the aqueous solutions were freshly prepared using purified de-ionized water with a specific resistivity of 18.2 MΩ cm at 25 °C from an ultrapure water purification system. UV-Vis spectra were collected at 25 ± 0.1 ℃ using a HP-8453 diode array spectrophotometer equipped with a Brinkman Lauda RM6 thermostatted system. The quartz cells for UV measurement are with path length of 1 mm or 1 cm. Kinetic data were collected on a Hi-Tech SF-51 stopped-flow spectrophotometer with 1 cm path length configuration with OLIS 4300 data acquisition and later analyzed by GraphPad PRISM 9. Optical cut-off filters were used between the sample and the detector with stopped-flow spectrophotometer for different kinetic studies. The k_{obs} and $k_{obs,2}$ values reported in this study are averages of at least seven trials. The absorbance change at 312 nm was monitored to obtain the concentration of Ni(III) and kinetic traces. ^{1}H-NMR spectra were recorded on a Bruker AV 500 or 600 MHz spectrometer by dissolving the sample in D_2O with 3-(trimethylsilyl)-1-propanesulfonic acid sodium salt (DSS) as internal standard unless otherwise stated.

3.2.3 UV-Vis Observation

UV-Vis spectrum of bis(1,4,7-triazacyclononane)nickel(III) in 0.1 M $HClO_4$ was collected as shown in Figure 3-1. Two absorbance peaks can be observed from the spectrum including a maximum at 312 nm and a secondary peak at 270 nm. Molar absorptivity of Ni(III) at 312 nm used for this study is $9.9 \times 10^3\ M^{-1}\ cm^{-1}$ (The value reported in the literature is $\varepsilon_{312} = (1.01 \pm 0.02) \times 10^4\ M^{-1}\ cm^{-1}$[9]).)

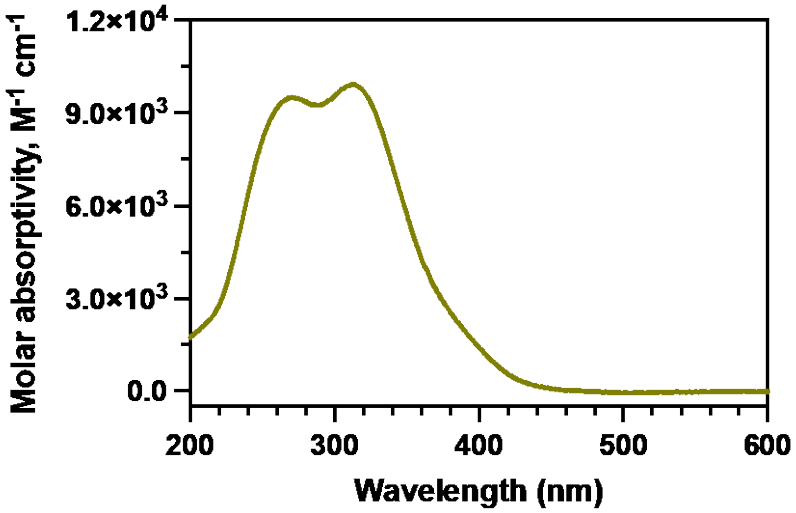

Figure 3-1. The UV spectrum of bis(1,4,7-triazacyclononane)nickel(III) in 0.1 M $HClO_4$.

3.3 Results

3.3.1 Stoichiometry

The stoichiometry of the reaction between MSA and $[Ni(tacn)_2]^{3+}$ was determined through spectrophotometric titration. 2 mL of 0.12 mM MSA with pH adjusted to 3 by $HClO_4$ was added to a cuvette and purged with argon for 30 minutes. Later, 0.06 mL aliquots of 0.72 mM $[Ni(tacn)_2]^{3+}$ at pH 3 were added into MSA solution using a gas-tight syringe under anerobic conditions and allowed to react for 30 minutes. The spectrum was recorded after each addition.

The titration was continued with 30 minutes interval till the end point was reached. The consumption ratio was determined to be $\frac{\Delta[\mathrm{Ni(tacn)_2}]^{3+}}{\Delta[\mathrm{MSA}]} = 0.9:1$.

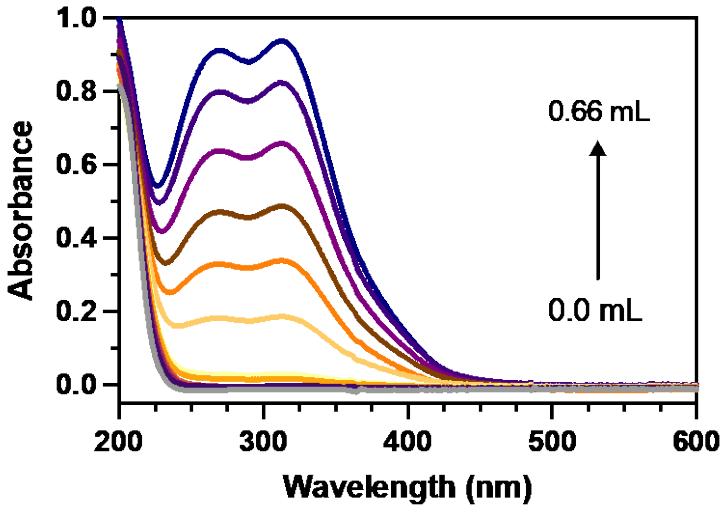

Figure 3-2. UV-vis spectrum after each addition.

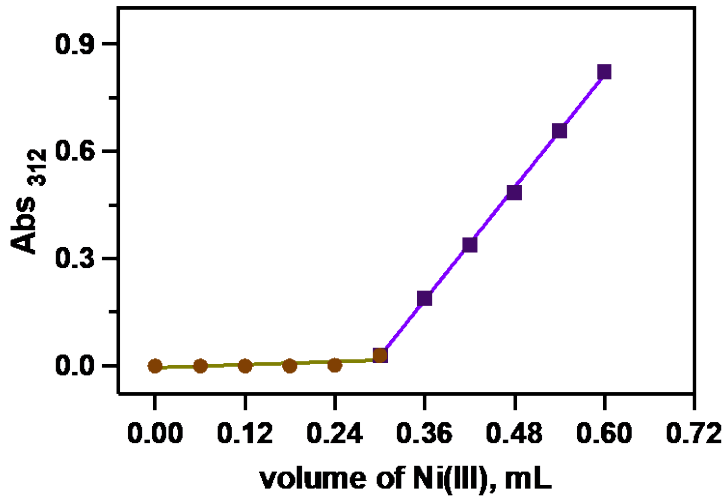

Figure 3-3. Titration curve.

Given that $[\mathrm{Ni(tacn)_2}]^{3+}$ is a one-electron oxidant, twice as much Ni(III) would thus be required for the conversion of sulfinic acid to the corresponding sulfonic acid. The observed nearly 1:1 ratio of the reactants herein can be possibly caused by something else which also oxidizes MSA. O_2 is most likely responsible because the oxidation of sulfite by one-electron oxidants is

quite sensitive to oxygen [13]. Thus, to optimize the anaerobic condition, the titration was performed in a glove box ($O_2 < 0.1$ ppm). 2 mL of 0.13 mM MSA with pH adjusted to 3 by $HClO_4$ was added to a cuvette and purged with argon for 40 minutes. Later, 0.08 mL aliquots of 0.688 mM $[Ni(tacn)_2]^{3+}$ at pH 2.7 with O_2 excluded was added into MSA solution using a gas tight syringe and allowed to react for at least 25 minutes. The spectrum at 312 nm after each addition was recorded from a 'Thermo Scientific Nanodrop One' UV-Vis instrument with 1 cm optical pathlength. The titration was continued till the end point was reached. The consumption ratio was determined to be $\frac{\Delta[Ni(tacn)_2]^{3+}}{\Delta[MSA]} = 1.90:1$.

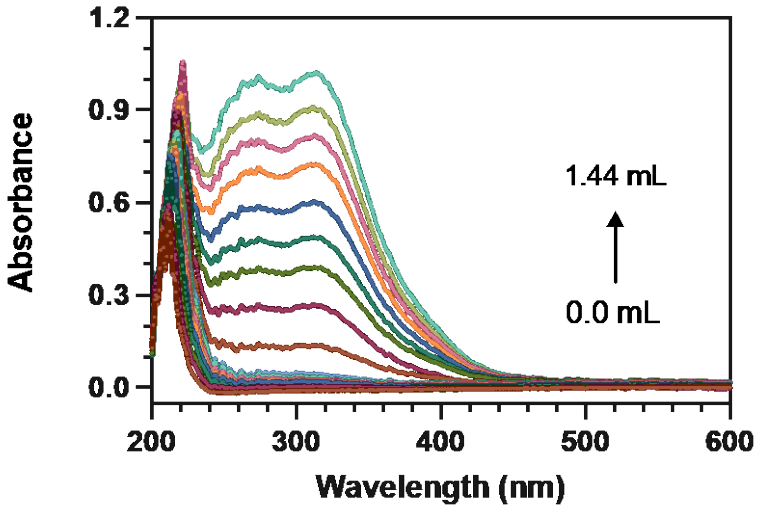

Figure 3-4. UV-vis spectrum after each addition.

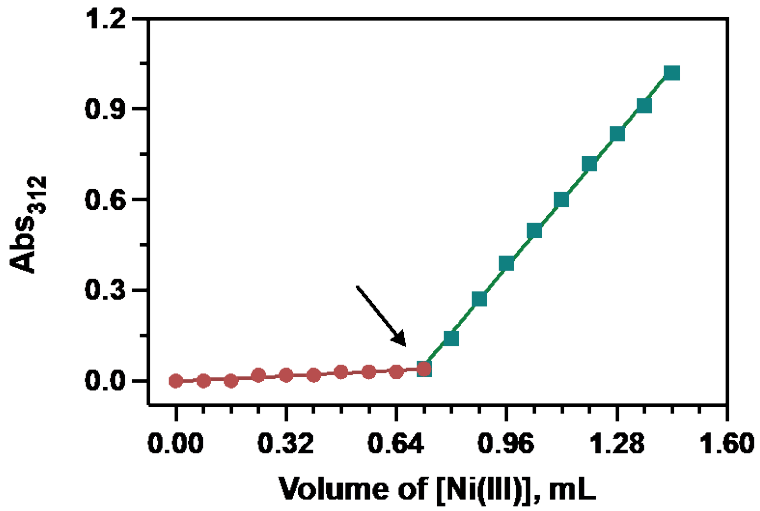

Figure 3-5. Titration curve for determining the reacting ratio.

3.3.2 Reaction Kinetics

3.3.2.1 Rate dependence on $[\mathbf{Ni(tacn)_2}]^{3+}$

The absorbance decay of the mixture of 0.013 mM Ni(III) and 0.96 mM MSA in pH 3.3 acetate buffer was obtained with no Ni(II) added. It turns out that Ni(III) can be easily reduced on addition of a large excess of MSA. Excellent pseudo-first-order dependence on [Ni(III)] was obtained according to the equation,

$$-\frac{\mathrm{d[Ni^{III}]}}{\mathrm{dt}} = k[\mathrm{MSA}][\mathrm{Ni(III)}] \qquad \text{Eq. 3-1}$$

When [MSA] >> [Ni(III)], $\Delta[\mathrm{MSA}] \approx 0$,

$$-\frac{\mathrm{d[Ni^{III}]}}{\mathrm{dt}} = k_{obs}[\mathrm{Ni(III)}] \qquad \text{Eq. 3-2}$$

Where k_{obs} is the observed first-order rate constant of the reaction.

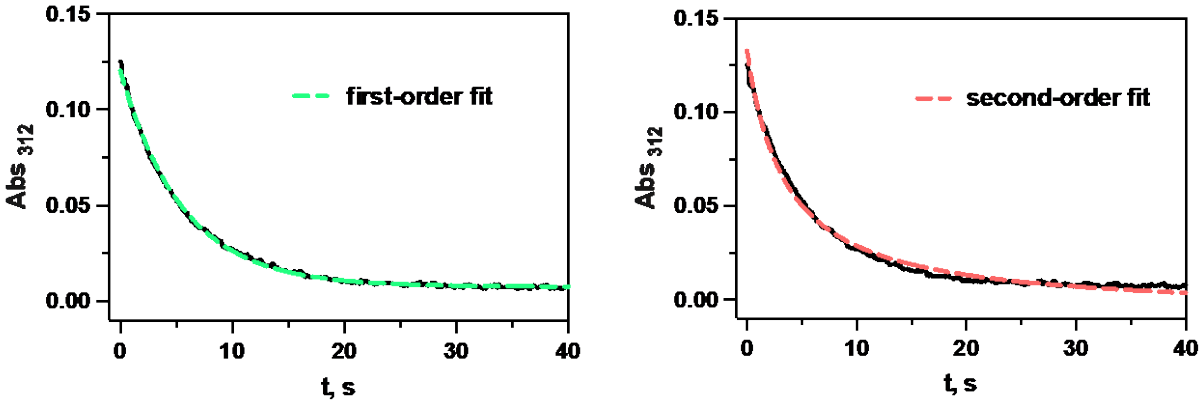

Figure 3-6. Kinetic trace of the mixture of Ni(III) with excess MSA. Left: first-order fit with k_{obs} = 0.18 s^{-1}. Right: second-order fit. Conditions: $[MSA]_0$ = 0.96 mM, $[Ni(III)]_0$ = 0.013 mM.

3.3.2.2 Rate dependence on $[Ni(tacn)_2]^{2+}$

The kinetic dependence on the product, $[Ni(tacn)_2]^{2+}$, was studied using stopped-flow methods by adding extra Ni(II) into the reaction solutions at pH 3.36 (acetate buffer), $\mu = 0.1$ M (NaCl). The kinetic traces were excellently fitted into pseudo-second-order rate law with the rate constants expressed as $k_{obs,2}$.

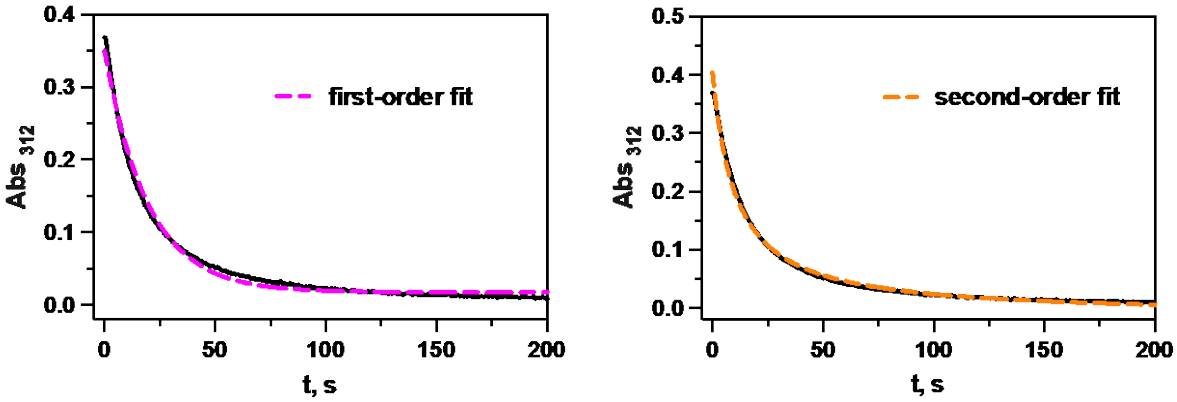

Figure 3-7. Kinetic trace at 312 nm of Ni(III)-MSA reaction. Left; first-order fit with k_{obs} = 0.1051 s^{-1}. Right: second-order fit. Conditions: $[MSA]_0 = 1.0$ mM, $[Ni(III)]_0 = 0.04$ mM, $[Ni(II)]_0 = 0.57$ mM.

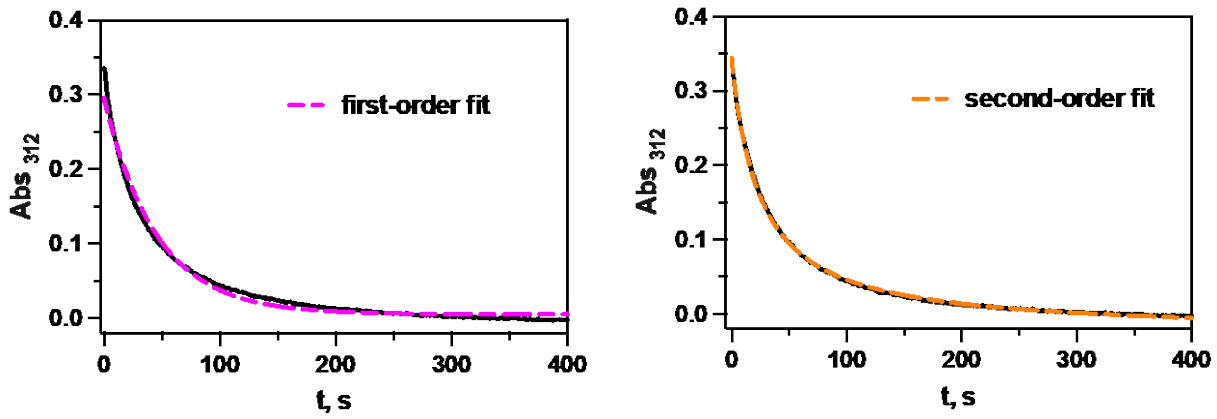

Figure 3-8. Kinetic trace of Ni(III)-MSA reaction. Left: first-order fit with k_{obs} = 0.022 s^{-1}. Right: second-order fit. Conditions: $[MSA]_0$ = 1.0 mM, $[Ni(III)]_0$ = 0.04 mM, $[Ni(II)]_0$ = 1.24 mM.

Ni(II) concentration was varied from 0.24 mM to 1.24 mM to determine its effect on the reaction rate. Strong inhibition from Ni(II) can be concluded from the fact that the increase in [Ni(II)] leads to a decrease of the rate constant. An inverse dependence of $k_{\mathrm{obs},2}$ on Ni(II) concentration is confirmed from the linear fit with negligible intercept.

Table 3-1. Data table for determination of rate dependence on [Ni(II)]

$\mathbf{[Ni(II)]_0, mM}$	$\mathbf{1/k_{obs,2}, M\ s}$
0.24	2.05×10^{-4}
0.57	4.38×10^{-4}
0.68	5.43×10^{-4}
1.02	7.54×10^{-4}
1.24	9.17×10^{-4}

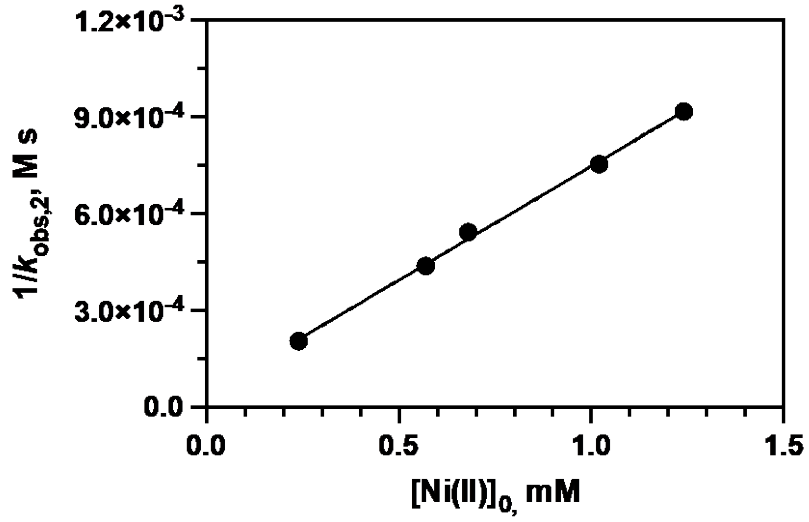

Figure 3-9. The plot of inverse $k_{obs,2}$ vs [Ni(II)]. Conditions: $[MSA]_0 = 1.0$ mM, $[Ni^{III}]_0 = 0.04$ mM, $[Ni^{II}]_0 = 0.24 - 1.24$ mM, pH 3.36 (acetate buffer). Straight line fit: slope $= (7.07 \pm 0.18) \times 10^{-1}$ s; Y − intercept $= (4.1 \pm 1.5) \times 10^{-5}$ M s.

The linear fit leads to the equation,

$$\frac{1}{k_{obs,2}} = k'[Ni^{II}] \qquad \text{Eq. 3-3}$$

Where $k' = (7.07 \pm 0.18) \times 10^{-1}$ s.

Based on [Ni(II)] and [MSA] dependence below in Figure 3-10, the rate law of the reaction can be expressed as,

$$-\frac{d[Ni^{III}]}{dt} = \frac{k''[Ni^{III}]^2[CH_3SO_2^-]}{[Ni^{II}]} \qquad \text{Eq. 3-4}$$

Here, k'' is a rate constant which is independent of pH under the selected condition. The value can be calculated from the equation,

$$k_{obs,2} = \frac{k''[CH_3SO_2^-]}{[Ni^{II}]} = \frac{1}{k'[Ni^{II}]} \qquad \text{Eq. 3-5}$$

$$k'' = \frac{1}{k'[MSA]} = (1.41 \pm 0.15) \times 10^3\ M^{-1}s^{-1} \qquad \text{Eq. 3-6}$$

3.3.2.3 Rate dependence on [MSA] with extra [Ni(II)]

The rate dependence on [MSA] with the presence of Ni(II) was investigated by mixing Ni(III) and various amounts of MSA with a large excess of Ni(II) in the solutions to maintain flooding conditions. The figure below displays a series of experiments with [MSA] varying from 5.25 mM to 27.95 mM. The linear fit with a negligible intercept provides an indication that the reaction rate has a first-order dependence of [MSA] when Ni(II) is included. The fit leads to the equation,

$$k_{\mathrm{obs},2} = k'''[\mathrm{MSA}]_{\mathrm{total}} \qquad \text{Eq. 3-7}$$

Where k''' is the slope of the linear fit with a value of $(9.14 \pm 0.45) \times 10^6\ \mathrm{M}^{-2}\ \mathrm{s}^{-1}$.

Table 3-2. Data table for determination of rate dependence on [MSA]

$[\mathbf{MSA}]_0, \mathbf{mM}$	$k_{obs,2}, \mathbf{M^{-1}\ s^{-1}}$
5.2	4.14×10^4
10.56	9.79×10^4
15.84	1.47×10^5
21.12	2.04×10^5
27.95	2.48×10^5

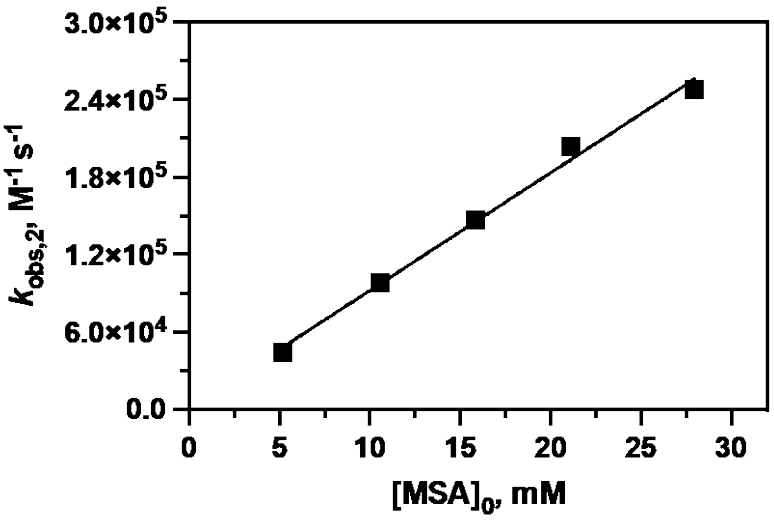

Figure 3-10. Dependence of $k_{obs,2}$ on [MSA] in the presence of Ni(II). Conditions: $[MSA]_0$ = 5.25-27.95 mM, $[Ni(III)]_0$ = 0.016 mM, $[Ni(II)]_0$ = 0.26 mM, pH 3.5 (acetate buffer). Straight line fit: slope = $(9.14 \pm 0.45) \times 10^6\ M^{-2}\ s^{-1}$; $Y - intercept = (5.27 \pm 81.5) \times 10^2\ M^{-1}\ s^{-1}$.

3.3.2.4 Spin trapping

To investigate the effect of a radical scavenger, PBN, on the reaction kinetics, the UV-vis spectra of 5 mM PBN and 0.095 mM Ni(III) at pH 2.26 (HCl) were recorded respectively. Then the spectrum of a Ni(III)/PBN mixture was taken prior to the kinetic study in order to select a wavelength at which only Ni(III) absorbs.

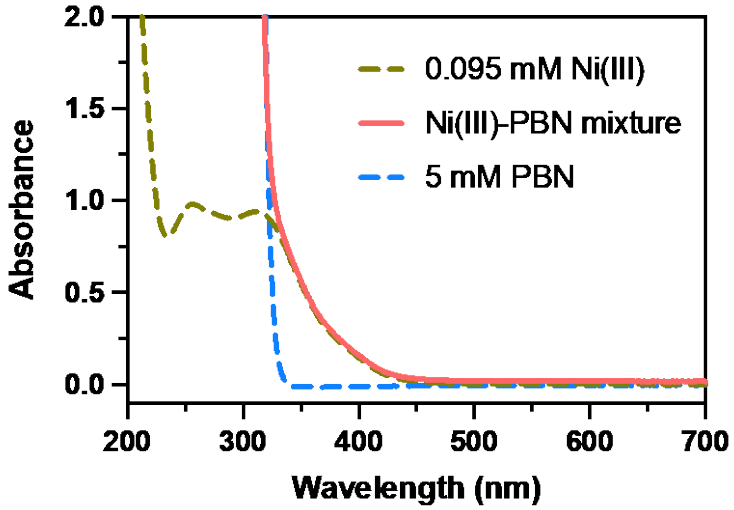

Figure 3-11. UV-vis spectra of Ni(III) and the mixture of PBN with Ni(III).

The absorbance changes at 360 nm were monitored for a series of experiments at pH 3.64 (acetate buffer), $\mu = 0.1$ M (NaCl). The concentration of Ni(III) and MSA were maintained constant. The concentration of PBN was varied from 0 mM to 5.0 mM. Pseudo-first-order rate constants were obtained to evaluate [PBN] dependence. It was found out that PBN has no distinguishable effect on the reaction rate.

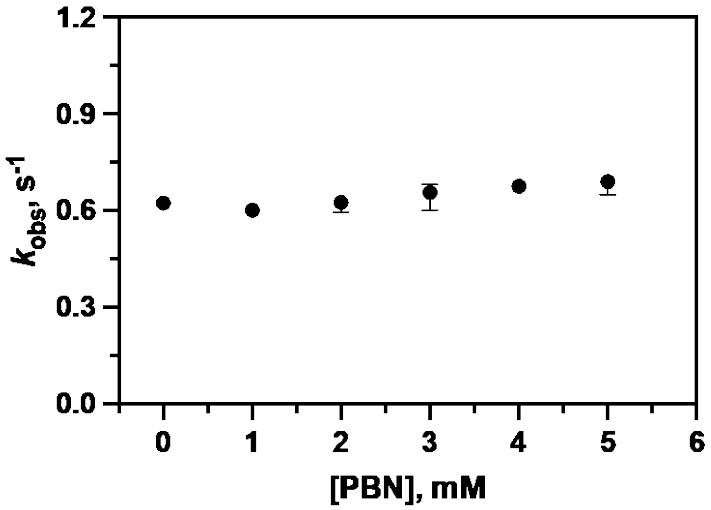

Figure 3-12. PBN effect on the reaction kinetics. Conditions: $[Ni(III)]_0 = 0.045$ mM, $[MSA]_0 = 2.5$ mM, $\mu = 0.1$ M (NaCl), pH 3.64, acetate buffer.

Theoretically, the reaction in the presence of PBN can occur via two ways, the first being the trapping of $CH_3SO_2^{\bullet}$ by PBN through the following process,

$$(M1) \quad Ni^{III} + CH_3SO_2^- \rightleftharpoons Ni^{II} + CH_3SO_2^{\bullet} \quad k_1 \qquad \text{Eq. 3-8}$$

$$PBN + CH_3SO_2^{\bullet} \rightarrow \text{Adduct } X^{\bullet} \qquad k_{PBN} \qquad \text{Eq. 3-9}$$

$$Ni^{III} + \text{Adduct } X^{\bullet} \rightarrow Ni^{II} + X^+ \qquad \text{Eq. 3-10}$$

And the second is the scavenging of $CH_3SO_2^{\bullet}$ by Ni^{III}. This reaction is likely to take place if the trapping rate constant of the radical, $k_{Ni(III)}$, is larger compared with k_{PBN}.

$$(M2) \quad Ni^{III} + CH_3SO_2^- \rightleftharpoons Ni^{II} + CH_3SO_2^{\bullet} \quad k_1 \qquad \text{Eq. 3-11}$$

$$Ni^{III} + CH_3SO_2^{\bullet} \rightarrow \text{Adduct M} \qquad k_{Ni(III)} \qquad \text{Eq. 3-12}$$

$$\text{Adduct M} + H_2O \rightarrow \text{products} \qquad \text{Eq. 3-13}$$

With [Ni(II)] = 0 mM, first-order kinetics on [Ni(III)] and $[CH_3SO_2^-]$ were obtained. The rate law for these two mechanisms can therefore be described as,

$$-\frac{d[Ni(III)]}{dt} = 2k_1[Ni(III)][CH_3SO_2^-] \qquad \text{Eq. 3-14}$$

Since the two mechanisms share the same rate constant, they cannot be distinguished from k_{obs} obtained from spin trap. Trapping experiments with various [Ni(II)] were performed next. A solution consisted of 3.3 mM MSA and 4.8 mM PBN was reacted with 0.045 mM Ni(III) at pH 3.5 (acetate buffer) with 0 mM, 2.76 mM, 5.25 mM Ni(II) present. First-order rate constant was obtained from the fitting of the kinetic trace. A slight decreasing of the reaction rate can be observed with an increasing of Ni(II) concentration. From [Ni(II)] dependence in Figure 3-9, we found that the reaction takes place slower when extra Ni(II) is added. However, the strong inhibition of Ni(II) cannot be observed when PBN is included, which indicates an effective trapping of $CH_3SO_2^{\bullet}$ from PBN.

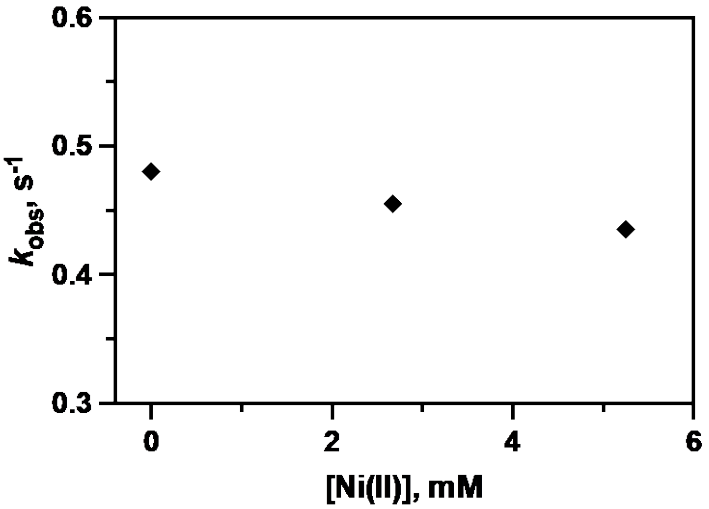

Figure 3-13. PBN effect on the reaction rate with various [Ni(II)]. Conditions: $[Ni(III)]_0$ = 0.045 mM, $[MSA]_0$ = 3.3 mM, $[Ni(II)]_0$ = 0 - 5.25 mM, μ = 0.1 M (NaCl), pH 3.5, acetate buffer.

3.3.3 Product Analysis

The product of the reaction between Ni(III) and MSA was characterized using ^{1}H-NMR spectrometry. A solution of MSA in D_2O with DSS as reference was purged with argon for 30 minutes in an NMR tube. The spectrum was obtained to determine the concentration of MSA. Next, $[Ni(tacn)_2]^{3+}$ was dissolved in acetic acid in D_2O and purged with argon. It was later mixed with MSA solution in the NMR tube using a gas-tight syringe with argon saturated for 20 minutes. The ^{1}H-NMR spectra were obtained to identify the intermediates and S-containing products. The pH of the mixture is 2.24. In the spectra, several singlets can be observed including the peak at 2.08 ppm from acetic acid, 2.45 ppm from the excess MSA, 2.80 ppm from $CH_3SO_3^-$, a major unknown peak at 3.58 ppm, and a minor one at 3.32 ppm. The peak at 3.58 ppm decays slowly, suggesting the presence of an intermediate during the reaction.

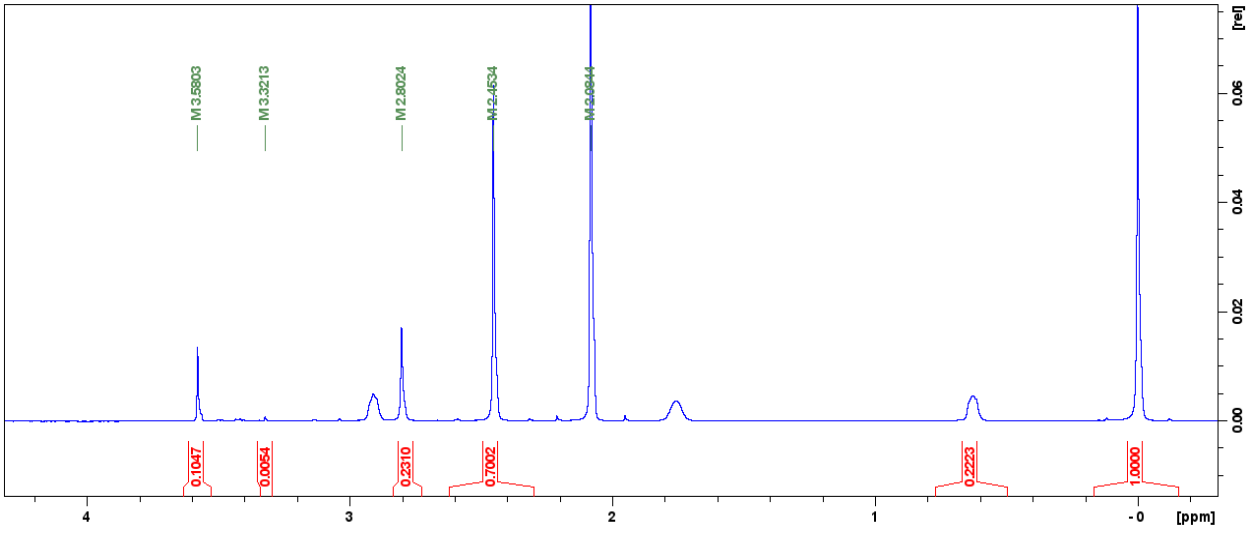

Figure 3-14. ^{1}H-NMR spectrum of the mixture of Ni(III) with excess MSA in D_2O after reacting 30 mins with DSS as reference. Conditions: [MSA] = 16.80 mM, [Ni(III)] = 4.67 mM, pH 2.24.

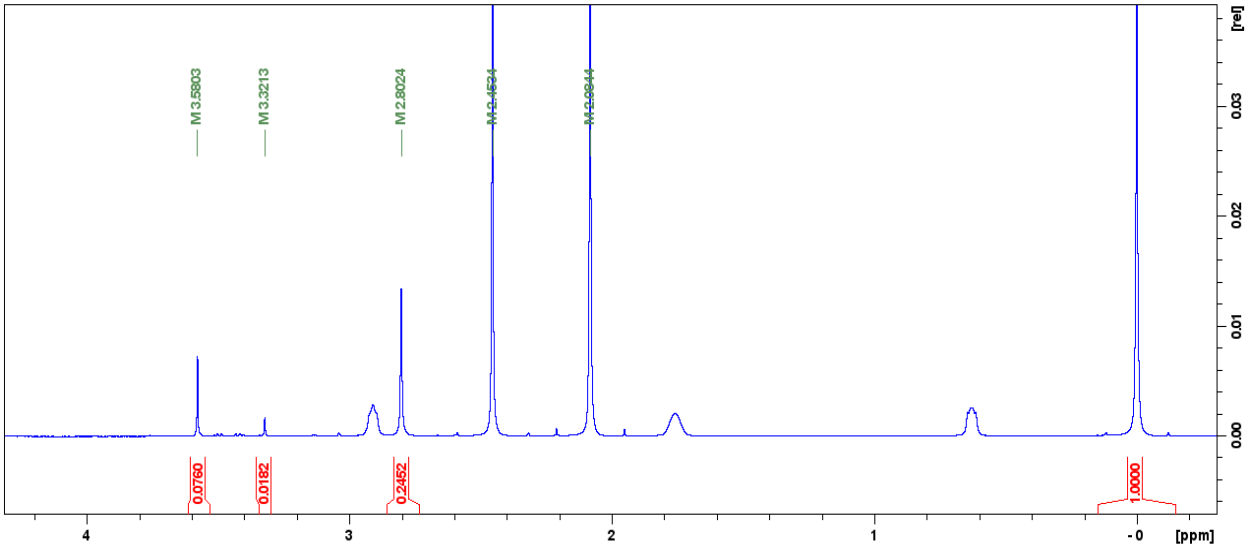

Figure 3-15. ^{1}H-NMR spectrum of the mixture of Ni(III) with excess MSA in D_2O after reacting 125 mins.

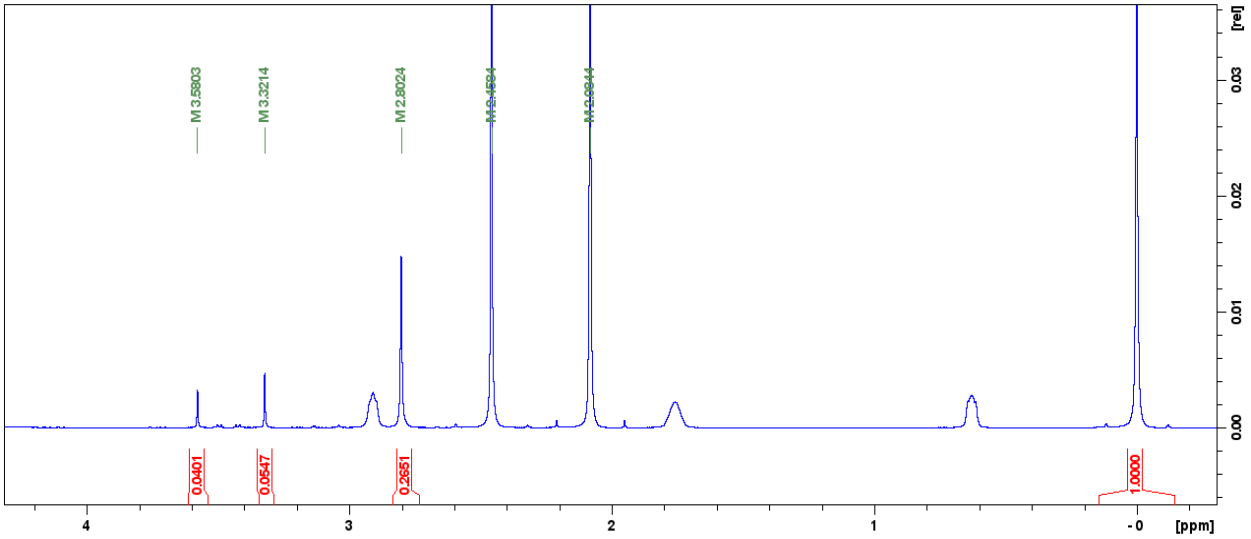

Figure 3-16. ^{1}H-NMR spectrum of the mixture of Ni(III) with excess MSA in D_2O after reacting 415 mins.

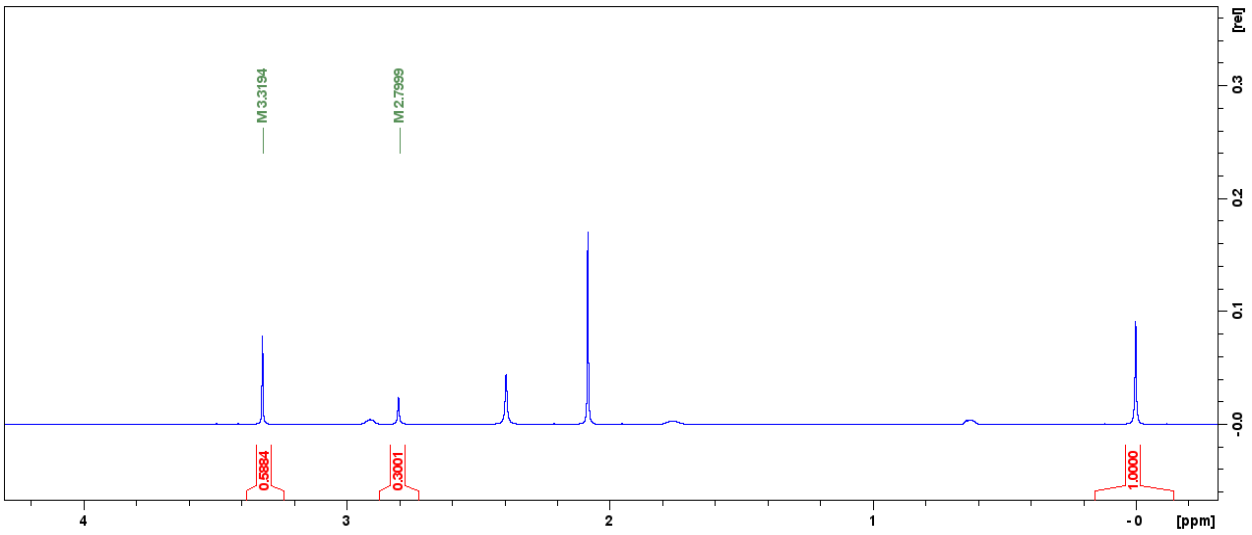

Figure 3-17. ^{1}H-NMR spectrum of the mixture of Ni(III) with excess MSA in D_2O after reacting 4 days.

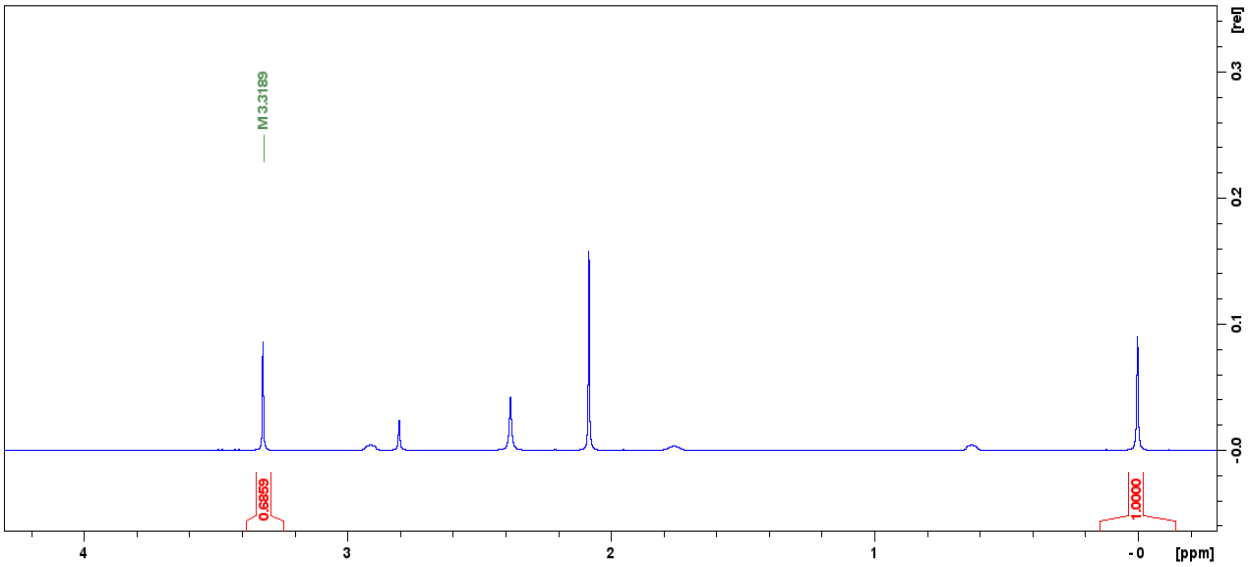

Figure 3-18. ^{1}H-NMR spectrum of the mixture of Ni(III) with excess MSA in D_2O after reacting 5 days.

Calculation on the yield of the products based on Figure 3-14-Figure 3-18:

In the mixture: $[\mathrm{MSA}]_{\mathrm{initial}} = 16.80\ \mathrm{mM}$

After reacting: $[\mathrm{MSA}]_{\mathrm{final}} = 11.28\ \mathrm{mM}$

$$\Delta[\mathrm{MSA}] = 16.80 - 11.28\ \mathrm{mM} = 5.52\ \mathrm{mM} \qquad \text{Eq. 3-15}$$

$$[\mathrm{CH_3SO_3^-}]_{\mathrm{total}} = [\mathrm{CH_3SO_3^-}\ \text{at 2.80 ppm}] + [\text{intermediate at 3.58 ppm}] = 4.83\ \mathrm{mM} \qquad \text{Eq. 3-16}$$

Ratio of the consumed [MSA] and $[CH_3SO_3^-]_{total} = \frac{5.52}{4.83} = 1.1$

The result indicates a complete conversion from methanesulfinic acid to methanesulfonic acid, which is consistent with the stoichiometric study.

NMR kinetics of the decomposition of the intermediate at 3.58 ppm and the formation of $CH_3SO_3^-$ were evaluated by plotting the integral against time and fitting the data with first-order rate law. The result is shown below.

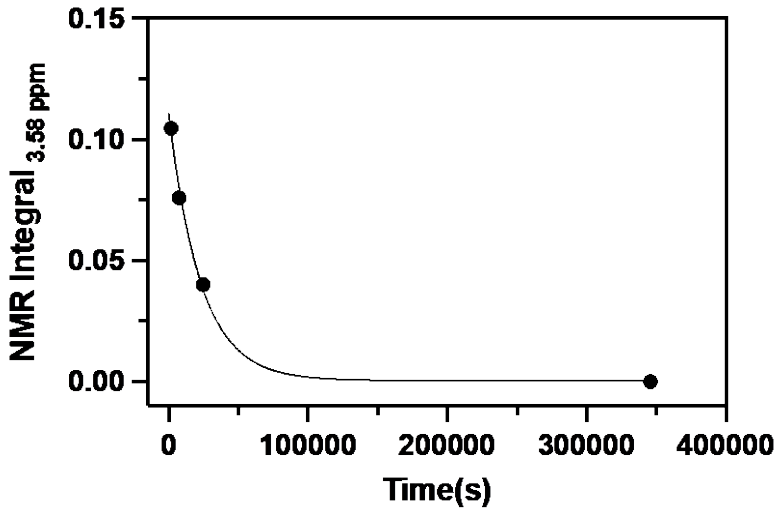

Figure 3-19. ^{1}H-NMR kinetics of the degradation of the intermediate (δ 3.58 ppm). Conditions: $[MSA]_0$ = 16.80 mM, $[Ni(III)]_0$ = 4.67 mM, pH 2.24.

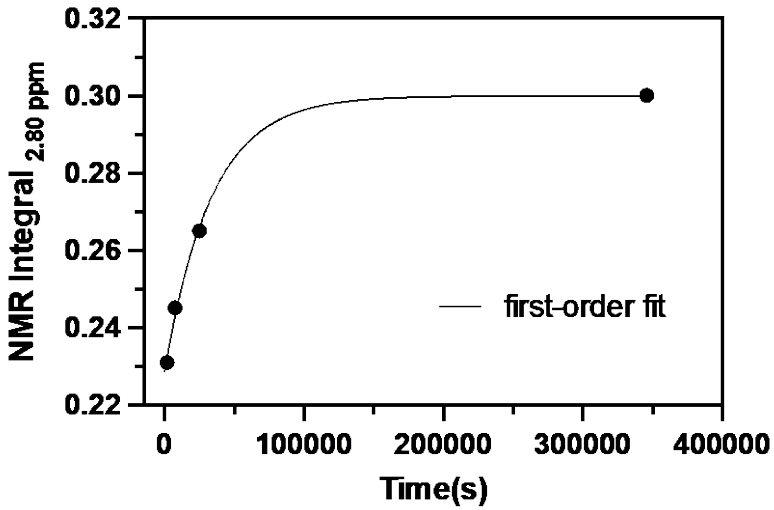

Figure 3-20. ^{1}H-NMR kinetics of the formation of $CH_3SO_3^-$ (δ 2.80 ppm). Conditions: $[MSA]_0$ = 16.80 mM, $[Ni(III)]_0$ = 4.67 mM, pH 2.24.

Table 3-3. Kinetic data for determining the fate of the intermediate.

	rate constant, s^{-1}	**$t_{1/2}$, s**
Intermediate	4.3×10^{-5}	2.3×10^{4}
$\mathbf{CH_3SO_3^-}$	3.0×10^{-5}	1.6×10^{4}

The rate constant of the decay of the intermediate (δ 3.58 ppm) is comparable to the formation of $CH_3SO_3^-$. We can thus infer that the unknown is a S-containing intermediate which eventually converts to the sulfonic acid.

To better characterize the unknown peaks shown in the NMR data from the reaction mixture, ^{1}H-NMR spectrum of 1,4,7-triazacyclononane (tacn) in D_2O was collected. A singlet at 3.35 ppm from the compound can be identified from the spectrum in Figure 3-21.

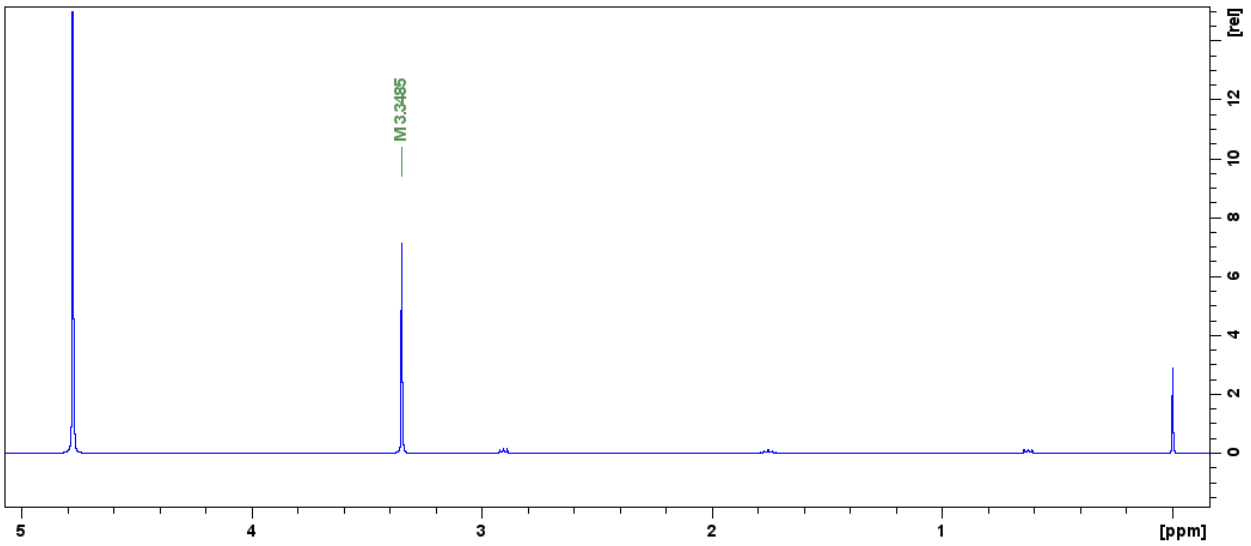

Figure 3-21. ^{1}H-NMR spectrum of 14.1 mM 1,4,7-tacn in D_2O with DSS as a reference.

Later, the product solution was spiked with tacn. The peak at 3.3 ppm become more intense in the resulting spectrum, suggesting that the ligand (tacn) of the Ni-complex might be released from the reaction.

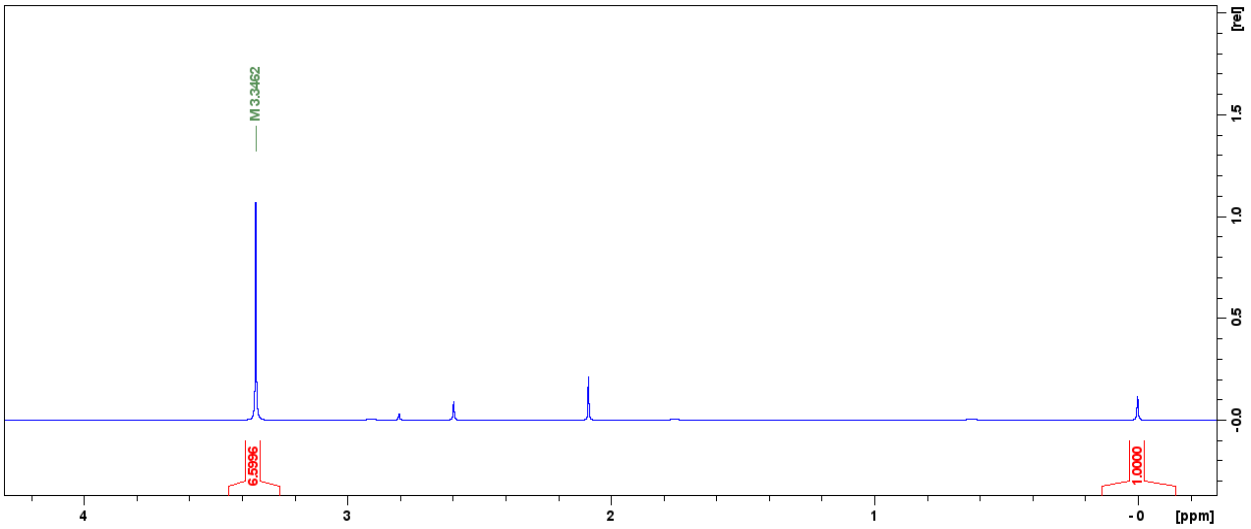

Figure 3-22. ^{1}H-NMR spectrum of 1,4,7-tacn spiking on the mixture of Ni(III) with excess MSA in D_2O.

To further confirm the presence of the ligand (tacn) and get a better understanding of the peak at 3.33 pm, ^{13}C-NMR experiments were conducted.

3.3.3.1 ^{13}C-NMR analysis

The solution of Ni(III) and MSA at pH 2 (acidic acid) in D_2O was purged with argon for 30 minutes before mixing in a NMR tube. Later, the mixture was allowed to react overnight under anerobic conditions. ^{13}C-NMR spectrum was taken (1053 scans, 500 MHz) and displayed below. (Note that the peak shape in Figure 3-23 might be affected by a poor shim.) Next, 30 mg tacn was added to Ni(III)/MSA mixture with the addition of 0.1 mL D_2O. The resulting ^{13}C-NMR spectrum (350 scans, 500 MHz) with tacn spiked is shown in Figure 3-24. The peak of MSA and tacn slightly shifted due to the pH change of the solution. It turns out that there is no additional peak arising, which confirms the singlet at 3.32 ppm in ^{1}H-NMR is from tacn.

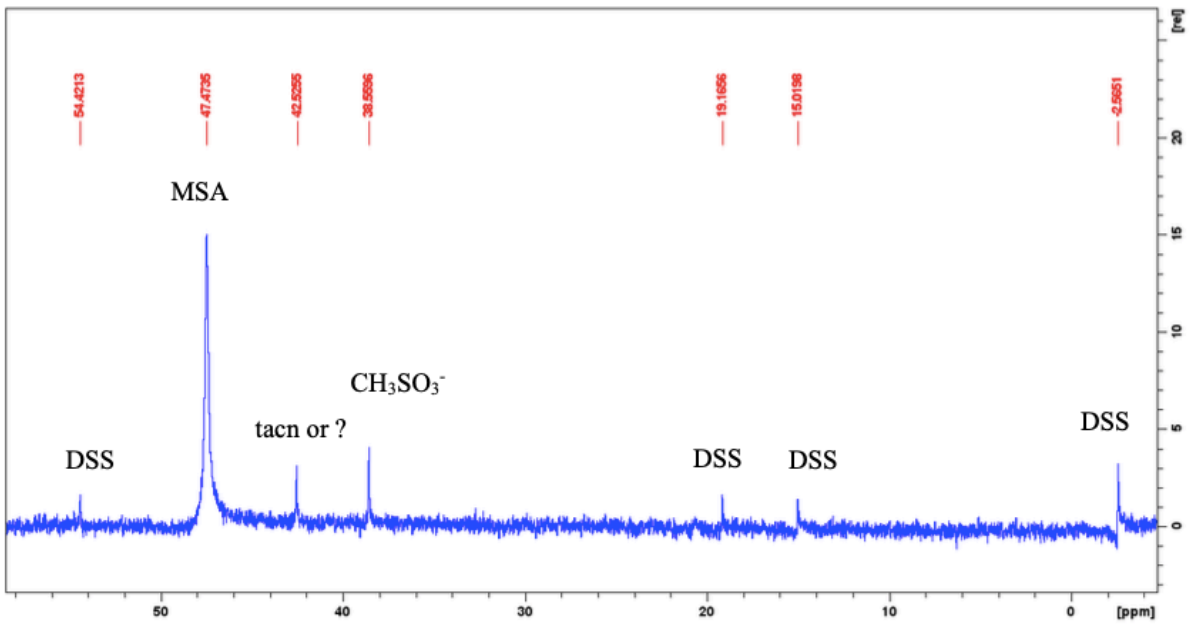

Figure 3-23. ^{13}C-NMR spectrum of the mixture of Ni(III) with excess MSA in D_2O after reacting overnight with DSS as reference. Conditions: [MSA] = 0.4 M, [Ni(III)] = 53.3 mM.

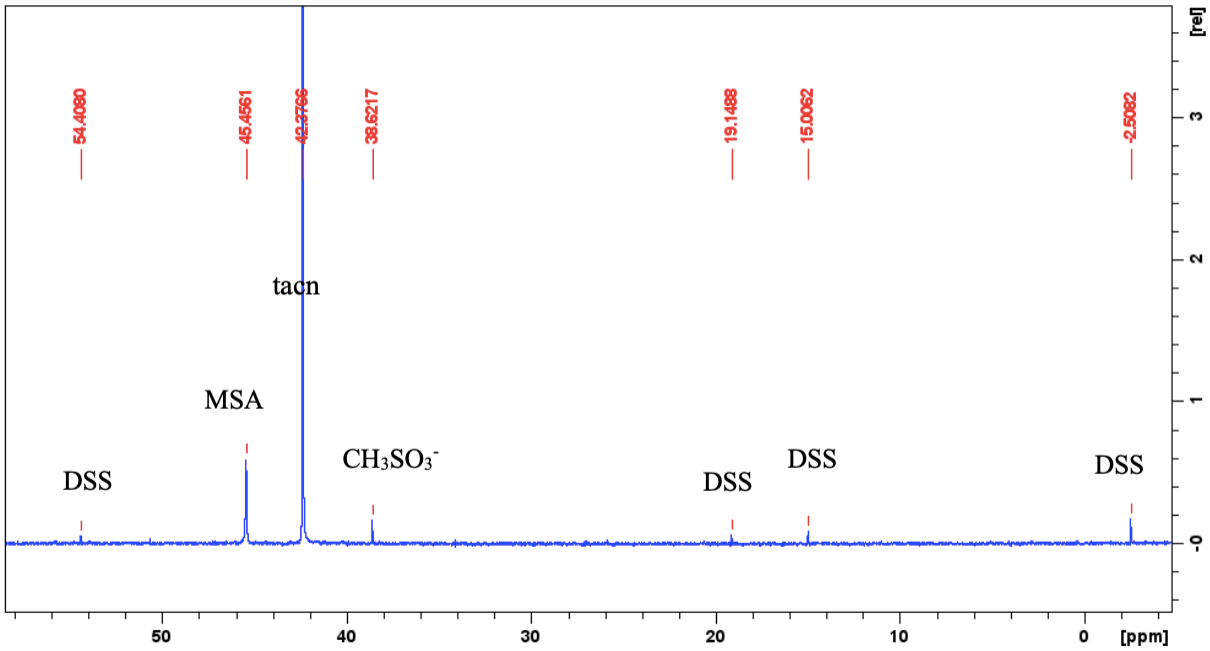

Figure 3-24. ^{13}C-NMR spectrum of the mixture of Ni(III) with excess MSA in D_2O, tacn spiked.

In order to check the formation of other Ni complexes, ^{1}H-NMR of Ni(III)/MSA solution with extra tacn at pH 2.2 (HOAc) was obtained in Figure 3-25. The mixture was afterward alkalized by adding 1 drop of 1M NaOH and followed by the addition of NaCN. After that, ^{1}H-NMR spectrum was recorded and displayed in Figure 3-26. The peak of MSA at 2.4 ppm, HOAc at 2.0 ppm and tacn at 3.3 ppm shifted because of the pH change in the system. As a result, the amount of MSA, $CH_3SO_3^-$ remains constant, and there is no special Ni-complex formed that can be detected from NMR.

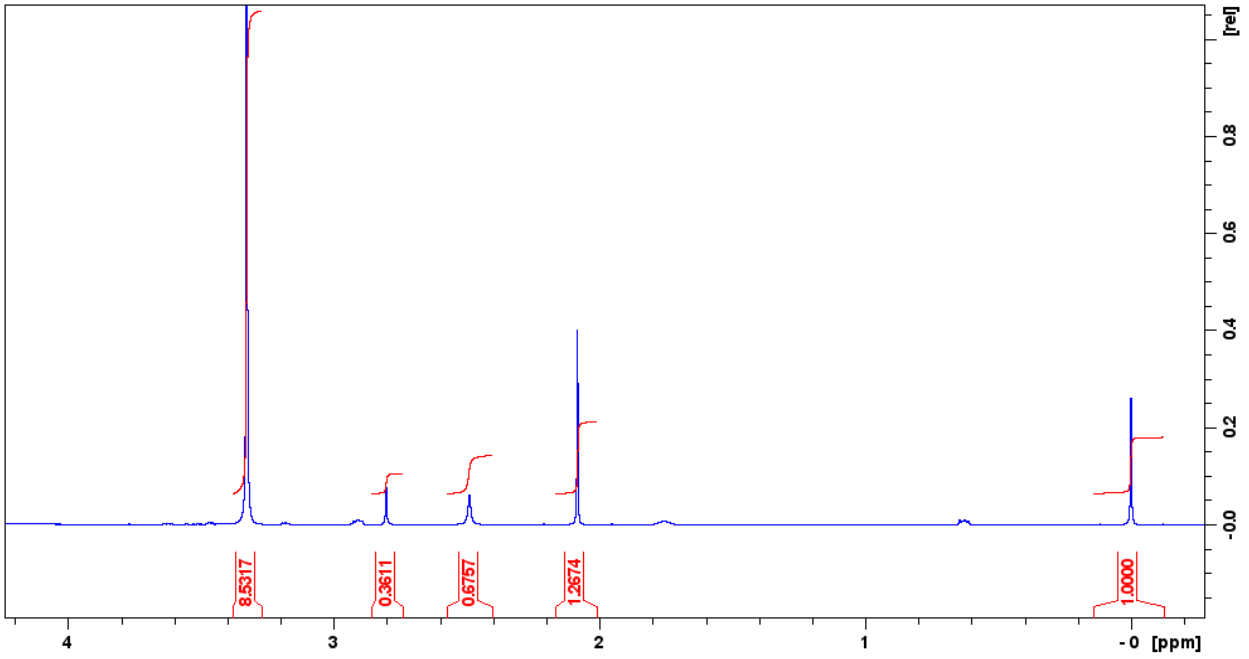

Figure 3-25. ^{1}H-NMR spectrum of the mixture of Ni(III) with excess MSA and tacn in D_2O.

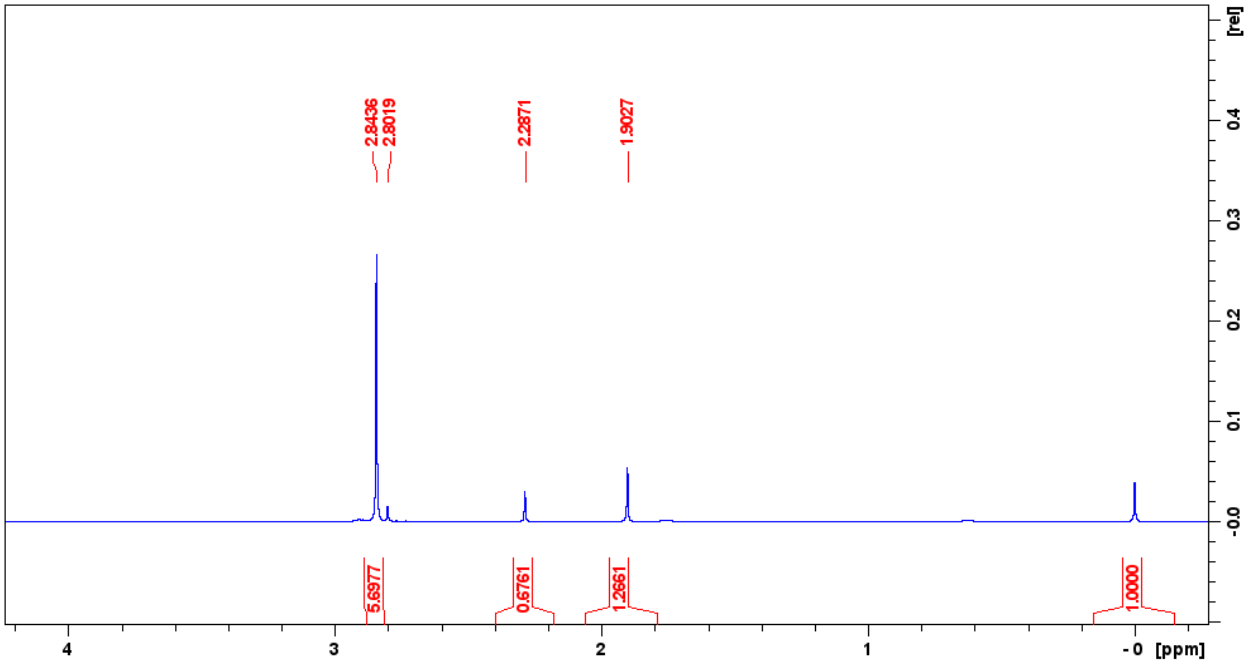

Figure 3-26. ^{1}H-NMR after the addition of NaCN to the mixture of Ni(III)/MSA in D_2O.

To check the stability of $[Ni(tacn)_2]^{2+}$ in acid media, the NMR experiment was carried out at pH 2.2 with acetic acid in D_2O with DSS as a reference.

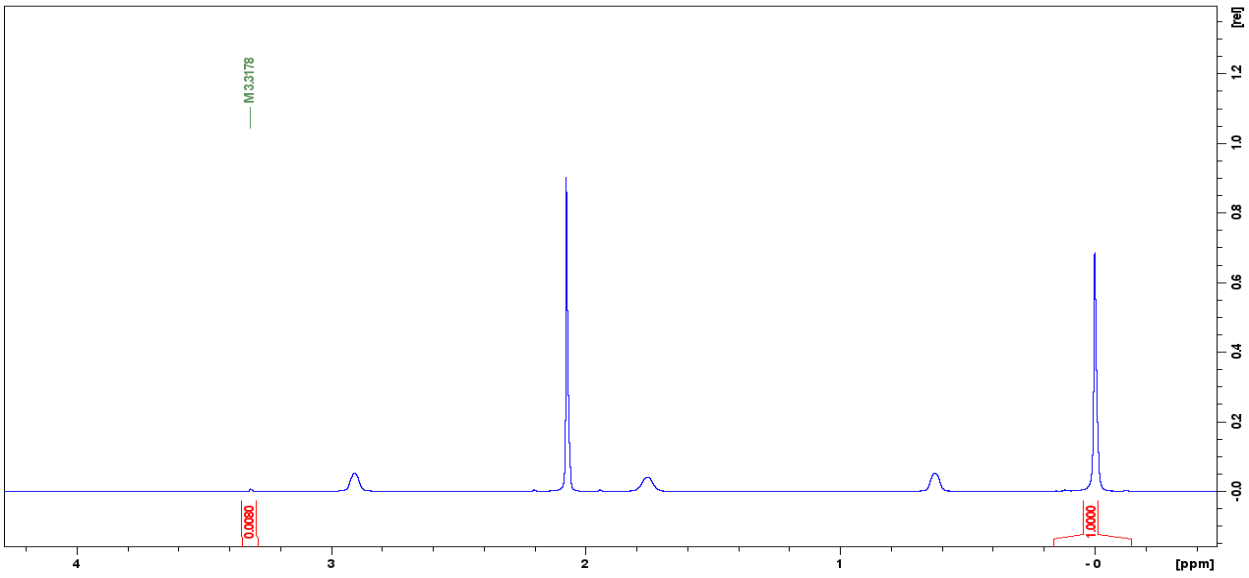

Figure 3-27. ^{1}H-NMR spectrum of 9.94 mM Ni(II) in acidic media after 20 minutes dissolving.

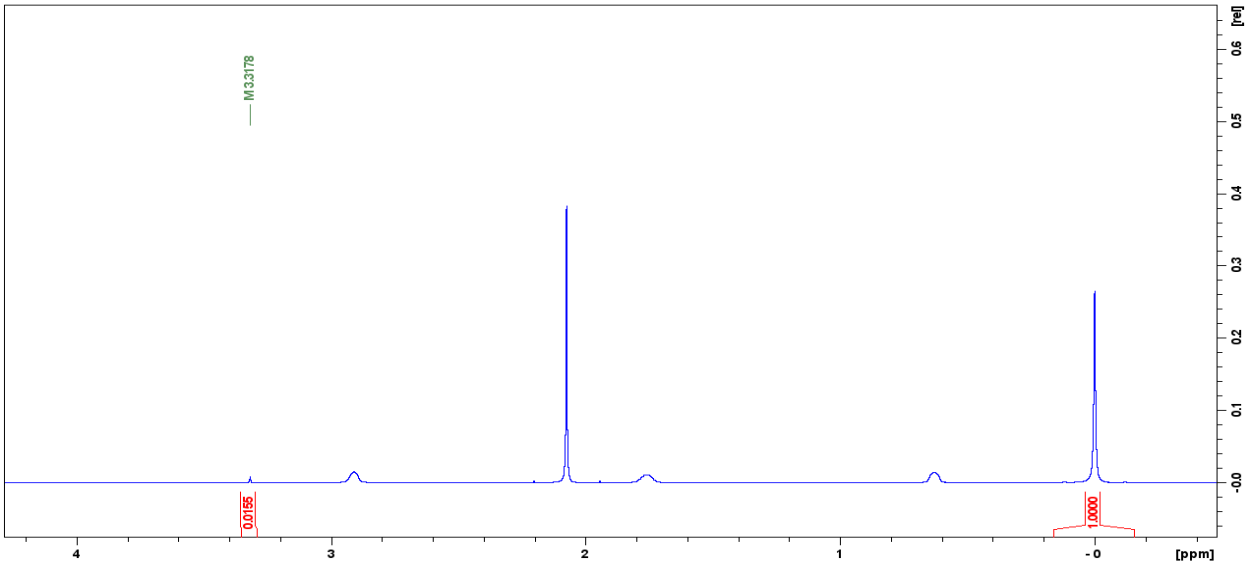

Figure 3-28. ^{1}H-NMR spectrum of Ni(II) in acidic media after 420 minutes dissolving

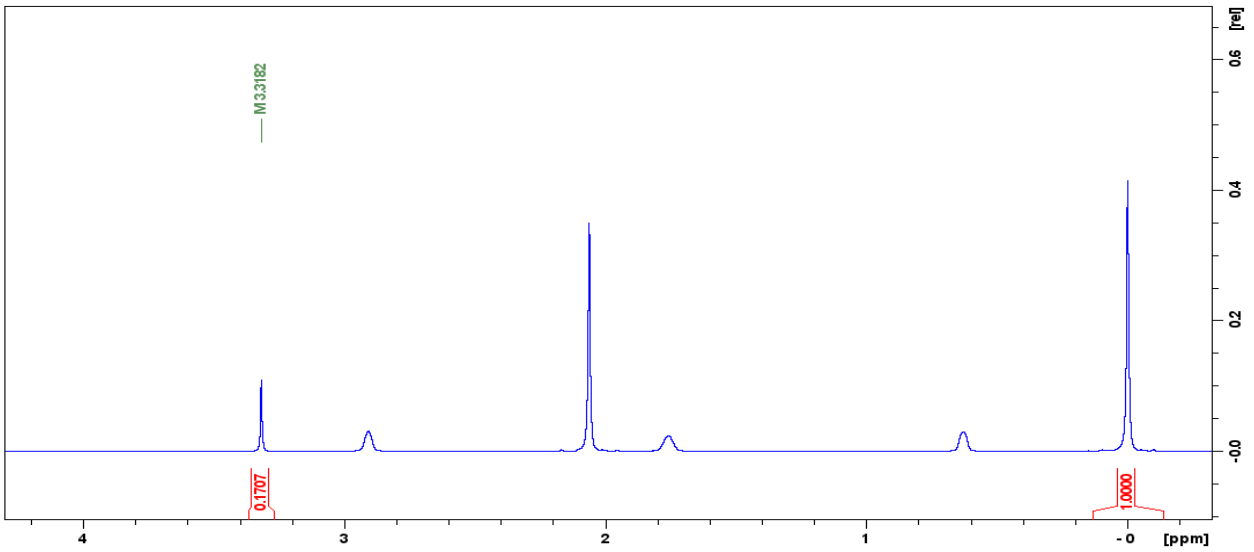

Figure 3-29. ^{1}H-NMR spectrum of Ni(II) in acidic media after 10 days.

In the same media, the degradation of $[Ni(tacn)_2]^{2+}$ and the production of tacn from Ni(III)/MSA mixture are kinetically established by getting the rate constants from the NMR integral at 3.32 ppm. Based on the kinetic data given in Table 3-4, the rate of the decay of $[Ni(tacn)_2]^{2+}$ is found to be comparable as that of the production of 1,4,7-tacn from the reaction. And therefore, it implies that tacn is formed from the decomposition of $[Ni(tacn)_2]^{2+}$ of our reaction mixture. The observed behavior of the NMR kinetics for these two solutions as shown in Figure 3-30 will be explained later in the discussion section.

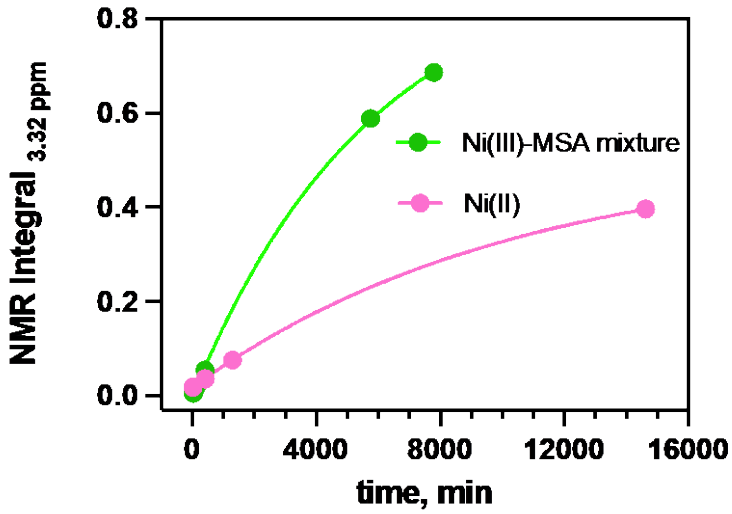

Figure 3-30. Kinetics of the decomposition of $[Ni(tacn)_2]^{2+}$ and the formation of 1,4,7-tacn from the reaction mixture. Conditions: Green: [MSA] = 16.80 mM, [Ni(III)] = 4.67 mM, pH 2.24; Red: $[Ni(tacn)_2]^{2+}$ = 9.92 mM, pH 2.2.

Table 3-4. Kinetic data of the formation of tacn.

Sample	k, s^{-1}	$t_{1/2}$, s
Ni(III)/MSA	2.88×10^{-6}	4.3×10^{5}
$\mathbf{[Ni(tacn)_2]^{2+}}$	1.60×10^{-6}	2.4×10^{5}

As it was confirmed that tacn was a product of the reaction mixture, free Ni(II) ion is therefore expected to be present in the solution as well. To detect the unbonded Ni(II), 4.24 mM $[Ni(tacn)_2]^{3+}$ was allowed to react with 20.0 mM MSA at pH 2.6 with N_2 purged for 5 days. The mixture solution was later alkalized with NaOH. UV-vis spectrum of the product solution was recorded and shown in the figure below. Later, a portion of the solution was separated and mixed with 0.074 mmole NaCN. UV-Vis spectrum of the resulting solution was taken after dilution to determine the formation of $[Ni(II)(CN)_4]^{2-}$. As a result, three peaks (at 267 nm, 285 nm, and 310 nm) can be detected from the spectrum, which are consistent with the spectral feature of

$[Ni(II)(CN)_4]^{2-}$ reported in literature [14]. ($\varepsilon_{267} = 1.16 \times 10^4\ M^{-1}\ cm^{-1}, \varepsilon_{285} = 4630\ M^{-1}\ cm^{-1}, \varepsilon_{310} = 750\ M^{-1}\ cm^{-1}$)

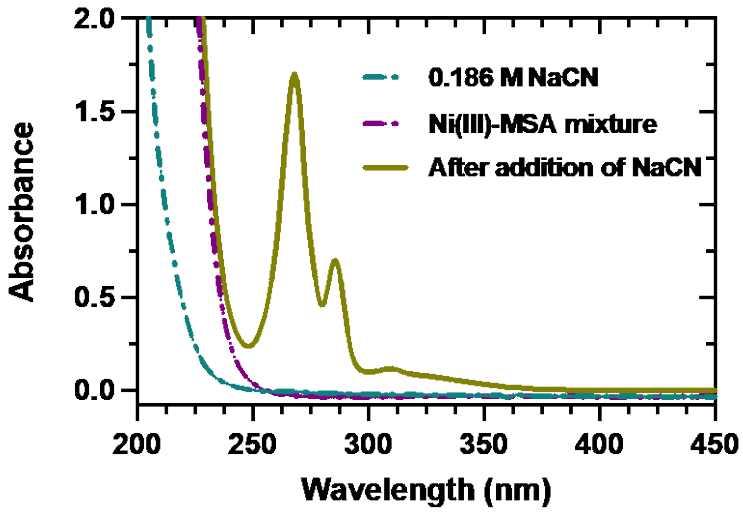

Figure 3-31. UV-vis spectra for determining the presence of free Ni(II).

Calculation on the yield of free Ni^{2+} from the decomposition of Ni-complex:

In the mixture: $[[Ni(III)(tacn)_2]^{3+}]_0 = 4.24$ mM; $[MSA]_0 = 20.0$ mM

After the addition of NaCN:

$$[Ni(II)(CN)_4]^{2-} = 1.20\text{mM}\ (\varepsilon_{267} = 1.16 \times 10^4\ M^{-1}\ cm^{-1}) \quad \text{Eq. 3-17}$$

$$\text{unbonded Ni(II) from Ni(III)} - \text{MSA mixture} = 1.20\ \text{mM} \quad \text{Eq. 3-18}$$

$$\text{Yield of the } Ni^{2+} = \frac{1.20}{4.24} \times 100 = 28.3\% \quad \text{Eq. 3-19}$$

To confirm the yield of the products from NMR with a better oxygen exclusion, both $[Ni(tacn)_2]^{3+}$ in acetic acid and MSA solutions were purged with argon for 50 minutes before mixing. A solution of $[Ni(tacn)_2]^{3+}$/MSA mixture was later prepared in a glove box and allowed to react for 1 hour. ^{1}H-NMR spectrum was obtained in D_2O with DSS as a reference.

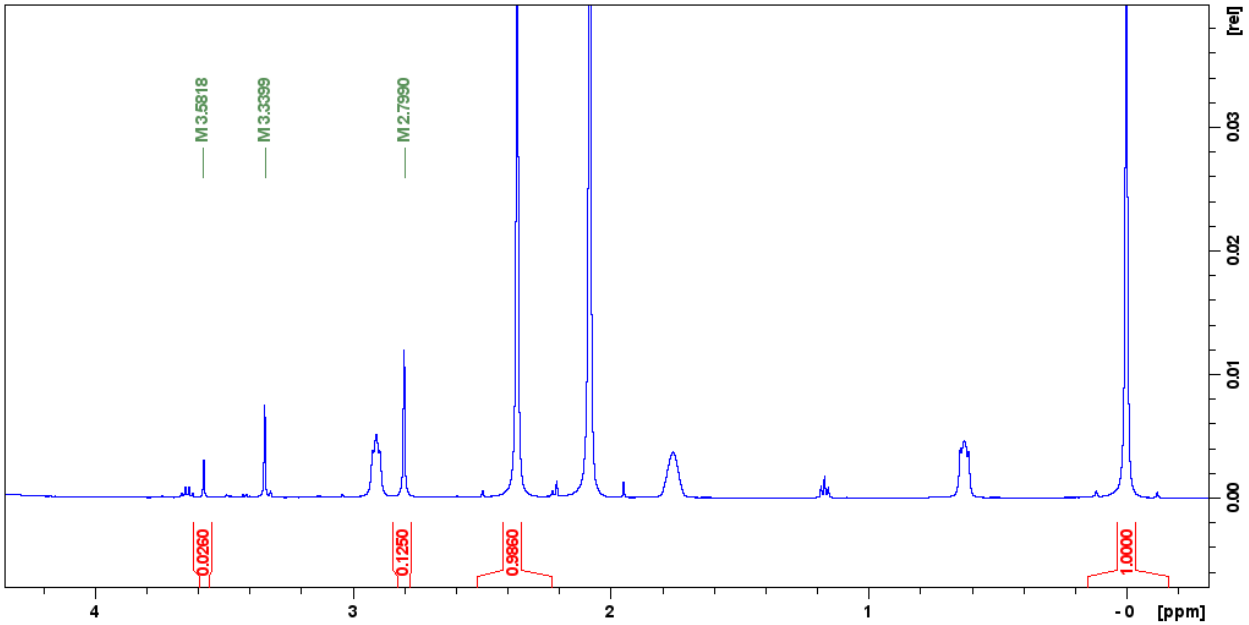

Figure 3-32. ^{1}H-NMR spectrum of the mixture of Ni(III) with excess MSA in D_2O after reacting 60 minutes. Conditions: [MSA] = 23.86 mM, [Ni(III)] = 4.56 mM.

$$[\mathrm{MSA}]_{\mathrm{initial}} = 23.86\ \mathrm{mM};\ [\mathrm{MSA}]_{\mathrm{final}} = 21.14\ \mathrm{mM} \quad \text{Eq. 3-20}$$

$$\Delta[\mathrm{MSA}] = 24.06 - 21.09\ \mathrm{mM} = 2.72\ \mathrm{mM} \quad \text{Eq. 3-21}$$

$$[\mathrm{CH_3SO_3^-}]_{\mathrm{total}} = [\mathrm{CH_3SO_3^-}\ \text{at 2.80 ppm}] + [\text{intermediate at 3.58 ppm}] = 2.74\ \mathrm{mM} \quad \text{Eq. 3-22}$$

$$\text{consumed [MSA]} / [\mathrm{CH_3SO_3^-}]_{\mathrm{total}} = \frac{2.72}{2.74} = 0.99 \quad \text{Eq. 3-23}$$

$$[\mathrm{Ni(tacn)_2}]^{3+}]/\ \text{consumed [MSA]} = \frac{4.56}{2.72} = 1.68 \quad \text{Eq. 3-24}$$

3.3.4 Oxygen effect on the intermediate decomposition

As for the unknown intermediate which has δ at 3.58 ppm in ^{1}H-NMR, oxygen is suspected to be a cause for its formation. Taking this into consideration, ^{1}H-NMR experiment was done by involving different amount of O_2 to the reaction solutions. All of the three samples included 23 mM MSA, 2.8 mM Ni(III), were dissolved in HOAc/ D_2O with DSS as reference. The solutions were separately treated with different gases including argon, air, and oxygen before mixing. Then

the reactants were mixed in the NMR tubes and allowed to react for 30 minutes. The spectra under each condition were recorded and displayed below.

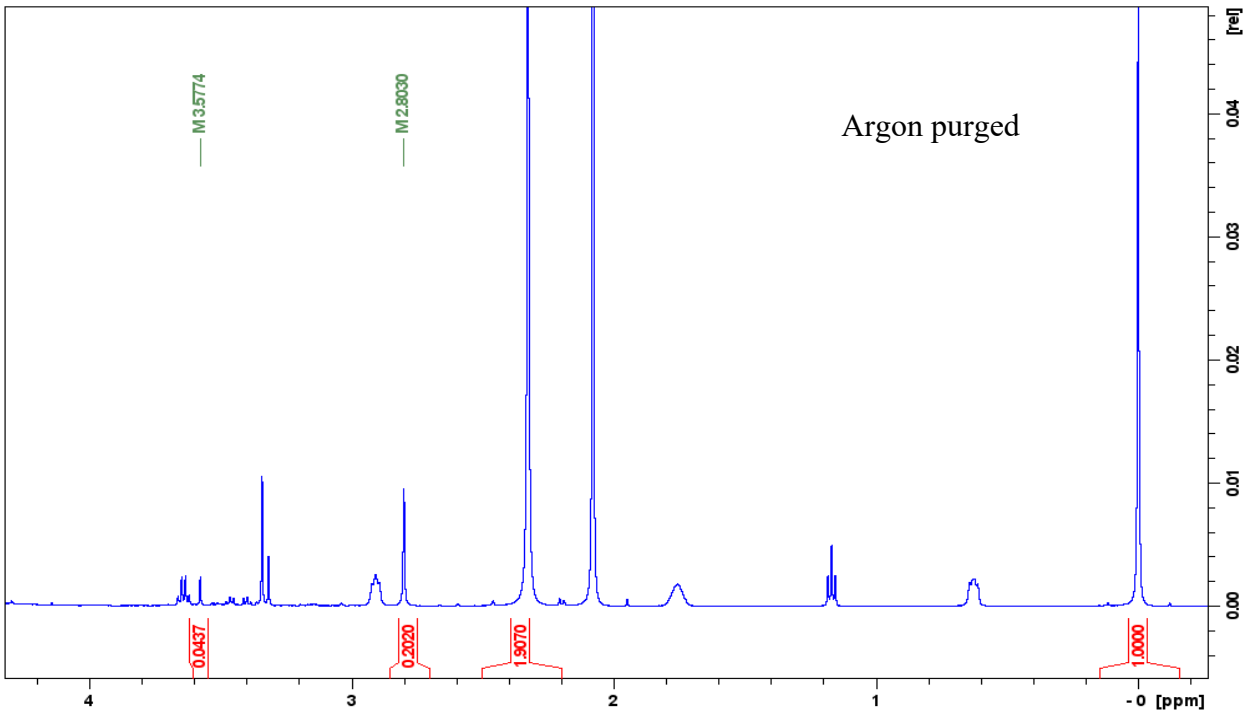

Figure 3-33. ^{1}H-NMR spectrum of the mixture of Ni(III) with excess MSA in D_2O with argon purged.

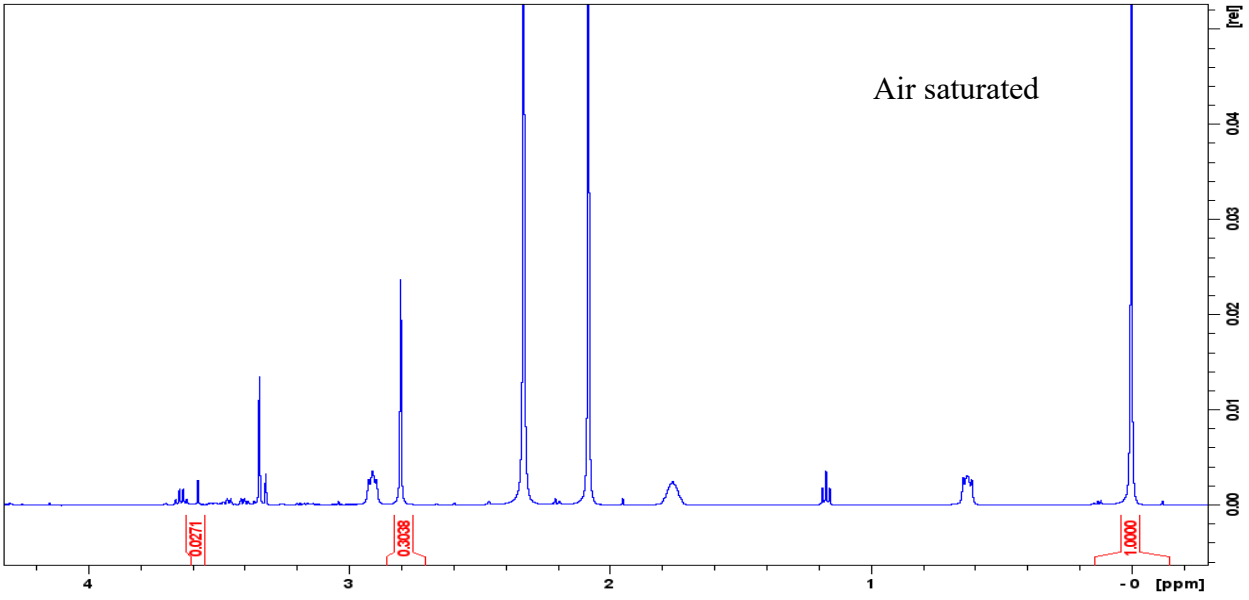

Figure 3-34. ^{1}H-NMR spectrum of the mixture of Ni(III) with excess MSA in D_2O with air saturated.

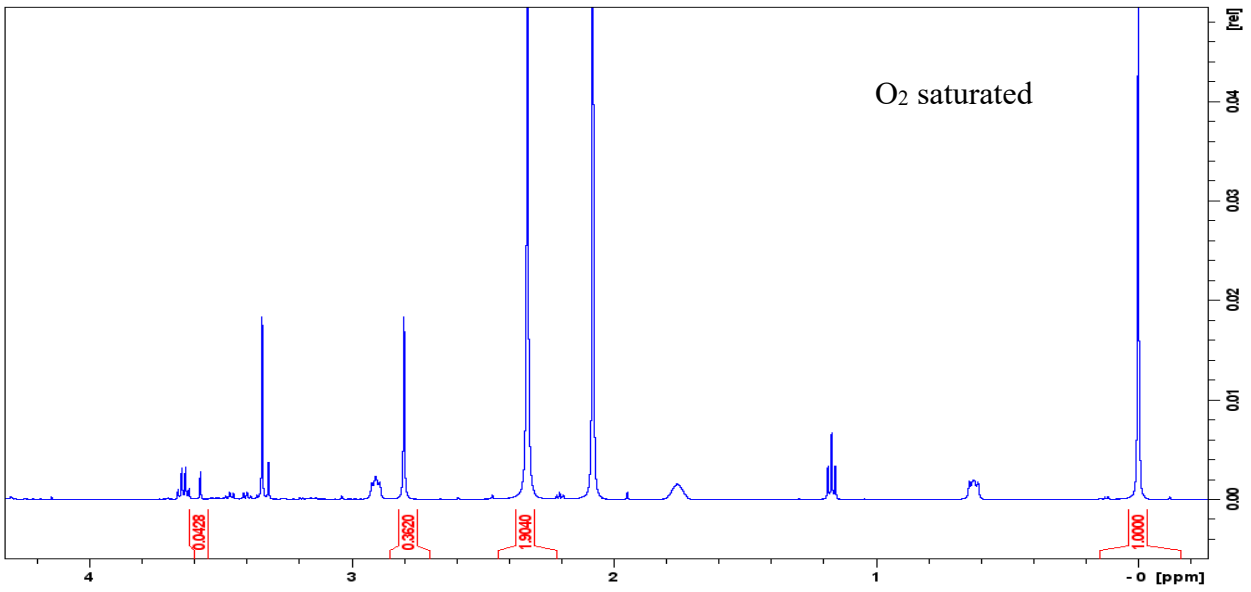

Figure 3-35. ^{1}H-NMR spectrum of the mixture of Ni(III) with excess MSA in D_2O with O_2 saturated.

The formation ratios (Δ[intermediate at 3.58 ppm]/ $\Delta[CH_3SO_3^-]$) based on the NMR integral are: 21.6% with argon purged; 8.9% with air saturated and 11.8% with oxygen purged. The result suggests that the intermediate is not quite oxygen sensitive.

3.3.5 Yield of Ni(II) from Ni(III)/MSA reaction

The yield of $[Ni(tacn)_2]^{2+}$ was investigated by oxidizing MSA with $[Ni(tacn)_2]^{3+}$ initially, followed by the re-oxidation of the mixture using excess sodium persulfate to convert of $[Ni(tacn)_2]^{2+}$complexes back to $[Ni(tacn)_2]^{3+}$. In the following experiments, $[Ni(tacn)_2]^{3+}$ and MSA were prepared in pH 1.9-2.0 acids and purged with gases accordingly. Acid effect on the yield of the product was examined by adjusting pH using HCl and $HClO_4$. The UV-vis spectra of $[Ni(tacn)_2]^{3+}$ solutions were taken prior to the reactions. MSA was added to $[Ni(tacn)_2]^{3+}$ solution afterward and allowed to react completely. After that, large amount of $Na_2S_2O_8$ was mixed into the reaction solution to re-produce $[Ni(tacn)_2]^{3+}$. The resulting spectra were obtained after the absorbances reached their maximum and became stable.

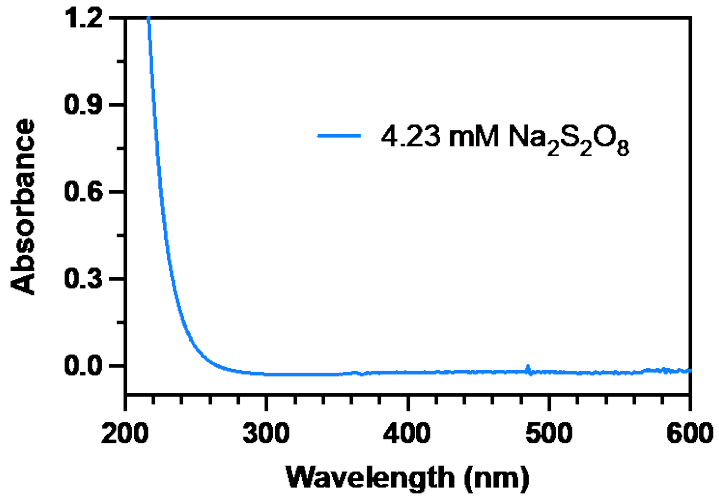

Figure 3-36. UV-vis spectrum of 4.23 mM $Na_2S_2O_8$ in 0.02 M $HClO_4$.

3.3.5.1 pH adjusted by $HClO_4$

The following UV-Vis experiments were carried out by changing the pH media or the type of gas saturated in the reaction mixture. The experimental conditions are listed below each figure.

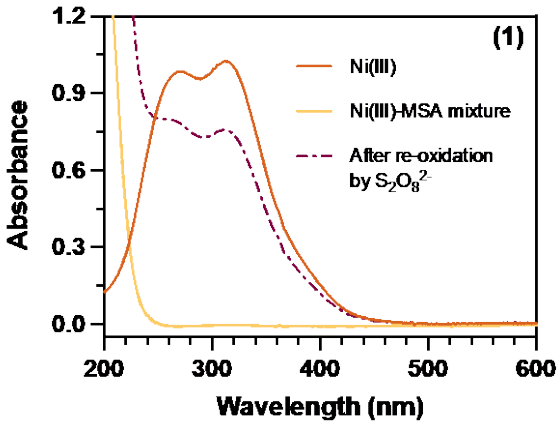

1) Argon purged:

$[MSA]_0$ = 0.15 mM, $[Ni(III)]_0$ = 0.10 mM, $[NaS_2O_8]_0$ = 7.53 mM, pH 2.0

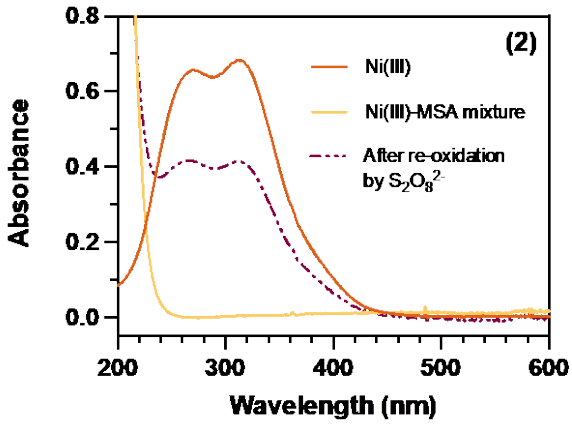

2) Argon purged + glovebox:

$[MSA]_0$ = 0.30 mM, $[Ni(III)]_0$ = 0.07 mM, $[NaS_2O_8]_0$ = 1.54 mM, pH 2.0

3.3.5.2 pH adjusted by HCl

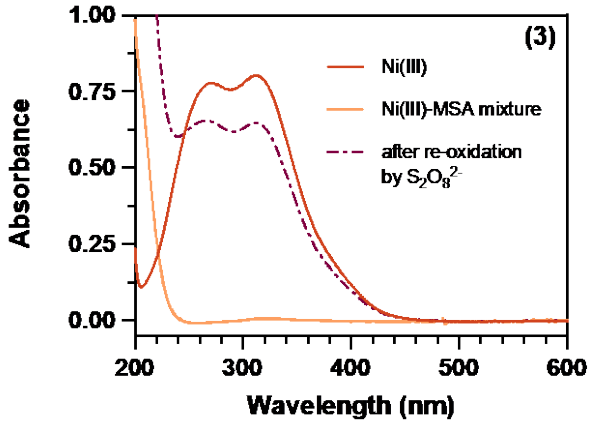

3) Argon purged:

$[MSA]_0$ = 0.043 mM, $[Ni(III)]_0$ = 0.08 mM, $[NaS_2O_8]_0$ = 3.85 mM, pH 1.9

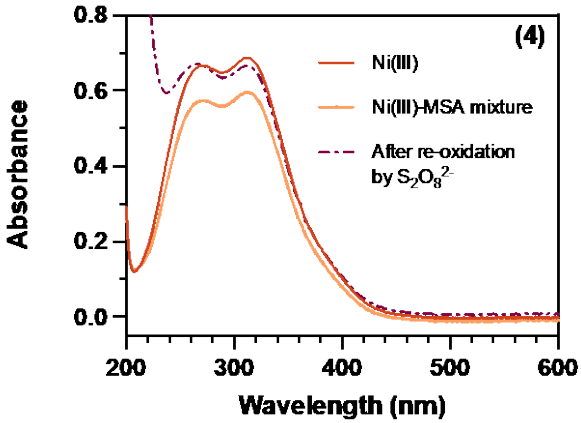

4) O_2 saturated:

$[MSA]_0$ = 0.052 mM, $[Ni(III)]_0$ = 0.07 mM, $[NaS_2O_8]_0$ = 3.86 mM, pH 1.9

Based on the condition **(2)** where the experiment was conducted under the best O_2 exclusion, the yield of $[Ni(tacn)_2]^{2+}$ was calculated to be 60.5% of the initial Ni(III).

As it was shown above, it is unusual that Ni(III) was not depleted after mixing with stoichiometric excess of MSA when the solution was saturated with O_2. Questions can thus be addressed upon whether Ni(III) loss was due to the reaction with MSA, or how much MSA was consumed from the system. To get the answers, ^{1}H-NMR studies of the reaction under the similar conditions were performed by preparing the reaction solutions in HOAc-D_2O with DSS as reference. At first, MSA concentration and the amount of methanesulfinate in the solution were measured by obtaining the spectrum after purging O_2. $[Ni(tacn)_2]^{3+}$ was added to the solution subsequently and allowed to react for 1 hour before taking NMR. The spectrum in Figure 3-37 shows that MSA reacted completely. Given that the amount of Ni(III) is stoichiometric less than MSA, it is reasonable to believe that part of the MSA was consumed by Ni(III), and the rest was

oxidized by O_2. The latter reaction, however, is likely to be catalyzed by Ni(II) ion released from the Ni(II)/MSA reaction.

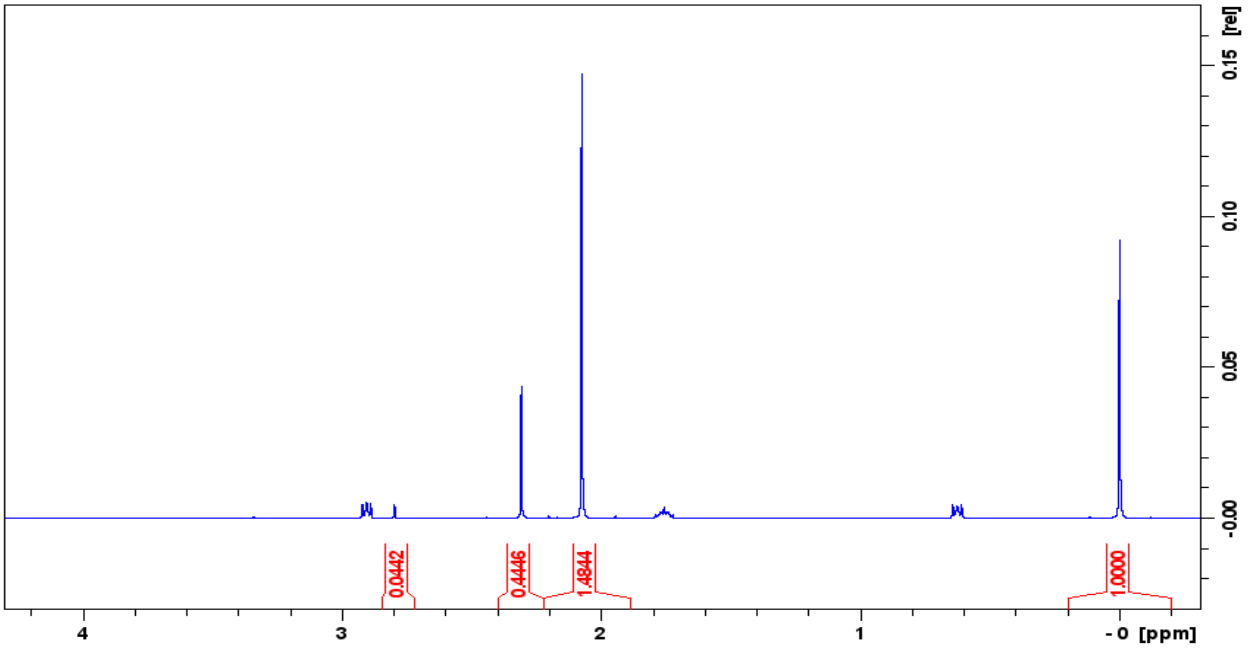

Figure 3-37. ^{1}H-NMR spectrum of MSA in HOAc-D_2O with O_2 saturated.

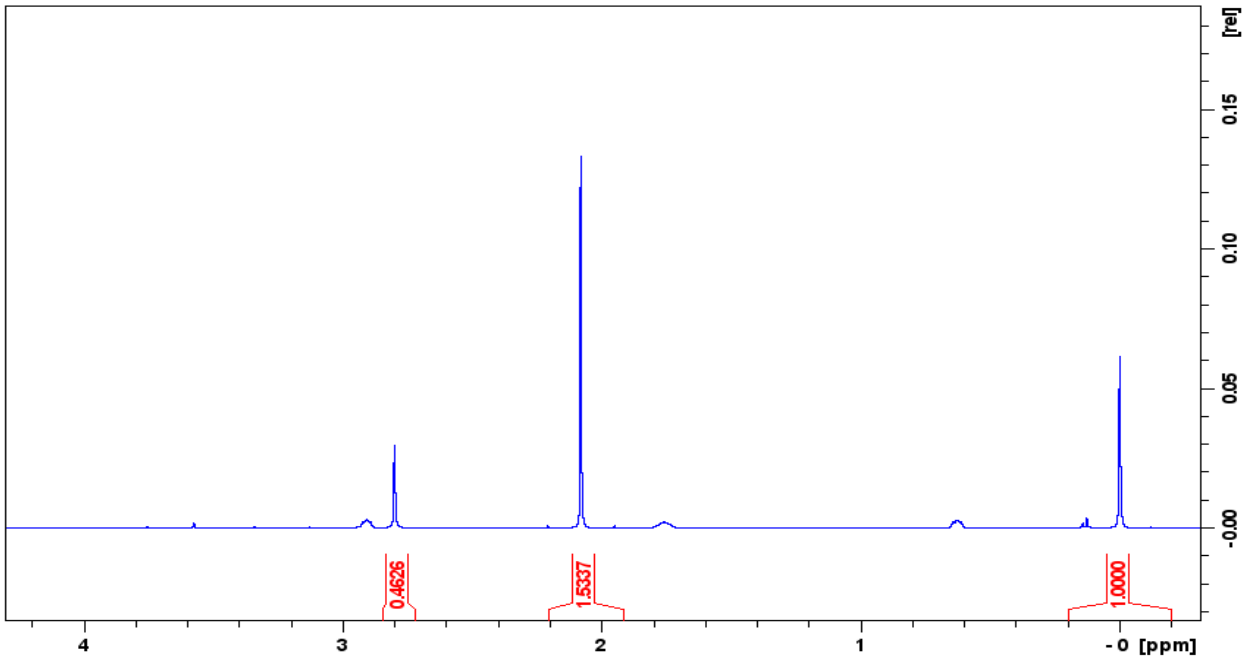

Figure 3-38. ^{1}H-NMR spectrum of Ni(III)/MSA mixture in HOAc-D_2O with O_2 saturated.

3.4 Discussion

3.4.1 Mechanism Scheme

With the evidence collected from the reaction kinetics, titration, NMR and UV-vis, a stoichiometric mechanism is proposed as,

$$[\mathrm{Ni(tacn)_2}]^{3+} + \mathrm{CH_3SO_2^-} \rightleftharpoons [\mathrm{Ni(tacn)_2}]^{2+} + \mathrm{CH_3SO_2^{\bullet}} \qquad k_1, k_{-1} \qquad \text{Eq. 3-25}$$

$$[\mathrm{Ni(tacn)_2}]^{3+} + \mathrm{CH_3SO_2^{\bullet}} \rightarrow [(\mathrm{Ni^{II}-tacn})(\mathrm{tacn-CH_3SO_2})]^{3+} \quad k_2 \qquad \text{Eq. 3-26}$$

$$[(\mathrm{Ni^{II}-tacn})(\mathrm{tacn-CH_3SO_2})]^{3+} + \mathrm{H_2O} \rightarrow [\mathrm{Ni^{II}-tacn}]^{2+} + [\mathrm{tacn-H}]^{+} + \mathrm{CH_3SO_3^-} + \mathrm{H^+} \quad k_3 \qquad \text{Eq. 3-27}$$

$$[\mathrm{Ni^{II}-tacn}]^{2+} \rightleftharpoons [\mathrm{Ni^{II}}]^{2+} + \mathrm{tacn} \qquad k_4, k_{-4}, K_4 \qquad \text{Eq. 3-28}$$

Here, k_3 is determined from the formation of $\mathrm{CH_3SO_3^-}$ in Figure 3-20 with a value of $3.0 \times 10^{-5}\ \mathrm{s^{-1}}$. k_4 is obtained from Figure 3-30 with a value of $2.9 \times 10^{-6}\ \mathrm{s^{-1}}$. Based on the reported value of K_4 $(= 10^{-16.2})$ from a literature [16], k_{-4} $\left(= \frac{k_4}{K_4}\right)$ can thus be calculated to be $4.6 \times 10^{10}\ \mathrm{M^{-1}\ s^{-1}}$. As discussed before, the NMR kinetics for Eq. 3-28 indicates that the ligand, tacn, is released from the decomposition of $[\mathrm{Ni(tacn)_2}]^{2+}$. Given that the reaction mixture produces a proton in Eq. 3-27, plus the rate constant is one magnitude faster compared with the formation of the ligand from Eq. 3-28, tacn should therefore be present mostly in its acid form. Consequently, the equilibrium of Eq. 3-28 will shift to right-side to produce more deprotonated tacn. Based on this fact, a rapid formation of tacn-H can be expected, and it was also evident from the NMR kinetic study. Followed by that is a slower process of the releasing of tacn-H, which can be predicted as well. The yield of $[\mathrm{Ni^{II}-tacn}]^{2+}$ therefore, is calculated with a value of 39.5 % from the subtraction of $[\mathrm{Ni(tacn)_2}]^{2+}$ from the total Ni(III).

3.4.2 Determination of Kinetic Coefficients

The rate law for the reaction under pH 3-5 can be expressed as,

$$-\frac{\mathrm{d}[\mathrm{Ni^{III}}]}{\mathrm{dt}} = \frac{k[\mathrm{Ni^{III}}]^2[\mathrm{CH_3SO_2^-}]}{[\mathrm{Ni^{II}}]} \quad \text{Eq. 3-29}$$

When steady-state approximation is applied to the radical $\mathrm{CH_3SO_2^{\bullet}}$

$$\frac{\mathrm{d}[\mathrm{CH_3SO_2^{\bullet}}]}{\mathrm{dt}} = k_1[\mathrm{Ni^{III}}][\mathrm{CH_3SO_2^-}] - k_{-1}[\mathrm{Ni^{II}}][\mathrm{CH_3SO_2^{\bullet}}]_{\mathrm{ss}} - k_2[\mathrm{Ni^{III}}][\mathrm{CH_3SO_2^{\bullet}}]_{\mathrm{ss}} = 0 \quad \text{Eq. 3-30}$$

$$[\mathrm{CH_3SO_2^{\bullet}}]_{\mathrm{ss}} = \frac{k_1[\mathrm{Ni^{III}}][\mathrm{CH_3SO_2^-}]}{k_{-1}[\mathrm{Ni^{II}}]+k_2[\mathrm{Ni^{III}}]} \quad \text{Eq. 3-31}$$

The general mechanism leads to the following rate law,

$$-\frac{\mathrm{d}[\mathrm{Ni^{III}}]}{\mathrm{dt}} = k_1[\mathrm{Ni^{III}}][\mathrm{CH_3SO_2^-}] - k_{-1}[\mathrm{Ni^{II}}][\mathrm{CH_3SO_2^{\bullet}}]+k_2[\mathrm{Ni^{III}}][\mathrm{CH_3SO_2^{\bullet}}] \quad \text{Eq. 3-32}$$

$$-\frac{\mathrm{d}[\mathrm{Ni^{III}}]}{\mathrm{dt}} = \frac{2k_1k_2[\mathrm{Ni^{III}}]^2[\mathrm{CH_3SO_2^-}]}{k_{-1}[\mathrm{Ni^{II}}]+k_2[\mathrm{Ni^{III}}]} \quad \text{Eq. 3-33}$$

Knowing the values of $E^0(\mathrm{Ni^{III}/Ni^{II}}) = 0.94\ \mathrm{V}$ and $E^0(\mathrm{CH_3SO_2^-/CH_3SO_2^{\bullet}}) = 1.017\ \mathrm{V}$, the redox potential of the first step reaction can be determined from,

$$\Delta\mathrm{E^0} = \mathrm{E^0_{(Ni^{III}/Ni^{II})}} - \mathrm{E^{\,0}_{(CH_3SO_2^-/CH_3SO_2^{\bullet})}} = -0.077\ V \quad \text{Eq. 3-34}$$

With the two equations regarding reaction Gibbs energy,

$$\Delta\mathrm{G^0} = -\mathrm{nF}\Delta\mathrm{E^0} = -1 \times 96485\ \mathrm{C\ mol^{-1}} \times -0.077\ V = 7.43 \times 10^3\ \mathrm{V} \quad \text{Eq. 3-35}$$

$$\Delta\mathrm{G^0} = -\mathrm{RTln}K_1 \quad \text{Eq. 3-36}$$

K_1 is calculated with a value of 0.05.

For Eq. 3-33, an assumption can be made as $k_{-1}[\mathrm{Ni^{II}}] \ll k_2[\mathrm{Ni^{III}}]$. With $k_{-1}[\mathrm{Ni^{II}}]$ term being neglected, the simplified equation is given as,

$$-\frac{\mathrm{d}[\mathrm{Ni^{III}}]}{\mathrm{dt}} = \frac{2k_1k_2[\mathrm{Ni^{III}}]^2[\mathrm{CH_3SO_2^-}]}{k_2[\mathrm{Ni^{III}}]} = 2k_1[\mathrm{Ni^{III}}][\mathrm{CH_3SO_2^-}] \quad \text{Eq. 3-37}$$

When $[\mathrm{CH_3SO_2^-}] \gg [\mathrm{Ni^{III}}]$,

$$k'_{obs} = 2k_1[\mathrm{CH_3SO_2^-}] \quad \text{Eq. 3-38}$$

Comparing Eq. 3-38 with the result obtained from [MSA] dependence in the absence of Ni(II) from [11], $2k_1$ equals to the slope of the linear fit:

$$2k_1 = (1.34 \pm 0.02) \times 10^2\ \mathrm{M^{-1}s^{-1}} \quad \text{Eq. 3-39}$$

k_1 is determined to be $(0.67 \pm 0.01) \times 10^2\ \mathrm{M^{-1}\ s^{-1}}$. This agrees with $k_1 (= 93.75\ \mathrm{M^{-1}\ s^{-1}})$ value obtained from [MSA] dependence from with $k_{obs} = 0.18\ \mathrm{s^{-1}}$ in Figure 3-6.

Another possibility is that $k_{-1}[\mathrm{Ni^{II}}] \gg k_2[\mathrm{Ni^{III}}]$, which results in a second-order kinetics on [Ni(III)] with the rate expression of,

$$-\frac{\mathrm{d}[\mathrm{Ni^{III}}]}{\mathrm{dt}} = \frac{2k_1k_2[\mathrm{Ni^{III}}]^2[\mathrm{CH_3SO_2^-}]}{k_{-1}[\mathrm{Ni^{II}}]} \quad \text{Eq. 3-40}$$

When $[\mathrm{CH_3SO_2^-}] \gg [\mathrm{Ni^{III}}]$,

$$k'_{obs,2} = \frac{2k_1k_2[\mathrm{CH_3SO_2^-}]}{k_{-1}[\mathrm{Ni^{II}}]} = \frac{2k_1k_2K_a[\mathrm{MSA}]_{\mathrm{total}}}{k_{-1}[\mathrm{Ni^{II}}](K_a + [\mathrm{H^+}])} \quad \text{Eq. 3-41}$$

$$\frac{1}{k'_{obs,2}} = \frac{k_{-1}(K_a + [\mathrm{H^+}])[\mathrm{Ni^{II}}]}{2k_1k_2K_a[\mathrm{MSA}]_{\mathrm{total}}} \quad \text{Eq. 3-42}$$

Comparing Eq. 3-42 to Eq. 3-43 which is formulated as a function of $[\mathrm{Ni^{II}}]$ $\left(\frac{1}{k_{\mathrm{obs,2}}} = k'[\mathrm{Ni^{II}}],\ k' = (7.07 \pm 0.18) \times 10^{-1}\ \mathrm{s^{-1}}\right)$ that has been determined from [Ni(II)] dependence, an equation can be deduced as,

$$k' = \frac{k_{-1}(K_a + [\mathrm{H^+}])}{2k_1k_2K_a[\mathrm{MSA}]_{\mathrm{total}}} = (7.07 \pm 0.18) \times 10^{-1}\ \mathrm{s^{-1}} \quad \text{Eq. 3-44}$$

Plus, $K_1, K_a\ (= 10^{-2.38}), [\mathrm{H^+}], [\mathrm{MSA}]$ are known, and $K_1 = \frac{k_1}{k_{-1}}$, k_2 is calculated with a value of $(1.56 \pm 0.04) \times 10^4\ \mathrm{M^{-1}\ s^{-1}}$.

Based on the calculated rate constants, the mechanism along with the corresponding parameters were obtained from the computational modelling. After various attempts, the rate constants were optimized and given in the table below.

Table 3-5. Mechanism Scheme 2 (M2).

Step	Reaction	Rate Constant
1	$\mathrm{Ni(III) + MSA = Ni(II) + MSA^{\bullet}}$	$150 \pm 45; 2300\ (K_1 = 0.065 \pm 0.02)$
2	$\mathrm{Ni(III) + MSA^{\bullet} \rightarrow M}$	$(1.5 \pm 0.3) \times 10^4$
3	$\mathrm{M + H_2O \rightarrow Ni - tacn + product}$	3×10^{-5}
4	$\mathrm{Ni - tacn = Ni + tacn}$	$2.9 \times 10^{-6};\ 4.6 \times 10^{10}$
5	$\mathrm{PBN + MSA^{\bullet} \rightarrow PBNM}$	2×10^5
6	$\mathrm{Ni(III) + PBNM \rightarrow Ni(II) + P}$	1200 ± 200

Based on the mechanism scheme 2, the reaction kinetics of [Ni(II)] dependence was simulated, and the result is shown in Figure 3-39 to compare with the experimental data.

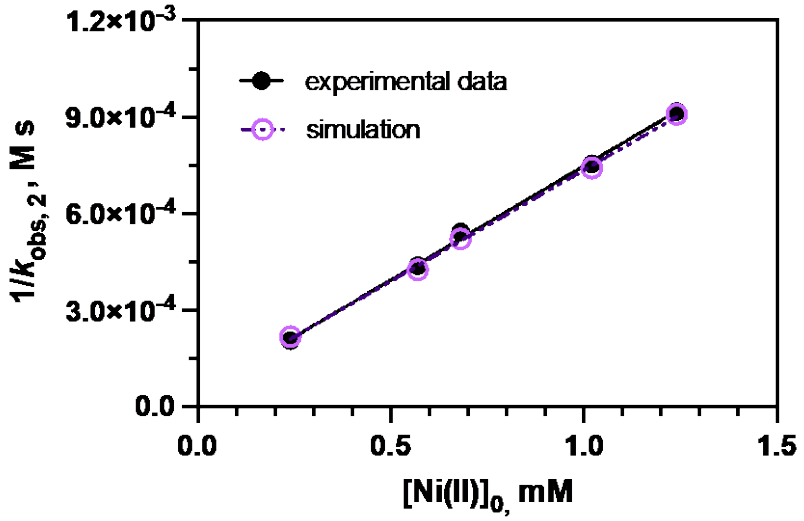

Figure 3-39. Simulation of [Ni(II)] dependence with M2. Conditions: $[\mathrm{MSA}]_0 = 1.0$ mM, $[\mathrm{Ni^{III}}]_0 = 0.04$ mM, $[\mathrm{Ni^{II}}]_0 = 0.24 - 1.24$ mM, pH 3.36 (acetate buffer).

Next, the data obtained from PBN trapping in the presence of extra Ni(II) is modeled. The kinetic traces and the first order rate constants were simulated using the mechanism, and later compared with the fitted values from the experiment. As a result, the two set of data were proved to be identical as can be seen from Figure 3-40.

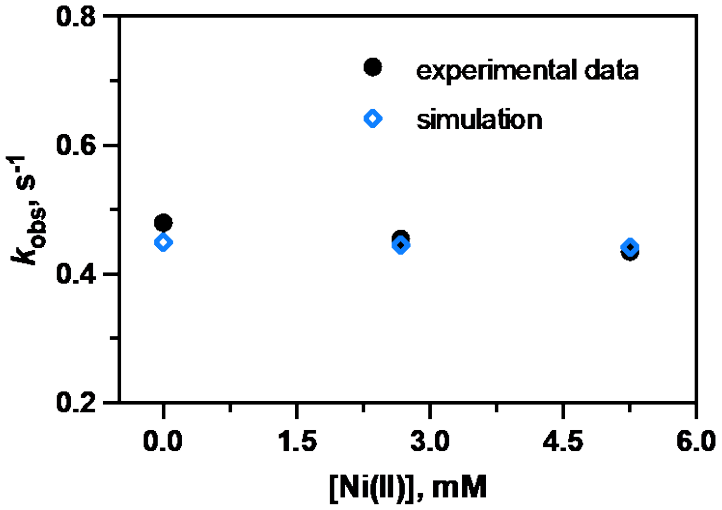

Figure 3-40. Simulation result of PBN trapping effect in the presence of Ni(II) with M2. Conditions: $[Ni(III)]_0$ = 0.045 mM, $[MSA]_0$ = 3.3 mM, $[PBN]_0$ = 4.8 mM, $[Ni(II)]_0$ = 0 mM, 2.76 mM, 5.25 mM, pH 3.5 acetate buffer.

For [MSA] dependence, it has come to our notice that when MSA concentration is relatively low, the kinetic trace in the presence of Ni(II) is well fitted into first-order decay, whereas the kinetics traces are better fitted with second-order rate law with the increasing of [MSA]. As the deviation appears, a more precise way to interpret the kinetic behavior regarding [MSA] dependence might be a two-phase decay including a rapid drop of the absorbance during the first period followed by the slow reaction in the second phase. Therefore, the kinetic result is investigated by plotting the first half-life, $t_{first,\frac{1}{2}}$, against MSA concentration, and then compared with the simulation as shown below. It turns out that the mechanism is valid for [MSA] dependence as well.

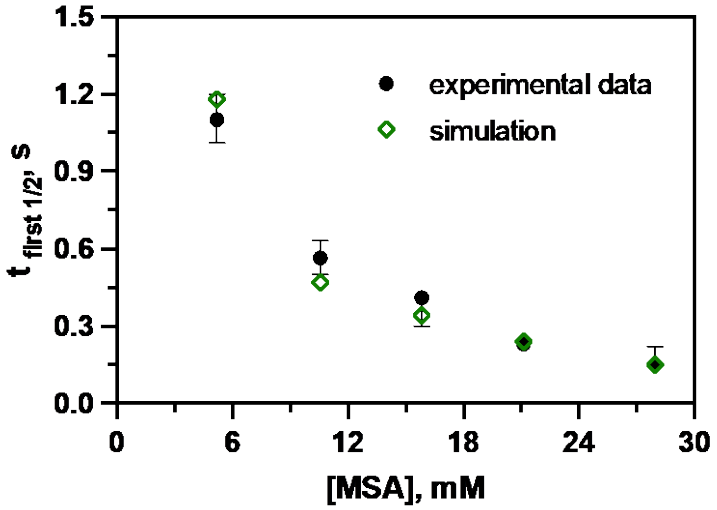

Figure 3-41. Simulation on [MSA] dependence with M2. Conditions: $[MSA]_0$ = 5.25-27.95 mM, $[Ni(III)]_0$ = 0.016 mM, $[Ni(II)]_0$ = 0.26 mM, pH 3.5 (acetate buffer).

The simulation of PBN trapping in the absent of Ni(II) is modeled as well. With the increase in PBN concentration, the simulated rate constants remain constant. This is consistent with the experimental result.

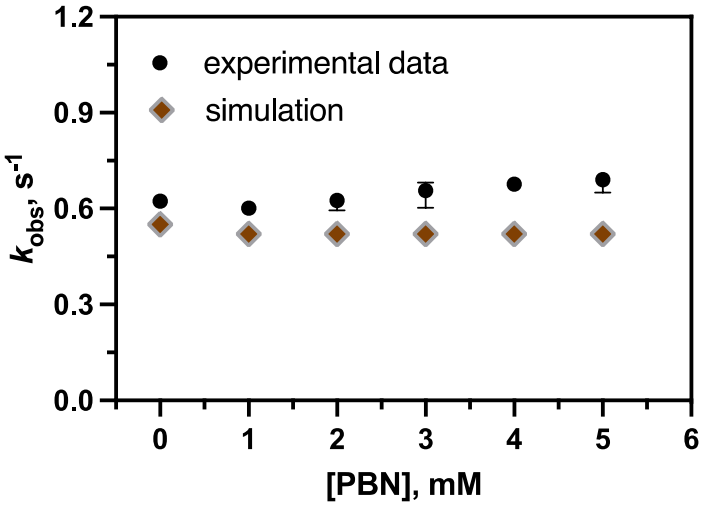

Figure 3-42. Simulation on [PBN] dependence in the absent of Ni(II) with M2. Conditions: $[MSA]_0$ = 2.5 mM, $[Ni(III)]_0$ = 0.0045 mM, pH 3.64 (acetate buffer).

3.4.3 Marcus Theory for Step 1

Considering that $[Ni(tacn)_2]^{3+}$ is coordinatively saturated, plus it is substitutionally inert, Marcus theory can be employed to better understand the first step reaction. According to Marcus cross correlation:

$$k_{12} = (k_{11}k_{22}K_{12}f)^{\frac{1}{2}}W_{12} \quad \text{Eq. 3-45}$$

Here, k_{12} is cross reaction rate of Ni(III) and MSA, k_{11} and k_{22} are the self-exchange rate constants of Ir(IV)/Ir(III) and $CH_3SO_2^-$/ $CH_3SO_2^{\bullet}$ redox couples, respectively. k_{11} is known with a value of $6 \times 10^3\ M^{-1}\ s^{-1}$ [16]. K_{12} $(= K_1 = 0.065 \pm 0.02)$ is the equilibrium constant of Eq. 3-25. The radii of $[Ni(tacn)_2]^{3+}$ and $CH_3SO_2^-$ are 3.8 A° [16] and 2.42 A°.

$$w_{12} = w_{[Ni(tacn)_2]^{3+}/CH_3SO_2^-} = \frac{17.7 \times (+3) \times (-1)}{(3.8\ + 2.42)\left(1 + 0.328 \times (3.8\ + 2.42) \times 0.1^{\frac{1}{2}}\right)} = -5.19\ \text{KJ mol}^{-1} \quad \text{Eq. 3-46}$$

$$w_{21} = w_{[Ni(tacn)_2]^{2+}/CH_3SO_2^{\bullet}} = \frac{17.7 \times (+2) \times 0}{(3.8\ + 2.42)\left(1 + 0.328 \times (3.8\ + 2.42) \times 0.1^{\frac{1}{2}}\right)} = 0 \quad \text{Eq. 3-47}$$

$$w_{11} = w_{[Ni(tacn)_2]^{3+}/[Ni(tacn)_2]^{2+}} = \frac{17.7 \times (+3) \times (+2)}{(3.8\ + 3.8)\left(1 + 0.328 \times (3.8\ + 3.8) \times 0.1^{\frac{1}{2}}\right)} = 7.81\ \text{KJ mol}^{-1} \quad \text{Eq. 3-48}$$

$$w_{22} = w_{CH_3SO_2^-/CH_3SO_2^{\bullet}} = \frac{17.7 \times (-1) \times 0}{(2.42\ + 2.42)\left(1 + 0.328 \times (2.42\ + 2.42) \times 0.1^{\frac{1}{2}}\right)} = 0 \quad \text{Eq. 3-49}$$

$$W_{12} = e^{\frac{-w_{12}-w_{21}+w_{11}+w_{22}}{2RT}} = e^{\frac{(5.19+7.81)\ \text{KJ mol}^{-1}}{2\times 8.314\times 10^{-3}\ \text{KJ mol}^{-1}\text{K}^{-1}\times 298.15\ \text{K}}} = 13.77 \quad \text{Eq. 3-50}$$

$$lnf_{12} = \frac{\left[lnK_{12} + \frac{w_{12} - w_{21}}{RT}\right]^2}{4\left[\ln\left(\frac{k_{11}k_{22}}{Z^2}\right) + (w_{11} + w_{22})/RT\right]}$$

$$= \frac{\left[\ln(0.065 \pm 0.02) + \frac{-5.19\ \text{KJ mol}^{-1}}{8.314 \times 10^{-3}\text{KJ mol}^{-1}\text{K}^{-1} \times 298.15\ \text{K}}\right]^2}{4\left[\ln\left(\frac{6 \times 10^3\ \text{M}^{-1}\ \text{s}^{-1} \times k_{22}}{(1 \times 10^{11}\text{M}^{-1}\text{s}^{-1})^2}\right) + 7.81\ \text{KJ}\frac{\text{mol}^{-1}}{8.314 \times 10^{-3}\text{KJ mol}^{-1}\text{K}^{-1} \times 298.15\ \text{K}}\right]} \quad \text{Eq. 3-51}$$

$$= \frac{23.30 \pm 2.97}{-155.226 + 4\text{In}k_{22}}$$

$$k_{12} = \left(6 \times 10^3 \times k_{22} \times (0.065 \pm 0.02) \times e^{\frac{23.30 \pm 2.97}{-155.226 + 4\ln k_{22}}}\right)^{\frac{1}{2}} \times 13.77 = (150 \pm 45) \quad \text{Eq. 3-52}$$

$$\ln k_{22} + \frac{23.30 \pm 2.97}{-155.226 + 4\ln k_{22}} = \ln(0.304 \pm 0.205) \quad \text{Eq. 3-53}$$

$$\ln k_{22} = -1.04 \pm 0.66 \quad \text{Eq. 3-54}$$

$$k_{22} = 0.35 \pm 0.23\ \mathrm{M^{-1}\ s^{-1}} \quad \text{Eq. 3-55}$$

3.5 Conclusions

The mechanism and kinetics of the oxidation of MSA by $[\mathrm{Ni(tacn)_2}]^{3+}$ in aqueous phase were presented in this project. The reaction was proved to be quite oxygen sensitive. The oxidation proceeds through a fast outer-sphere electron transfer equilibrium between Ni(III) and $\mathrm{CH_3SO_2^{\bullet}}$. The second step is the capture of the radical by another Ni(III) to form this adduct cation, $[(\mathrm{Ni^{II}-tacn})(\mathrm{tacn-CH_3SO_2})]^{3+}$, followed by its hydrolysis to release $[\mathrm{Ni^{II}-tacn}]^{2+}$ and a protonated ligand, $[\mathrm{tacn-H}]^{+}$. $[\mathrm{Ni^{II}}]^{2+}$ ion is produced from the decomposition of $[\mathrm{Ni^{II}-tacn}]^{2+}$. It is expected that the reactivity of MSA towards Ni(III) is smaller compared to Ir(IV), given that the latter one has a higher reduction potential, plus the difference in the charge of the oxidants. The NMR results in this study, however, show unusual kinetic behavior of the intermediates and reaction pathways compared with the reaction of MSA with $[\mathrm{IrCl_6}]^{2-}$ and the reaction between MSA with $[\mathrm{Os(phen)_3}]^{3+}$. The self-exchange rate of $\mathrm{CH_3SO_2^-}$/ $\mathrm{CH_3SO_2^{\bullet}}$ redox couple determined from this kinetics study is rather small, which requires us to give more thoughts into the kinetic behavior.

3.6 References

[1] Walsh, C. T.; Orme-Johnson, W. H. "Nickel enzymes." *Biochem.* **1987***, 26,* 4901-4906.

[2] Lappin, A. G.; McAuley, A. *Adv. Inorg. Chem.* **1988,** *32*, 241-295.

[3] Dirkert, G.; Konheiser, U.; Piechulla, K.; Thauer, R.; *Journal of Bacteriology*. **1981***, 148,* 459-464.

[4] Duin, E. C. *Role of Coenzyme F430 in Methanogenesis*. Springer, New York, **2009,** 352-374.

[5] Hung, M.-L.; Stanbury, D. M. *Inorg. Chem.* **1994***, 33,* 4062–4069.

[6] McAuley, A.; Spencer, L.; West, P. R. *Can. J. Chem.* **1985***, 63,* 1198–1203.

[7] Sarala, R.; Stanbury, D. M. *Inorg. Chem.* **1992***, 31,* 2771–2777.

[8] McAuley, A.; Norman, P. R.; Olubuyide, O. *Inorg. Chem.* **1984***, 23,* 1938–1943.

[9] McAuley, A.; Norman, P. R.; Olubuyide, O. *J. Chem. Soc., Dalton Trans.* **1984**, 1501-1505.

[10] DeMaine, M. M.; Stanbury, D. M. *Inorg. Chem.* **1991***, 30,* 2104–2109.

[11] Rajakaruna, P. R. *Reaction Mechanisms of One- and Two-Electron Oxidations of Alkanesulfinates in Aqueous Media*. 2021. Dissertation, Auburn University, Auburn, AL.

[12] Sonnberger, B.; Hühn, P.; Waßerburger, A.; Wasgestian, F. *Inorg. Chim. Acta.* **1992***, 196,* 65–71.

[13] Sarala, R.; Stanbury, D. M. *Inorg. Chem.* **1990***, 29,* 3456–3460.

[14] Beach, M. W.; Margerum, D. W. *Inorg. Chem.* **1990***, 29,* 1225-1232.

[15] Yang, R.; Zompa. L. J. *Inorg. Chem.* **1976***, 15,* 1499–1501.

[16] Hung, M.-L.; Stanbury, D. M. *Inorg. Chem.* **1994**, *33*, 4067.

4 Kinetics and Mechanism of Reaction of Thiols with Iodine/Iodate

4.1 Introduction

Thiols are the organosulfur compounds with a form of R-SH, where R can be alkyl group or some other organic substituents. Typically, reactions involving a thiol can be its deprotonation, substitution reaction, and its oxidation to disulfides. As part of our sulfur-based redox reaction research, we focus our kinetic and mechanism study on the oxidation of several thiols to disulfides in order to extend the knowledge of such field.

Thiols are the most direct and essential precursors to disulfides, and since disulfides are vital vulcanizing agents, oils for rubbers and elastomers [17],[18], and protecting groups for proteins, interest in developing efficient and ecological methods for converting thiols into disulfides is of much interest in both biological and industrial field. The research upon thiol oxidation to disulfides mainly includes two aspects: one is the investigation and modification of the oxidants, and another being the exploration of the potential catalysts. The methods of thiol/disulfide conversion have been extensively reported over the years regarding various reagents such as oxygen [1], dimethyl sulfoxide [2], peroxide [3],[15],[16], halogens and their derivatives [4],[5], transition metal complexes such as copper(II) [6],[11], cerium(IV) [8], iridium(IV) [9], ferric salt [7], chromate compounds [10] and ruthenium complexes [12],[13],[14]. Most of the reactions terminate after a long period of time, and therefore require the assistance of a catalyst. Some of them have drawbacks such as the high cost of using reagents for the oxidation, due to which, finding a better reagent to obtain disulfides from thiols is always the primary goal for researchers.

From a mechanistic point of view, the oxidative process can be exceptionally significant in biological, synthetical, and medical areas as they are highly connected to bioactivities and

cellular control, especially in the aspect of metabolic regulation [33],[36], signal transduction [34],[35] and regulation of enzymatic activity of proteins [35]. The mechanisms of the processes can involve electron-transfer, oxygen transfer, proton transfer pathways, etc. For example, at least three types of cysteine-based redox couples are present in enzymes and serving different purposes as shown in Table 4-1. Specifically, the understanding of mechanisms for thiol oxidation can be beneficial for purposefully modifying the oxidative function of -SH groups in proteins in order to enhance their selectivity and efficiency. Considering cysteine as an example, the thiol group contained in the residue can be oxidized to a wide range of products as shown in Figure 4-1 [29] using various oxidants [20],[21] along with the release of a wide range of species such as reactive species.

Table 4-1. Cysteine-based redox couples present in enzymes.

Redox couple	Functional group	Sulfur oxidation states (R = +1)	Redox mechanism	Examples of occurrence in proteins
Thiol/disulfide	RSH/RSSR	−2/−1	Thiol disulfide exchange Two-electron transfer	Commonly observed, *e.g.* Glutathione reductase
Thiol/thiyl radical	RSH/RS·	−2/−1	One-electron transfer Hydrogen atom transfer	Ribonucleotide reductase Pyruvate formate lyase Benzylsuccinate synthase
Thiol/sulfenic acid	RSH/RSOH	−2/0	Oxygen atom transfer with subsequent thiol/disulfide exchange or hydride transfer	Peroxiredoxins Bacterial NADH oxidases and peroxidases

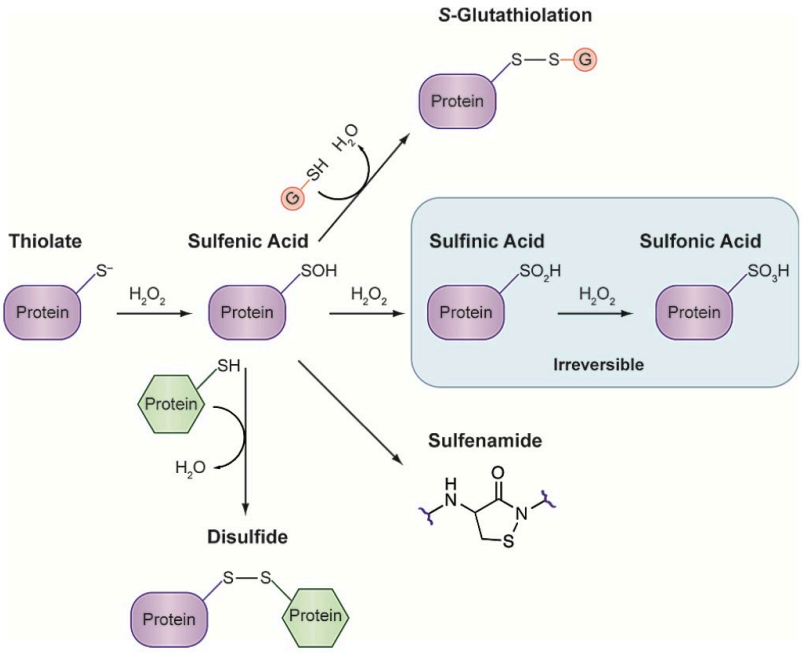

Figure 4-1. Oxidative modifications of protein cysteine residues through H_2O_2.

Notably, some of the reactive species generated through the oxidation process such as ROS ($O_2^{\bullet-}, OH^{\bullet}, H_2O_2$), reactive sulfur species ($RSOH, H_2S$), and reactive nitrogen species ($NO^{\bullet}, N_2O_3$), can be consumed by thiols, and thus form the products such as disulfides (RSSR) [22],[23], sulfenic acids (RSOH) [24],[25], sulfinic acids (RSO_2H) [26],[27],[28], sulfonic acids (RSO_3H) [26],[28], sulfenamides [29],[30], and persulfides [31],[32]. Despite the crucial role of thiols as regulators in organisms, sometimes it can be harmful as well due to the fact that the number of reactive species and toxic ions can be increased with the oxidative modifications. However, with a control of the level and site of the oxidants, the damage caused by cell regulation can be reduced and prevented.

The reactivity and function of different thiols can be very diverse, largely determined by their solvent accessibility, pK_a, and functional groups present in the thiols. For example, the reactivities of glutathione, and cysteamine towards hydrogen peroxide are different (pH 7.4, 37

ºC) as it was stated by Winterbourn and Metodiewa [37]. The rate constants of the reactions are listed below.

Table 4-2. Rate constants for the reaction of thiols with H_2O_2.

	pK_a of -SH group	Rate constant (M^{-1} s^{-1})
glutathione	8.8	0.87 ± 0.03
cysteamine	8.3	2.9 ± 0.1
penicillamine	7.9	4.5 ± 0.5

Generally, the reactive species in proteins are the fully ionized thiolate groups and are highly likely to determine the reaction reactivity [38],[39]. However, the ionization is not the only element to affect the reaction rates [37],[38]. Perez-Benito demonstrated that reactivity of the oxidation of thiols by chromium(VI) can be affected by the neighboring group of -SH [71]. It was also mentioned that the acidic proton of the functional group, for example, H of -COOH compared with -$COOEt_2$, is more favorable for a larger rate constant, and so are electron donating substituents. Since the reactivity of thiols oxidation can be determined by many factors such as pH, inhibitors, ionic strength, etc., the kinetic studies on the reactions will provide valuable information for the selective modification of the oxidation process. Furthermore, the effective trapping of the intermediates, and the isolation of oxidative products might be used for developing more potential chemical probes.

4.2 Motivation and Background

Research regarding halogen based organosulfur chemistry has been going on for decades. This involves the understanding of various reactions and their underlying mechanisms by investigating different sulfur species and halogen. For example, Simoyi's group studied the reaction of cysteamine ($N_2HCH_2CH_2SH$) with iodine and iodate under both neutral and mildly acidic conditions [40]. They found that the reaction between iodine and the thiol is slow with a

rate constant less than 3 $M^{-1}\ s^{-1}$. The stoichiometry was found to be dependent on the ratio of the reactants. This group has also reported the kinetics and mechanism of the oxidation between methionine ($H_3CSCH_2CH_2NH_2COOH$) and iodine/acidified iodate [41]. The reaction overall was determined to be a simple 2-electron oxidation with methionine sulfoxide formed as final product. The reaction proceeds through a transient iodine generation followed by a slow consumption of iodine by methionine. A network with 11 reactions was proposed to explain the kinetic behavior and mechanism. However, some of the equilibrium and rate coefficients appeared questionable. As mentioned by Dr. Stanbury [42], the iodine/iodate part of the reaction mechanism clearly disagrees with the principle of detailed balancing. He noted that the relationship of the following three independent reactions should satisfy the equation $\frac{k_1}{k_{-1}} = \left(\frac{k_2}{k_{-2}}\right)\left(\frac{k_3}{k_{-3}}\right)$, where k is the rate constant of each step, based on the principle of detailed balancing.

$$IO_3^- + I^- + 2H^+ \rightleftharpoons HIO_2 + HOI \mid k_1, k_{-1} \qquad \text{Eq. 4-1}$$

$$HIO_2 + I^- + H^+ \rightleftharpoons 2HOI \mid k_2, k_{-2} \qquad \text{Eq. 4-2}$$

$$IO_3^- + HOI + H^+ \rightleftharpoons 2HIO_2 \mid k_3, k_{-3} \qquad \text{Eq. 4-3}$$

It is worth to mention that works published with aqueous iodine/iodate system by many researchers are significant as they provide critical information for understanding reactions mentioned above. However, some of the kinetic coefficients might deviate by large amount from the practical values due to the complexity of the reaction systems and the violation of the principle of detailed balancing. Thus, evaluations and re-calculations on the mechanisms of thiol-iodine/oxy-iodine reactions using more rigorous and accurate methods can be very meaningful.

Prior to our work, we re-examined the reaction between cysteamine (CA) and iodine in acidic media as it was discussed by Chanakira et al previously [40]. They reported a rate constant of 2.7 $M^{-1}\ s^{-1}$ for the oxidation of CA by iodine. However, when performing the experiments

under similar conditions, we got very different results that suggest the reaction should be several orders of magnitude faster. The reaction completed in a matter of milliseconds and the full kinetic trace cannot be recorded by stopped-flow instrument as shown in the figures below.

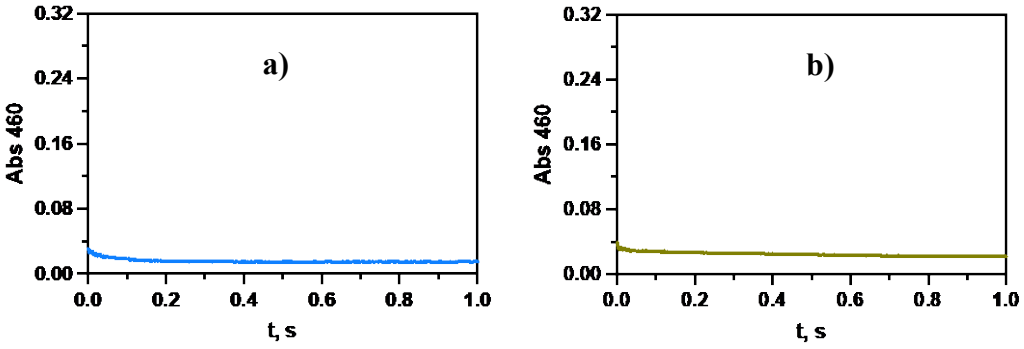

Figure 4-2. Kinetic trace of CA-iodine reaction. Conditions: $[I_2]$ = 0.435 mM, $[I^-]$ = 0 M, [CA] = 0.99 mM, μ = 1 M, a) $[H^+]$ = 0.001 M, b) $[H^+]$ = 0.004 M.

To seek strong evidence and establish a more reliable and well-founded mechanism system for reactions between thiols and iodine species, we began our work with studying and interpreting of the kinetic behavior between two thiols (mercaptoethansulfonate, MESNA and 2-mercpatoethanol, BME) with iodine/iodate in acidic media so as to infer the role each of the reaction steps plays.

Sodium 2-mercaptoethansulfonate (MESNA), $HSCH_2CH_2SO_3Na$, also known as coenzyme M (CoM), was selected as the reductant for this research, not only because it is a highly soluble thiol with low molecular weight, but also for its biological significance. CoM is one of the cofactors that can be found in methyl transfer reactions in methanobateria [43]. Primarily, it is synthesized by methanogenic archaea to participate in the reduction of CO_2 to methane as a methyl carrier [44]. It was later discovered to be a cofactor, present in the pathway of propylene metabolism as well and engaging in binding and orienting conjugated substrates for catalysis [45],[46],[47]. Apart from its enzymatic importance, MESNA is also frequently used as a

protective agent, antioxidant, and mucolytic agent in pharmaceutical and surgical fields [48],[49]. To our knowledge, mechanism upon the oxidation of MESNA by iodine/oxy-iodine species has not been systematically established. The oxidation of this thiol might terminate when disulfide is formed, or it could go further. Because of the simple structure of MESNA (the only other functional group being a sulfonic acid that is inactive), this thiol can be a good candidate to work on the kinetic studies. In addition, to gain more knowledge on how MESNA can act as an antioxidant, it is believed to be important to detect its corresponding derivatives which are often intermediates or products formed during and after its oxidation.

The oxidants employed for this research are iodine and iodate. The properties and importance of the two species were discussed in Chapter 1. Generally, iodine has several main effects on proteins, one of the most essential one is the oxidation of -SH groups [50],[51]. The most commonly suggested level of the oxidation process is to form disulfides, however the production of other sulfur species is up for debate [52]. We selected iodine as a substance for this study mainly because of its fundamental role in human body in forming thyroid hormones. An in-depth exploration of its oxidation levels and mechanisms will therefore be used as a guide for regulating and activating the relevant hormone to keep human body in a healthy condition. Compared with iodine, iodate is less powerful as an oxidizing regent. However, it can be a dominant species occurring in iodine solution. Hence, we believe it is necessary to include the reaction of iodate with thiols to make the kinetics and mechanism more complete.

4.3 Overview

This work is divided into two sub-projects: 1) Kinetics and mechanism of the oxidation of MESNA by iodine/iodate in acidic media; 2) Kinetics and mechanism of the reaction between BME and

iodine/iodate. With the results discussed here, deeper insight into the oxidation events at the mechanistical level is provided and could be beneficial for later research in other fields.

4.4 Materials and Methods

4.4.1 Reagent and solutions

MESNA (Sodium 2-mercaptoethane sulfonic acid sodium) (Alfa Aesar), BME (2-mercaptoethanol) (TCI, > 99%), 2-hydroxyethyl disulfide (TCI), sodium iodide (Alfa Aesar), potassium iodide (Fisher Scientific), perchloric acid (Fisher Scientific), sodium perchlorate monohydrate (Alfa Aesar), sodium acetate (Sigma), sodium oxalate (99.8%), hydrochloric acid (Fisher Scientific), ethanol (99.95% Sigma-Aldrich), stabilized 30% H_2O_2 (Sigma-Aldrich), 3-(trimethylsilyl)-1-propanesulfonic acid sodium salt (DSS) (sigma-Aldrich), D_2O 99.8% isotopic (Alfa Aesar), dimedone (Sigma-Aldrich).

All the aqueous solutions were freshly prepared using purified de-ionized water with a specific resistivity of 18.2 MΩ cm at 25 °C from an Ultrapure water purification system. Reagent grade crystalline iodine was purified by sublimation. The concentration of iodine was determined through UV-Vis spectrophotometry at 460 nm. Stock solutions of I_2/I_3^- was prepared by dissolving sublimed pulverized iodine in water with the addition of sodium iodide. I_3^- solution for experiments was obtained by diluting the stock solution and then standardized spectrophotometrically prior to each experiment. All of the iodine and triiodide solutions were freshly prepared and well-protected from light.

4.4.2 Methods

UV-Vis spectra were recorded at 25 ± 0.1°C by an Agilent HP 8453 diode array spectrophotometer with quartz cells having calibrated 1 cm path lengths. Rapid kinetic studies were performed at 25 ± 0.1°C on a Hi-Tech SF-51 stopped-flow spectrophotometer equipped with

a thermostat apparatus and a quartz cell with a light path of 10 mm using Olis 4300 data acquisition and analysis software. Optical filters were adjusted to different absorbance measurement. The kinetic data was analyzed using GraphPad Prism version 8.3.1. The equilibrium data analysis was performed through DataFit. Computational simulation was conducted using COPASI 4.22 and Kintecus based on the proposed mechanism and steps. ^{1}H-NMR spectra of the reactants and products were obtained on a Bruker AV 500 MHz and 600 MHz spectrometer other than noted. Mass spectrometry data were recorded with a Waters Q-Tof Premier mass spectrometer after direct electrospray ionization in the negative mode.

When iodine is mixed with iodide, a considerable rapid equilibrium (I_2/I_3^-) proceeds with the formation of triiodide as a product. The UV-Vis spectrum of iodine solution shows a maximum peak at 460 nm with molar absorptivity determined to be $750\ M^{-1}\ cm^{-1}$. The molar coefficient of triiodide at 352 nm was obtained from UV-Vis with a value of $2.6 \times 10^4\ M^{-1}\ cm^{-1}$. The equilibrium constant of $(K_{I_3^-})$ used for this research is $740\ M^{-1}$ [72].

4.4.3 UV-Vis Observation

Sodium oxalate was employed to inhibit copper catalyzed reaction in the solutions, given that dioxygen might react with iodide when trace of Cu^{2+} is present as a catalyst. UV-Vis spectra of the mixture solutions between the different reactants with oxalate were obtained to exclude the effect from $C_2O_4^{2-}$.

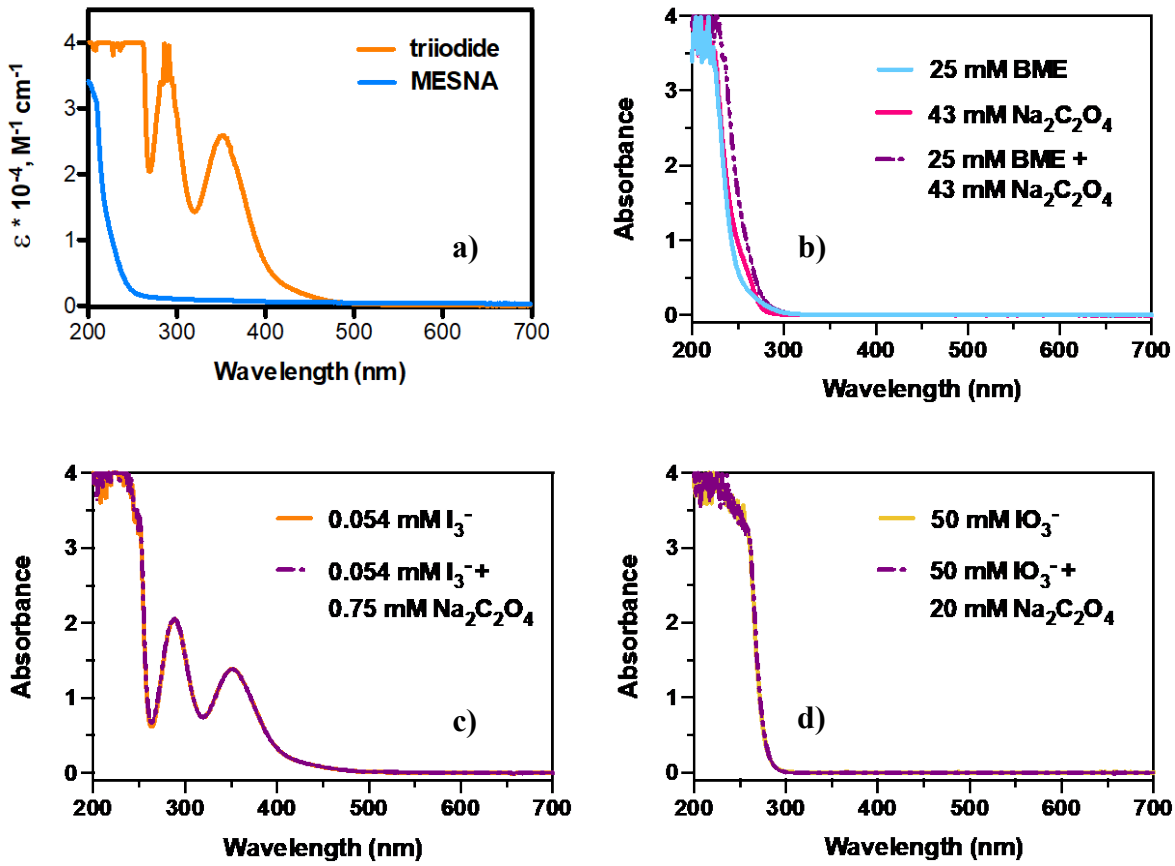

Figure 4-3. UV-Vis spectrum of a) MESNA and triiodide; b) BME and BME-oxalate mixture; c) I_3^- and I_3^--oxalate mixture; d) IO_3^- and IO_3^--oxalate mixture.

4.5 Part I: Oxidation of MESNA by Iodine/Iodate in Acidic Media

4.5.1 Stoichiometry of MESNA/triiodide Reaction

Iodometric titrations were employed to determine the stoichiometry of the reaction between MESNA and triiodide. The data was collected through UV-Vis spectrophotometry. 2 mL 0.05 mM acidified iodine solution was added to a quartz cuvette and the spectrum was recorded. Later, 0.1 mL 0.16 mM MESNA was injected to the iodine solution using gastight syringe and was allowed to react for 5 mins in the cuvette. The change of the spectrum at 352 nm suggests the loss of triiodide. The end point was found when all I_3^- was reacted and the absorbance reached to zero. The total volume of MESNA added was 0.6 mL, from which the consumption ratio of ΔMESNA/Δ I_3^- was determined to be 2.00 ± 0.04.

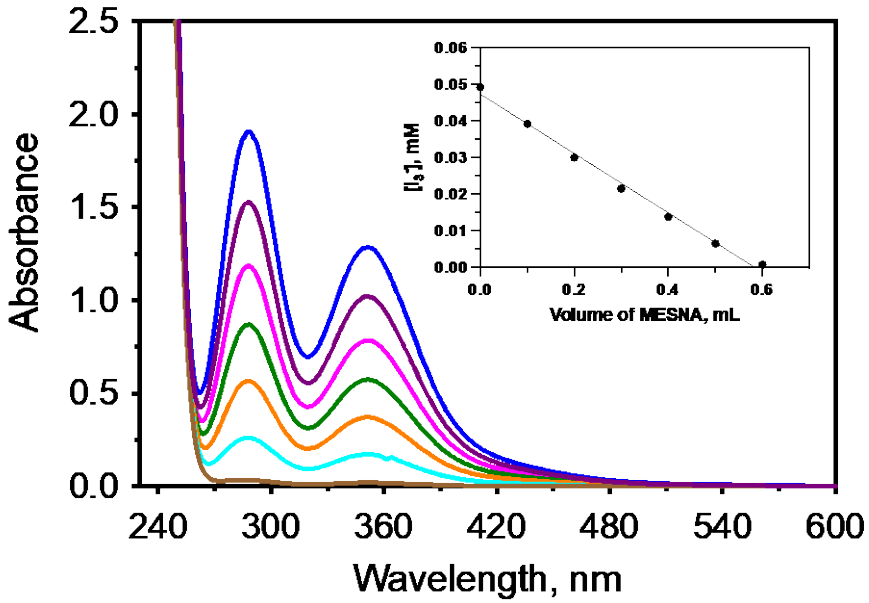

Figure 4-4. The absorbance decay of the mixture of MESNA with triiodide and titration curve.

4.5.2 Kinetic Result of MESNA/triiodide Reaction

4.5.2.1 [Iodide] dependence

Effect of $[I^-]$ on the reaction kinetics is shown in the figure below. The experiments were carried out by adding various amount of iodide to MESNA solution, followed by mixing MESNA-I^- with I_3^- and monitoring the absorbance change at 352 nm. From the kinetic traces, it is evident that the reaction rate can be accelerated with the increase in [iodide].

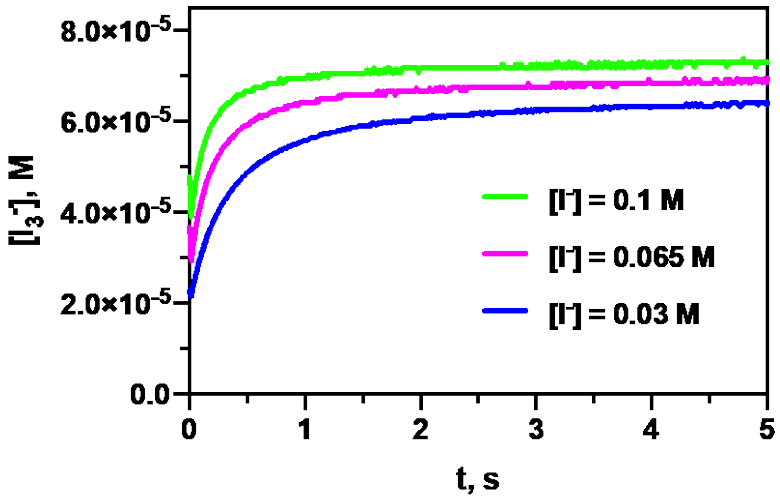

Figure 4-5. $[I^-]$ effect on the reaction kinetics. Conditions: $[I_3^-]_0 = 0.12$ mM, $[\text{MESNA}]_0 = 0.095$ mM, $[H^+]_0 = 0.1$ M, $[C_2O_4^{2-}]_0 = 0.02$ M, $\mu = 0.35$ M ($NaClO_4$).

4.5.2.2 pH dependence

The acid effect on the reaction kinetics was investigated by varying $HClO_4$ concentration of the reaction mixture and keeping the concentration of the reactants as constant. Consequently, the reaction rate is independent of pH under the selected range as when $[H^+]$ increases from 0.02 M to 0.12 M, there is no detectable change in the half-life of the reaction kinetics.

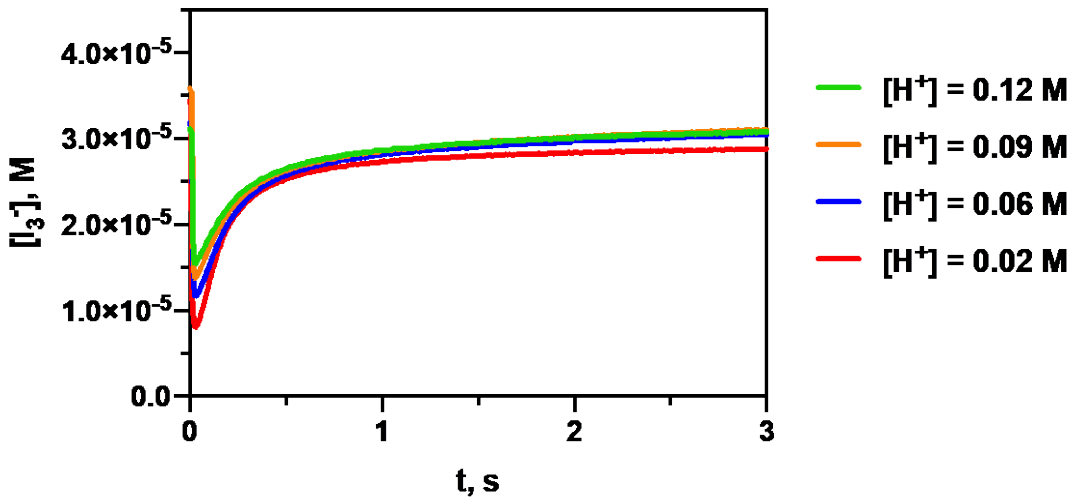

Figure 4-6. pH dependence on the reaction kinetics. Conditions: $[I_3^-]_0 = 0.10$ mM, $[\text{MESNA}]_0 = 0.123$ mM, $[I^-]_0 = 0.3$ M.

4.5.2.3 [MESNA] dependence

[MESNA] dependence was investigated by changing MESNA concentration from equimolar to excess as compared to I_3^-. The figure below shows a sharp and instant triiodide loss when MESNA is mixed with I_3^-. At high [MESNA] and low $[I^-]$, I_3^- is completely converted to the disulfide. The 2:1 stoichiometric ratio can be graphically determined from the residual absorbance at 352 nm as well.

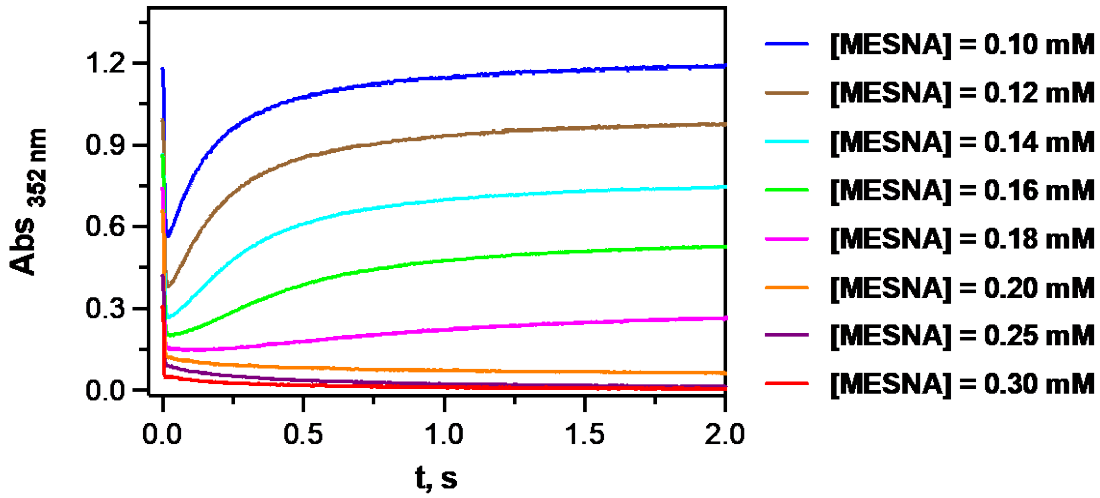

Figure 4-7. Kinetic traces of MESNA reaction triiodide at various MESNA concentrations. Conditions: $[I_3^-]_0 = 0.1$ mM, $[I^-]_0 = 0.25$ M, $[H^+]_0 = 0.1$ M, , $\mu = 0.35$ M ($NaClO_4$).

Kinetics data was also obtained under the same conditions within 0.02 seconds at 352 nm to study the first phase of the reaction, where a reactive intermediate X forms in the process.

$$2RSH + I_3^- \rightarrow \text{Intermediate X} \qquad \text{Eq. 4-4}$$

By using excess of MESNA, it could simplify the kinetic study as the reaction under such conditions is expected to be pseudo-first order. The kinetic trace is thus fitted with pseudo-first order law.

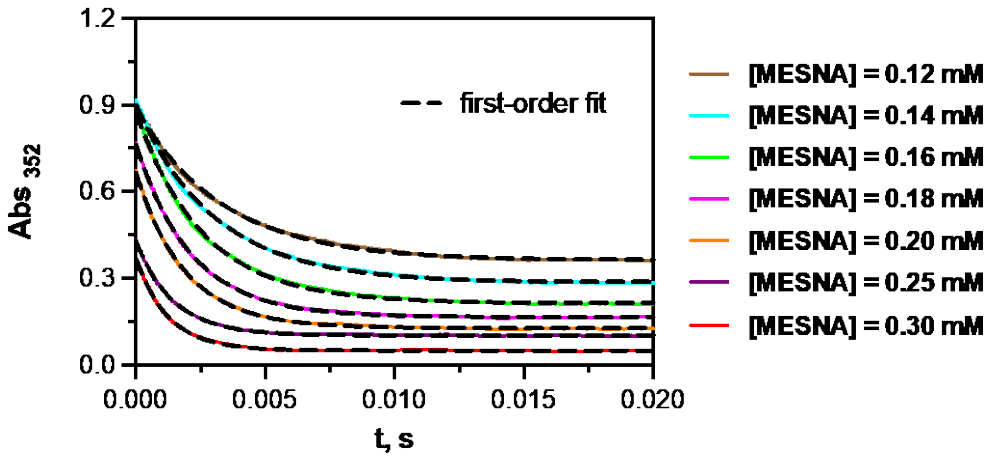

Figure 4-8. Kinetic traces in 0.02 seconds with first order fit. Conditions: $[I_3^-]_0 = 0.1$ mM, $[I^-]_0 = 0.25$ M, $[H^+]_0 = 0.1$ M.

Given that the reaction takes place within 20 ms, the observed rate constant, k_{obs}, was corrected using the equation $1/k_{obs} = 1/k_{real} + 1/k_{mix}$, where k_r (1540 s^{-1}) is the mixing rate constant of the stopped-flow instrument.

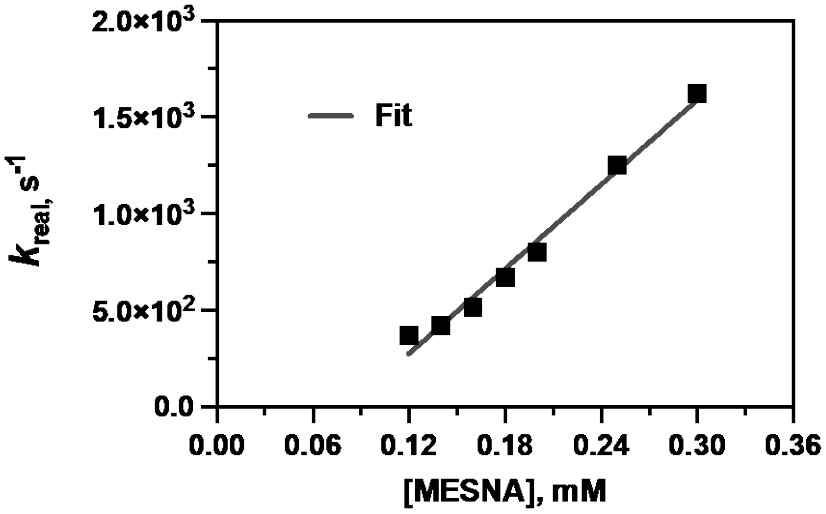

Figure 4-9. First-order dependence of k_{obs} on [MESNA].

Table 4-3. Corrected rate constant for determining [MESNA] dependence.

[MESNA], mM	k_{real}, s^{-1}
0.12	371.0
0.14	418.4
0.16	516.9
0.18	672.3
0.20	798.8
0.25	1253.4
0.30	1622.1

The corrected rate constant, k_{real}, is plotted against [MESNA] and fitted with a linear regression. The slope of the straight-line fit is $(7.3 \pm 0.4) \times 10^6\ \mathrm{M^{-1}\ s^{-1}}$, and Y-intercept is $(-601 \pm 80)\ \mathrm{s^{-1}}$.

4.5.3 Equilibrium Study of MESNA/triiodide Reaction

Quantitative determination of the sulfur-iodide intermediate can be tricky on account of its short lifetime. In our case, initial values of [RSH] are known, and [I_2] can be obtained

spectrophotometrically. As the reaction proceeds, the remaining [RSH] is determined by the subtraction of $[I_3^-]$ from initial [RSH].

Since the intermediate cannot be directly discerned from the overall kinetic trace, we attempt to understand the mechanism by proposing two equilibria stoichiometrically and checking their effectiveness. Among the two pathways, the right-hand side of the equations can be differentiated by the number of iodine atoms bonded to the sulfur center.

$$RSH + I_3^- \rightleftharpoons RSI_2^- + I^- + H^+ \quad \mathbf{M1} \qquad \text{Eq. 4-5}$$

$$RSH + I_3^- \rightleftharpoons RSI + 2I^- + H^+ \quad \mathbf{M2} \qquad \text{Eq. 4-6}$$

A series of quantitative measurements of the absorbance change at 352 nm with various [MESNA], $[I^-]$, $[I_3^-]$, $[H^+] = 0.1$ M was performed at 25.0 ± 0.5 °C using stopped-flow instrument. Two fitting equations were derived, where final [RSH] is described as a function of absorbance change of triiodide, S-containing product, K_{eq}, final concentration of iodide as well as triiodide.

	RSH	$\mathbf{I_3^-}$	**RSI**
Initial	$[RSH]_0$	$[I_3^-]_0$	0
Δ	$[RSI]_{final}$	$[RSI]_{final}$	$[RSI]_{final}$
Equilibrium	$[RSH]_{final}$	$[I_3^-]_{final}$	$[RSI]_{final}$

$$\Delta[I_3^-] = [I_3^-]_0 - [I_3^-]_{final} = [RSI]_{final} \qquad \text{Eq. 4-7}$$

$$Abs_{final} = Abs_{(I_3^-)} + Abs_{(RSI)} \qquad \text{Eq. 4-8}$$

$$Abs_{final} = \epsilon_{I_3^-} \times [I_3^-]_{final} + \epsilon_{RSI} \times [RSI]_{final} \qquad \text{Eq. 4-9}$$

$$[I_3^-]_{final} = \frac{Abs_{final} - \epsilon_{RSI} \times [RSI]_{final}}{\epsilon_{I_3^-}} \qquad \text{Eq. 4-10}$$

$$[I_3^-]_0 - [RSI]_{final} = \frac{Abs_{final} - \epsilon_{RSI} \times [RSI]_{final}}{\epsilon_{I_3^-}} \qquad \text{Eq. 4-11}$$

$$\frac{Abs_0}{\epsilon_{I_3^-}} - \frac{Abs_{final}}{\epsilon_{I_3^-}} = [RSI]_{final} - \frac{\epsilon_{RSI}}{\epsilon_{I_3^-}}[RSI]_{final} \qquad \text{Eq. 4-12}$$

$$\frac{\Delta\text{Abs}}{\epsilon_{I_3^-}} = [\text{RSI}]_{\text{final}}\left(1 - \frac{\epsilon_{\text{RSI}}}{\epsilon_{I_3^-}}\right) \quad \text{Eq. 4-13}$$

$$[\text{RSI}]_{\text{final}} = \frac{\frac{\Delta\text{Abs}}{\epsilon_{I_3^-}}}{\frac{\epsilon_{I_3^-} - \epsilon_{\text{RSI}}}{\epsilon_{I_3^-}}} = \frac{\Delta\text{Abs}}{\epsilon_{I_3^-} - \epsilon_{\text{RSI}}} \quad \text{Eq. 4-14}$$

$$[\text{RSH}]_{\text{final}} = [\text{RSH}]_0 - \frac{\Delta\text{Abs}}{\epsilon_{I_3^-} - \epsilon_{\text{RSI}}} \quad \text{Eq. 4-15}$$

$$[I_3^-]_{\text{final}} = [I_3^-]_0 - \frac{\Delta\text{Abs}}{\epsilon_{I_3^-} - \epsilon_{\text{RSI}}} \quad \text{Eq. 4-16}$$

$$K = \frac{[\text{RSI}][\text{H}^+][\text{I}^-]^2}{[\text{RSH}][I_3^-]} \quad \text{Eq. 4-17}$$

$$K = \frac{\left(\frac{\Delta\text{Abs}}{\epsilon_{I_3^-} - \epsilon_{\text{RSI}}}\right)[\text{H}^+][\text{I}^-]^2}{\left([\text{RSH}]_0 - \frac{\Delta\text{Abs}}{\epsilon_{I_3^-} - \epsilon_{\text{RSI}}}\right)\left([I_3^-]_0 - \frac{\Delta\text{Abs}}{\epsilon_{I_3^-} - \epsilon_{\text{RSI}}}\right)} \quad \text{Eq. 4-18}$$

$$K = \frac{\Delta\text{Abs} \times 0.1 \times [\text{I}^-]^2}{(26{,}000 - \epsilon_{\text{RSI}})\left([\text{RSH}]_0 - \frac{\Delta\text{Abs}}{26{,}000 - \epsilon_{\text{RSI}}}\right)\left([I_3^-]_0 - \frac{\Delta\text{Abs}}{26{,}000 - \epsilon_{\text{RSI}}}\right)} \quad \text{Eq. 4-19}$$

$$K = \frac{0.1 \times \Delta\text{Abs} \times [\text{I}^-]^2}{(26{,}000 - \epsilon_{\text{RSI}})\left(\frac{26{,}000[\text{RSH}]_0 - \epsilon_{\text{RSI}}[\text{RSH}]_0 - \Delta\text{Abs}}{26{,}000 - \epsilon_{\text{RSI}}}\right)\left(\frac{26{,}000[I_3^-]_0 - [I_3^-]_0\epsilon_{\text{RSI}} - \Delta\text{Abs}}{26{,}000 - \epsilon_{\text{RSI}}}\right)} \quad \text{Eq. 4-20}$$

$$K = \frac{0.1 \times \Delta\text{Abs} \times [\text{I}^-]^2}{\frac{(26{,}000[\text{RSH}]_0 - \epsilon_{\text{RSI}}[\text{RSH}]_0 - \Delta\text{Abs})(26{,}000[I_3^-]_0 - [I_3^-]_0\epsilon_{\text{RSI}} - \Delta\text{Abs})}{26{,}000 - \epsilon_{\text{RSI}}}} \quad \text{Eq. 4-21}$$

$$K = \frac{0.1 \times \Delta\text{Abs} \times [\text{I}^-]^2(26{,}000 - \epsilon_{\text{RSI}})}{(26{,}000[\text{RSH}]_0 - \epsilon_{\text{RSI}}[\text{RSH}]_0 - \Delta\text{Abs})(26{,}000[I_3^-]_0 - [I_3^-]_0\epsilon_{\text{RSI}} - \Delta\text{Abs})} \quad \text{Eq. 4-22}$$

$$K(26{,}000[\text{RSH}]_0 - \epsilon_{\text{RSI}}[\text{RSH}]_0 - \Delta\text{Abs}) = \frac{0.1 \times \Delta\text{Abs} \times [\text{I}^-]^2(26{,}000 - \epsilon_{\text{RSI}})}{(26{,}000[I_3^-]_0 - [I_3^-]_0\epsilon_{\text{RSI}} - \Delta\text{Abs})} \quad \text{Eq. 4-23}$$

$$[\text{RSH}]_0(26{,}000 \times K - K \times \epsilon_{\text{RSI}}) - K \times \Delta\text{Abs} = \frac{0.1 \times \Delta\text{Abs} \times [\text{I}^-]^2(26{,}000 - \epsilon_{\text{RSI}})}{(26{,}000[I_3^-]_0 - [I_3^-]_0\epsilon_{\text{RSI}} - \Delta\text{Abs})} \quad \text{Eq. 4-24}$$

$$\textbf{\textit{Fitting}}\ (\boldsymbol{Eq_2})\ \textit{for}\ \boldsymbol{M2}\text{: } [\text{RSH}]_0 = \frac{\frac{0.1 \times \Delta\text{Abs} \times [\text{I}^-]^2(26{,}000 - \epsilon_{\text{RSI}})}{(26{,}000[I_3^-]_0 - [I_3^-]_0\epsilon_{\text{RSI}} - \Delta\text{Abs})} + (K \times \Delta\text{Abs})}{(26{,}000 \times K - K \times \epsilon_{\text{RSI}})} \quad \text{Eq. 4-25}$$

$$\textbf{\textit{Fitting}}\ (\boldsymbol{Eq_1})\ \textit{for}\ \boldsymbol{M1}\text{: } [\text{RSH}]_0 = \frac{\frac{0.1 \times \Delta\text{Abs} \times [\text{I}^-]\left(26{,}000 - \epsilon_{\text{RSI}_2^-}\right)}{\left(26{,}000[I_3^-]_0 - [I_3^-]_0\epsilon_{\text{RSI}_2^-} - \Delta\text{Abs}\right)} + (K \times \Delta\text{Abs})}{\left(26{,}000 \times K - K \times \epsilon_{\text{RSI}_2^-}\right)} \quad \text{Eq. 4-26}$$

The experimental data are fitted with the deduced equations. The graph shown below includes three independent variables (ΔAbs, [I^-], [I_3^-]) and a dependent variable [RSH].

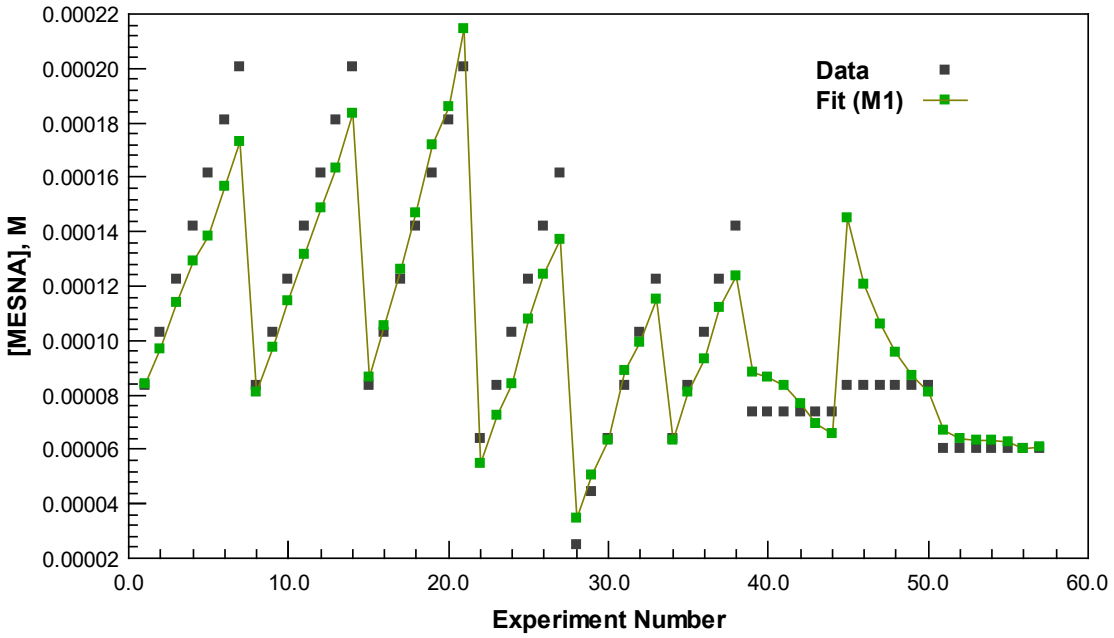

Figure 4-10. Experimental result and fitting result using (Eq_1).

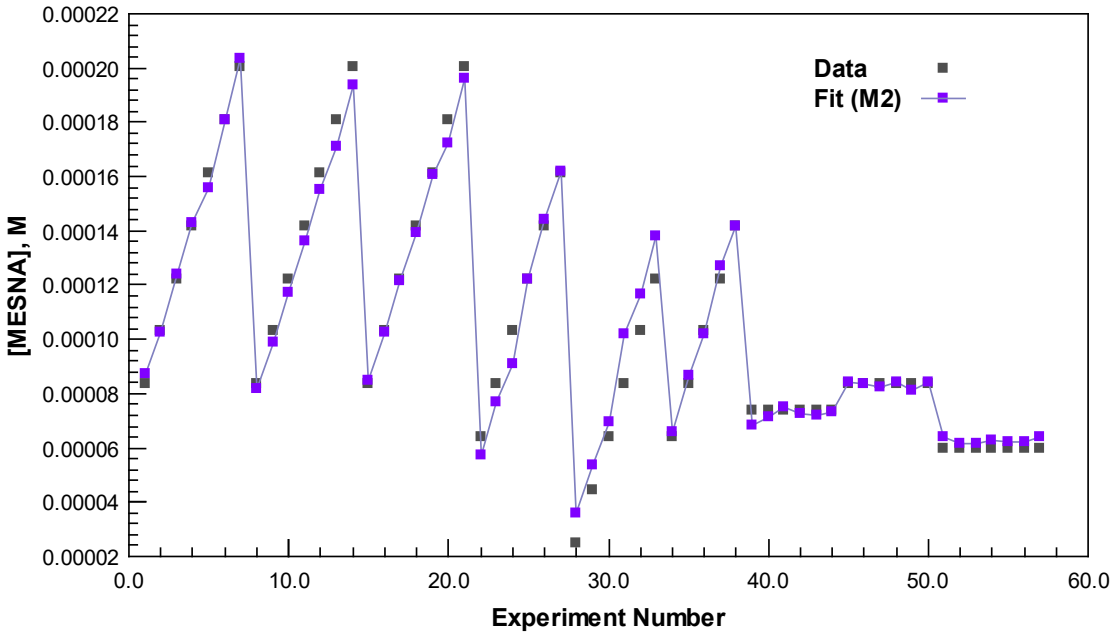

Figure 4-11. Experimental result and fitting result using (Eq_2).

As the only unknown of the fitting equation above, the equilibrium constant K for each mechanism is solved to be: $K_{eq}(1) = 6300 \pm 294\ M$ (4.67 % error) and $K_{eq}(2) = 1100 \pm 19\ \mathrm{M}^2$ (1.69 % error). With a smaller uncertainty of the solved K_2, M2 can be considered as a better explanation of how the reaction takes places. However, given that the fitting results are close to each other, more evidence regarding the valid pathway remains to be collected.

4.5.4 Stoichiometry of MESNA-Iodate Reaction

It should be stated that both MESNA and IO_3^- have no distinguishable UV-Vis features at an extensive wavelength, the appearance of the product formed at 460 nm therefore permits us to study the reaction and monitor the kinetic behavior.

Indirect iodometric titration was carried out to study the stoichiometry of the reaction between MESNA and iodate. UV-Vis spectrum of the reaction mixture was collected by injecting 0.05 mL 44.33 mM MESNA to acidic iodate solution in a quartz cuvette with 5 mins intervals. The end point was determined when the absorbance at 460 nm reached to the maximum and became stable. The ratio of the consumed MESNA and formed iodine is calculated to be $\frac{\Delta[\mathrm{MESNA}]}{\Delta[\mathrm{Iodine}]} = 10 \pm 0.16$.

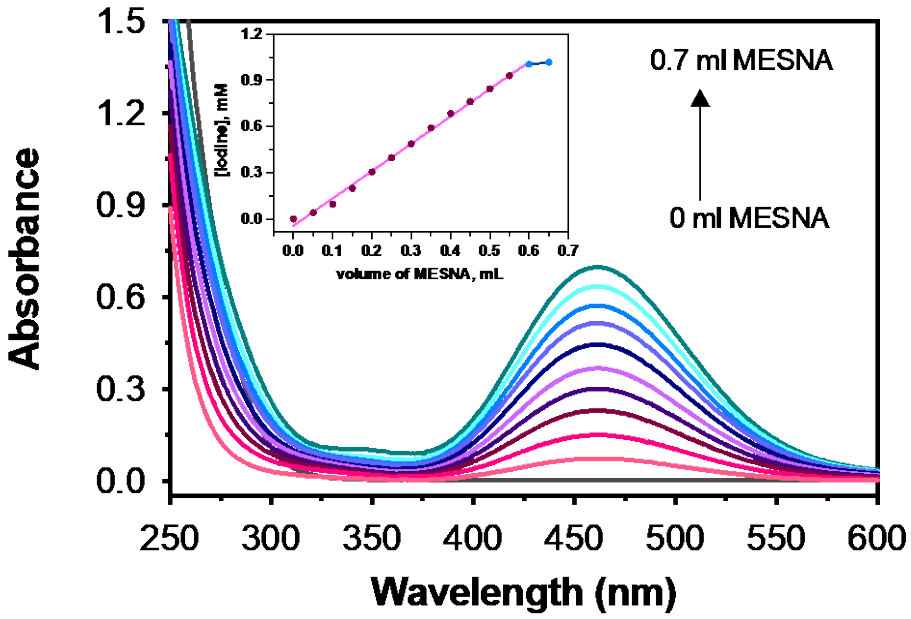

Figure 4-12. The absorbance changes of the mixture of MESNA with iodate and titration curve.

4.5.5 Kinetic Result of MESNA-Iodate Reaction

Kinetic trace of the reaction between MESNA and iodate displays a two-phase reaction: a rapid formation of the product within a second, and a generation of the reaction product in a relatively slower rate soon after. The first step is detectable yet subtle. The trend of the two processes is quite alike when compared with each other, making it reasonable to speculate that the same product might be generated during both two phases. To confirm our suspicion, experiments of the reaction were performed at different wavelengths varying from 440 nm to 500 nm.

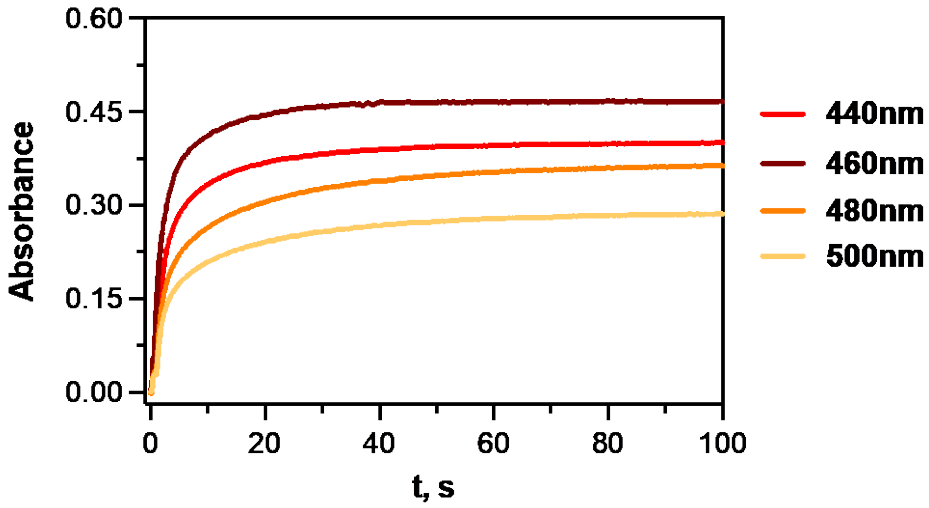

Figure 4-13. Kinetic traces of the reaction mixture at various wavelengths. Conditions: $[IO_3^-]_0 =$ 5.0 mM, $[MESNA]_0 = 5.0$ mM, $[H^+]_0 =$ 0.02 M.

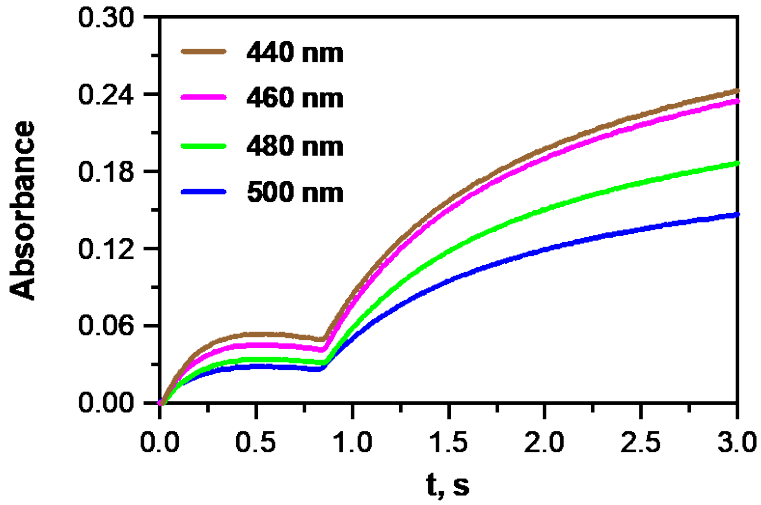

Figure 4-14. Kinetic traces of the reaction mixture at various wavelength within 3 seconds. Same condition as Figure 4-13.

Table 4-4. Ratio of absorbance at 3 second and 0.5 second at various wavelengths.

Wavelength	440 nm	460 nm	480 nm	500 nm
$\frac{\text{abs at 3 sec}}{\text{abs at 0.5 sec}}$	4.6	5.2	5.5	5.1

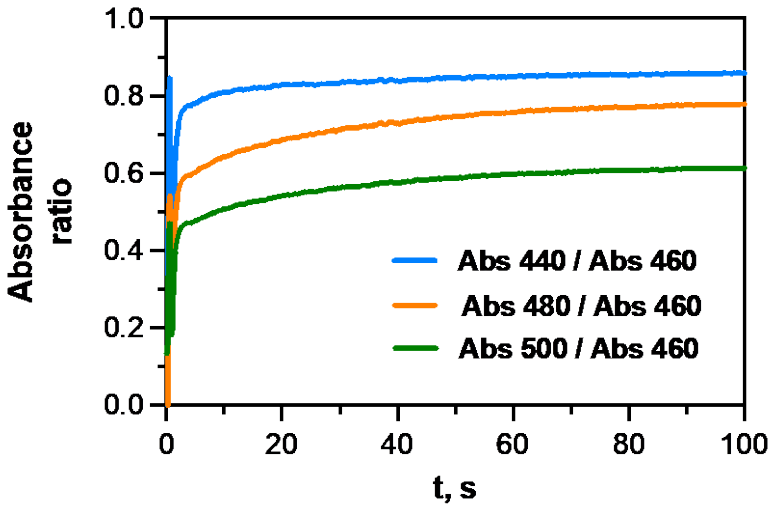

Figure 4-15. Absorbance ratio as a function of time.

The identical ratios of the two absorbances at each wavelength, plus the nearly parallel trace of the absorbance ratio against time strongly confirm that a same product formed during the two processes.

4.5.5.1 O_2 Dependence

O_2 dependence of the reaction kinetics between MESNA and IO_3^- was examined in the presence of 5 mM MESNA, 1 mM iodate, 0.02 M $HClO_4$, and μ = 0.1 M ($NaClO_4$). The absorbance changes at 460 nm were obtained by performing the experiments under air included, argon purged, and O_2 saturated conditions. The overlap of the traces indicates that O_2 has no distinct effect on the reaction kinetics.

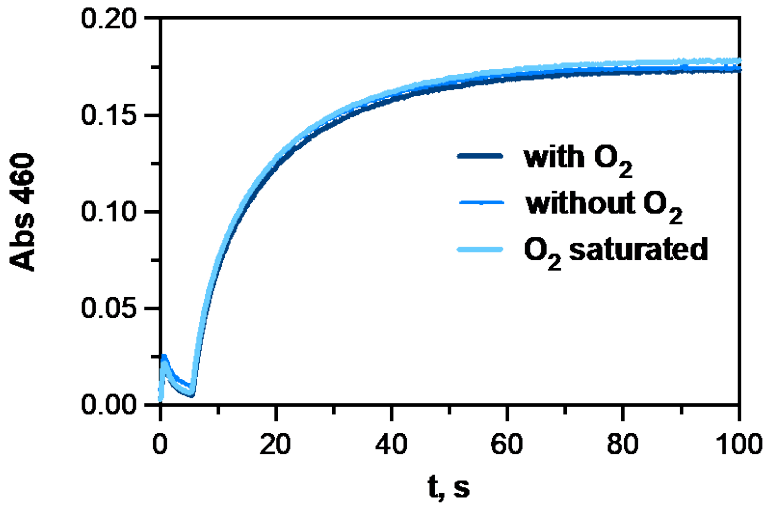

Figure 4-16. O_2 effect on the reaction kinetics. Conditions: $[IO_3^-]_0 = 1.0$ mM, $[MESNA]_0 = 5.0$ mM, $[H^+]_0 = 0.02$ M.

4.5.5.2 [Iodate] Dependence

The kinetic dependence on the iodate concentration was determined by mixing various [iodate] with MESNA. The kinetic traces here also indicate that the reaction ratio of the oxidant-to-reductant is 1 to 5. This can be evident because all iodate was consumed when [MESNA] is in stoichiometric excess, and the resulting product will be further depleted by the excess MESNA. In addition, a higher rate of iodine formation along with an increased amount of iodine can be detected when $[IO_3^-]$ is increased.

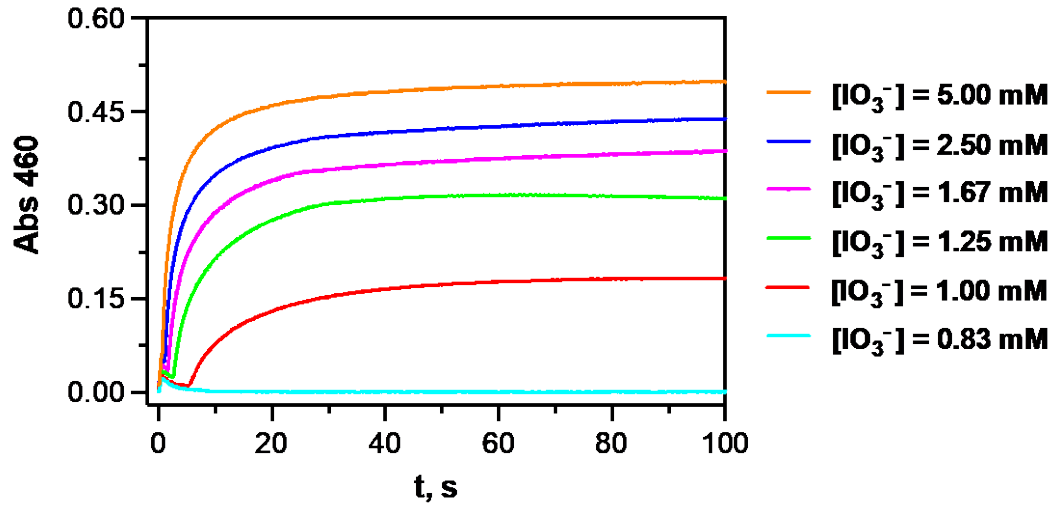

Figure 4-17. [Iodate] dependence of the reaction kinetics. Conditions: $[IO_3^-]_0 = 0.83 - 5$ mM, $[MESNA]_0 = 5.0$ mM, $[H^+]_0 = 0.02$ M.

Apart from the large increase in the absorbance, the kinetic behavior that involves a slight enhancement within first few seconds, as shown in Figure below, can be attributed to the iodine clock reaction.

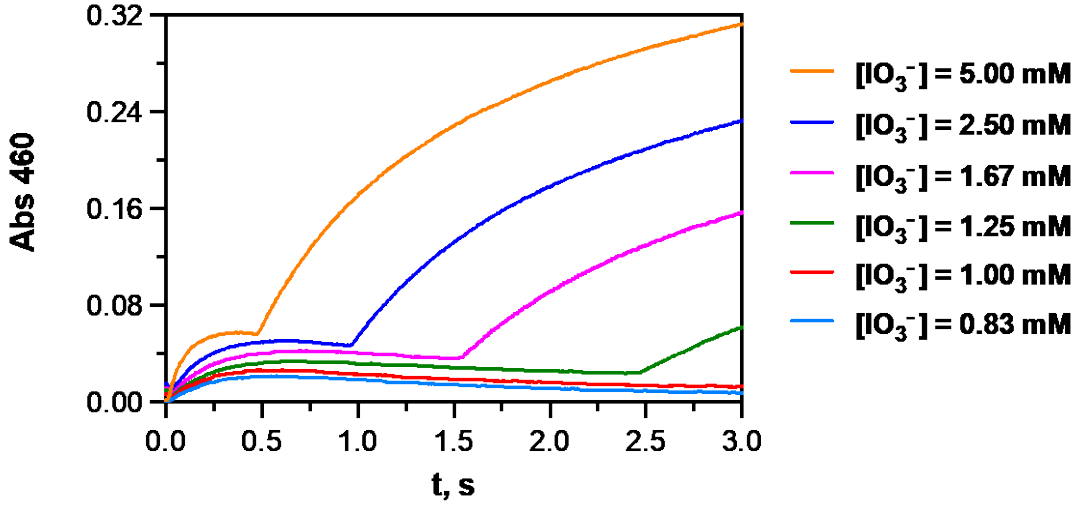

Figure 4-18. Iodine clock reaction with various [iodate]. Same conditions as Figure 4-17.

A typical iodine clock reaction can be the appearance of color in a reaction mixture after a short induction time when iodine is formed in the system. Based on the observation and UV-vis

feature of the reaction, two types of dynamics are proposed for the overall reaction of MESNA with iodate: a) clock reaction; b) formation of iodine as the main product.

4.5.5.3 pH Dependence

Acid effect was studied by changing the concentration of $HClO_4$ of the solution. It can be concluded from the figure below that the increase in acid concentration results in a faster formation of iodine. We thus infer that the acid acts as a catalyst for the overall reaction to facilitate the generation of iodine. This deduction is reasonable, given that acid is known to catalyze the Dushman reaction ($IO_3^- + 5I^- + 6H^+ \rightarrow 3I_2 + 3H_2O$).

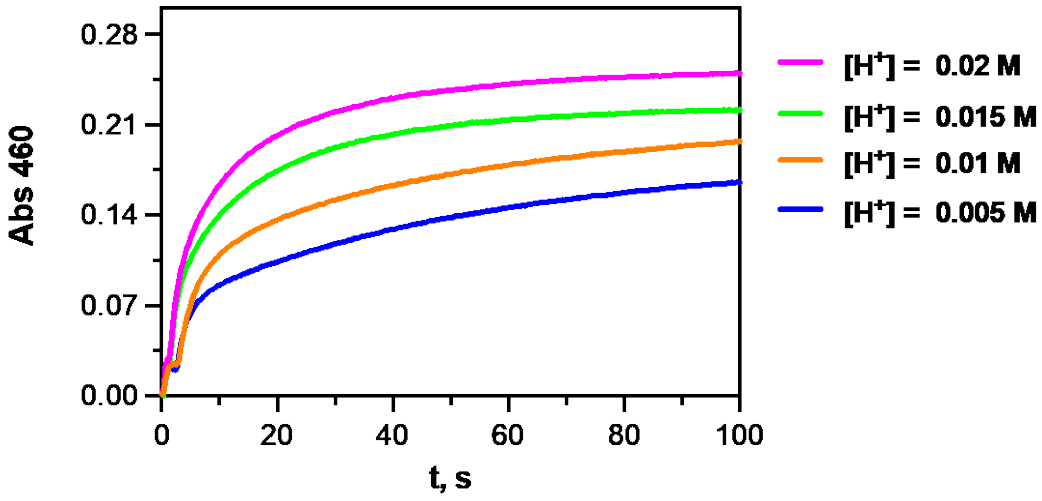

Figure 4-19. pH dependence of the reaction kinetics. Conditions: $[IO_3^-]_0 = 2.5$ mM, $[MESNA]_0 = 2.5$ mM, $[H^+]_0 = 0.005 - 0.02$ M.

4.5.5.4 [MESNA] Dependence

The kinetic dependence on [MESNA] was investigated by mixing various [MESNA] with an iodate solution. An increased rate of iodine formation can be observed from the kinetic traces.

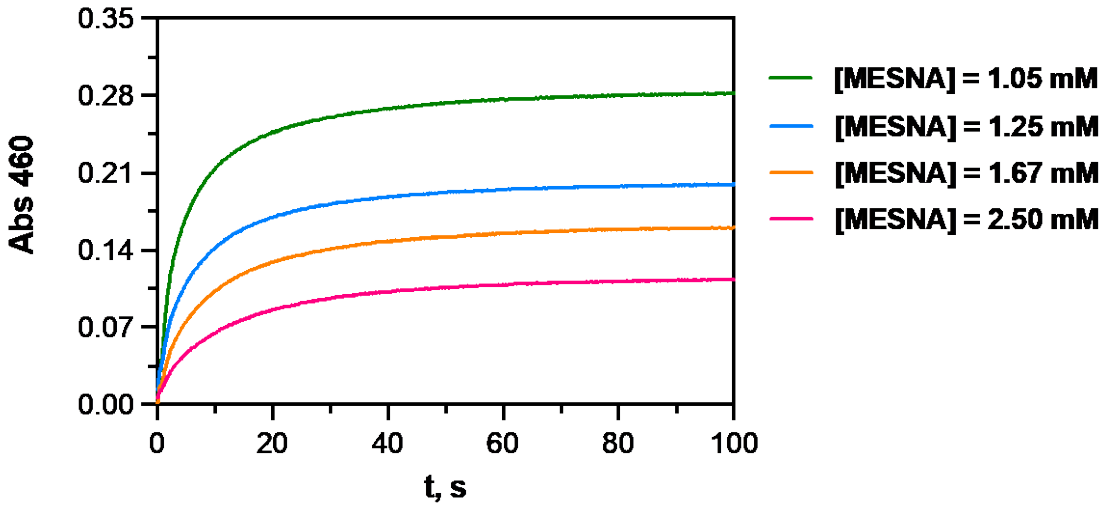

Figure 4-20. [MESNA] dependence of the reaction kinetics. Conditions:$[IO_3^-]_0 = 5.0$ mM, $[MESNA]_0 = 1.05 - 2.5$ mM, $[H^+]_0 = 0.02$ M.

4.5.5.5 [Iodide] dependence

Iodide effect on the reaction kinetics was studied by adding I^- to MESNA solution before the two reactants were mixed. The absorbance change at 460 nm was monitored. Increased final absorbance can be seen from the kinetic traces when more iodide is included in the mixture. This can be explained by the reason that Dushman reaction is accelerated, not only by the iodide produced from the reaction itself, but also by the extra iodide added to the solution. Meanwhile, a larger quantity of iodine is released with the addition of iodide.

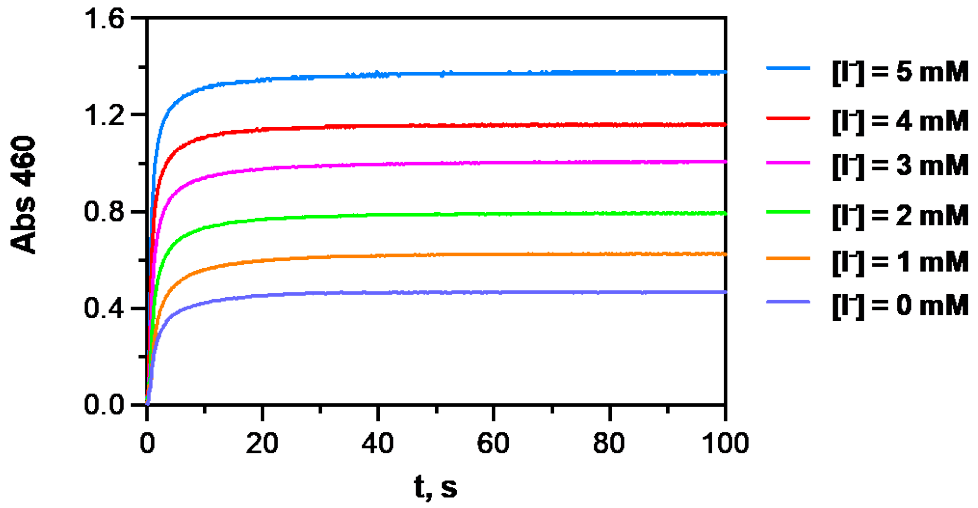

Figure 4-21. [Iodide] effect on the reaction kinetics. Conditions: $[IO_3^-]_0 = 5.0$ mM, $[MESNA]_0 = 5.0$ mM, $[I^-]_0 = 0 - 5$ mM, $[H^+]_0 = 0.02$ M.

4.5.6 Product Analysis

4.5.6.1 Synthesis of disulfide

MESNA-disulfide, SEDS, was synthesized through the oxidation of MESNA by H_2O_2. MESNA was mixed with 30 % H_2O_2 solution with NaI as a catalyst. The mixture was allowed to react for 60 mins at ambient temperature. The resulting product was obtained after removing the solvent using rota-evaporator. Later, the crude was dissolved in a minimum amount of water. After that, ethanol was added dropwise to the solution till white precipitate could be detected. The resulting solid was eventually obtained by filtration and dried overnight.

4.5.6.2 Characterization of the product

To characterize the synthesized compound, ^{1}H-NMR and ESI-MS are recorded as shown next. ^{1}H-NMR spectrum of the compound was recorded after dissolving the solid into D_2O with DSS as reference. A pair of triplets appears in the spectrum which can be assigned to the -CH_2 groups of the disulfide.

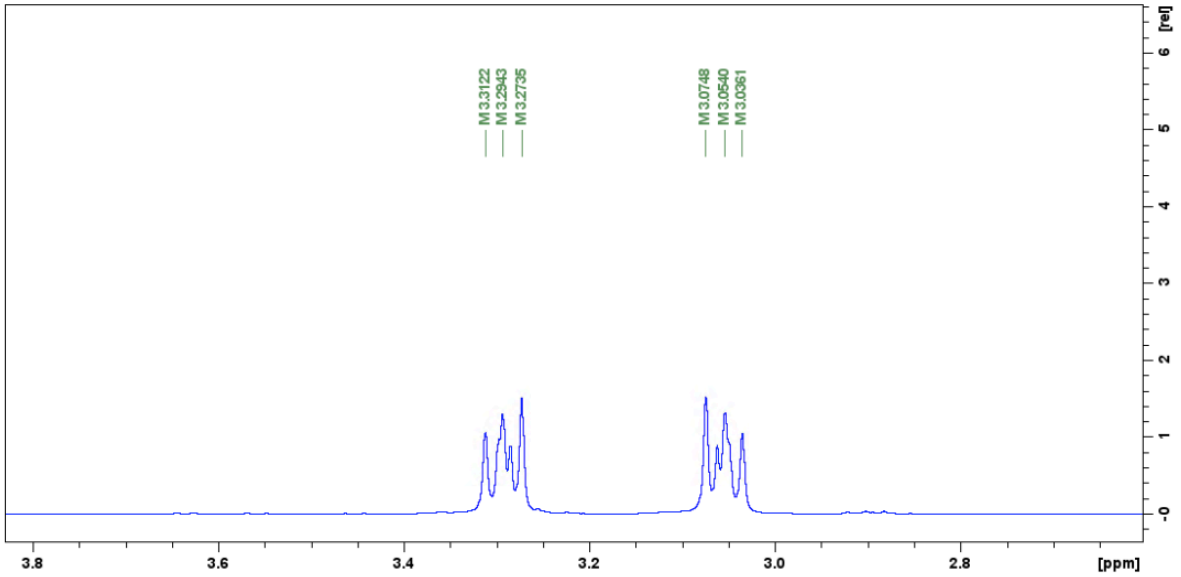

Figure 4-22. ^{1}H-NMR Spectrum of the synthesized disulfide in D_2O.

ESI-MS (negative mode) spectrum of the compound is shown below. The highest peak with $m/z = 302.9066$ was identified as arising from $NaSO_3(CH_2)_2SS(CH_2)_2SO_3^-$.

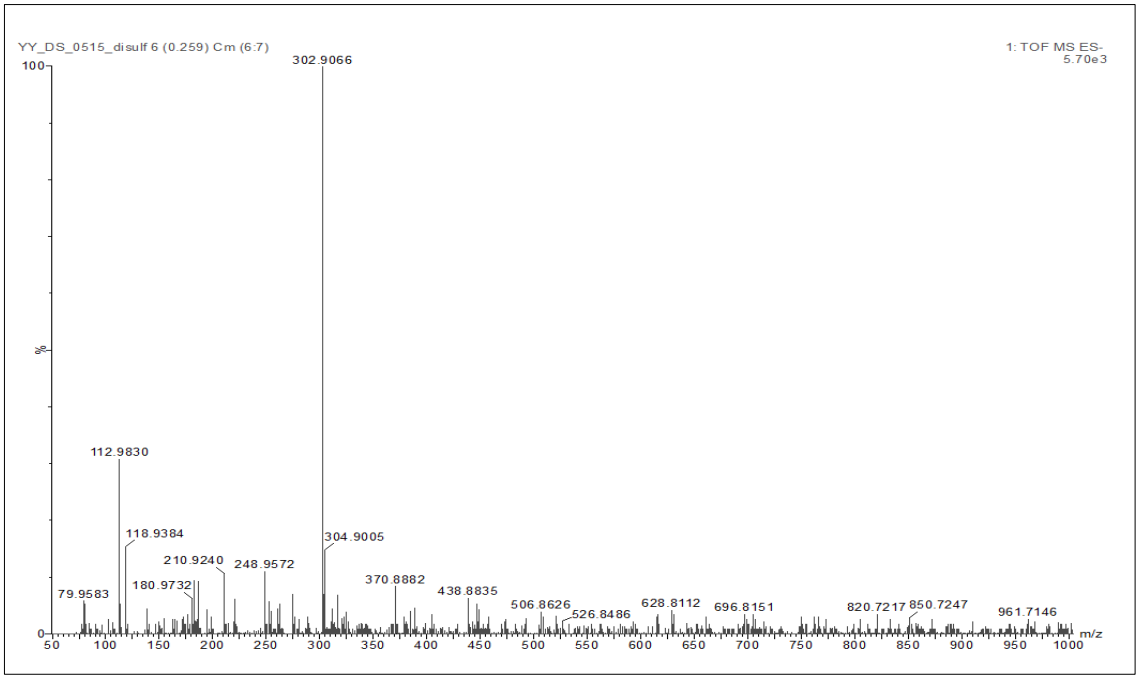

Figure 4-23. MS spectrum of the synthesized compound.

The following three ^{1}H-HMR spectra include MESNA, mixture of MESNA and I_3^-, MESNA/IO_3^- solution and the synthesized disulfide.

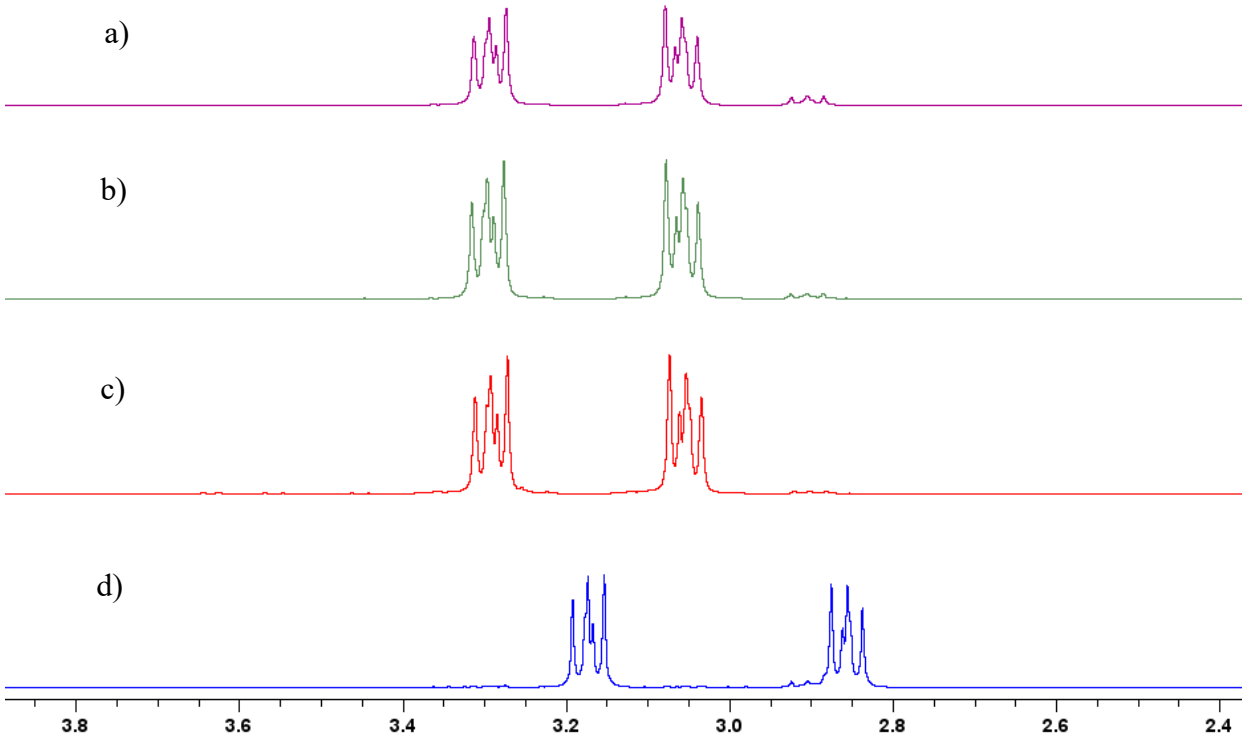

Figure 4-24. ^{1}H-NMR Spectrum of a) reaction mixture of MESNA/I_3^-; b) MESNA/IO_3^- solution; c) synthesized disulfide; d) MESNA in D_2O.

As displayed in the figure above, both reaction solution, MESNA/triiodide and MESNA/iodate, yield the same sulfur product which is proved to be the disulfide.

With the evidence collected from stoichiometry, kinetics study, and product characterization, the overall reaction is justified and formulated as,

$$10HS(CH_2)_2SO_3^- + 2IO_3^- + 2H^+ \rightarrow 5SO_3^-(CH_2)_2SS(CH_2)_2SO_3^- + 6H_2O + I_2$$

4.6 Part II: Oxidation of BME by Iodine/Iodate in Acidic Media

4.6.1 Background

The kinetic behaviors of the reaction between MESNA with iodine/iodate are very complex as can be seen from their rather complicated UV-vis trace at both 352 nm and 460 nm. It is obvious that the kinetics traces are not a simple first-order or second order decay, and thus it can be very hard to elaborate the mechanism by deriving a simple rate law. Nevertheless, some of the dynamics are quite uncommon. For instance, I^- is generally detected as an inhibitor of nucleophilic attack on iodine/iodate species, whereas in MESNA-iodate reaction, it was found to be an accelerator. A primary explanation for the effect of iodide can be understood from its role in the Dushman reaction. However, there might be some other interpretation for the behavior as it involves iodine oscillation in the system that can be quite elusive. In order to better explore the relevant kinetics and ensure that the reaction observations between MESNA and iodine/iodate are not random, we extend our study to another reaction by employing another thiol, 2-mercaptoethanol (BME), $OHCH_2CH_2SH$.

BME is widely used as a biological antioxidant to scavenge hydroxyl radicals [53], and also utilized as a protecting group in some organic synthesis [54]. It is capable of maintaining protein activity by inhibiting the oxidation of free sulfhydryl residues [55]. BME is water-soluble, plus the hydroxyl group contained in this thiol is not reactive, the kinetic study on its -SH group can therefore be more advantageous.

4.6.2 Reaction Stoichiometry

Spectrophotometric titration was carried out to determine the consumption ratio of the reaction between BME and IO_3^-. UV-Vis spectra of the reaction mixture were collected by injecting aliquots 57.76 mM BME to acidic iodate solution in a quartz cuvette with 5 mins intervals with a gastight syringe. The break point was found when the absorbance at 460 nm reached to the peak and then followed by the decline at the same wavelength with more BME added. The ratio of consumed BME and formed iodine is $\frac{\Delta \text{BME}}{\Delta \text{Iodine}} = 4.85:1$.

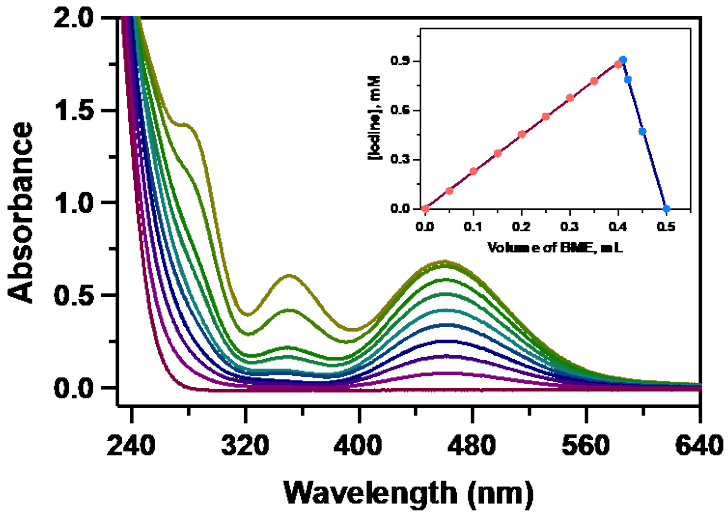

Figure 4-25. Titration of iodate with BME.

The stoichiometric ratio of the reaction between triiodide and BME was determined by direct iodometric titration. 2 mL 0.056 mM acidic I_3^- was titrated by BME in a cuvette using a gastight syringe till the endpoint was reached. The ratio of the consumed triiodide and BME was determined to be 1.84:1.

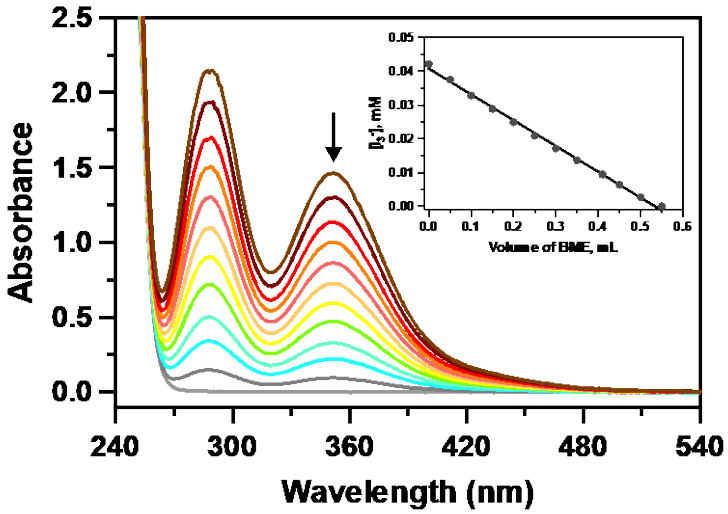

Figure 4-26. Titration of I_3^- with BME.

4.6.3 Product Analysis

^{1}H-NMR spectrum of BME in D_2O with DSS as reference is displayed below. The spectrum consists of two triplets at 2.67 ppm and 3.69 ppm.

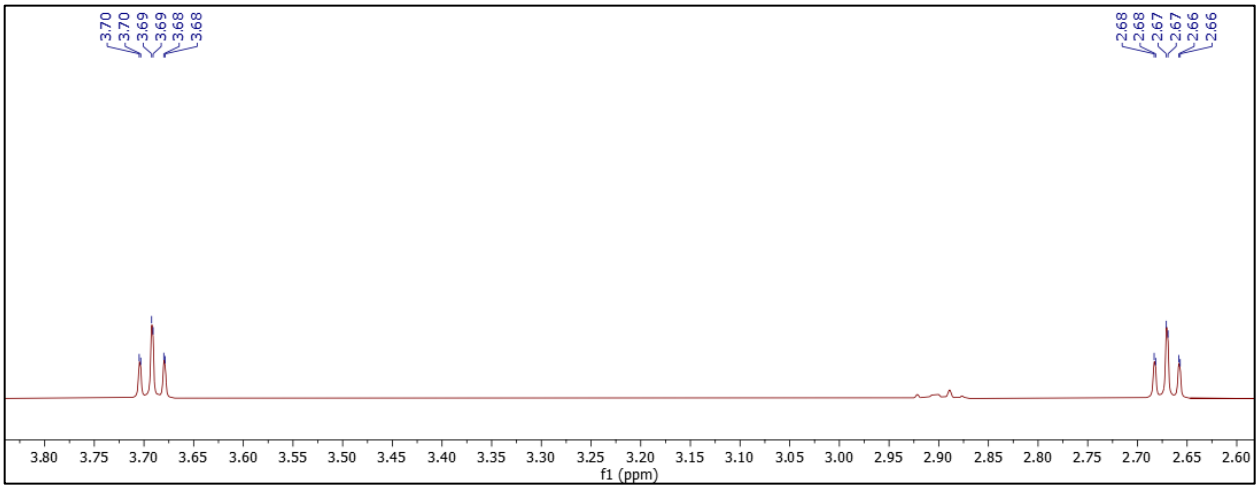

Figure 4-27. Standard ^{1}H-NMR Spectrum of BME in D_2O.

^{1}H-NMR spectrum of the corresponding disulfide, HEDS (2-hydroxyethyldisulfide) in D_2O with DSS as reference was also obtained to compare with the thiol. The spectrum shows two signals at 2.89 ppm and 3.86 ppm.

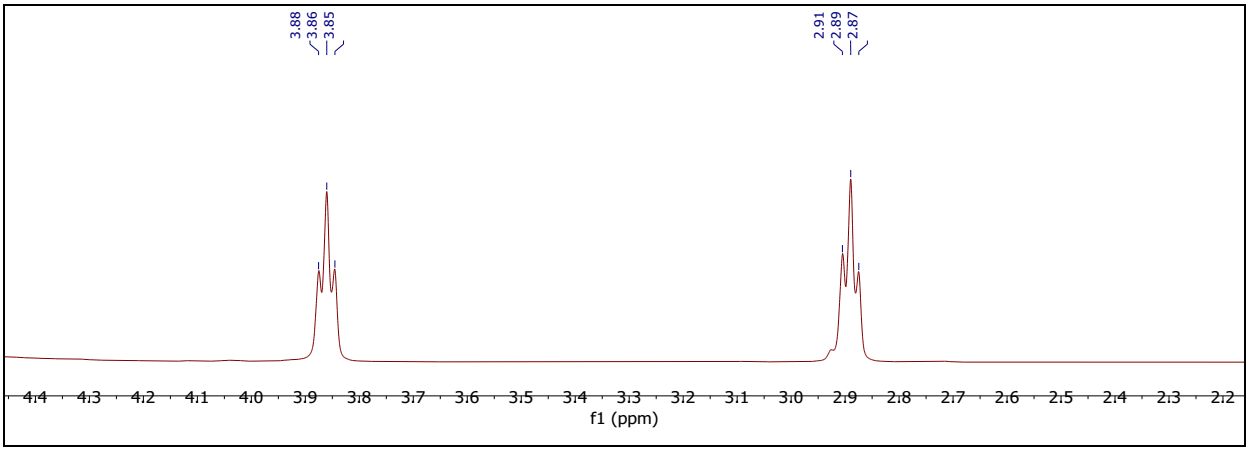

Figure 4-28. Spectrum of 2-hydroxyethyldisulfide in D_2O

Next, a mixture solution of BME and IO_3^- in D_2O was prepared under the conditions of $[IO_3^-]$ = 24.3 mM, [BME] = 28.1 mM, [DSS] = 2.70 mM. Then the spectrum was recorded with DSS as reference. Two triplets are detected at 3.86 ppm and 2.89 ppm, respectively. They are assigned to the two -CH_2 groups of the sulfur-containing product.

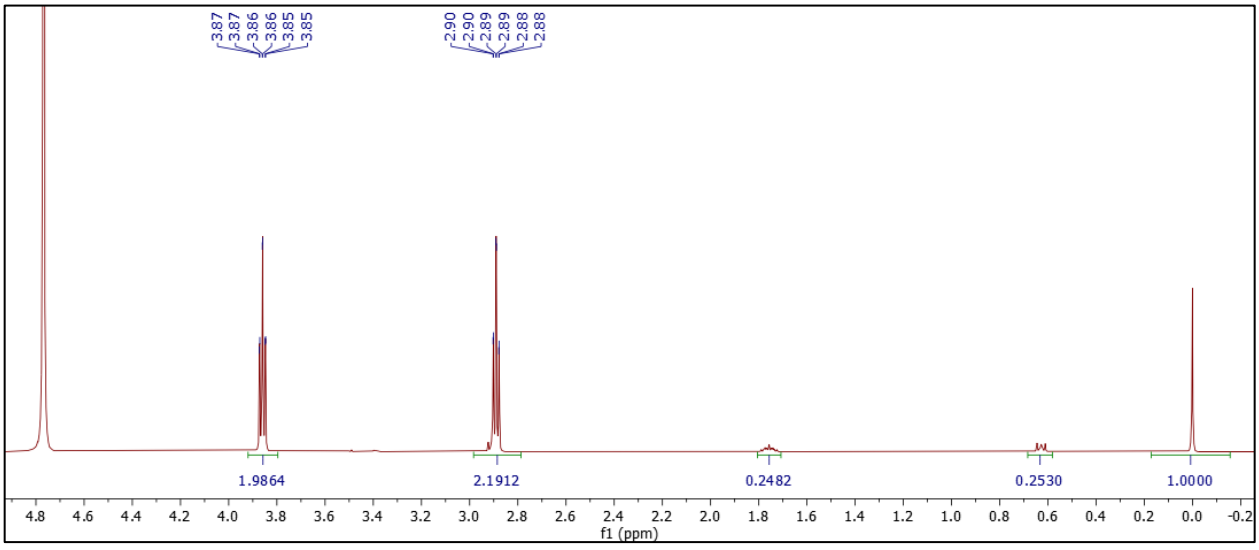

Figure 4-29. ^{1}H NMR Spectrum of BME and IO_3^- mixture in D_2O.

To confirm that the sulfur containing product of the reaction to be a disulfide, HEDS was added to the reaction mixture. After spiking, the peaks become much more intense, concluding that the couple of triplets is arising from the disulfide.

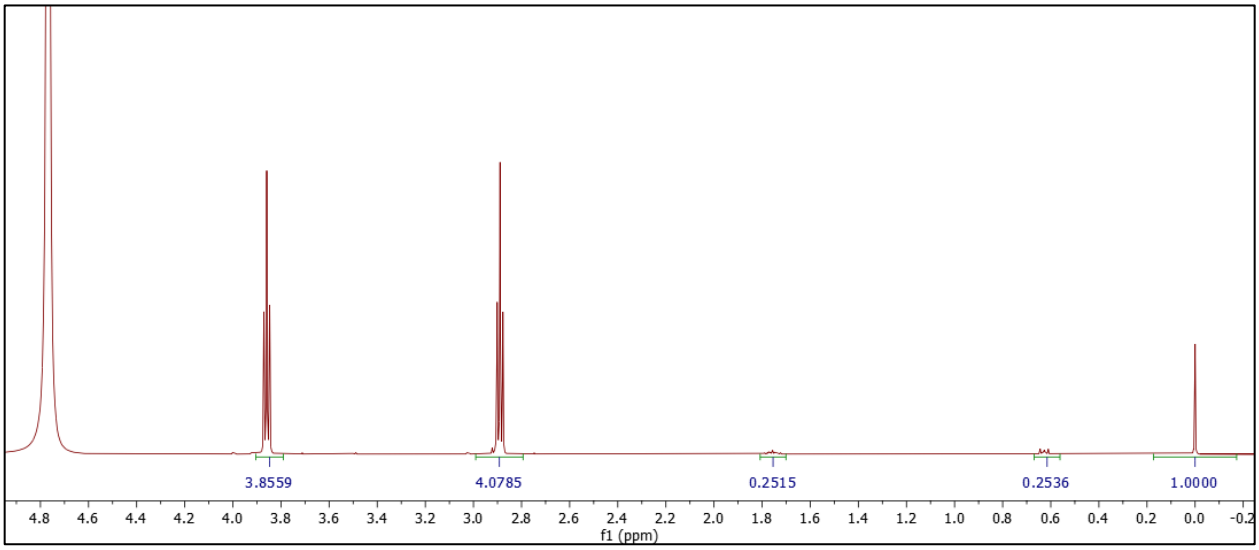

Figure 4-30. ^{1}H-NMR Spectrum of HEDS spiking on the reaction mixture.

Figure 4-31 below displays the spectrum of the product from the reaction solution of I_3^- and BME under the conditions of [I_3^-] = 28.0 mM, [BME] = 28.1 mM, [DSS] = 3.14 mM. The spectrum shows two triplets. This is later identified as arising from HEDS through spiking the authentic disulfide on the reaction mixture, which can be seen in Figure 4-32.

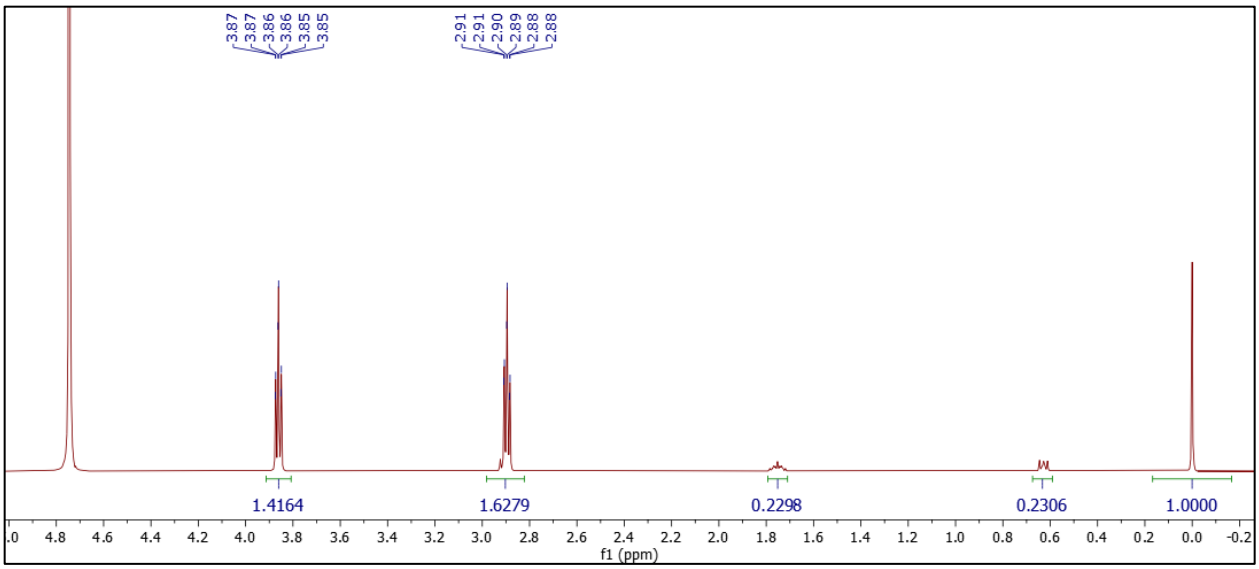

Figure 4-31. ^{1}H-NMR Spectrum of BME and I_3^- mixture in D_2O.

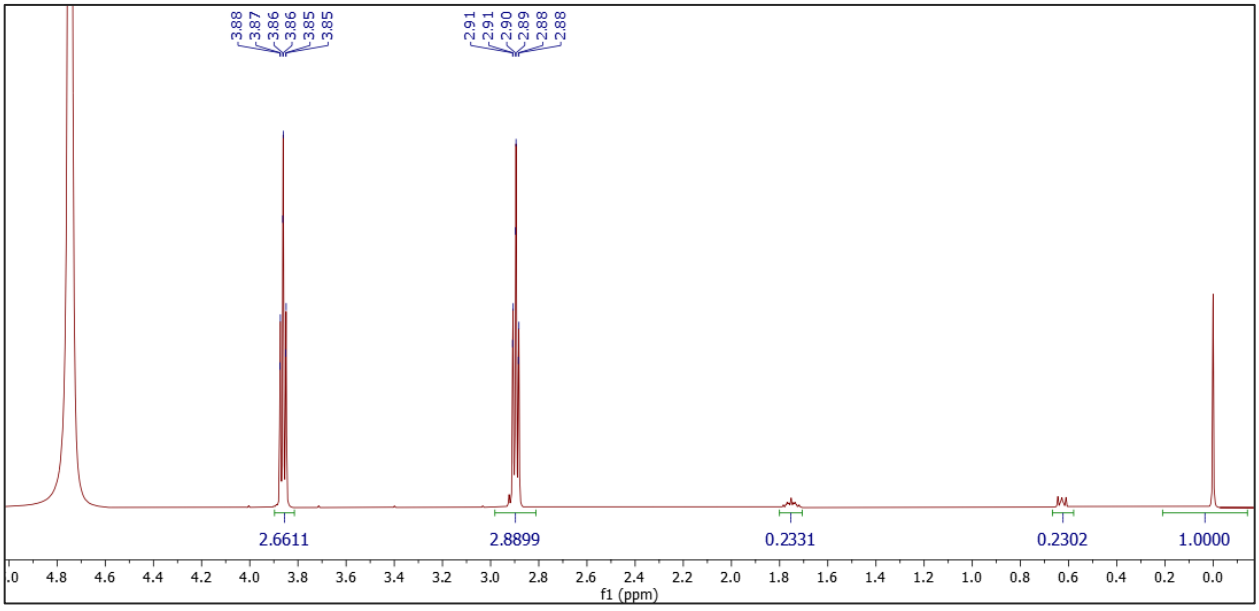

Figure 4-32. ^{1}H-NMR Spectrum of HEDS spiking on the mixed sample.

4.6.4 Kinetic Results of the Reaction between BME and I_3^-

4.6.4.1 [BME] Dependence

Rate dependence on [BME] of the reactions between triiodide and BME in the presence of large excess of iodide was examined at 352 nm under the conditions of $[I_3^-]$ = 0.115 mM, $[I^-]$ = 0.5 M, $[H^+]$ = 0.1 M, and [BME] varying from 0.15 mM to 0.235 mM. The reaction undergoes

two steps, a sharp absorbance drop followed by an increase at the same wavelength. Such behavior suggests the formation of a sulfur-contained intermediate and followed by the formation of 2-hydroxyethyl disulfide as product.

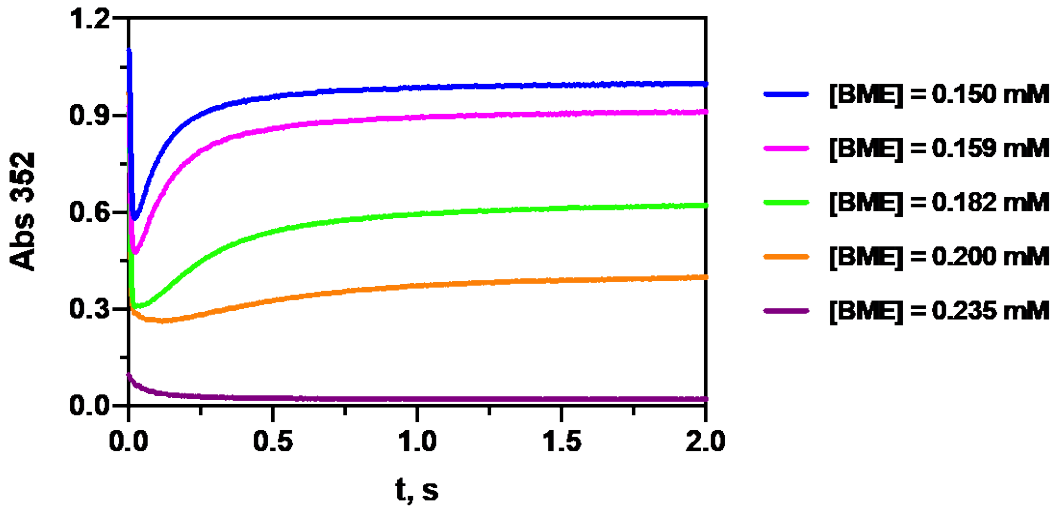

Figure 4-33. [BME] dependence of the BME-I_3^- reaction. Conditions: $[I_3^-]_0 = 0.115$ mM, $[I^-]_0 = 0.5$ M, $[H^+]_0 = 0.1$ M, $[NaClO_4]_0 = 0.2$ M, $[C_2O_4^{2-}]_0 = 0.2$ mM.

4.6.4.2 pH Dependence

pH effect on the kinetics was studied by varying the concentration of $HClO_4$ of the reaction mixture. The kinetic traces were recorded, suggesting that the reaction rate is independent of [acid] over the range investigated.

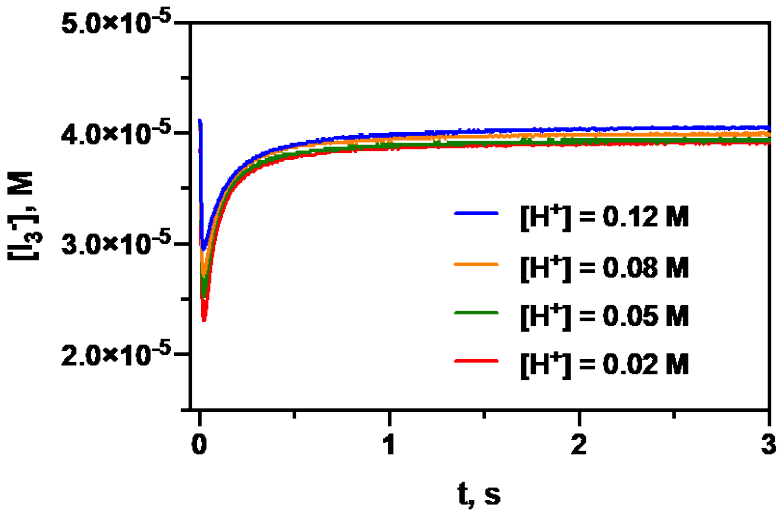

Figure 4-34. pH effect on the reaction kinetics. Conditions: $[I_3^-]_0 = 0.115$ mM, $[I^-]_0 = 0.4$ M, $[BME]_0 = 0.147$ mM.

4.6.5 Equilibrium Study

The equilibrium between BME and triiodide with the formation of BME-sulfenyl iodide was evaluated by performing series of measurement of absorbance loss of triiodide with various [BME], $[I_3^-]$, $[I^-]$ using stopped-flow instrument. Very similar to MESNA/triiodide reaction, the initial step of BME/I_3^- is also a first-order decay, and the final absorbance of which is measurable.

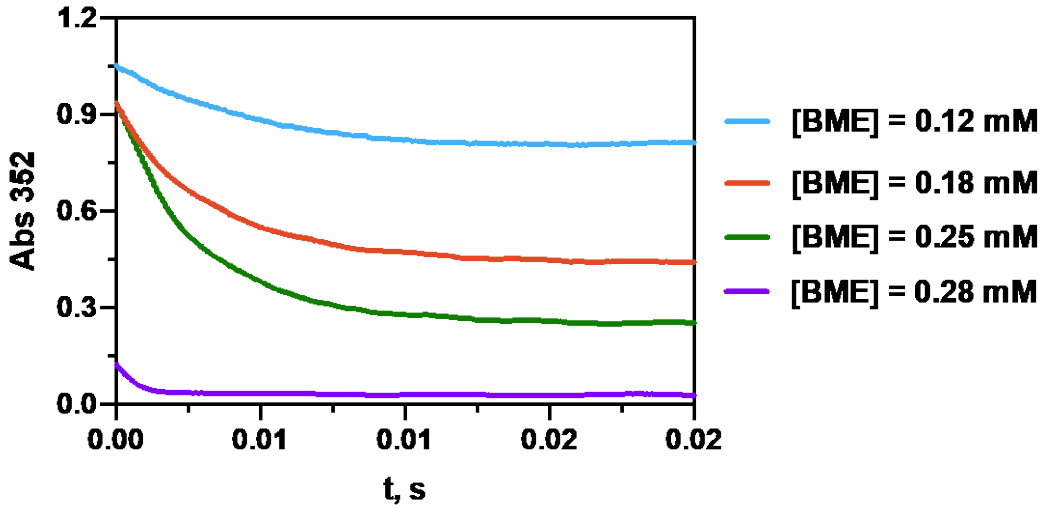

Figure 4-35. Kinetic trace at 352 nm of BME-I_3^- reaction within 0.02 s. Conditions: $[I_3^-]_0 = 0.1$ mM, $[I^-]_0 = 0.5$ M, $[H^+]_0 = 0.1$ M, $[NaClO_4]_0 = 0.2$ M, $[C_2O_4^{2-}]_0 = 0.2$ mM.

The change of [BME] during the formation of the intermediate was calculated by getting the absorbance at 0.02 s and then subtracting from the initial [I_3^-]. Two fitting equations based on the following two mechanisms were derived to fit the experimental data. The algorithm deduction can be found from Eq. 4-18 in **Part I.**

M1 $$RSH + I_3^- \rightleftharpoons RSI + 2I^- + H^+ \qquad K_1$$

M2 $$RSH + I_3^- \rightleftharpoons RSI_2^- + I^- + H^+ \qquad K_2$$

Fitting Equation:

$$[BME] = \frac{(2600 \times \Delta Abs \times [I^-]^2 + 26000 \times K_1 \times \Delta Abs \times [I_3^-] - K_1 \times \Delta Abs^2}{676000000 \times K_1 \times [I_3^-] - 26000 \times K_1 \times \Delta Abs} \qquad (1)$$

$$[BME] = \frac{(2600 \times \Delta Abs \times [I^-] + 26000 \times K_1 \times \Delta Abs \times [I_3^-] - K_1 \times \Delta Abs^2}{676000000 \times K_1 \times [I_3^-] - 26000 \times K_1 \times \Delta Abs} \qquad (2)$$

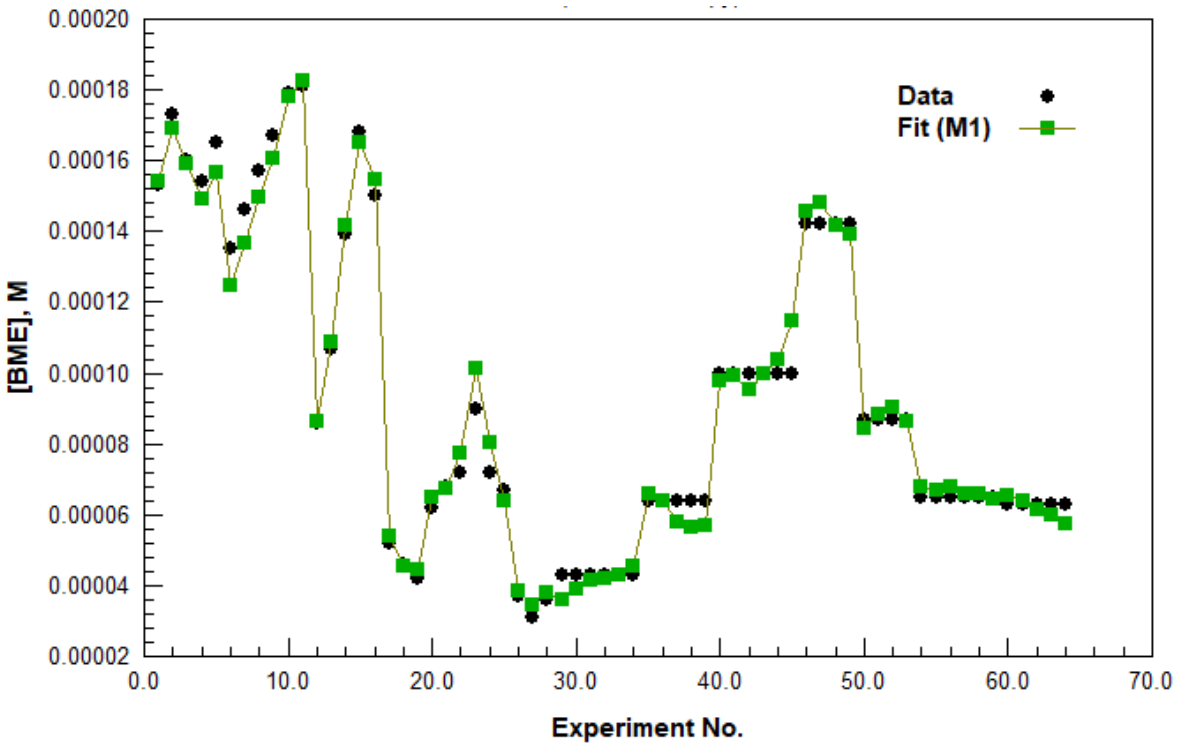

Figure 4-36. 4-D plot fitted by equation (1).

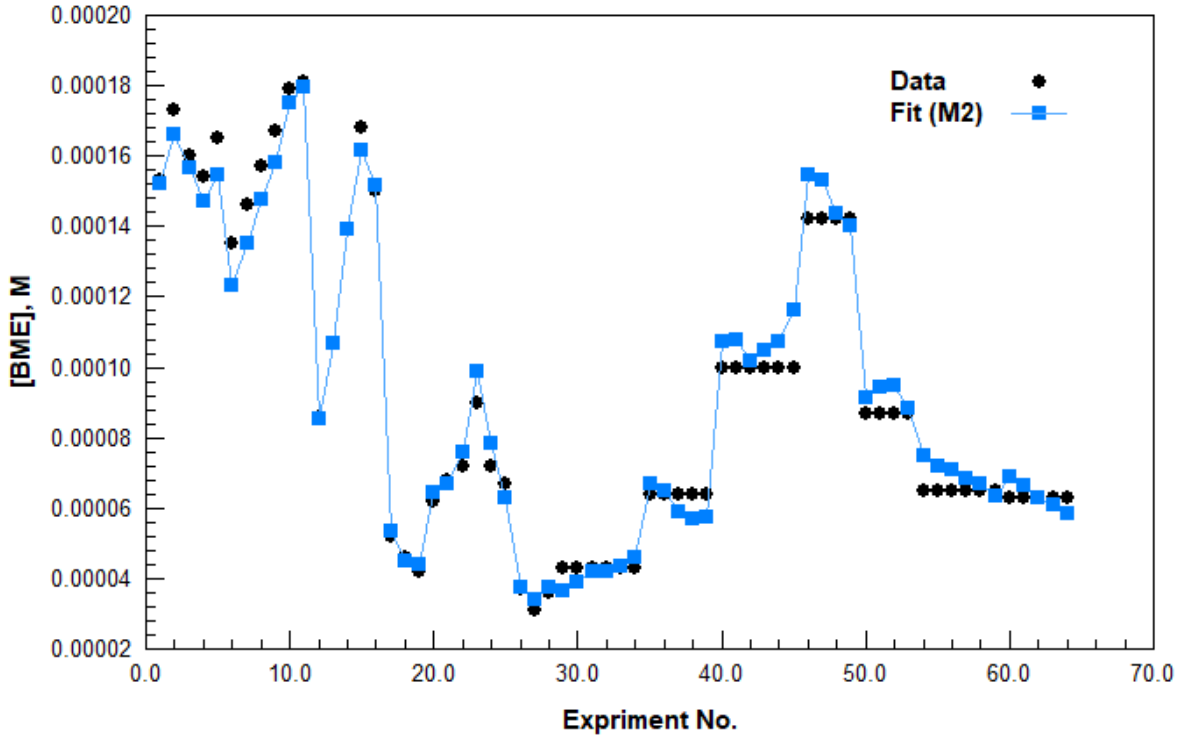

Figure 4-37. 4-D plot fitted by equation (2).

The fitting result from the two mechanisms is

$$K_{eq}(1)_{BMEI} = 2313 \pm 40\ \mathrm{M}^2 \quad (1.73\ \%\ \text{error})$$

$$K_{eq}(2)_{BMEI} = 4882 \pm 109\ \mathrm{M} \quad (2.23\ \%\ \text{error})$$

The surprisingly close standard uncertainty of the two equilibrium constants for the two mechanism suggests that the reaction between BME and I_3^- might take places in both pathways. It is likely that two iodide atoms attack the center sulfur to form the anion adduct, RSI_2^-. The stability of the reactive anion, however, is yet to be determined from further experiment and simulation.

From the equilibrium study above, it is certain that reactive sulfenyl-iodide or the corresponding anion adduct participates in the reaction. Nevertheless, it is also a fact that the spectral evidence on the presence of intermediates is insufficient. We therefore performed experiments to see whether the intermediate absorption happens. The experiment of $[I_3^-]$ dependence on the kinetics for the reaction of BME-I_3^- with excess BME was conducted under the

conditions of [BME] = 0.1 mM, $[I^-]$ = 0.5 M, $[H^+]$ = 0.1 M, and $[I_3^-]$ varying from 0.019 mM to 0.026 mM. With excess BME, the absorbance of each reaction mixture decreases to 0.03 instead of zero, suggesting the intermediates might absorb.

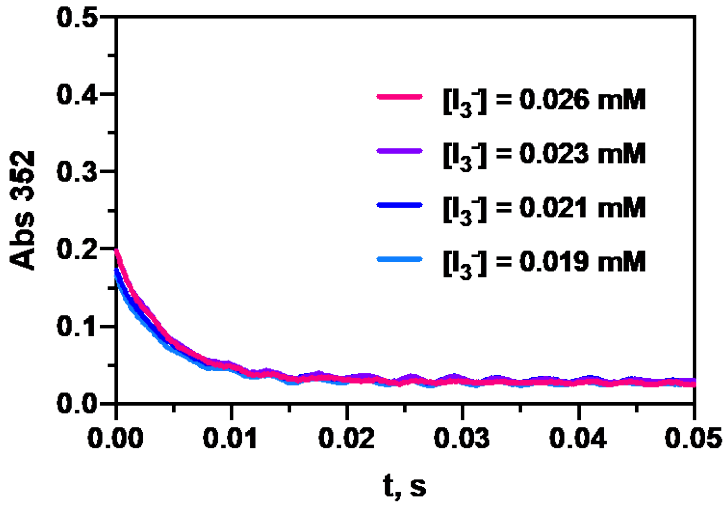

Figure 4-38. Kinetic traces for BME-I_3^- reaction at various [triiodide] within 0.05 s. (Note that the wiggles of the kinetic traces are caused by the instrument error in such a short time scale.) Conditions: $[BME]_0 = 0.1$ mM, $[I^-]_0 = 0.5$ M, $[H^+]_0 = 0.1$ M.

Table 4-5. Absorbance reading at 352 nm at various $[I_3^-]$.

$[I_3^-]$, mM	**0.026**	**0.023**	**0.021**	**0.019**
Initial Abs	0.669	0.592	0.538	0.494
Abs at 0.03 s	0.031	0.033	0.028	0.033

With the absorbance of the sulfenyl-iodide intermediate included, new equations were derived as following to fit the experimental data.

$$RSH + I_3^- \rightleftharpoons RSI + H^+ + 2I^-$$

	RSH	**I_3^-**	**RSI**
Initial	$[RSH]_0$	$[I_3^-]_0$	0
Δ	$[RSI]_{final}$	$[RSI]_{final}$	$[RSI]_{final}$
Equilibrium	$[RSH]_{final}$	$[I_3^-]_{final}$	$[RSI]_{final}$

$$\Delta[I_3^-] = [I_3^-]_0 - [I_3^-]_{final} = [RSI]_{final}$$
$$Abs_{final} = Abs_{(I_3^-)} + Abs_{\{RSI)}$$

$$Abs_{final} = \epsilon_{I_3^-} \times [I_3^-]_{final} + \epsilon_{RSI} \times [RSI]_{final}$$

$$[I_3^-]_{final} = \frac{Abs_{final} - \epsilon_{RSI} \times [RSI]_{final}}{\epsilon_{I_3^-}}$$

$$[I_3^-]_0 - [RSI]_{final} = \frac{Abs_{final} - \epsilon_{RSI} \times [RSI]_{final}}{\epsilon_{I_3^-}}$$

$$\frac{Abs_0}{\epsilon_{I_3^-}} - \frac{Abs_{final}}{\epsilon_{I_3^-}} = [RSI]_{final} - \frac{\epsilon_{RSI}}{\epsilon_{I_3^-}}[RSI]_{final}$$

$$\frac{\Delta Abs}{\epsilon_{I_3^-}} = [RSI]_{final}\left(1 - \frac{\epsilon_{RSI}}{\epsilon_{I_3^-}}\right)$$

$$[RSI]_{final} = \frac{\frac{\Delta Abs}{\epsilon_{I_3^-}}}{\frac{\epsilon_{I_3^-} - \epsilon_{RSI}}{\epsilon_{I_3^-}}} = \frac{\Delta Abs}{\epsilon_{I_3^-} - \epsilon_{RSI}}$$

$$[RSH]_{final} = [RSH]_0 - \frac{\Delta Abs}{\epsilon_{I_3^-} - \epsilon_{RSI}}$$

$$[I_3^-]_{final} = [I_3^-]_0 - \frac{\Delta Abs}{\epsilon_{I_3^-} - \epsilon_{RSI}}$$

$$K = \frac{[RSI][H^+][I^-]^2}{[RSH][I_3^-]}$$

$$K = \frac{\left(\frac{\Delta Abs}{\epsilon_{I_3^-} - \epsilon_{RSI}}\right)[H^+][I^-]^2}{\left([RSH]_0 - \frac{\Delta Abs}{\epsilon_{I_3^-} - \epsilon_{RSI}}\right)\left([I_3^-]_0 - \frac{\Delta Abs}{\epsilon_{I_3^-} - \epsilon_{RSI}}\right)}$$

$$K = \frac{\Delta Abs \times 0.1 \times [I^-]^2}{(26{,}000 - \epsilon_{RSI})\left([RSH]_0 - \frac{\Delta Abs}{26{,}000 - \epsilon_{RSI}}\right)\left([I_3^-]_0 - \frac{\Delta Abs}{26{,}000 - \epsilon_{RSI}}\right)}$$

$$K = \frac{0.1 \times \Delta Abs \times [I^-]^2}{(26{,}000 - \epsilon_{RSI})\left(\frac{26{,}000[RSH]_0 - \epsilon_{RSI}[RSH]_0 - \Delta Abs}{26{,}000 - \epsilon_{RSI}}\right)\left(\frac{26{,}000[I_3^-]_0 - [I_3^-]_0\epsilon_{RSI} - \Delta Abs}{26{,}000 - \epsilon_{RSI}}\right)}$$

$$K = \frac{0.1 \times \Delta\text{Abs} \times [\text{I}^-]^2}{\frac{(26{,}000[\text{RSH}]_0 - \epsilon_{\text{RSI}}[\text{RSH}]_0 - \Delta\text{Abs})(26{,}000[\text{I}_3^-]_0 - [\text{I}_3^-]_0\epsilon_{\text{RSI}} - \Delta\text{Abs})}{26{,}000 - \epsilon_{\text{RSI}}}}$$

$$K = \frac{0.1 \times \Delta\text{Abs} \times [\text{I}^-]^2(26{,}000 - \epsilon_{\text{RSI}})}{(26{,}000[\text{RSH}]_0 - \epsilon_{\text{RSI}}[\text{RSH}]_0 - \Delta\text{Abs})(26{,}000[\text{I}_3^-]_0 - [\text{I}_3^-]_0\epsilon_{\text{RSI}} - \Delta\text{Abs})}$$

$$K(26{,}000[\text{RSH}]_0 - \epsilon_{\text{RSI}}[\text{RSH}]_0 - \Delta\text{Abs}) = \frac{0.1 \times \Delta\text{Abs} \times [\text{I}^-]^2(26{,}000 - \epsilon_{\text{RSI}})}{(26{,}000[\text{I}_3^-]_0 - [\text{I}_3^-]_0\epsilon_{\text{RSI}} - \Delta\text{Abs})}$$

$$[\text{RSH}]_0(26{,}000 \times K - K \times \epsilon_{\text{RSI}}) - K \times \Delta\text{Abs} = \frac{0.1 \times \Delta\text{Abs} \times [\text{I}^-]^2(26{,}000 - \epsilon_{\text{RSI}})}{(26{,}000[\text{I}_3^-]_0 - [\text{I}_3^-]_0\epsilon_{\text{RSI}} - \Delta\text{Abs})}$$

$$\textbf{\textit{Fitting Eq1}}': \qquad [\text{RSH}]_0 = \frac{\frac{0.1 \times \Delta\text{Abs} \times [\text{I}^-]^2(26{,}000 - \epsilon_{\text{RSI}})}{(26{,}000[\text{I}_3^-]_0 - [\text{I}_3^-]_0\epsilon_{\text{RSI}} - \Delta\text{Abs})} + (K \times \Delta\text{Abs})}{(26{,}000 \times K - K \times \epsilon_{\text{RSI}})}$$

$$\text{RSH} + \text{I}_3^- = \text{RSI}_2^- + \text{I}^- + \text{H}^+$$

$$\textbf{\textit{Fitting Eq2}}': \qquad [\text{RSH}]_0 = \frac{\frac{0.1 \times \Delta\text{Abs} \times [\text{I}^-]\left(26{,}000 - \epsilon_{\text{RSI}_2^-}\right)}{\left(26{,}000[\text{I}_3^-]_0 - [\text{I}_3^-]_0\epsilon_{\text{RSI}_2^-} - \Delta\text{Abs}\right)} + (K \times \Delta\text{Abs})}{\left(26{,}000 \times K - K \times \epsilon_{\text{RSI}_2^-}\right)}$$

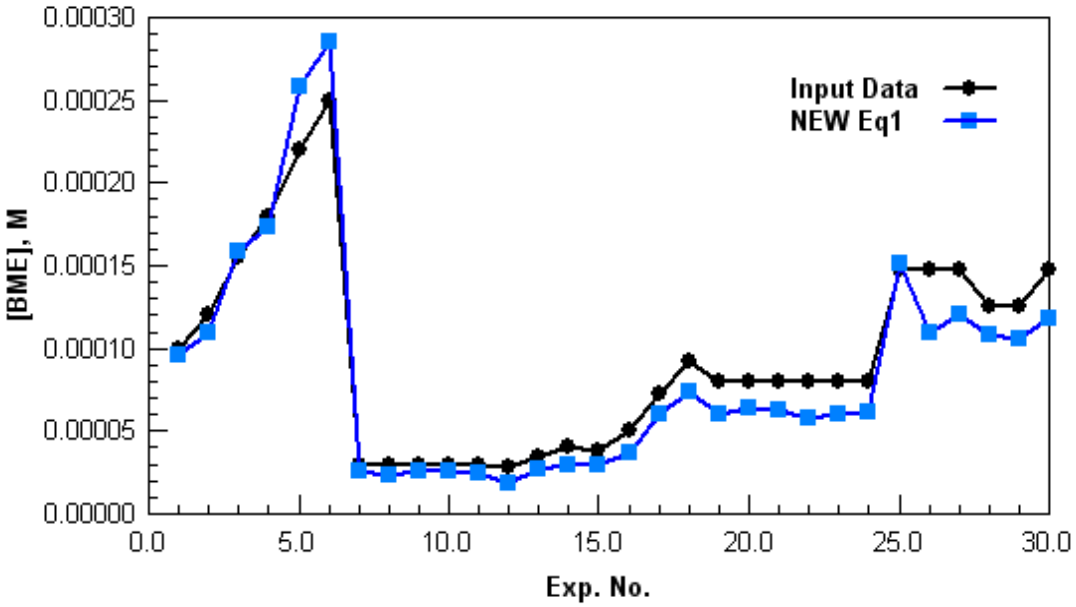

Figure 4-39. 4-D plot fitted by *Eq1'*.

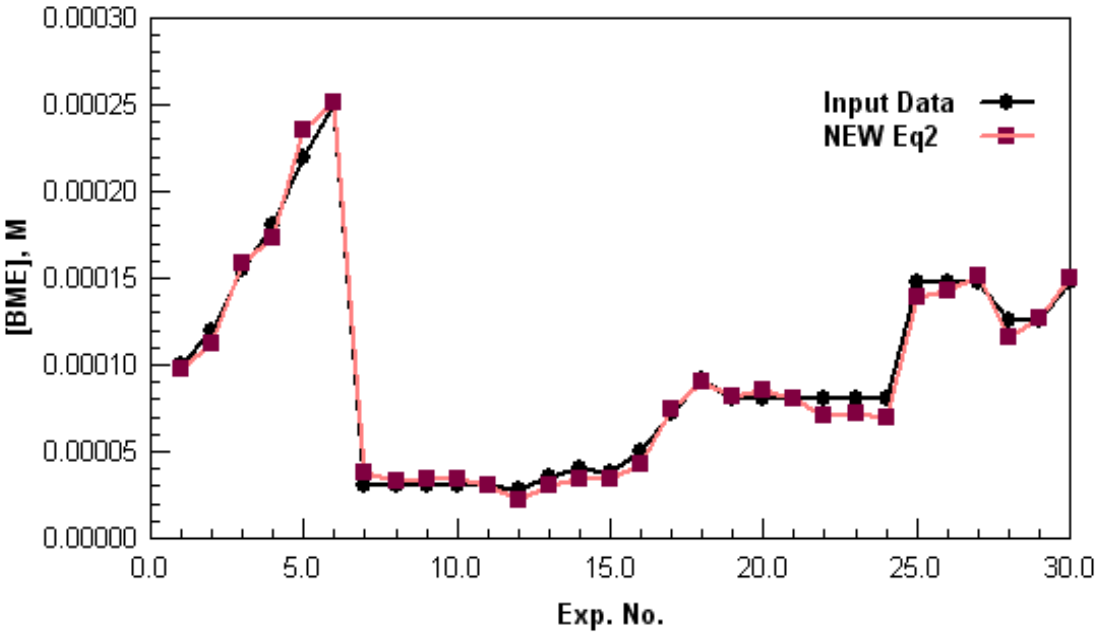

Figure 4-40. 4-D plot fitted by *Eq2'*.

The calculated coefficient of the intermediate, ε_{RSI}, from the two equations are listed in the table. They are not large enough to contribute to the absorbance, and therefore, further investigations will not consider the spectral effect from the reactive sulfenyl-iodide species.

Table 4-6. Data for determine the UV spectral feature of the intermediates.

	K_{eq}	ϵ_{RSI}
M1	2503 ± 254 M^2	244 ± 300 M^{-1} cm^{-1}
M2	5967 ± 740 M	599 ± 331 M^{-1} cm^{-1}

4.6.6 Kinetic Results of the Reaction between BME and IO_3^-

4.6.6.1 Oxygen dependence

Oxygen effect was investigated by purging nitrogen gas and oxygen into the reactants prior to the mixing. The experimental conditions are $[IO_3^-]$ = 2.5 mM, [BME] = 2.5 mM, $[H^+]$ = 0.02 M. The two kinetic traces were compared with the reaction kinetics obtained in the presence of air. As a result, no distinguishable difference can be seen from the reaction kinetics.

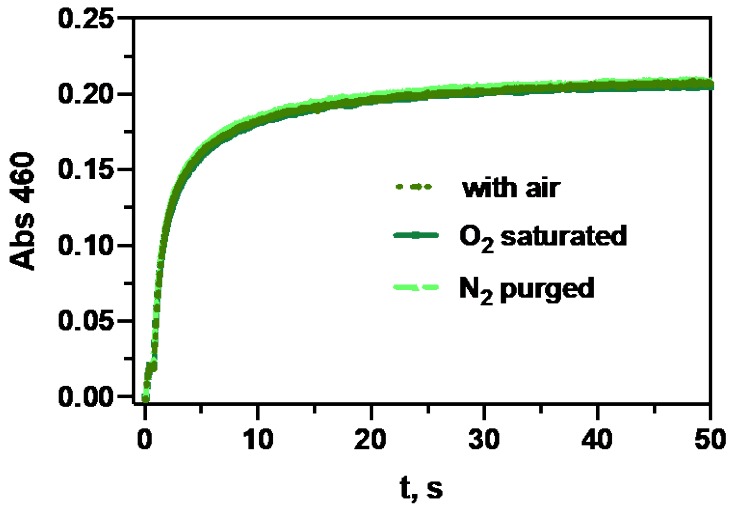

Figure 4-41. O_2 effect on the reaction kinetics.

Given that there is no effect upon saturating the solutions with O_2 or N_2, the following reactions were all carried out without purging.

4.6.6.2 pH dependence

Effect of varying acid concentration on the reaction between BME and iodate was studied under the conditions of $[IO_3^-]$ = 2.5 mM, [BME] = 2.5 mM, and $[HClO_4]$ varying from 0.03 M to 0.07 M. The reaction kinetics were examined at 460 nm spectrophotometrically. As shown below, at a lower pH, the reaction proceeds faster.

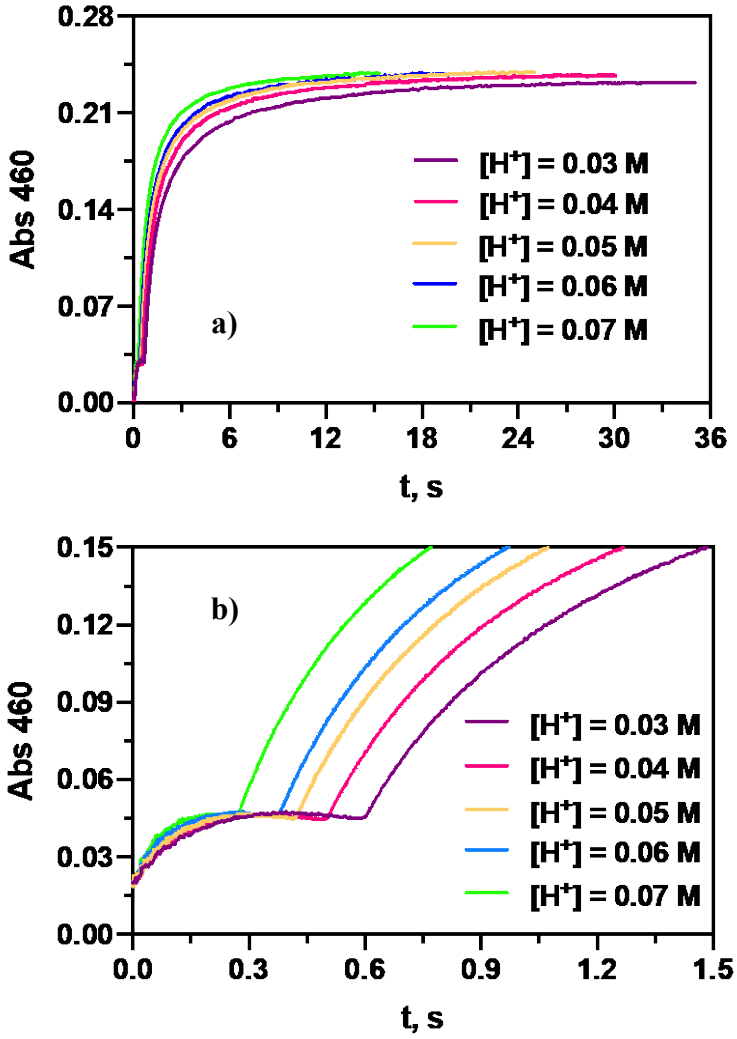

Figure 4-42. pH dependence on the a) reaction kinetics and b) clock reaction. Conditions: $[IO_3^-]_0$ = 2.5 mM, $[H^+]_0$ = 0.03– 0.07 mM, $[BME]_0$ = 2.5 m , μ = 0.1 M ($NaClO_4$), $[C_2O_4^{2-}]_0$ = 0.2 mM.

4.6.6.3 [IO_3^-] Dependence

Kinetic dependence on $[IO_3^-]$ was determined by mixing 2.5 mM BME with iodate concentration varying from 0.83 mM to 2.5 mM at constant $[H^+]$. The kinetic traces show that the rate of iodine formation is increased at higher $[IO_3^-]$. This is evident from both clock reaction and the subsequent iodine formation. Such behavior can be attributed to the effect of $[IO_3^-]$ term on the rate law of Dushman reaction with an expression of Rate $= k[H^+]^2\,[I^-]^2\,[IO_3^-]$, where k is the rate constant.

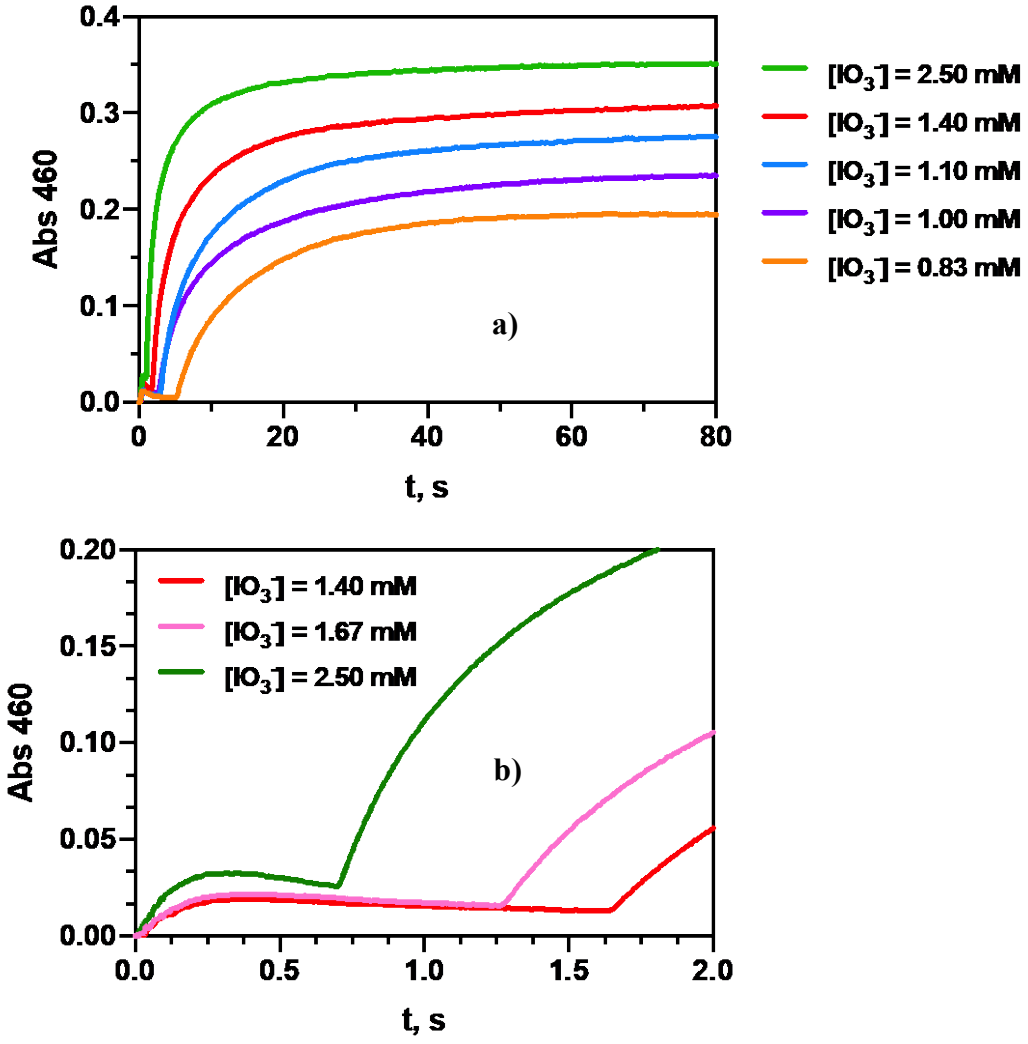

Figure 4-43. [IO_3^-] dependence on the a) reaction kinetics and b) clock reaction. Conditions: $[BME]_0 = 2.5$ mM, $[IO_3^-]_0 = 0.83 - 2.5$ mM, $[H^+]_0 = 0.02$ M.

4.6.6.4 [BME] dependence

[BME] dependence of the reaction kinetics was monitored by performing the experiments with different [BME] and keeping the rest components as constant. It turns out that the reaction completes faster when the concentration of BME is increased.

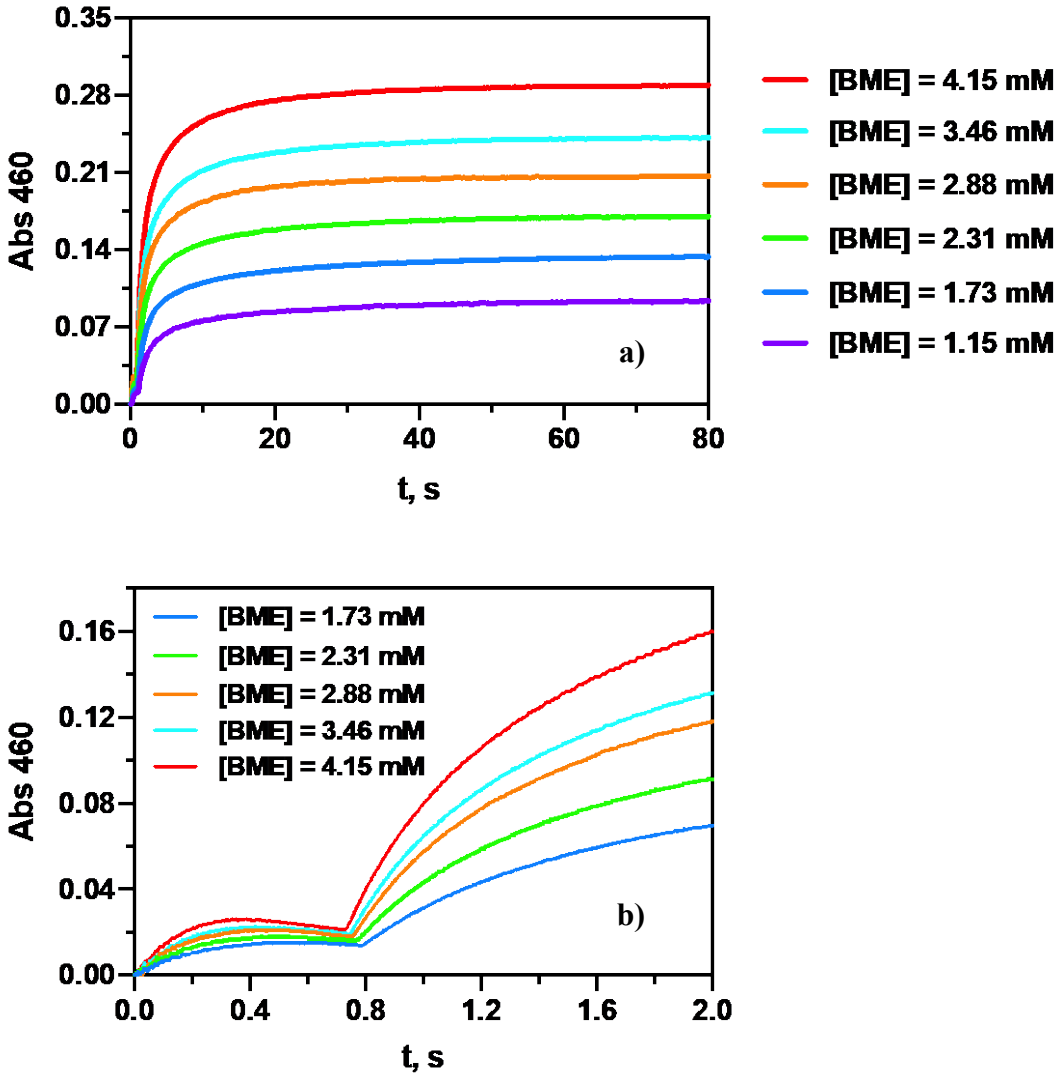

Figure 4-44. Effect of [BME] on the a) overall reaction and b) clock reaction. Conditions: $[IO_3^-]_0 = 2.5\ \text{mM}, [\text{BME}]_0 = 1.15\ \text{mM} - 4.15\ \text{mM}, [H^+]_0 = 0.02\ \text{M}$.

4.6.6.5 [Iodide] dependence

Rate dependence on $[I^-]$ was explored by increasing [iodide] of the reaction mixture. Iodide was added to BME solution before the reactants were mixed. The reaction solution contained 2.5 mM iodate, 2.5 mM BME, 0.02 M H^+ and various amount of iodide. The enhancement of the reaction rate by I^- can be observed from the sharp kinetic traces. This effect on the reaction kinetics can be hard to elaborate by a simple equation or rate law, given that iodide is involved in multiple steps of the reaction system.

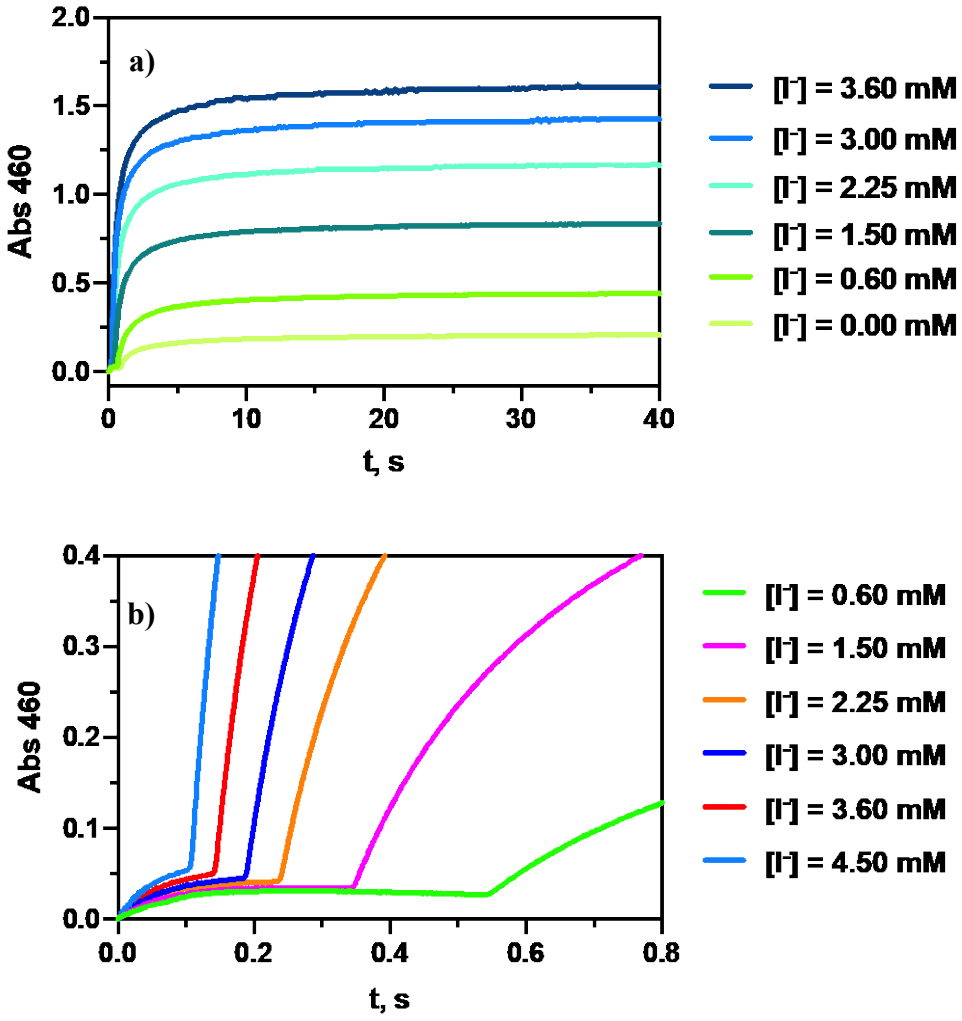

Figure 4-45. [iodide] effect on the a) overall process and b) clock reaction. Conditions: $[IO_3^-]_0 = 2.5\ \text{mM}, [\text{BME}]_0 = 2.5\ \text{mM}, [\text{I}]_0 = 0 - 4.5\ \text{mM}, [\text{H}]_0 = 0.02\ \text{M}$.

4.7 Discussion

In aqueous phase, a thiol can deprotonate to form the corresponding thiolate through the equilibrium $RSH \rightleftharpoons RS^- + H^+$ (K_a). The acidity of a thiol, known as pK_a, can be determined from $-logK_a$, where K_a is the equilibrium constant of the deprotonation [56]. For a typical -SH group, the pK_a value is in the range of 8-9, but it can be varied due to its solvent environment [60]. The studies we perform regarding thiol-iodine/iodate reactions are under highly acidic solutions, and therefore the thiol should be present in its protonated form.

4.7.1 Thiol-iodine Reactions

A general mechanism of the reactions between the two thiols (MESNA and BME) with triiodide is displayed in Table 4-7 including 4 steps.

Table 4-7. Proposed mechanism of thiol-triiodide reaction.

Step	Reaction	Rate Constant
1	$RSH + I_3^- \rightleftharpoons RSI + 2I^- + H^+$	$k_1; k_{-1}; K_1$
2	$RSI + H_2O \rightleftharpoons RSOH + H^+ + I^-$	$k_2; k_{-2}; K_2$
3	$RSOH + RSH \rightarrow RSSR + H_2O$	k_3
4	$RSI + RSH \rightarrow RSSR + H^+ + I^-$	k_4

To solve the unknown kinetic parameters, value of K_1 determined from the equilibrium study in **Part I,** for the first-step reaction is taken to be $K_{eq1}(= 1100 \pm 19\ M^2)$ for both MESNA and BME reaction with iodine. The kinetic traces were modeled using Kintecus software with the coefficients being calculated accordingly. The simulated results of the kinetic dependence on various factors are displayed below.

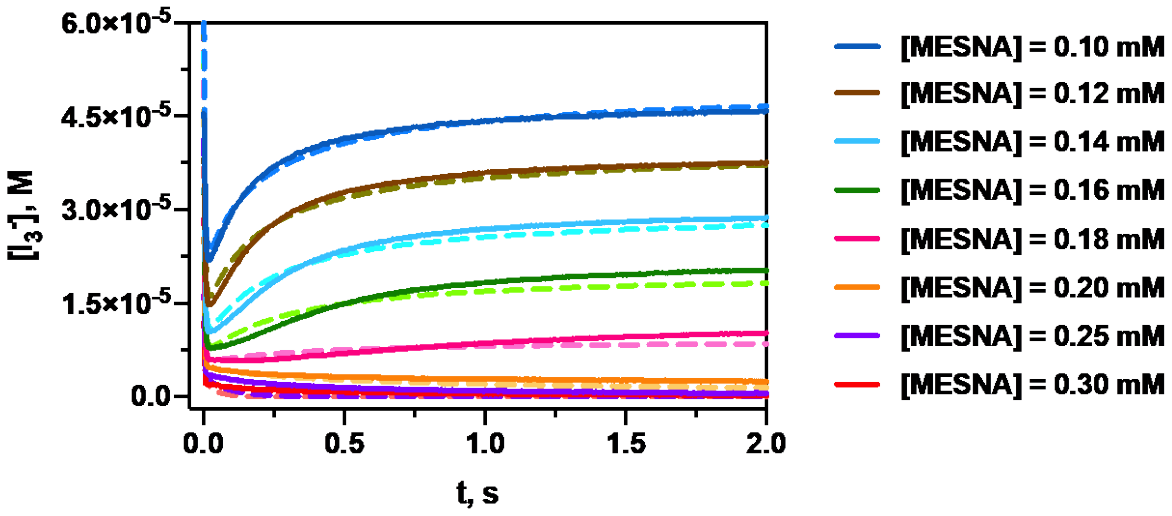

Figure 4-46. [MESNA] dependence of the reaction kinetics (solid line: experiment data; dashed line: simulation). Conditions: $[I_3^-]_0 = 0.1$ mM, $[I^-]_0 = 0.25$ M, $[H^+]_0 = 0.1$ M.

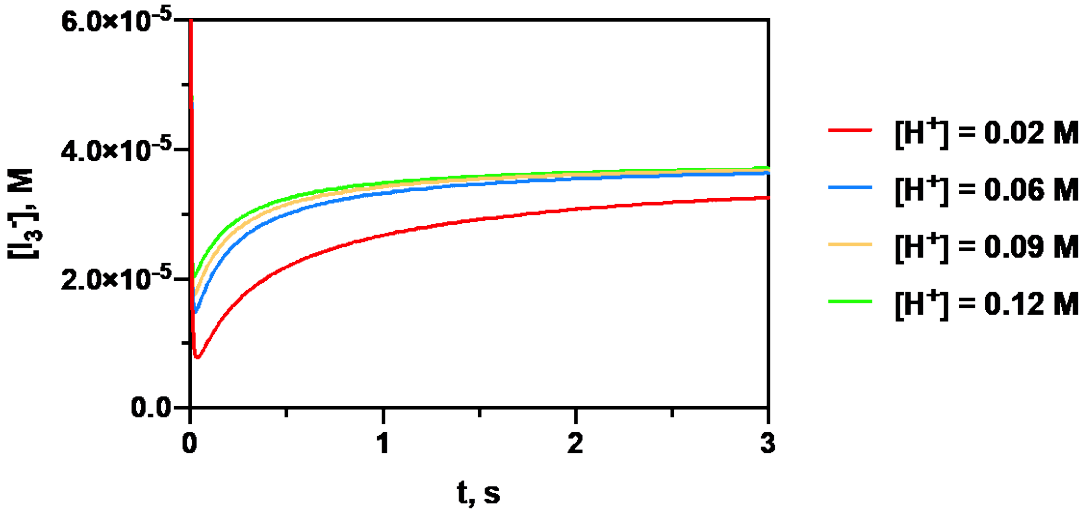

Figure 4-47. Simulation of the pH dependence. Note: Y-axis truncated to highlight the long-time behavior. Conditions: $[I_3^-]_0 = 0.1$ mM, $[I^-]_0 = 0.3$ M, $[MESNA]_0 = 0.123$ M.

Based on the proposed mechanism and simulation, the solved rate constants of the reaction between MESNA with iodine are given in the scheme.

Table 4-8. Calculated kinetic coefficient of MESNA-iodine reaction from simulation.

Reaction	Calculated Rate Constant	K_{eq}
1	$k_1 = (3.64 \pm 0.20) \times 10^6\ \mathrm{M^{-1}\ s^{-1}}$; $k_{-1} = (3.16 \pm 0.26) \times 10^3\ \mathrm{M^{-3}\ s^{-1}}$	$(1150 \pm 70)\ \mathrm{M^2}$
2	$k_2 = (3.74 \pm 0.31) \times 10^4\ \mathrm{M^{-1}\ s^{-1}}$; $k_{-2} = (2.99 \pm 0.24) \times 10^7\ \mathrm{M^{-2}\ s^{-1}}$	0.00125 M
3	$k_3 = (1.45 \pm 0.34) \times 10^5\ \mathrm{M^{-1}\ s^{-1}}$	
4	$k_4 = (2.43 \pm 0.04) \times 10^5\ \mathrm{M^{-1}\ s^{-1}}$	

Computational modelling was also performed for the reaction between BME and iodine. The resulting simulation for [BME] dependence and pH dependence are used to fit the experimental traces.

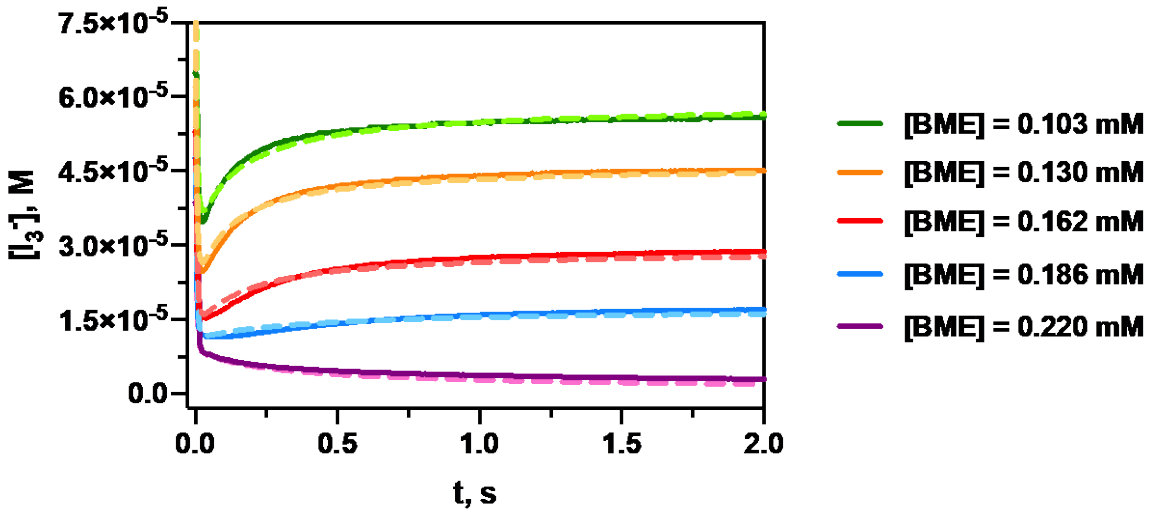

Figure 4-48. Experiment data (solid line) vs simulation (dashed line). Note: Y-axis truncated to highlight the long-time behavior. Conditions: $[I_3^-]$ = 0.11 mM, $[I^-]$ = 0.49 M, $[H^+]$ = 0.05 M.

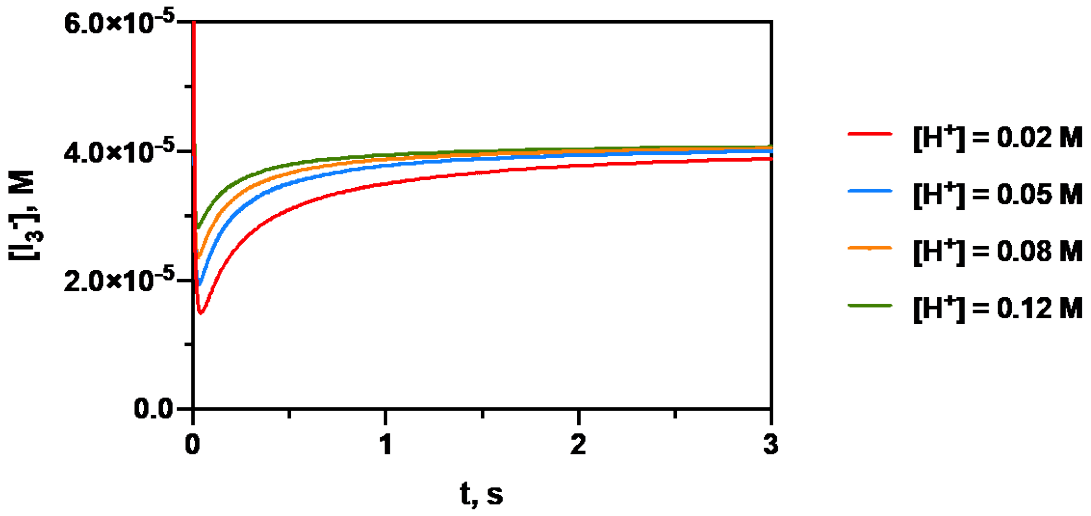

Figure 4-49. Simulation on the pH dependence. Note: Y-axis truncated to highlight the long-time behavior. Conditions: $[I_3^-]$ = 0.115 mM, $[I^-]$ = 0.4 M, [BME] = 0.147 mM.

With the equilibrium constant of $K_1 (= (1150 \pm 70)\ \mathrm{M}^2)$ obtained from the experimental and fitting result, the solved kinetic parameters for each step are determined and listed below.

Table 4-9. Calculated kinetic coefficient of BME-iodine reaction from simulation.

Reaction	Calculated Rate Constant	K_{eq}
1	$k_1 = (2.05 \pm 0.12) \times 10^6\ \mathrm{M^{-1}\ s^{-1}}$; $k_{-1} = (1.78 \pm 0.15) \times 10^3\ \mathrm{M^{-3}\ s^{-1}}$	$(1150 \pm 70)\ \mathrm{M}^2$
2	$k_2 = (2.34 \pm 0.33) \times 10^4\ \mathrm{M^{-1}\ s^{-1}}$; $k_{-2} = (1.87 \pm 0.26) \times 10^7\ \mathrm{M^{-2}\ s^{-1}}$	0.00125 M
3	$k_3 = (7.67 \pm 0.56) \times 10^4\ \mathrm{M^{-1}\ s^{-1}}$	
4	$k_4 = (2.61 \pm 0.12) \times 10^5\ \mathrm{M^{-1}\ s^{-1}}$	

The simulated results of thiol-iodine reactions fit excellently with the experimental data, and therefore provide reliable proof to the proposed 4-step mechanism. On account of the addition of large excess of iodide, the free iodine should be present in all conditions as triiodide. The first step is a process of nucleophile (Nu^-) attack on triiodide by thiol to form the intermediates. The

intermediate, however, cannot be detected spectrally or isolated as it is kinetically reactive. Equilibrium study successfully proved the presence of transient species to be the corresponding sulfenyl-iodide, $IS(CH_2)_2SO_3^-$ and $HO(CH_2)_2SI$. Sulfenyl iodides (RSI) are generally generated from the reaction of thiols and iodine. It was first proposed by Fraenkel-Conrat based on the observation that tobacco mosaic virus consume two equivalents of iodine because of the formation of RSI group [57]. In regard to its physiological function, sulfenyl iodides play an important role in participating in iodination and deiodination process in thyroid [69],[70]. Since the species is highly unstable, it can easily disproportionate. It is also worth noting that the fate of RSI can be determined by the surrounding environment. In biological systems, some sulfenyl iodides can be stable and kinetic favorable in protein due to the steric isolation by the rigid scaffold of the biomolecules [58],[59]. Whereas in other systems that lack well-defined spatial constraints, it might be challenging to trap the elusive species and study it quantitively. In our case, we prove the formation of RSI through a I^+ transfer mechanism expressed as $Nu^- + I_3^- \rightleftharpoons NuI + 2I^-$.

The second step of the reaction is the decomposition of sulfenyl iodide to generate sulfenic acid (RSOH). Given that sulfenic acids are transient species, and they tend to degrade through over-oxidation, nucleophile reaction to produce disulfide, and self-condensation to form thiosulfinates [20], the large rate constant solved for k_{-2} and k_3 is justified to be reasonable. The third step is a reaction between sulfenic acid and the thiol to release disulfide. This, however, is not the only path to produce disulfide in the system. As the oxidation state of sulfonyl iodide is not stable, it further reacts with the thiol to form disulfide as shown in step 4 as well.

4.7.2 Thiol-iodate Reactions

Generally, the reactions and species involved in acidic iodate solutions are considerably complex. It is quite challenging to determine and isolate the reactive species occurring in the

system as they are mostly short-lived. Based on this fact, it is believed that using a rate law to explain the kinetic behaviors can be very difficult, and hence, we attempt to propose a network with multiple steps of the reaction based on experimental results and theoretical knowledge. The scheme displayed below presents the general underlying mechanism network elaborating the reaction between two thiols with iodate which include 15 steps reaction.

Table 4-10. Proposed mechanism for thiol-iodate reactions.

Step	Reaction	k_f	k_r	K_{eq}
1	$H^+ + IO_3^- \rightleftharpoons HIO_3$	2.53×10^8	1×10^8	2.53 [a]
2	$HIO_3 + H^+ + I^- \rightleftharpoons I_2O_2 + H_2O$	2.5×10^8 [a]	40 [a]	
3	$I_2O_2 + H_2O + H^+ \rightleftharpoons HIO_2 + HOI + H^+$	1.1×10^4 [b]		
4	$HIO_2 \rightleftharpoons IO_2^- + H^+$	3.1×10^6	1×10^{10}	3.1×10^{-4} [a]
5	$I_2O_2 + I^- \rightarrow I_2 + IO_2^-$	130 [a]		
6	$HIO_2 + H^+ + I^- \rightleftharpoons 2HOI$	1×10^{10}	1.3	7.5×10^8 [d]
7	$HOI + H^+ + I^- \rightleftharpoons I_2 + H_2O$	1.7×10^9 [c]	1.8×10^{-3} [c]	9.4×10^{11} [c]
8	$I_2 + I^- \rightleftharpoons I_3^-$	6×10^9	8×10^6	
9	$RSH + I_3^- \rightleftharpoons RSI + H^+ + 2I^-$	3.64×10^6 [M]	3.16×10^3	1150 ± 70
		2.05×10^6 [B]	1.78×10^3	
10	$RSI + H_2O \rightleftharpoons RSOH + H^+ + I^-$	3.74×10^4 [M]	2.99×10^7	
		2.34×10^4 [B]	1.78×10^7	
11	$RSH + HIO_3 \rightarrow RSOH + HIO_2$	50		
12	$RSH + HIO_2 \rightarrow RSOH + HOI$	1000		
13	$RSH + HOI \rightarrow RSOH + H^+ + I^-$	500		
14	$RSH + RSOH \rightarrow RSSR + H_2O$	1.45×10^5 [M]		
		7.67×10^4 [B]		
15	$RSH + RSI \rightarrow RSSR + H^+ + I^-$	2.43×10^5 [M]		
		2.61×10^5 [B]		

References:

[*a*] Horváth, V.; Epstein, I. R.; Kustin, K. *J. Phys. Chem. A* **2016**, *120*, 1951−1960.

[*b*] Xu. L; Horváth, A. K. *J. Phys. Chem.* **2014**, *118*, 6172-6180.

[c] Schmitz, G. E.; Furrow, S. D., *Reaction Kinetics, Mechanisms and Catalysis*. **2022**. DOI: org/10/1007/s11144-022-02155-4.

[d] Schmitz, G. *J. Chem. Kinet*. **2008,** *40*, 647-652.

[M] MESNA-Iodine part of this work.

[B] BME-Iodine part of this work.

The addition of reaction 1, 2 and 3 in Table 4-10 lead to an equation

$$R_{total}: \quad IO_3^- + 2H^+ + I^- \rightleftharpoons HIO_2 + HOI \quad (K_{tot})$$

According to the principle of detailed balancing, the equilibrium constant of the total reaction is $K_{tot} = K_1 \times K_2 \times K_3 = K_1 \times K_2 \times (k_3/k_{-3})$. With K_1, K_2, k_3 values known from the table, and K_{tot} being reported recently by Furrow & Schmitz [c] with a value of 6.1 M^{-1}, k_{-3} can therefore be calculated to be 2.83×10^{10}. When the backward reaction with the solved rate constant is included to the overall reaction scheme in Table 4-10, the simulated half-time of reaction kinetics is nearly 3 times faster compared to that without the reverse step.

Suppose R12 is reversable, $K_{12} = K_6 \times K_7 \times K_9 \times K_{10}$ can be obtained from the reaction scheme, where the only unknown is k_{-12}. This can be solved based on the values in the table to be 9.8×10^{-19}. Similarly, when R13 is reversable, K_{13} equals to $K_7 \times K_9 \times K_{10}$, and k_{-13} is found to be 3.7×10^{-10}. The surprisingly large equilibrium constant for both R12, R13 indicates that the backward reaction for this two reactions are not favorable. To avoid the complexity caused by detailed balancing, k_{-7} can be omitted, and k_{-12}, k_{-13} is therefore not required. With the backward step of R7 excluded in the mechanism, the simulation on the reaction kinetics does not make any detectable change.

The overall reaction scheme begins with displaying the Dushman reaction of the reduction of iodate to iodine through several steps (R1 to R7). R1, R2, R4, R6, R7 are rapidly established equilibria. Among them, R1 and R4 involve the protonation of iodate anion and the equilibrium of

iodous acid (HIO_2), the rate constants of which are estimated to be nearly diffusion-controlled limit in the favorable direction. R7 can be interpreted as the backward reaction of iodine hydrolysis. The rate of this step can be largely affected by the concentration of iodide and pH as it was discussed by Schmitz (2004) [62],[63]. The rate coefficients of these steps are either adopted from the recent reports or obtained from our simulation on the overall reaction.

Reaction 8 is the well-known I_2/I^- equilibrium to form I_3^- which is a relatively inert electrophile as compare with aqueous iodine. This reaction has been widely reported with $K_{I_3^-}$ values of (720 ± 30) M [61],[62]. Kinetic data regarding the change of I_3^- at 360 nm is shown below, where a rapid formation of I_3^- due to the iodine equilibrium in few seconds can be detected, followed by the consumption of it by the reductant. The rate of this equation is described as $k_f[I_2]I - k_b[I_3^-]$ which is first-order in $[I^-]$. This explains the kinetic behavior in the figure that the reaction goes faster with the increase in $[I^-]$ at the first place.

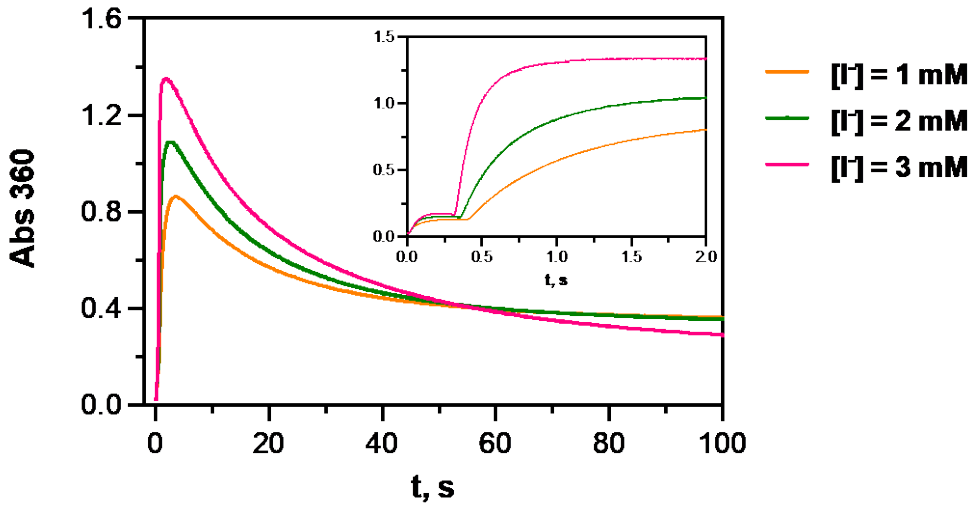

Figure 4-50. Kinetic traces at 360 nm with different $[I^-]$. Conditions: $[MESNA] = 5.0$ mM, $[IO_3^-] = 5$ mM, $[H^+] = 0.02$ M.

Starting from reaction 8, thiol participates in various reaction process as a nucleophile. Triiodide attacks the sulfur center of the thiol to produce sulfenyl iodide (RSI) as discussed earlier

in this work, followed by the release of sulfenic acid (RSOH) as a reactive intermediate. As not only iodine is capable of oxidizing the thiol in solution, various oxy-iodine species including iodic acid (HIO_3), iodous acid (HIO_2), hypoiodous acid (HOI) are capable of reacting with the nucleophile as well. The direct oxidation of RSH by these species should also give RSOH as products, and hence makes RSOH an essential component of the formation of final product.

Sulfenic acids are mostly thought as an early oxidation product of the reaction of biological thiols with reactive species such as ROS, RNS, and thus regarded as a potential biomarker for oxidative stress and redox regulator [20],[64]. Over the years, researchers have been looking for effective and rapid methods to detect various sulfenic acids. Some well-accepted techniques include the use of chemical probes such as dimedone and its derivatives [65]-[67] or biotin switch methods [68]. Given that the thiol we investigate has a low molecular weight, dimedone is expected to be an optimized scavenger for trapping MESNA-sulfenic acid once it occurs in the MESNA-iodate mixture. The effective trap of dimedone on the targeting RSOH will generate a stable product, the corresponding thioether. The reaction is described below.

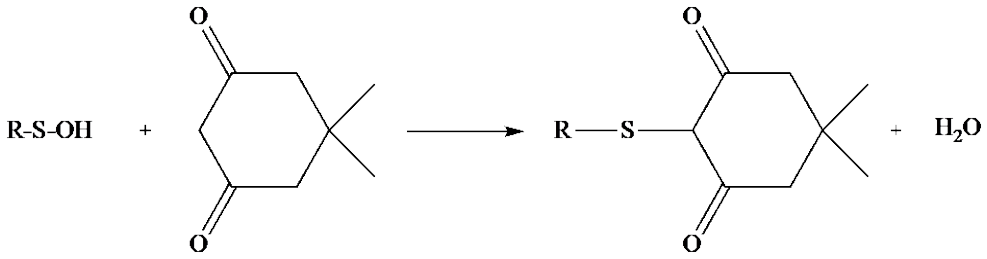

Prior to the trapping experiment of the reaction solution, UV-Vis spectrum of dimedone was recorded. It turns out that dimedone does not absorb at the wavelength range we investigate.

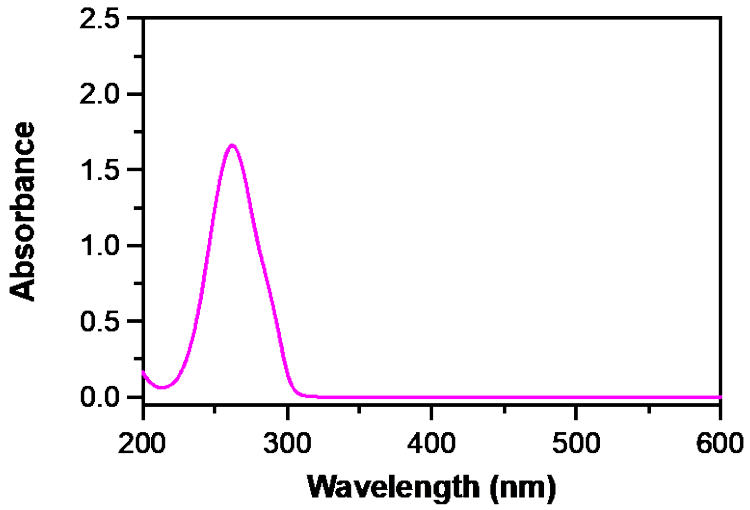

Figure 4-51. UV-Vis spectrum of the 0.12 mM recrystallized dimedone.

Next, the kinetic traces from UV-Vis spectrophotometer at 460 nm of the reaction mixture in the presence or absence of dimedone is obtained. It can be observed from the spectrum that the reaction will not proceed to form iodine when dimedone is included, implying that dimedone has effect on the reaction mixture.

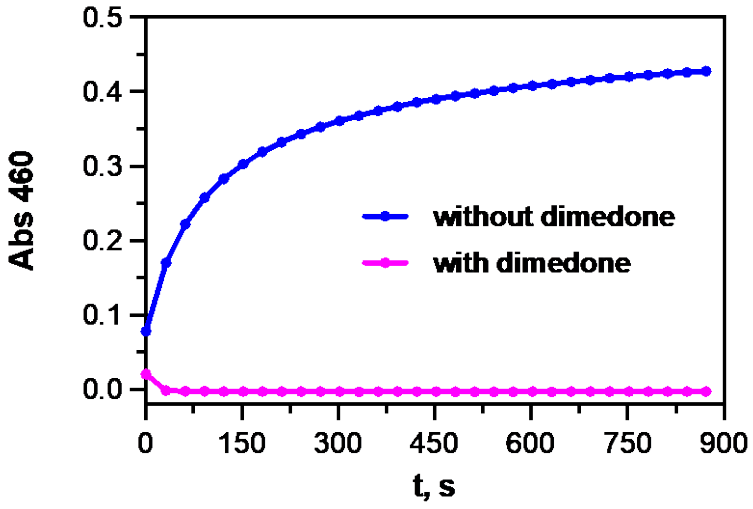

Figure 4-52. UV-Vis kinetics of the mixture of MESNA and iodate with/without dimedone. Conditions: $[\text{MESNA}] = 10\ \text{mM}, [IO_3^-] = 2\ \text{mM},\ [\text{Dimedone}] = 7.5\ \text{mM},\ [H^+] = 0.02\ \text{M}$.

Later, an MS sample was prepared by mixing 10 mM MESNA with 2 mM iodate and 20 mM dimedone in 2 mM $HClO_4$. After reacting 30 minutes, the sample was monitored through ESI-MS with positive mode. As shown in the spectrum below, the peak at m/z = 325.0137 was identified to be the sodium thioether with the formula of $C_{10}H_{15}O_5S_2Na$ with an extra Na^+ bonded.

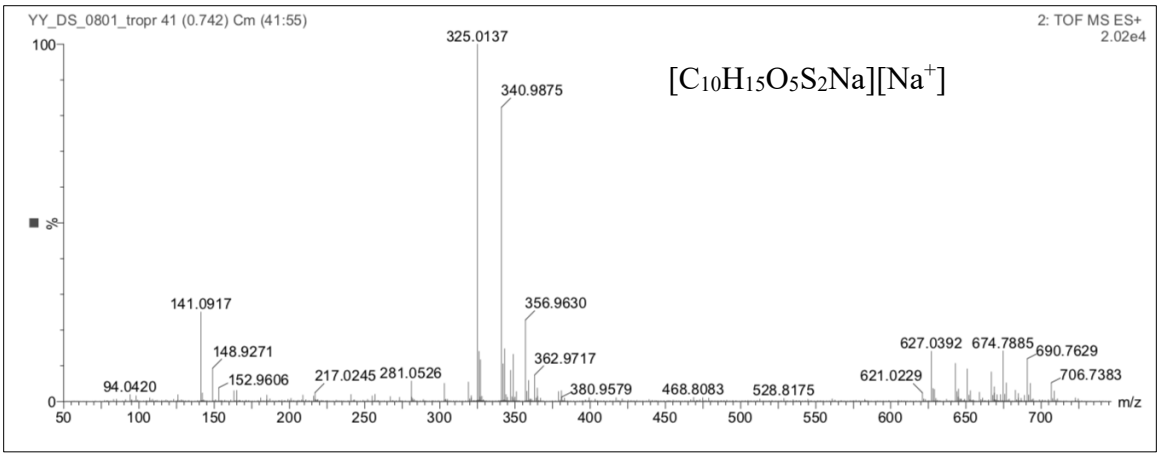

Figure 4-53. ESI-MS spectrum of the trapping product.

With the evidence collected from UV-Vis and MS, the formation of sulfenic acid in the reaction is strongly justified. The rate constants of the reactions between RSOH and the three protonated oxy-iodine species are simulated through computational modeling. The eventual production of disulfide is achieved from the reaction of the thiol with RSI and RSOH. The kinetic coefficients were used from the simulation of thiol-I_3^- reaction discussed earlier in this work.

When the trapping step

$$\mathrm{RSOH} + \mathrm{dimedone} \rightarrow \mathrm{adduct} + \mathrm{H_2O}$$

with an estimated rate constant of 1×10^{10} is added to the reaction scheme in Table 4-10, step 10 should be irreversible given that sulfenic acid is largely consumed by the trapping reagent, and reaction 14 will not take place. Using this mechanism, the simulation in the presence of dimedone under Figure 4-52 conditions yields an identical result that the reaction is quenched by the scavenger.

4.8 Conclusions

In this study, we proposed a comprehensive mechanism scheme of the oxidation of two thiols, MESNA and BME, by iodine/iodate in acidic media, proving the thiols can be potential antioxidants used for reducing the toxicity induced by some reactive sulfur species, such as sulfenic acid. In addition, the thiols can act as powerful regulators for adjusting hormone level in the biological environment based on their reactions with various oxy-iodine species. The rapid oxidation of MESNA by iodine/iodate to produce the corresponding MESNA-disulfide provides an effective method for synthesizing 2-sulfonatoethyl disulfide (SEDS) without the assistance of additional catalyst. More importantly, the reactions regarding aqueous iodine system are better investigated by strictly following the principle of detailed balancing. The dynamic coefficients reported in this work, for instance, the hydrolysis and decomposition of the sulfenyl-intermediates including RSI, RSOH will provide applicable information for the regulation of metabolism and enzyme activities in living cells.

4.9 References

[1] Bagiyan, G. A.; Koroleva, I. K.; Soroka, N. V.; Ufimtsev, A. V. *Russ. Chem. Bull.* **2003**, *52*, 1135-1141.

[2] Sanz, R.; Aguado, R.; Pedrosa, M. R.; Arnaiz, F. J. *Synthesis*. ***2002,*** *7*, 0856-0858.

[3] Tidei, C.; Piroddi, M.; Galli, F.; Santi, C. *Tetrahedron Lett*. **2012**, *53*, 232-234.

[4] Wu, X.; Rieke, R. D.; Zhu, L. *Synth. Commun*. **1996**, *26*, 191-196.

[5] Ali, M. H.; McDermott, M. *Tetrahedron Lett*. **2002**, *43*, 6271-6273.

[6] Smith, R. C.; Reed, V. D.; Hill, W. E. *Phosphorus, Sulfur, and Silicon and the Relat. Elem*. **1994**, *90,* 147-154.

[7] Iranpoor, N.; Zeynizadeh, B. *Synthesis*. **1999**, *1*, 49-50.

[8] Dhar, D. N.; Bag, A. K. *Ind. J. Chem.* **1984**, *23B*, 974.

[9] Bhattarai, N.; Stanbury, D. M. *Inorg. Chem.* **2012**, *51*, 13303-13311.

[10] Ghammamy, S.; Tajbakhsh, M. *J. Sulfur Chem.* **2005**, *26*, 145.

[11] Scarpa, M.; Momo, F.; Viglino, P.; Vianello, F.; Rigo, A. *Biophys. Chem.* **1996**, *60*, 53.

[12] Frasca, D. R.; Clarke, M. J. *J. Am. Chem. Soc.* **1999**, *121*, 8523.

[13] Chatterjee, D.; Pal, U.; Ghosh, S.; van Eldik, R. *Dalton Trans.* **2011**, *40*, 1302.

[14] Nayak, S.; Brahma, G. S.; Reddy, K. V. *Aust. J. Chem.* **2012**, *65*, 113.

[15] Kevasan, V.; Bonnet-Dulpon, D.; Bégué, J. P. *Synthesis*, **2000**, *2*, 223.

[16] Ravikumar, K.S.; Kesavan, V.; Crousse, B.; Bonnet-Delpon, D.; Bégué, J. P. *Org. Synth.* **2003**, *80*, 184-189.

[17] Holbrook, D. L. *Handbook of Petroleum Refining Processes*, Edited by: Meyers, R. A. New York: McGraw-Hill. **1996**, Ch. 11.3.

[18] Sengupta, D.; Roy, B.; Basu, B. *Curr. Med. Chem*. **2017**, *24*, 4627-4637.

[19] Jacob, C.; Holme, A. L.; Fry, F. H. *Org. Biomol. Chem.* **2004**, *2*, 1953-1956.

[20] Alcock, L. J.; Perkins, M. V. ; Chalker, J. M. *Chem. Soc. Rev.* **2018**, *47*, 231-268.

[21] Paulsen, C. E.; Carroll, K. S. *Chem. Rev.* **2013**, *113*, 4633-4679.

[22] Jacob, C.; Giles, G. I.; Giles, N. M.; Sies, H. *Angew. Chem.* **2003,** *115,* 4890-4907.

[23] Miseta, A.; Csutora, P. *Mol. Biol. Evol.* **2000**, *17*, 1232-1239.

[24] Nagy, P.; Ashby, M. T. *J. Am. Chem. Soc*. **2007**, *129*, 14082-14091.

[25] Pople, J. M.; Chalker, J. M. *Curr. Opin. Chem. Biol.* **2021**, *60*, 55-65.

[26] Yang, K.S.; Kang, S.W.; Woo, H. A.; Hwang, S.C.; Chae, H. Z.; Kim, K.; Rhee, S. G. *J. Bio. Chem.* **2002**, *277*, 38029-38036.

[27] Reddie, K. G.; Carroll, K. S. *Curr. Opin. Chem. Biol*. **2008**, *12*, 746-754.

[28] Wang, Y.; Vivekananda, S.; Men, L.; Zhang, Q. *J. Am. Soc. for Mass Spectrom.* **2004**, *15*, 697-702.

[29] Paulsen, C. E.; Carroll, K. S. *ACS Chem. Biol.***2010**, *5*, 47-62.

[30] Poole, L. B.; Nelson, K. J. *Curr. Opin. Chem. Biol.* **2008**, *12*, 18-24.

[31] Poole, L. B.; Furdui, C. M.; King, S. B. *Essays Biochem*. **2020**, *64*, 1-17.

[32] Ida, T.; Sawa, T.; Ihara, H.; Tsuchiya, Y.; Watanabe, Y.; Kumagai, Y.; Suematsu, M.; Motohashi, H.; Fujii, S.; Matsunaga, T.; Yamamoto, M. *Proc. Natl. Acad. Sci.* **2014**, *111*, 7606-7611.

[33] Ziegler, D. M. *Annu. Rev. Biochem.* **1985**, *54*, 305-329.

[34] Sen, C. K. *Curr. Top. Cell. Regul*. **2001**, *36*, 1-30.

[35] Baba, S. P.; Bhatnagar, A. *Curr. Opin. Toxicol*. **2018**, *7*, 133-139.

[36] Dickinson, D. A.; Forman, H. J. *Biochem. Pharmacol.* **2002**, *64*, 1019-1026.

[37] Winterbourn, C. C.; Metodiewa, D. *Free Radic. Biol*. **1999**, *27*, 322-328.

[38] Denu, J. M.; Tanner, K. G. *Biochem*. **1998**, *37*, 5633-5642.

[39] Denu, J. M.; Zhou, G.; Guo, Y.; Dixon, J. E. *Biochem.* **1995**, *34*, 3396-3403.

[40] Chanakira, A.; Chikwana, E.; Peyton, D. H.; Simoyi, R. H. *Can. J. Chem.* **2006**, *84*, 49-57.

[41] Chikwana, E.; Davis, B.; Morakinyo, M. K.; Simoyi, R. H. *Can. J. Chem.* **2009**, *87*, 689-697.

[42] Stanbury, D. M. *J. Phys. Chem.* **2018,** *15*, 3956-3957.

[43] Taylor, C. D.; Wolfe, R. S. *J. Biol. Chem.* **1974,** *15*, 4879-4885.

[44] Balch, W. E.; R. S. Wolfe. *Appl. Environ. Microbiol.* **1976***, 32*, 781-791.

[45] Allen, J. R.; Clark, D. D.; Krum, J. G.; Ensign, S. A. *Proc. Natl. Acad. Sci.* **1999***, 96*, 8432-8437.

[46] Ensign, S. A.; Allen, J. R. *Annu. Rev. Biochem.* **2003**, *72*, 55-76.

[47] Krishnakumar, A. M.; Sliwa, D. l; Endrizzi, J. A.; Boyd, E. S.; Ensign, S. A.; Peters, J. W. *Microbiol. Mol. Biol. Rev.* **2008**, *72*, 445-456.

[48] Ant, A.; Karamert, R.; Kulduk, G.; Ekinci, Ö.; Tutar, H.; Göksu, N. *Surg. Neurol. int.* **2015**, *6*.

[49] Casale, M.; Di Martino, A.; Salvinelli, F.; Trombetta, M.; Denaro, V. *Expert. Opin. Investig. Drugs.* **2010**, *19*, 699-707.

[50] Alexander, N. M. *J. Biol. Chem.* **1959,** *234*, 1530-1533.

[51] Anson, M. L. *J. Gen. Physiol.* **1941,** *24*, 399-421.

[52] Cunningham, L. W.; Nuenke, B. J. *J. Biol. Chem.* **1959,** *234*, 1447-1451.

[53] Wong, S.; Kirkland, J. L.; Schwanz, H. A.; Simmons, A. L.; Hamilton, J. A.; Corkey, B. E.; Guo, W. *Life Sci.* **2014**, *107*, 32-41.

[54] Sartori, G.; Ballini, R.; Bigi, F.; Bosica, G.; Maggi, R.; Righi, P. *Chem. Rev.* **2004**, *104*, 199-250.

[55] Sariri, R.; Jafarian, V.; Sajedi, R. H.; Khajeh, K. *J. Mol. Liq.* **2006**, *128*, 175-177.

[56] Zheng, Y.; Zheng, W.; Zhu, D.; Chang, H. *New J. Chem.* **2019**, *43*, 5239-5254.

[57] Fraenkel-Conrat, H. *J. Biol. Chem.* **1955**, *217*, 373.

[58] Yee, K. K.; Wong, Y. L.; Xu, Z. *Dalton Trans*. **2016**, *45*, 5334-5338.

[59] Kratochwil, N. A.; Ivanov, A. I.; Patriarca, M.; Parkinson, J. A.; Gouldsworthy, A. M.; del Socorro Murdoch, P.; Sadler, P. J. *J. Am. Chem. Soc.* **1999**, *121*, 8193-8203.

[60] Ferrer-Sueta, G.; Manta, B.; Botti, H.; Radi, R.; Trujillo, M.; Denicola, A. *Chem. Res. Toxicol.* **2011**, *24*, 434-450.

[61] Ruasse, M.; Aubard, J.; Galland, B.; Adenier, A. *J. Phys. Chem.* **1986**, *90*, 4382-4388.

[62] Schmitz, G. *Int. J. Chem. Kinet.* **2004**, *36*, 480-493.

[63] Schmitz, G. E.; Furrow, S. D. *React. Kinet. Mech. Catal*. **2022**, 1-16.

[64] Denu, J. M.; Tanner, K. G. *Biochem*. **1998**, *37*, 5633-5642.

[65] Paulsen, C. E.; Truong, T. H.; Garcia, F. J. Homann, A.; Gupta, V.; Leonard, S. E.; Carroll, K. S. *Nat. Chem. Biol.* **2012**, *8*, 57-64.

[66] Reddie, K. G.; Carroll, K. S. *Curr. Opin. Chem. Biol.* **2008**, *12*, 746-754.

[67] Kohr, M. J.; Sun, J.; Aponte, A.; Wang, G.; Gucek, M.; Murphy, E.; Steenbergen, C. *Circ. Res.* **2011**, *108*, 418-426.

[68] Saurin, A. T.; Neubert, H.; Brennan, J. P.; Eaton, P. *Proc. Natl. Acad. Sci.* **2004**, *101*, 17982-17987.

[69] Fawcett, D. M. *Can. J. Biochem.* **1968**, *46*, 1433-1441.

[70] Yee, K. K.; Wong, Y. L.; Xu, Z. *Dalton Trans*. **2016**, *45*, 5334-5338.

[71] Perez-Benito, J. F.; Saiz, N.; Amat, E. *J. Mol. Catal. A Chem*. **1998**, *135*, 1-10.

[72] Turner, D. H.; Flynn, G. W.; Sutin, N.; Beitz, J. V. *J. Am. Chem. Soc.* **1972**, *94*, 1554-1559.

5 Kinetics and Mechanism of the Reaction of Disulfides (RSSR) with Iodine

5.1 Introduction

Disulfides (RSSR) are a type of compounds which have sulfur-sulfur bonds. They are generally derived from the coupling of two thiol (-SH) groups and are present in many proteins. In biological environments, S-S bonds are covalent links between two cysteine residues [1],[2]. The physiological importance of disulfides in proteins are especially highlighted by the fact that they can stabilize proteins' structure and regulate enzyme activities. Formation and cleavage of S-S bonds have been extensively explored due to their significance in biology, agriculture, and food industry [3],[4]. The stability of the bond can be affected by temperature, pH, ionic strength, etc. [5],[6]. For example, an intramolecular S-S bond of a wine protein was found to be able to unfold under a heat stress (at 70 ℃) in the presence of sulfur dioxide to release thiol and the reduced form of the protein upon cooling [6],[7]. Early studies from the Kharasch group have shown that electrophilic attack on disulfides by halogens such as chlorination of disulfide gives sulfenyl halides. The reaction can be catalyzed by sulfuric acid [8],[9]. Halogens are two-electron oxidants that are reactive to many other species. The mechanism of the reaction between halogens and some reductants can be complex and subtle due to their special features and high reactivity in aqueous phase. Questions can be addressed on whether the oxidation takes place through an electron-transfer mechanism or halogen cation transfer pathways followed by halide ion elimination [10]-[12]. To better address the question, iodine is typically selected as a reactant for studying these reactions, not only because it is a powerful two-electron oxidant, but also because it is known as a vital component of hormones that participates in the biosynthesis and metabolism among human tissue [24]. Studies on the reaction of iodine/triiodide with nucleophiles have been on-going for decades. Kinetics and mechanism of the oxidation of a base, hydroxylamine (NH_2OH), by

iodine/triiodide was reported by Margerum in 1995 [10]. The reaction was found to obey a first-order rate law with excess NH_2OH under a certain pH range. The proposed mechanism included a rapid reaction between I_2 and NH_2OH and followed by general-base assisted deprotonation of I_2NH_2OH to produce INHOH. Inhibition of the reaction rate by H^+ and I^- were also stated owing to the loss of base assistance. Notably, the reaction mechanism was described as I^+ transfer and subsequent I^- elimination instead of electron-transfer pathways. In 1998, the reaction between hydrazine ($N_2H_5^+/N_2H_4$) and iodine/triiodide was examined [13]. The overall mechanism turned out to be similar as that of I_2/NH_2OH reaction, whereas some kinetic behaviors were distinct. One example is the reaction sensitivity towards pH. Different intermediates were proposed accordingly at various pH: the formation of $IN_2H_4^+$ as a steady-state species at low pH (<3) and the production of $I_2N_2H_4$ adduct at high pH, the latter of which undergoes deprotonation, and subsequently reacts with I_2 to release N_2 as a final product. Interestingly, the reaction rate decreases as I^- concentration increases at low pH, whereas the inhibition is not evident in acetate and phosphate buffer due to the direct reaction of $I_2N_2H_4$ and the base. General base effect on the reaction rate instead of forming N_2H_4-buffer ion complexes was considered as an explanation for the rate dependence on the buffers. Later reports were extended to the study of oxidation of dimethylthiourea [14], cysteamine [15], methionine [16],[44], pentathionate [17], thiourea dioxide [18], etc. Short-lived intermediates are generally produced in these reactions from the rapid equilibrium established by halogen species. Buffers are normally recognized as a major influence on the reaction pathways, mostly depending on their intrinsic property and concentration [18]. In terms of halogen ion effect on the reaction kinetics, iodide for instance, can either inhibit the reaction rate or uninfluential. To clarify the kinetic dependence on iodide, evaluations often proceed based on whether the reversibility of the reaction or the formation of I_3^- is dominant in the system [17],[21]-[23].

Despite the extensive studies on halogen-sulfur redox chemistry, kinetics and mechanisms of these reactions can be very tricky and questionable. In addition, research on the reactions of S-S bond mostly involve its breaking using reducing agents-namely dithiothreitol and 2-mercaptoethanol [25], whereas the mechanism of the oxidation of disulfides has not been extensively studied and reported. Methods for preparing some derivatives of disulfide and sulfenic acid such as thiosulfinic acid and thiosulfonic acid are also limited, mainly using m-chloroperbenzoic acid (MCPBA) or Cl_2/AcOH at a very low temperature. Our exploration on the kinetics and mechanism of the oxidation of three disulfides at (25 ± 0.1) ℃ including MESNA (methansulfonate)-RSSR, 2-hydroxyethyl disulfide, 3,3'-dithiodipropionic acid by iodine would provide more efficient methods for preparing disulfide derivatives and contribute to halogen-sulfur chemistry in a mechanistic level. More specifically, the study will make the following aspects clear: 1) whether I_2/I_3^- can be a good candidate for S-S bond cleavage or S=O bond formation; 2) what are the causes that affect the kinetics of iodine-disulfides reactions; 3) the reactivity of different disulfides with electrophiles. Most importantly, the knowledge and insights gained from this study could perhaps get us a better understanding on regulating hormone using sulfur-containing species.

5.2 Experimental Preparation and Methods

5.2.1 Reagents and Solution

Reagents and solutions used in the study are listed. MESNA (Sodium 2-mercaptoethane sulfonic acid sodium) (Alfa Aesar), 2-hydroxyethyl disulfide (TCI), 3,3'-dithiodipropionic acid (Aldrich), sodium iodide (Alfa Aesar), potassium iodide (Fisher Scientific), perchloric acid (Fisher Scientific), sodium perchlorate monohydrate (Alfa Aesar), sodium acetate (Sigma), glacial acetic acid (Fisher Scientific), 3-bromopropionic acid, sodium sulfite, hydrochloric acid (Fisher

Scientific), stabilized hydrogen peroxide 30% (Sigma-Aldrich), ethyl alcohol 99.95% (Fisher Scientific), methanol (Fisher Scientific), acetonitrile (Fisher Scientific), 3-(trimethylsilyl)-1-propanesulfonic acid sodium salt (DSS) (sigma-Aldrich), D_2O 99.8% isotopic (Alfa Aesar), methanol-d_4 99.8% isotopic (Alfa Aesar).

All the aqueous solutions were freshly prepared using purified de-ionized water with a specific resistivity of 18.2 MΩ cm at 25 °C from an ultrapure water purification system. Reagent grade crystalline iodine was purified by sublimation. Saturated iodine solutions were prepared prior to experiment by dissolving pulverized I_2 in hot water, followed by overnight cooling. The excess iodine was removed through filtration. The concentration of iodine was determined through UV-Vis spectrophotometry at 460 nm. Stock solutions of I_2/I_3^- were prepared by dissolving solid sublimed iodine in water with the addition of sodium iodide. Triiodide solutions for different uses were obtained by diluting the stock solution and then standardized spectrophotometrically prior to each experiment. All the iodine and triiodide solutions were well-protected from light.

5.2.2 Instruments and Methods

Kinetics of the reactions with a long-time scale were monitored by an Agilent HP 8453 diode array spectrophotometer with quartz cells having calibrated 1 cm path lengths. Rapid kinetic studies were performed at 25 ± 0.1°C on a Hi-Tech SF-51 stopped-flow spectrophotometer equipped with a thermostat apparatus and a quartz cell with a light path of 10 mm using Olis 4300 data acquisition and analysis software. Optical filters were used for different stopped-flow experiments. The kinetic data was analyzed using GraphPad Prism version 8.3.1. pH measurements were carried out using a corning 450 $p[H]^+$ meter with a Mettler Toledo Inlab 421 pH electrode. Mass spectra of the solutions were recorded with a Waters Q-Tof Premier mass spectrometer after direct electrospray ionization in the negative mode. ^{1}H-NMR data of the

reagents and reaction solutions were collected on Bruker AV 500 MHz and 600 MHz spectrometers.

5.2.3 UV-Vis Observations

The UV-Vis spectrum of iodine solution was obtained by dissolving sublimated iodine in water. The molar absorptivity (ε_{eff}) of iodine at 460 nm was found to be $750\ \text{M}^{-1}\ \text{cm}^{-1}$. While iodine is mixed with iodide, an extremely rapid equilibrium proceeds with the formation of triiodide as a product. The molar coefficient of triiodide at 352 nm was measured from UV-Vis with a value of $2.6 \times 10^4\ \text{M}^{-1}\ \text{cm}^{-1}$. The equilibrium constant of I_2/I_3^- ($K_{I_3^-}$) used for this project is $740\ \text{M}^{-1}$ [45].

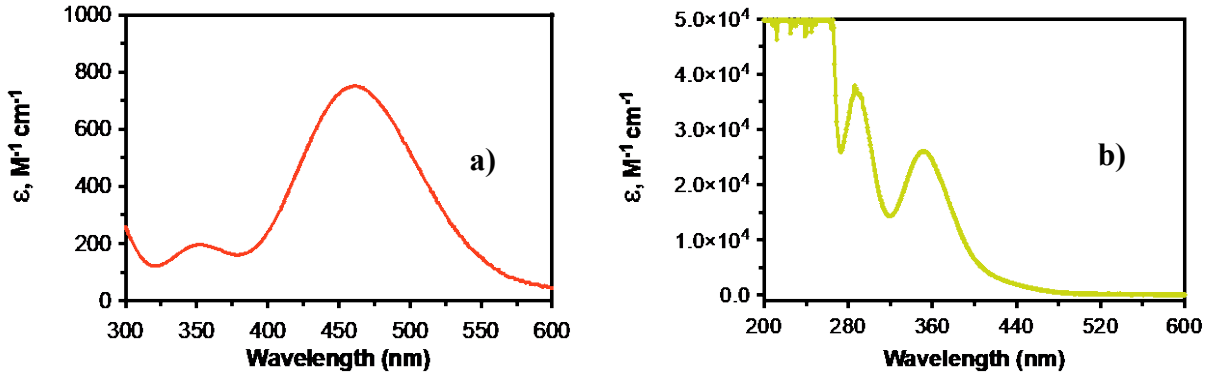

Figure 5-1. The UV-Vis spectrum of aqueous (a) iodine (b) triiodide.

5.3 Part-I: Oxidation of 2-Sulfonatoethyl Disulfide (SEDS) by Iodine

5.3.1 Background

As a two-electron oxidant, iodine can convert thiols into disulfides. The detailed mechanism and kinetics of the oxidation of two typical thiols (MESNA, BME) by iodine are elaborated in Chapter 4. One might expect that these reactions terminate at the point where disulfide forms. However, it turns out that the oxidation can go further. From the evidence collected, a thorough discussion on the kinetics and mechanism of the oxidation of SEDS by iodine

is provided in this chapter. More specifically, reaction stoichiometry, product analysis, equilibrium, and rate dependence on [SEDS], [iodide] and buffers are discussed in this part.

5.3.2 Preliminary Observation

As a starting point of this research, the absorbance changes of the mixture of SEDS (synthesized through oxidizing MESNA by H_2O_2 with NaI as catalyst and characterized as discussed in Chapter 4) and iodine in both water and $HClO_4$ were monitored using UV-Vis spectrophotometry. The increase of the absorbance at 352 nm with time under both conditions suggests the formation of triiodide in the solution.

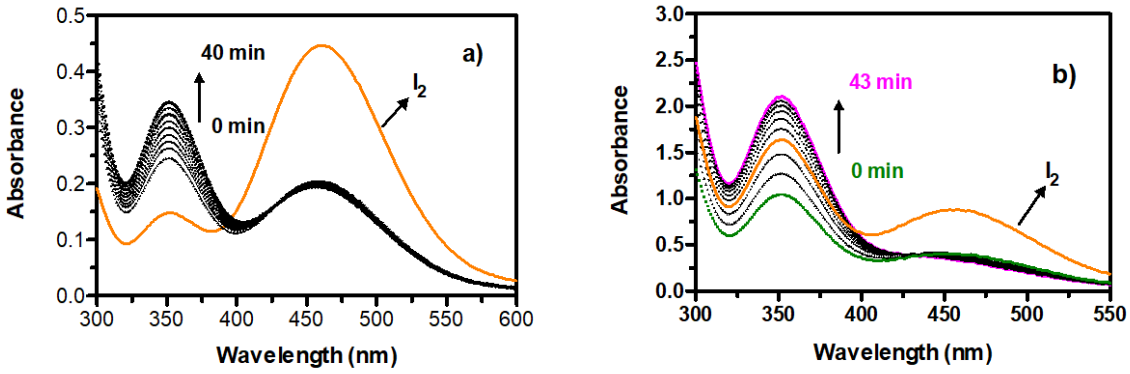

Figure 5-2. The absorbance changes of the mixture of SEDS with iodine. Orange trace: UV spectrum of iodine; black traces: spectra of iodine/disulfide mixture. a) Reaction mixture in water with $[SEDS]_0 = 3.13\ mM, [I_2]_0 = 0.6\ mM$; b) Reaction mixture in $HClO_4$ with $[SEDS]_0 = 5.0\ mM, [I_2]_0 = 1.0\ mM, [HClO_4] = 0.02\ M$.

The UV-Vis spectrum of iodine solution and SEDS solution were recorded to evaluate the stability of the two species in aqueous phase, where there was no change in the spectra after a long period of time (2.5 hours). The speculation of the degradation of the reactants can thus be ruled out.

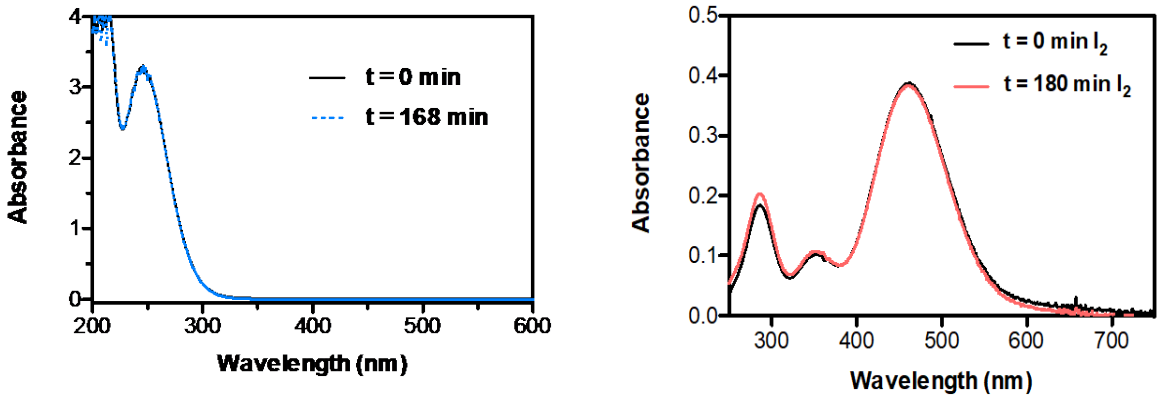

Figure 5-3. The UV-Vis spectrum of (left) 10 mM SEDS (right) 0.5 mM I_2.

5.3.3 Stoichiometry

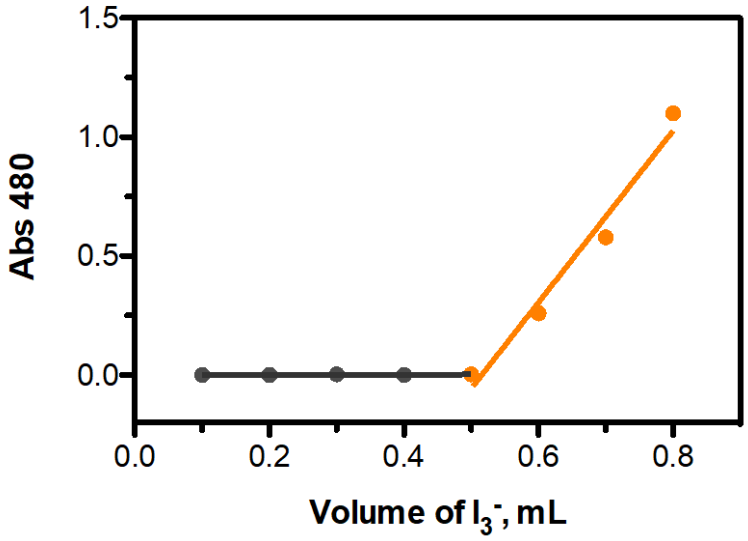

Figure 5-4. Titration curve for determining the reaction stoichiometry.

The stoichiometry of the reaction between iodine and SEDS was examined by spectrophotometric titration. The experiment began with recording the UV-vis spectrum of 2 mL 1.308 mM SEDS. Next, 0.1 mL aliquots of 10.29 mM I_3^- with 50 mM [I^-] was added to the disulfide solution in a cuvette using gastight syringe till the endpoint was reached. When the amount of I_3^- is sufficiently high, a sharp rise of the absorbance at 480 nm permitted us to

determine the complete consumption of RSSR by I_3^-. As a result, the ratio of the consumed triiodide and RSSR was found to be 1.97:1.

5.3.4 Reaction Kinetics

The UV-Vis experiments of the reaction between SEDS and iodine were carried out by recording the absorbance change at 352 nm upon mixing the reactants to monitor the formation of triiodide. Meanwhile, data at 460 nm was collected to assess the consumption of iodine. The kinetic trace at 352 nm in Figure 5-5 shows a rapid formation and a subsequent slow consumption of I_3^-. The absorbance decay of iodine indicates a complete reaction of I_2 with large excess of disulfide. The trace at 460 nm was then fitted into first-order rate law with a rate constant of $1.49 \times 10^{-4}\ s^{-1}$ ($t_{1/2} = 4653$ s), which suggests a pseudo-first order rate dependence on $[I_2]$.

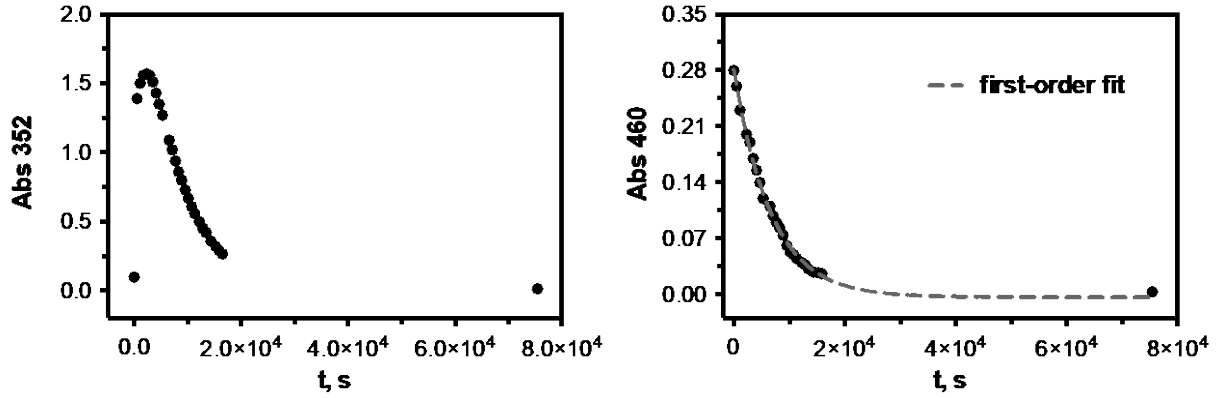

Figure 5-5. Kinetic trace of the mixture of SEDS and iodine at (left) 352 nm (right) 460 nm. Conditions: $[SEDS]_0 = 10$ mM, $[I_2]_0 = 0.5$ mM.

To examine [disulfide] effect on the reaction kinetics, a series of experiments with 0.48 mM iodine and various [SEDS] were carried out. The reaction was monitored at 352 nm spectrophotometrically through UV-Vis to record the formation of triiodide present in the rapid iodine equilibrium. As shown from the traces below, the increase in RSSR concentration resulted in the increase of the rate of the formation of triiodide.

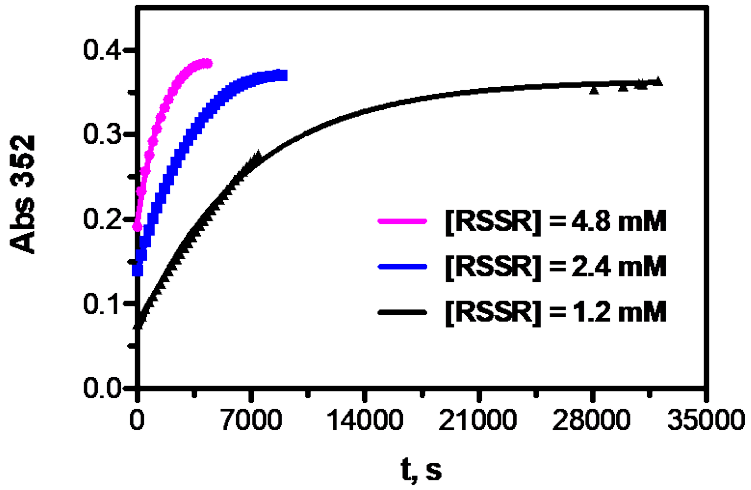

Figure 5-6. SEDS effect on the formation of triiodide. Conditions: $[SEDS]_0 =$ 1.2 mM, 2.4 mM, 4.8 mM, $[I_2]_0 = 0.48$ mM, μ ($NaClO_4$) = 0.1 M.

Table 5-1. [SEDS] dependence of $k_{obs,\ triiodide}$.

[SEDS]	k_{obs,I_3^-}, s^{-1}	$t_{1/2}$, s
4.8 mM	6.78×10^{-3}	1008
2.4 mM	3.04×10^{-3}	2276
1.2 mM	1.49×10^{-3}	4657

5.3.4.1 Buffer effect on the reaction kinetics

To determine the effect of buffer on the reaction kinetics, the experiments in water and in 0.1 M pH 4.87 acetate buffer were performed. For the latter one, two reactant solutions were prepared in acetate buffer prior to mixing. The absorbance changes at 460 nm were recorded using UV-Vis. The values of the two rate constants $k_{unbuffered} = 2.13 \times 10^{-3}\ s^{-1}$ and $k_{buffered} = 2.20 \times 10^{-3}\ s^{-1}$ were determined from the pseudo-first order fit of the kinetic traces. It can be concluded that buffer has no effect on the reaction rate. Thus, the following kinetic studies were carried out in water unless otherwise noted.

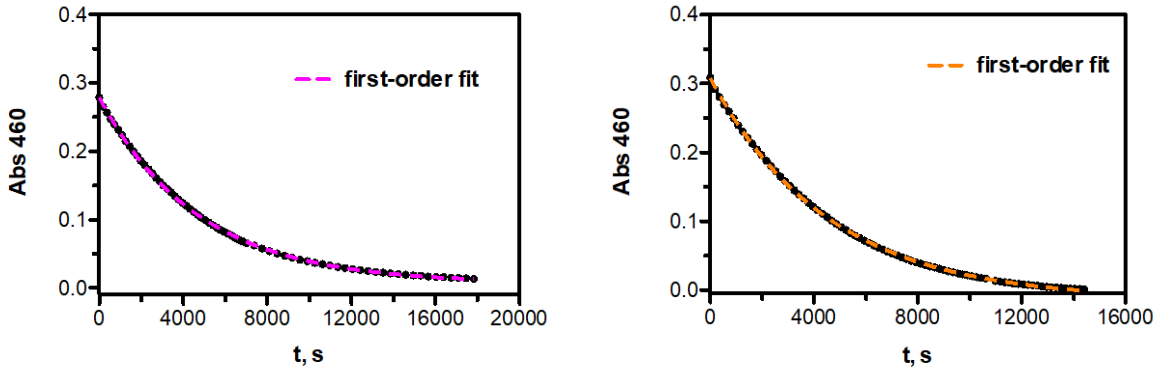

Figure 5-7. Kinetic trace of SEDS reaction with iodine in different media. (left) In water: $[\mathrm{SEDS}]_0 = 11.9$ mM, $[\mathrm{I_2}]_0 = 0.42$ mM; (right) in acetate buffer: $[\mathrm{SEDS}]_0 = 13.8$ mM, $[\mathrm{I_2}]_0 = 0.48$ mM.

5.3.4.2 Rate dependence on [SEDS]

Given the fact that the reaction of SEDS with iodine is rather slow, the rate dependence on [SEDS] was studied using a pH meter by mixing iodine with various RSSR. The pH of the two reactants, 5.0 mM SEDS and 0.47 mM iodine, over a long period of time was examined prior to the reaction. The pH values indicates that the two substances are stable enough in aqueous media for further kinetic study.

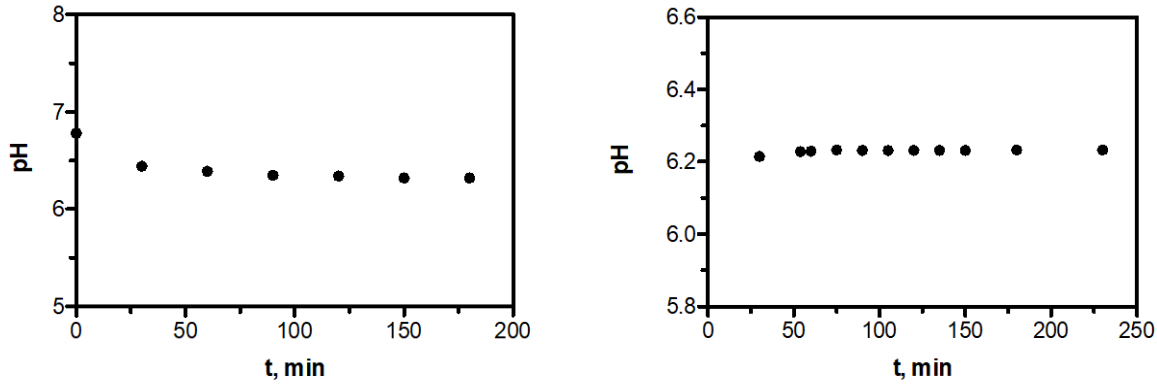

Figure 5-8. pH changes of (left) 5.0 mM SEDS solution with 0.1 M $NaClO_4$ and (right) 0.47 mM iodine solution with 0.1 M $NaClO_4$.

The following experiments are performed with ionic strength adjusted to 0.1 M with $NaClO_4$. pH data of the reaction mixture was collected continuously till the reading became stable. The data was well-fitted into first-order rate law. A first-order dependence of k_{obs} on [SEDS] can be evident from the excellent linear regression with a negligible intercept.

The change of pH (Δ pH) is determined to be 2.98 through the subtraction of initial pH of the solutions from the final pH of the reaction. Based on that, the ratio of produced H^+ and consumed iodine is calculated $\Delta[H^+]/\Delta[I_2] = 2.11$.

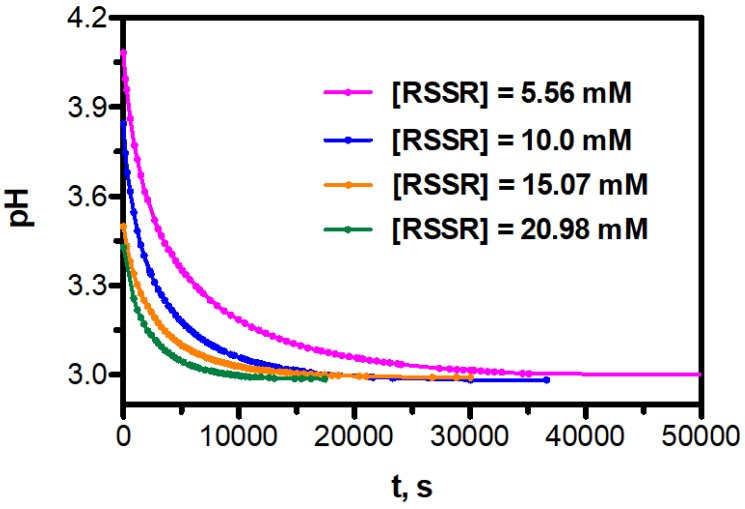

Figure 5-9. pH changes of the mixture of iodine and SEDS. Conditions: $[SEDS]_0 = 5.56 - 20.98$ mM, $[I_2]_0 = 0.49$ mM.

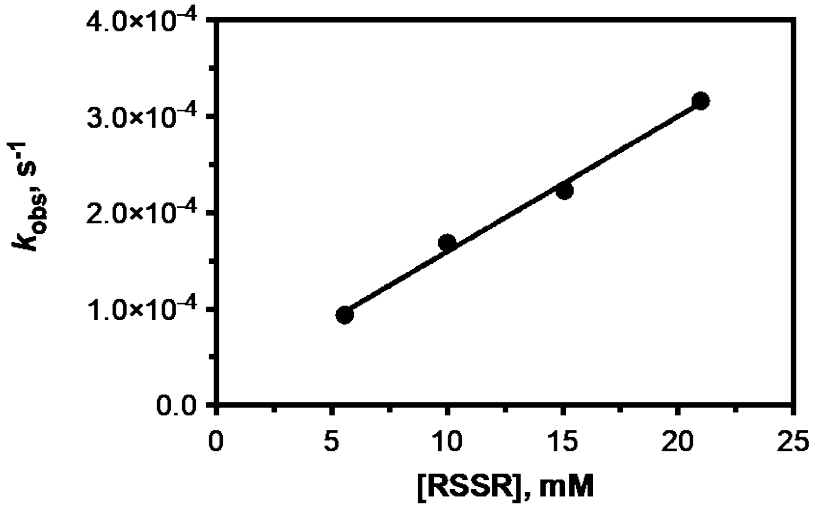

Figure 5-10. [SEDS] dependence of k_{obs}. Linear fit with slope $= (1.40 \pm 0.08) \times 10^{-2}\ \mathrm{M^{-1}\ s^{-1}}$; Y − intercept $= (1.93 \pm 1.09) \times 10^{-5}\ \mathrm{s^{-1}}$. Conditions: $[\mathrm{SEDS}]_0 = 5.56 - 20.98$ mM, $[\mathrm{I_2}]_0 = 0.49$ mM.

A general expression for the loss of iodine is displayed in Eq. 5-1,

$$-\frac{\mathrm{d}[\Delta \mathrm{H}^+]}{\mathrm{dt}} = k[\mathrm{SEDS}][\Delta \mathrm{H}^+] \qquad \text{Eq. 5-1}$$

Given that [SEDS] is at least 10-fold excess of $[\mathrm{I_2}]$, the equation can be rewritten as,

$$-\frac{\mathrm{d}[\Delta \mathrm{H}^+]}{\mathrm{dt}} = k_{obs}[\Delta \mathrm{H}^+] \qquad \text{Eq. 5-2}$$

Where $k_{obs} = k[\mathrm{SEDS}]$ with $k = 0.014\ \mathrm{M^{-1}\ s^{-1}}$.

Table 5-2. Kinetic data for determining the rate dependence on [SEDS].

[SEDS], mM	$\boldsymbol{k_{obs}\ (\times 10^4), \mathrm{s^{-1}}}$
5.56	0.94
10.00	1.69
15.07	2.23
20.98	3.16

To better solve the kinetics, the reaction is divided into two steps **(M_1; M_2)**, where I_2/I_3^- equilibrium is also taken into consideration of the reaction process. Such expression can be of importance for determining the fate of triiodide because the reaction rate can be strongly dependent on the reverse step of the equilibrium. To solve the kinetic coefficient, it was considered helpful to get the rate law by deriving an equation with the approximation that the reaction of I_3^- with SEDS can be neglected with no I^- added. The reaction process regarding the consumption of iodine can be given as,

M1 $$I_2 + I^- \rightleftharpoons I_3^-; \qquad k_1, k_{-1}$$ Eq. 5-3

M2 $$I_2 + \text{SEDS} \rightarrow \text{product} + 2I^-; \qquad k_2$$ Eq. 5-4

The rate law based on the assumption is,

$$-\frac{d[I_2]}{dt} = k_1[I_2][I^-] - k_{-1}[I_3^-] + k_2[I_2][\text{SEDS}]$$ Eq. 5-5

$$K_{I_3^-} = \frac{[I_3^-]}{[I_2][I^-]}; \qquad [I_3^-] = K_{I_3^-}[I_2][I^-]$$ Eq. 5-6

$$[I_2]_{\text{total}} = [I_2] + K_{I_3^-}[I_2][I^-]; \qquad [I_2] = \frac{[I_2]_{\text{total}}}{1 + K_{I_3^-}[I^-]}$$ Eq. 5-7

$$-\frac{d[I_2]}{dt} = k_1[I_2][I^-] - k_{-1}K_{I_3^-}[I_2][I^-] + k_2[I_2][\text{SEDS}]$$ Eq. 5-8

$$= [I_2]\left(k_1[I^-] - k_{-1}K_{I_3^-}[I^-] + k_2[\text{SEDS}]\right)$$ Eq. 5-9

$$= k_2[I_2][\text{SEDS}]$$ Eq. 5-10

$$= k_2\left(\frac{[I_2]_{\text{total}}}{1 + K_{I_3^-}[I^-]}\right)[\text{SEDS}]$$ Eq. 5-11

$$[I^-] = [I^-]_{\text{total}} - [I_3^-]$$ Eq. 5-12

$$[I^-] = 2[I_2]_{\text{total}} - [I_3^-]$$ Eq. 5-13

$$[I^-] = 2[I_2]_{\text{total}} - K_{I_3^-}[I_2][I^-]$$ Eq. 5-14

$$[\mathrm{I^-}] = 2[\mathrm{I_2}]_{\mathrm{total}} - \frac{K_{\mathrm{I_3^-}}[\mathrm{I^-}][\mathrm{I_2}]_{\mathrm{total}}}{1 + K_{\mathrm{I_3^-}}[\mathrm{I^-}]} \quad \text{Eq. 5-15}$$

$$[\mathrm{I^-}] + K_{\mathrm{I_3^-}}[\mathrm{I^-}]^2 + K_{\mathrm{I_3^-}}[\mathrm{I^-}] = 2[\mathrm{I_2}]_{\mathrm{total}} + 2K_{\mathrm{I_3^-}}[\mathrm{I_2}]_{\mathrm{total}}[\mathrm{I^-}] \quad \text{Eq. 5-16}$$

$$K_{\mathrm{I_3^-}}[\mathrm{I^-}]^2 + \left(1 - K_{\mathrm{I_3^-}}[\mathrm{I_2}]_{\mathrm{total}}\right)[\mathrm{I^-}] - 2[\mathrm{I_2}]_{\mathrm{total}} = 0 \quad \text{Eq. 5-17}$$

$$[\mathrm{I^-}] = \frac{K_{\mathrm{I_3^-}}[\mathrm{I_2}]_{\mathrm{total}} - 1 + \sqrt{\left(K_{\mathrm{I_3^-}}^2[\mathrm{I_2}]_{\mathrm{total}}^2 + 6K_{\mathrm{I_3^-}}[\mathrm{I_2}]_{\mathrm{total}} + 1\right)}}{2K_{\mathrm{I_3^-}}} \quad \text{Eq. 5-18}$$

$$-\frac{\mathrm{d}[\mathrm{I_2}]}{\mathrm{dt}} = k_2[\mathrm{RSSR}]\left(\frac{2[\mathrm{I_2}]_{\mathrm{total}}}{K_{\mathrm{I_3^-}}[\mathrm{I_2}]_{\mathrm{total}} + \sqrt{\left(K_{\mathrm{I_3^-}}^2[\mathrm{I_2}]_{\mathrm{total}}^2 + 6K_{\mathrm{I_3^-}}[\mathrm{I_2}]_{\mathrm{total}} + 1\right)} + 1}\right) \quad \text{Eq. 5-19}$$

Due to the complexity in the denominator of the equation, another approximation is considered where $\mathbf{M_2}$ pathway is dominant despite the presence of $\mathrm{I_2}/\mathrm{I_3^-}$ equilibrium. This is a fair assumption since most $\mathrm{I^-}$ is not converted to $\mathrm{I_3^-}$ as initial iodine is in a small amount, leading to a new rate law shown in Eq. 5-21.

$$[\mathrm{I_2}]_{\mathrm{total}} = [\mathrm{I_2}]_0 - \frac{1}{2}[\mathrm{I^-}];\ [\mathrm{I^-}] = 2([\mathrm{I_2}]_0 - [\mathrm{I_2}]_{\mathrm{total}}) \quad \text{Eq. 5-20}$$

$$-\frac{\mathrm{d}[\mathrm{I_2}]_{\mathrm{total}}}{\mathrm{dt}} = k_2[\mathrm{I_2}][\mathrm{RSSR}] \quad \text{Eq. 5-21}$$

$$-\frac{\mathrm{d}[\mathrm{I_2}]_{\mathrm{total}}}{\mathrm{dt}} = \frac{k_2[\mathrm{I_2}]_{\mathrm{total}}[\mathrm{RSSR}]}{1 + K_{\mathrm{I_3^-}}[\mathrm{I^-}]} \quad \text{Eq. 5-22}$$

$$-\frac{\mathrm{d}[\mathrm{I_2}]_{\mathrm{total}}}{\mathrm{dt}} = \frac{k_2[\mathrm{I_2}]_{\mathrm{total}}[\mathrm{RSSR}]}{1 + K_{\mathrm{I_3^-}}\left(2([\mathrm{I_2}]_0 - [\mathrm{I_2}]_{\mathrm{total}})\right)} \quad \text{Eq. 5-23}$$

$$-\frac{(1 + 2K_{\mathrm{I_3^-}}([\mathrm{I_2}]_0 - [\mathrm{I_2}]_{\mathrm{total}})}{[\mathrm{I_2}]_{\mathrm{total}}}\mathrm{d}[\mathrm{I_2}]_{\mathrm{total}} = k_2[\mathrm{RSSR}] \times \mathrm{dt} \quad \text{Eq. 5-24}$$

Integrating $[\mathrm{I_2}]_{\mathrm{total}}$ from $[\mathrm{I_2}]_0 \rightarrow [\mathrm{I_2}]_{\mathrm{total}}$; and t from $0 \rightarrow \mathrm{t}$

$$-\ln[\mathrm{I_2}]_{\mathrm{total}} + \ln[\mathrm{I_2}]_0 + 2K_{\mathrm{I_3^-}}([\mathrm{I_2}]_{\mathrm{total}} - [\mathrm{I_2}]_0 - [\mathrm{I_2}]_0 \ln[\mathrm{I_2}]_{\mathrm{total}} + [\mathrm{I_2}]_0 \ln[\mathrm{I_2}]_0) = k_2[\mathrm{RSSR}] \times \mathrm{t} \quad \text{Eq. 5-25}$$

$$-\ln[I_2]_{total} + \ln[I_2]_0 + 2K_{I_3^-}[I_2]_{total} - 2K_{I_3^-}[I_2]_0 - 2K_{I_3^-}[I_2]_0 \ln[I_2]_{total} + 2K_{I_3^-}[I_2]_0 \ln[I_2]_0 = k_2[RSSR] \times t \quad \text{Eq. 5-26}$$

$$2K_{I_3^-}[I_2]_{total} - \ln[I_2]_{total}\left(1 + 2K_{I_3^-}[I_2]_0\right) = k_2[RSSR] \times t + 2K_{I_3^-}[I_2]_0 - \ln[I_2]_0\left(1 + 2K_{I_3^-}[I_2]_0\right) \quad \text{Eq. 5-27}$$

Here,

$K_{I_3^-} = 750\ M^{-1}$, $[I_2]_0 = 0.00042\ M$, $[RSSR] = 0.0119\ M$

$$1500 \times [I_2]_{total} - 1.63 \times \ln[I_2]_{total} = 0.0119 \times k \times t + 13.30 \quad \text{Eq. 5-28}$$

Solving implicitly,

$$[I_2]_t = \frac{(0.0119 \times k_2 \times t) + 13.30 + 1.63 \times \ln[I_2]_t}{1500} \quad \text{Eq. 5-29}$$

Using the simplified Eq. 5-29, the value of the rate constant k_2 was calculated to be $0.022\ M^{-1}\ s^{-1}$.

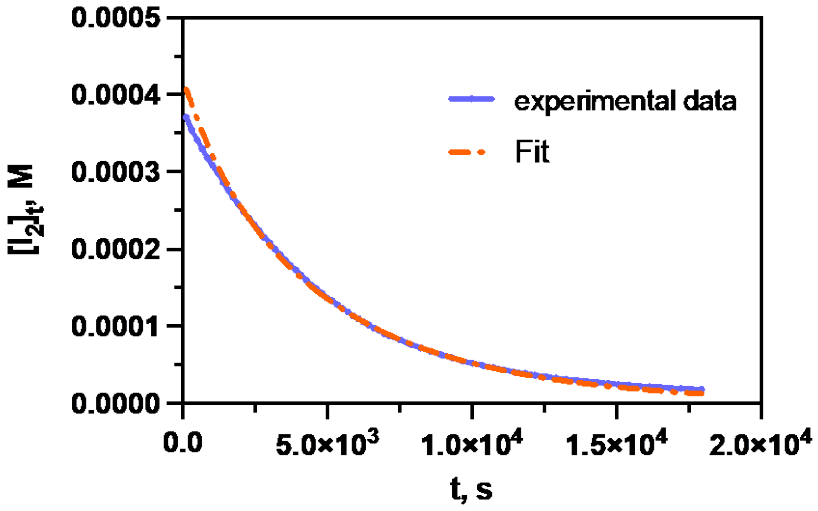

Figure 5-11. Kinetic trace of the reaction and fit with Eq. 5-29. Conditions: $[SEDS]_0 = 11.9$ mM, $[I_2]_0 = 0.42$ mM.

5.3.4.3 Rate dependence on [iodide]

Many reports have shown that the kinetics of nucleophiles reacting with iodine/ triiodide can be greatly affected by iodide concentration [17],[18],[22],[23], thus, it is believed to be important to postulate the mechanism including this term.

The kinetics of the reaction between SEDS and iodine with iodide concentration varying from 0 mM to 5.0 mM were studied using UV-Vis spectrophotometer under the conditions of [iodine] = 0.42 mM, [SEDS] = 11.9 mM. The final pH values of the reaction mixtures were found to be (2.93 ± 0.01). The kinetic traces were fitted with first-order rate law. A plot of series k_{obs} as a function of $[I^-]$ is displayed in Figure 5-13.

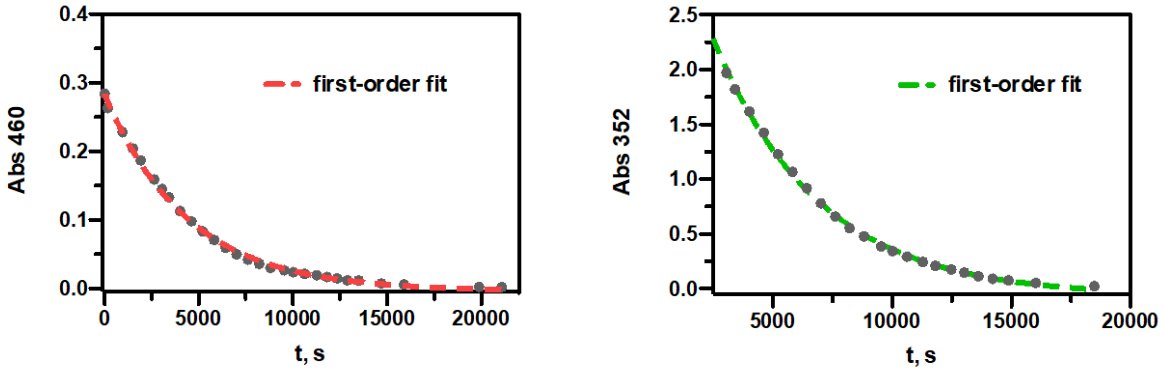

Figure 5-12. Kinetic trace with 0.5 mM [I-] at (left) 460 nm (right) at 352 nm. (left) $k_{obs,460\,nm} = 2.26 \times 10^{-4}\ s^{-1}$; (right) $k_{obs,352\,nm} = 2.26 \times 10^{-4}\ s^{-1}$.

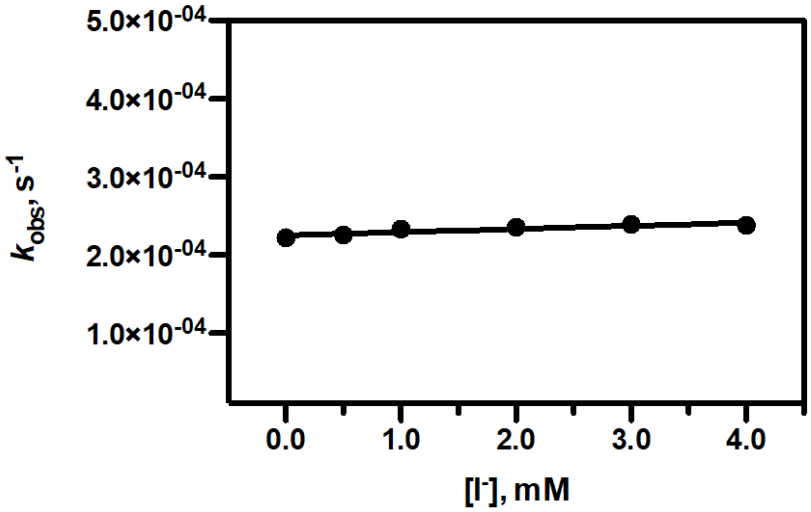

Figure 5-13. k_{obs} dependence of [I-]. Conditions: $[SEDS]_0 = 11.0$ mM, $[I_2]_0 = 0.42$ mM, $[I^-]_0 = 0 - 5.0$ mM.

Table 5-3. Kinetic data for determining the rate dependence on [I^-].

[I^-], mM	k_{obs}, s^{-1}	[I^-], mM	k_{obs}, s^{-1}
0	2.22×10^{-4}	2.0	2.26×10^{-4}
0.5	2.26×10^{-4}	3.0	2.39×10^{-4}
1.0	2.23×10^{-4}	4.0	2.38×10^{-4}

The slope of the linear fit is statistically indistinguishable from zero, indicating that the reaction rate is independent of [I^-]. This result is unusual as iodide is generally found to be a rate inhibitor of such reactions. To include iodide effect into the mechanism, it was assumed that the reaction proceeds through the initial formation of an $RSSRI^+$, followed by an equilibrium between $RSSRI^+$ and $RSSR^{2+}$. Notably, the conversion of the reactive species is considered as mainly governing the reaction kinetics. A rate law is herein derived in Eq. 5-33 based on an established equation from a literature [23].

$$I_2 + I^- \rightleftharpoons I_3^- \qquad K_{I_3^-} \qquad \text{Eq. 5-30}$$

$$SEDS + I_2 \rightleftharpoons SEDSI^+ + I^- \qquad k_2, k_{-2} \qquad \text{Eq. 5-31}$$

$$SEDSI^+ \rightarrow SEDS^{2+} + I^- \qquad k_3 \qquad \text{Eq. 5-32}$$

The original equation (**Eq. 12** from Kerek's report in 2007) was modified to include the experimental conditions and mechanism discussed and is shown below.

$$-\frac{1}{2}\frac{d[I_2]_{total}}{dt} = [SEDS][I_2]_{total}\frac{k_2 k_3 [I^-]}{k_{-2}[I^-] + K_{I_3^-}k_{-2}[I^-]^2} \qquad \text{Eq. 5-33}$$

$$\frac{d[I_2]_{total}}{dt} = -2[SEDS][I_2]_{total}\frac{k_2 k_3 [I^-]}{k_{-2}[I^-] + K_{I_3^-}k_{-2}[I^-]^2} \qquad \text{Eq. 5-34}$$

$$k_{obs} = 2[SEDS]\frac{k_2 k_3}{k_{-2} + K_{I_3^-}k_{-2}[I^-]} \qquad \text{Eq. 5-35}$$

Assuming $k_{-2} \gg K_{I_3^-}k_{-2}[I^-]$, the above equation can be simplified as,

$$k_{\text{obs}} = 2[\text{SEDS}]\frac{k_2 k_3}{k_{-2}} = 2[\text{SEDS}]K_2 k_3 \qquad \text{Eq. 5-36}$$

which explains the iodide dependence on the reaction kinetics. Based on Figure 5-13, $K_2 \times k_3$ can be calculated to be 0.01 $\text{M}^{-1}\,\text{s}^{-1}$.

5.3.5 Product Analysis

5.3.5.1 ^{1}H-NMR of the reaction mixture

7.6 mM I_3^- was mixed with 5.2 mM SEDS into D_2O. The mixture was stirred at room temperature for 5 days. ^{1}H-NMR was recorded with DSS as reference after the reaction was completed. In the spectrum, four multiplets from 3.0 ppm to 4.0 ppm can be observed from the product of the reaction mixture.

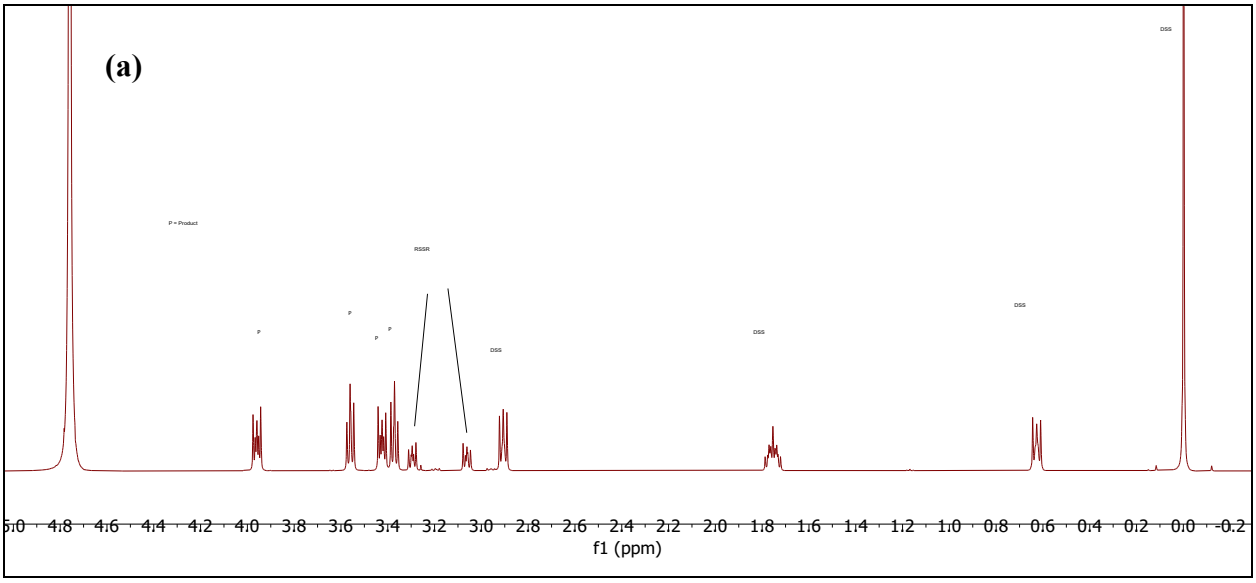

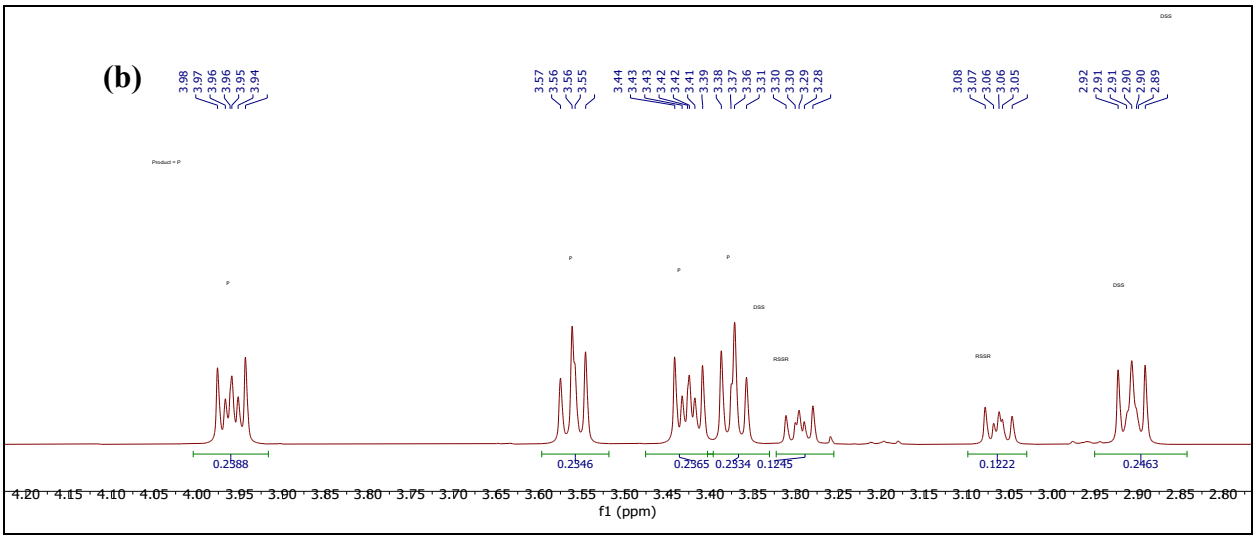

Figure 5-14. ^{1}H-NMR spectra of the product from the reaction mixture: (a) Full spectrum; (b) zoom in on spectrum (a). Conditions: $[\mathrm{SEDS}]_0 = 5.7$ mM, $[\mathrm{I_2}]_0 = 7.6$ mM, $[\mathrm{DSS}]_0 = 2.84$ mM.

5.3.5.2 ESI-MS of the reaction mixture

A sample of a mixture solution including 7.5 mM SEDS and 17.0 mM $\mathrm{I_3^-}$ (prepared from iodine and NaI) was prepared for mass spectrometry. After reacting 9 days, the spectrum of ESI-MS (in negative mode) was obtained from the reaction solution. It shows the major product, highly likely to be the corresponding thiosulfonate ($\mathrm{NaSO_3C_2H_4S(O)_2SC_2H_4SO_3^-}$) with a value of m/z to be 334.90.

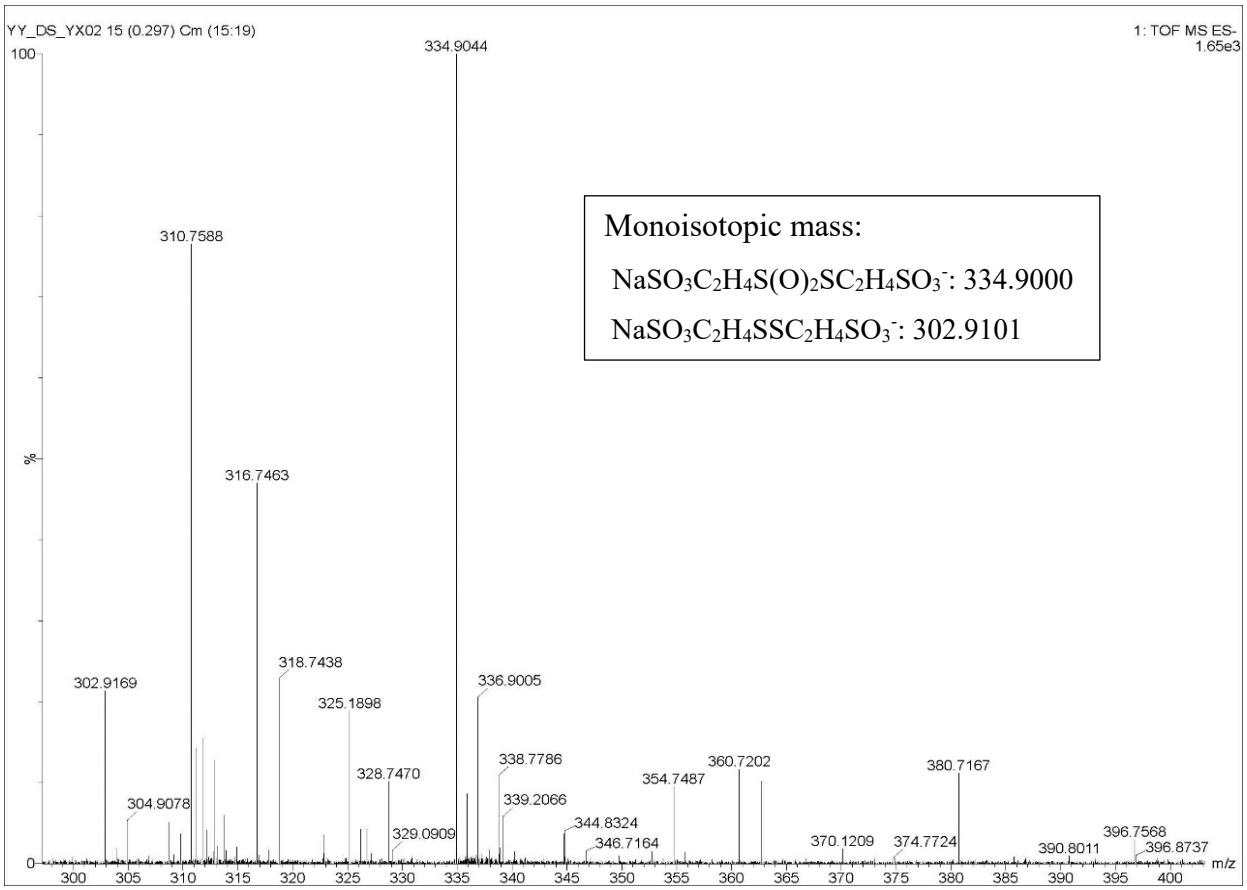

Figure 5-15. ESI-MS (-) spectrum of the reaction mixture.

5.3.5.3 Synthesis of MESNA-thiosulfonate

(MESNA-RS(O)$_2$SR) To confirm the product, effort was made to synthesize MESNA-thiosulfonate. A solution containing 100 mg (0.306 mmol) SEDS, 0.783 mmol 30% H_2O_2, and 0.013 mmol NaI was stirred in 1.5 mL H_2O at room temperature. After running 19 hours, half of the mixture solution was taken for subsequent experiment, and the rest was allowed to react longer. The separated solution was treated with 50 mL ethanol, resulting in white precipitate upon cooling at 4 °C for 1 hour. The crude product was later washed with ethanol, filtered, and dried for further characterization.

5.3.5.4 ^{1}H-NMR of the synthesized product

^{1}H-NMR was recorded after dissolving the resulting product into D_2O with DSS as reference. The spectrum displayed below shows that the species has identified signals (P) from 3.35 ppm to 4.00 ppm. The four triplets are the signals from the -CH_2 group of the compound. Besides, it can be evident from the integral that nearly half of the initial disulfide was reacted.

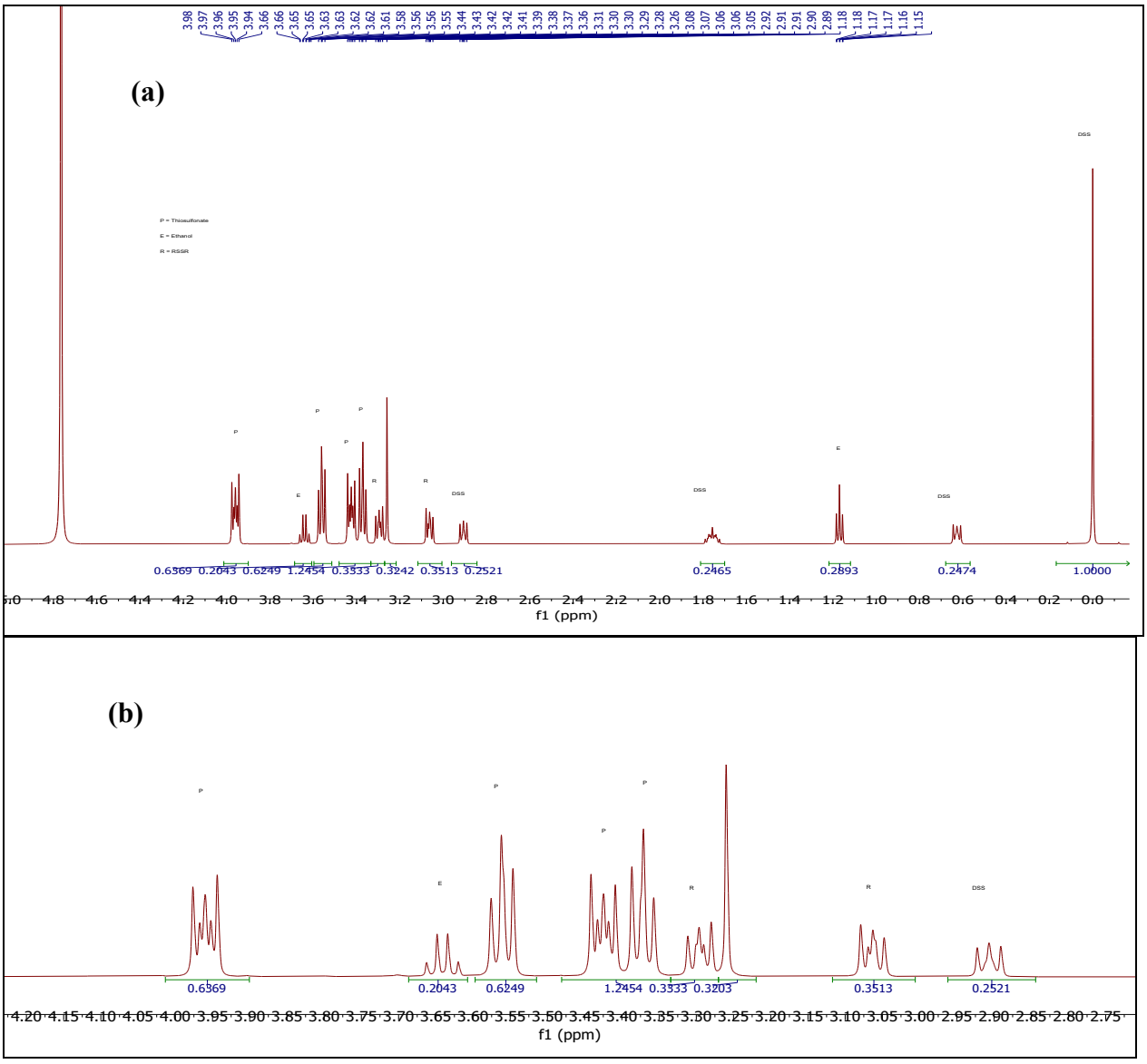

Figure 5-16. ^{1}H-NMR spectra of the synthesized product: (a) Full spectrum; (b) zoom in on spectrum (a). Conditions: mass of the product = 5.76 mg, DSS = 0.75 mg; volume of D_2O = 0.55 mL.

After reacting 48 hours, the remaining half of the solution was transferred into 50 mL ethanol and allowed to cool down at 4 °C for 40 mins before it was washed and filtered. The resulting solid was dried overnight. Afterwards, 4.25 mg of the synthesized product was dissolved into 0.6 ml D_2O for ^{1}H-NMR with 0.5 mg DSS as reference. As shown in Figure 5-17, SEDS was completely consumed by H_2O_2 and fully converted into the corresponding thiosulfonate.

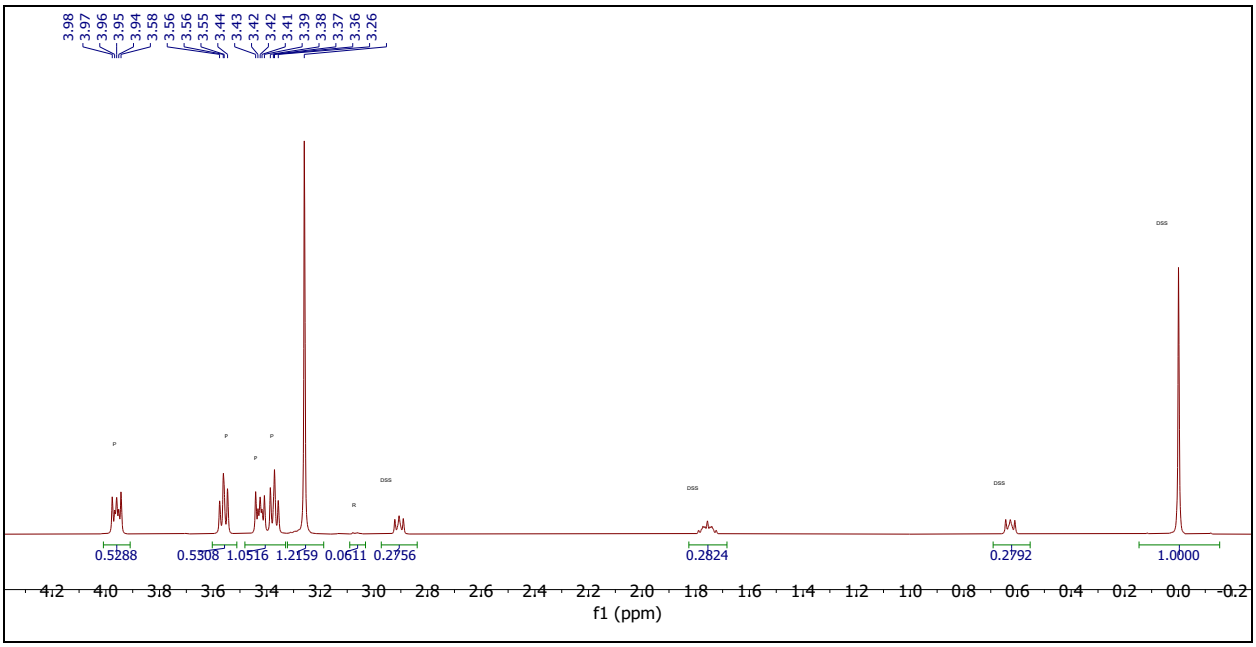

Figure 5-17. ^{1}H-NMR spectrum of the synthesized product after complete reaction.

5.3.5.5 ESI-MS of the synthesized product

To further verify that the synthesized product is MESNA-thiosulfonate, ESI-MS [MH^-] was conducted with dissolving 0.95 mg compound into 1 mL H_2O. A major peak with m/z = 334.90 from the thiosulfonate was perceived in the mass spectrum.

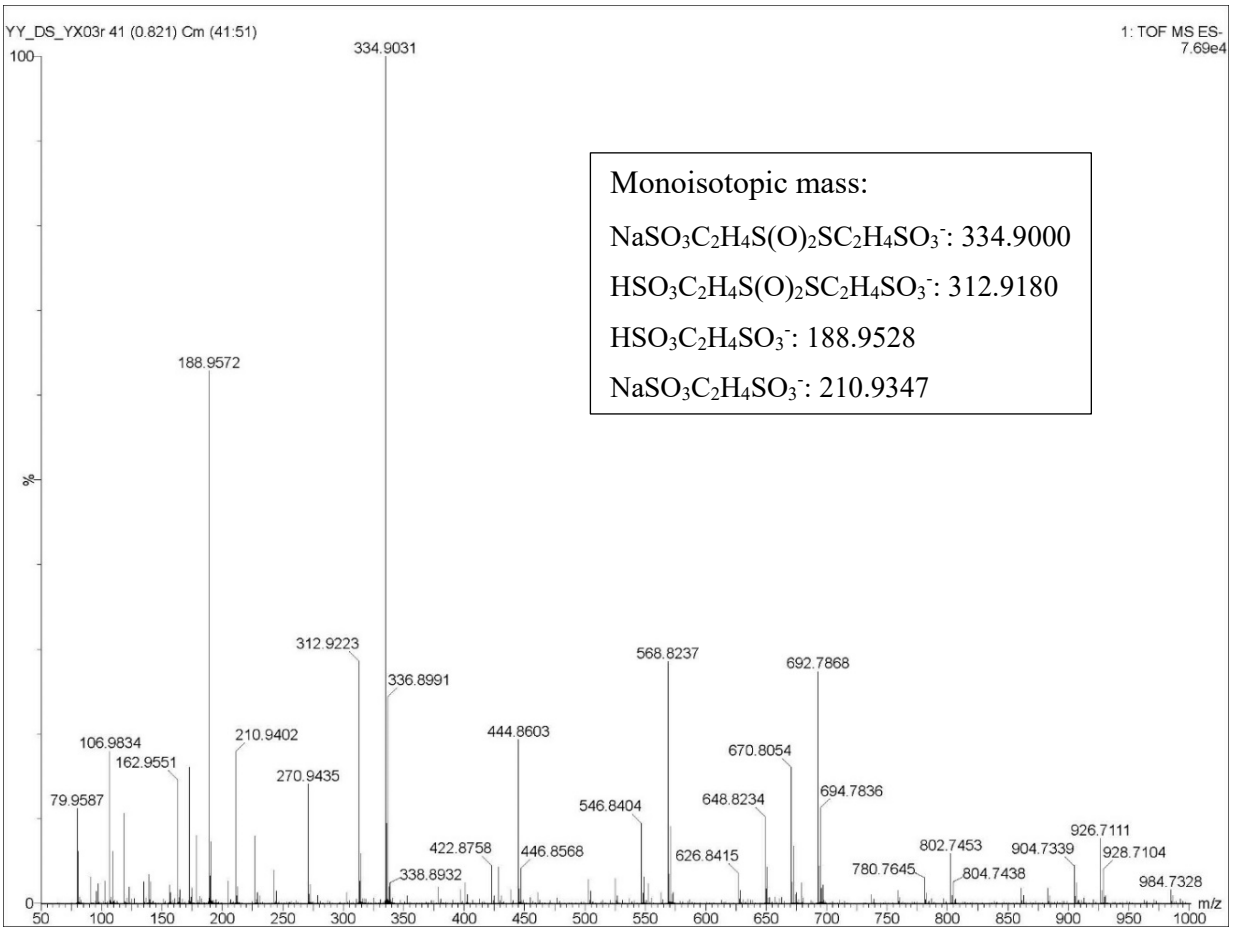

Figure 5-18. ESI-MS (-) of the synthesized thiosulfonate.

5.3.5.6 Synthesized product spiking on the NMR

^{1}H-NMR spectrum of the reaction mixture of 9.6 mM I_3^- and 5.2 mM SEDS in D_2O was obtained primarily after reacting 7 days as shown in Figure 5-19**(a)**. In addition, the reaction mixture was spiked with 16.05 mg of the synthesized thiosulfonate. The peaks assigned to the thiosulfonate (P) become more intense as shown in Figure 5-19**(b)**, confirming the formation of MESNA-thiosulfonate from the oxidation of SEDS by iodine.

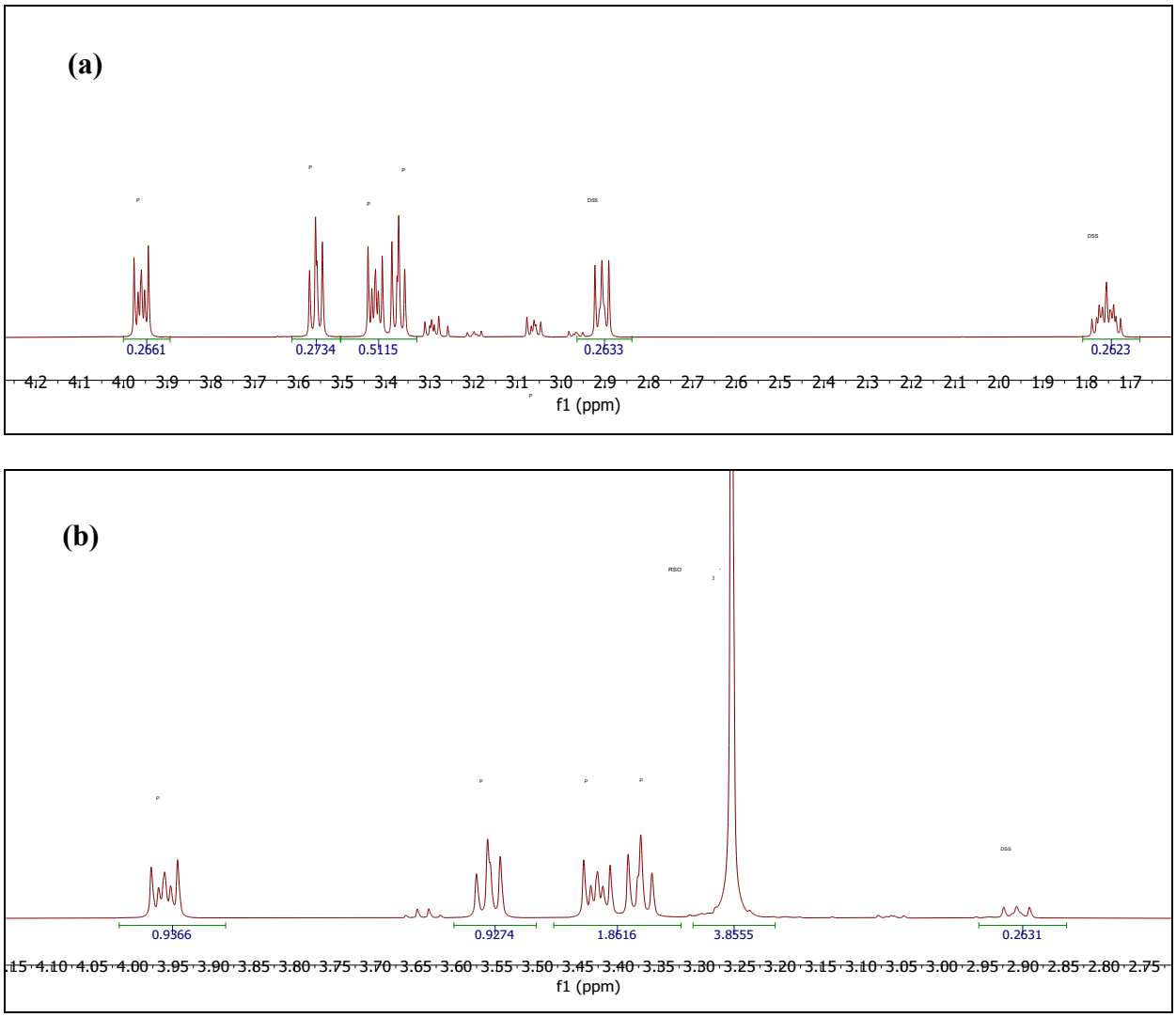

Figure 5-19. ^{1}H-NMR spectrum of (a) I_3^-/RSSR mixture and (b) the reaction mixture with MESNA-thiosulfonate spiked.

5.3.6 Overall reaction

Based on the evidence from titration, kinetic studies and product identification, the overall reaction is determined as one equivalent of SEDS consuming 2-fold iodine to produce stoichiometrically equivalent amount of MESNA-thiosulfonate along with the release of iodide. The reaction is formulated as

$$(NaSO_3CH_2CH_2S)_2 + 2I_2 + 2H_2O \rightarrow NaSO_3CH_3CH_2S(O)_2SCH_2CH_2\ SO_3Na + 4I^- + 4H^+$$

5.4 Part-II: Oxidation of 2-Hydroxyethyl Disulfide ($(HOCH_2CH_2S)_2$) by Iodine

5.4.1 Background

2-Hydroxyethyl disulfide (HEDS), $(OHCH_2CH_2S)_2$ is a commercially available disulfide with low molecular weight. It is soluble, inexpensive, and known for its role in determining the presence, activity, and enzyme kinetics of glutaredoxins from organisms and other sources based on the thiol-disulfide interchange [26]-[28]. In addition, the inactive feature of -OH site of this substrate makes it a good candidate. Besides, given that the study regarding the kinetics and mechanism of the oxidation of its reduced form, 2-mercaptoethanol, by iodine/iodate presented earlier in Chapter 4, it is believed to be important to look into the following reaction as the oxidation of HEDS by iodine will reveal deeper insights with respect to the understanding of organosulfur-halogen chemistry.

5.4.2 Stoichiometric

The consumption ratio of the reaction between HEDS and iodine was determined through spectrophotometric titration. The process was carried out by titrating HEDS with 99.72 mM I_3^- and meanwhile monitoring the absorbance change at 500 nm. The spectrum of 2 mL 25.23 mM HEDS was recorded initially, followed by getting the absorbance change after adding aliquots of triiodide till the end point was reached. Totally, 0.56 mL I_3^- was depleted to complete the reaction. The stoichiometric ratio was eventually calculated to be $\frac{\Delta[\mathrm{HEDS}]}{\Delta[I_3^-]} = 1.11:1$.

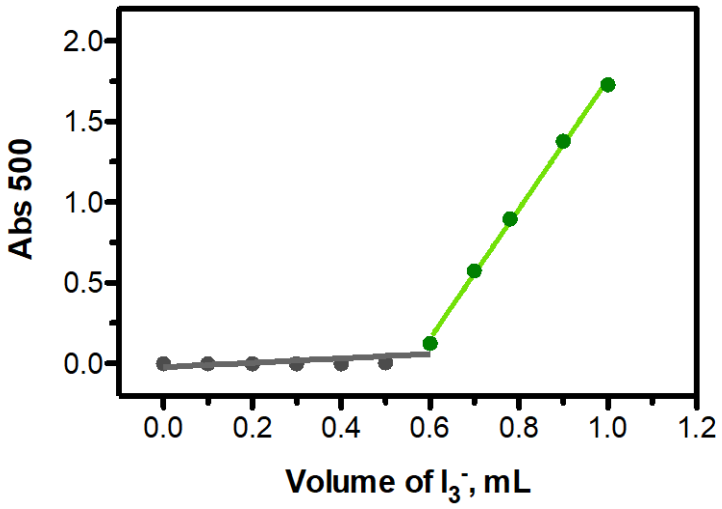

Figure 5-20. Titration curve for determining the reacting ratio of HEDS/Iodine.

5.4.3 Determination of the presence of I^-

A stock solution of the mixture of 0.43 mM I_2 and 17.4 mM HEDS was prepared and was diluted 10 times afterwards. UV-Vis spectra (red trace) was recorded after the dilution. The spectrum of the disulfide with 0.1 M $NaClO_4$ is also displayed. The amount of I^- produced from the reaction was calculated to be 0.89 mM from the known molar coefficient of iodide at 226 nm ($\varepsilon_{I^-} = 1.34 \times 10^4\ M^{-1}cm^{-1}$) where the maximum peak appears in the UV-Vis. In addition, the ratio of iodide produced from the reaction and iodine consumed is determined to be $\Delta[I^-]/\Delta[I_2] = 2.08$.

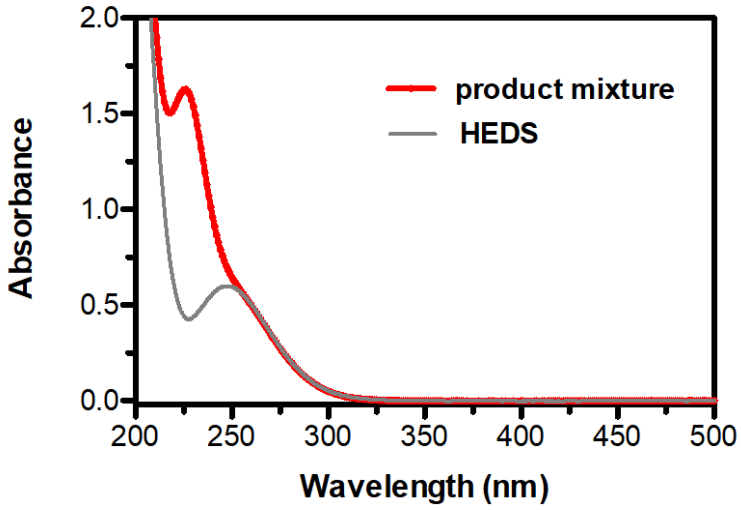

Figure 5-21. UV-Vis spectrum of HEDS and the product mixture after dilution.

5.4.4 pH study on the reaction

With the aim of investigating the formation of H^+, pH change of the disulfide and the reaction mixture was recorded as a function of time. The final pH of the reaction mixture was found to be 3.06. The ratio of the produced $[H^+]$ and consumed $[I_2]$ was calculated to be 2.01.

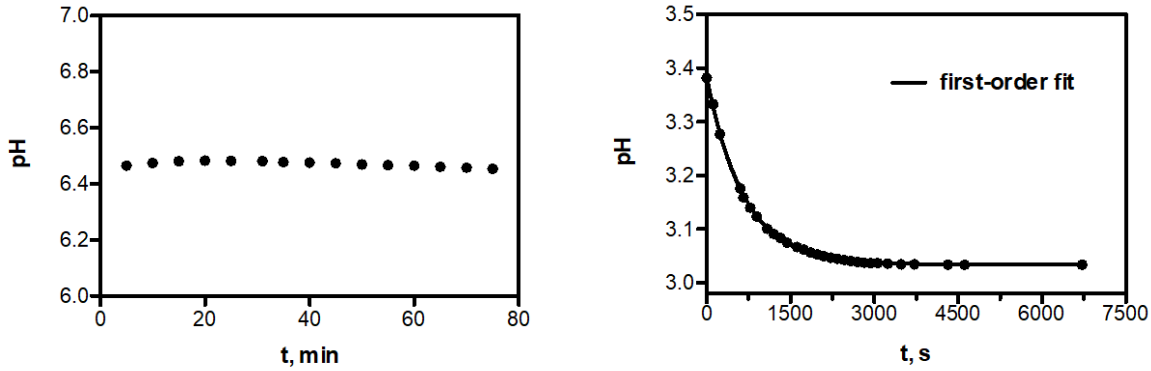

Figure 5-22. (left) pH change of HEDS as a function of time; (right) pH kinetics of the reaction mixture with the first-order fit. Conditions: (left) $[\mathrm{HEDS}]_0 = 10.0$ mM; (right) $[\mathrm{HEDS}]_0 = 10.0$ mM, $[\mathrm{I_2}]_0 = 0.43$ mM, $\mu = 0.1$ M.

5.4.5 Determination of the presence of IO_3^-

To test for the formation of IO_3^-, the product mixture of HEDS and iodine was titrated by iodide. This titration method is used because the rapid release of iodine can be detected through UV-Vis after mixing IO_3^- and iodide in acidic media. Prior to the titration, the mixture of 17.4 mM disulfide and 0.43 mM iodine was acidified with 0.1 M $HClO_4$. After that, 2 mL of the mixture solution was titrated with 2.95 mM I^-. The absorbance change was monitored by UV-Vis. No distinguishable difference of the spectrum can be observed after each addition, which suggests that there is no IO_3^- formed in the system.

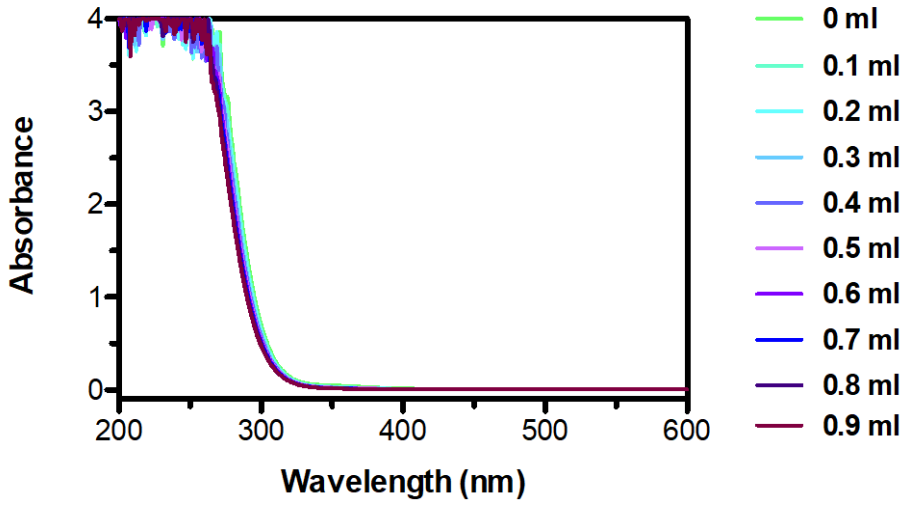

Figure 5-23. Spectrophotometric titration of IO_3^- using I^-.

To further confirm the above conclusion, the solution with the presence of extra I^- from the titration was diluted 10 times, and UV-Vis reading (red trace) of the diluted solution was recorded to compare with the spectrum of the acidic solution before titration (orange trace) and the spectrum of HEDS (blue trace). As a result, it turns out that 86% of the initial iodide was consumed after titration.

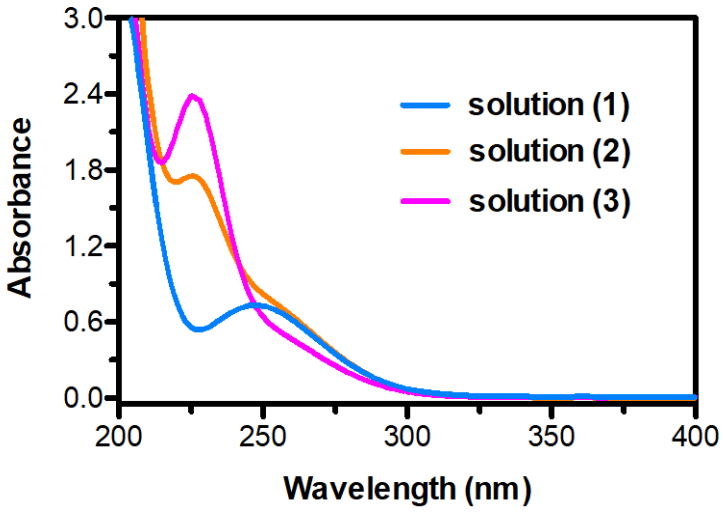

Figure 5-24. UV-Vis spectrum of solution (1): HEDS; solution (2): acidified reaction solution; solution (3): diluted solution after titration.

The calculated result ensures that the iodide was mostly consumed, which might be due to the formation of HEDS $-$ IO_3^- adduct. Later, UV-Vis spectrum was recorded for 2 mM IO_3^-, 2 mM HEDS, and the mixture of equimolar of the two species as shown in the figure below.

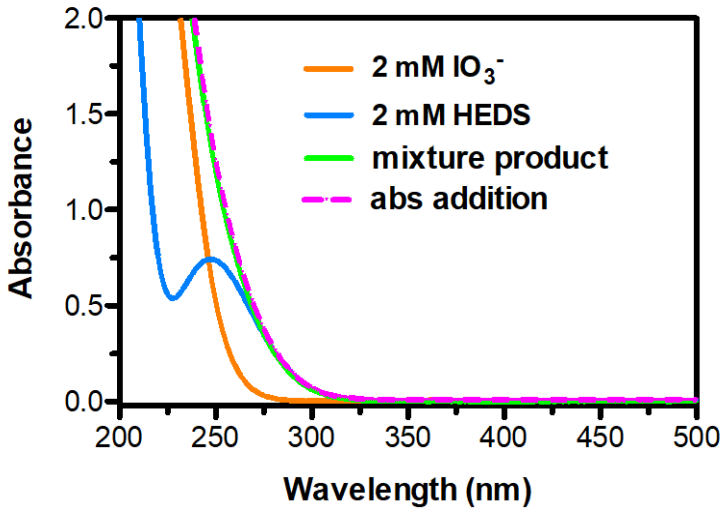

Figure 5-25. UV-Vis spectra for determining the presence of HEDS-IO_3^- adduct.

The total absorbance obtained from the addition of two separate spectrum was calculated to compare with the spectra of the mixture product. The complete overlap of the two traces indicates that there is no adduct forming in the solution, given that the adduct should yield a different UV spectrum. This result further confirms the lack of iodate formation in the disulfide-iodine mixture.

The evidence collected above leads to the conclusion that the reaction is not iodine hydrolysis, and therefore disulfide is not serving as a catalyst for the process. Therefore, the oxidation of HEDS by iodine should be more promising based on the following facts: first, iodine is a strong oxidizing agent; second, the redox reaction between MESNA-disulfide and iodine was determined and strongly proved. To confirm the speculation, experiments regarding the reaction kinetics, stoichiometry, and product identifications were conducted from different aspects and discussed in the following sections.

5.4.6 Kinetic Study

The absorbance changes of the mixture solution of HEDS (OHRSSROH) and iodine was monitored using UV-Vis spectrophotometer at both 352 nm and 460 nm. Meanwhile, the spectrum of HEDS was also collected to check the stability of the disulfide.

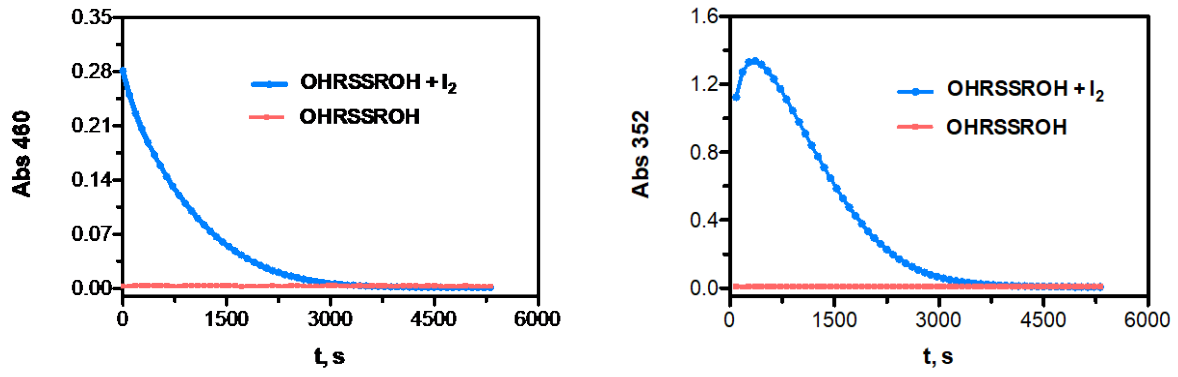

Figure 5-26. Kinetic traces of HEDS and the reaction mixture at (left) 460 nm and (right) 352 nm.

The kinetic trace at 460 nm is better fitted into a first-order rate law compared with the second-order fit, which indicates a first-order rate dependence on iodine.

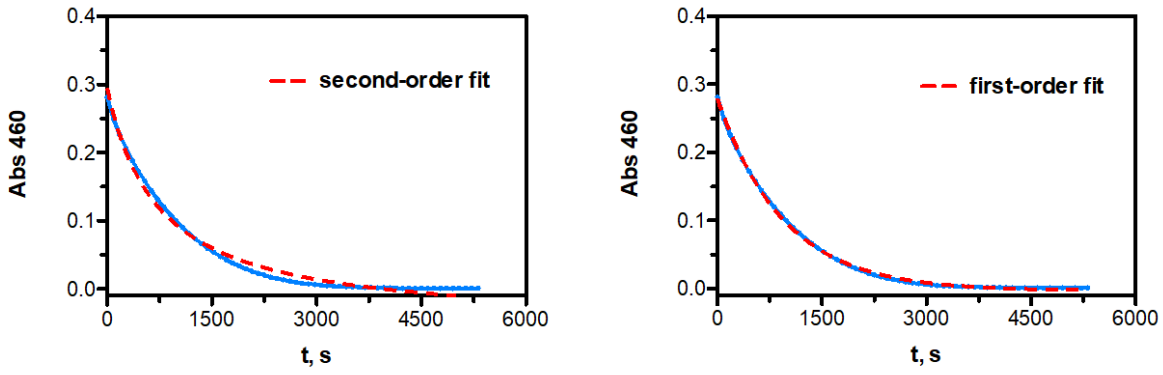

Figure 5-27. Kinetic trace with (left) second-order fit and (right) first-order fit. Conditions: $[\mathrm{HEDS}]_0 = 17.4\ \mathrm{mM}, [\mathrm{I_2}]_0 = 0.43\ \mathrm{mM}$.

To investigate the filter and UV light effect on the reaction kinetics, spectrophotometric experiments were performed with and without 420 nm cut-off filter. The numbers of scanning was changed. It was found out that the two factors have no discerned effect on the reaction kinetics.

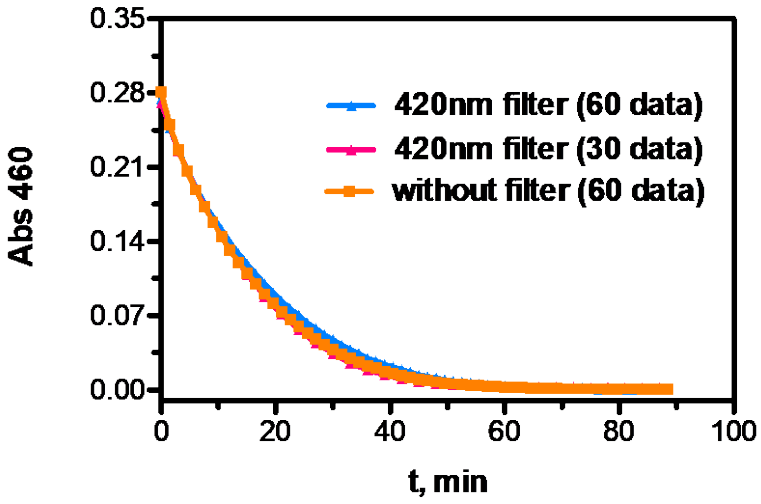

Figure 5-28. Kinetic traces for determining the effect of the numbers of data collection and filter. Conditions: $[\mathrm{HEDS}]_0 = 17.4\ \mathrm{mM}, [\mathrm{I_2}]_0 = 0.43\ \mathrm{mM}$.

To test out the possibility that the kinetic behavior is caused by iodine hydrolysis, and at the same time the disulfide is acting as a catalyst, experiments were performed involving the following aspects.

5.4.6.1 Oxygen effect on the reaction

To investigate the effect of oxygen to the reaction mixture of HEDS and iodine, UV experiment was carried out after purging argon to the solutions. The result was compared to the experiment that was performed under similar conditions except the latter one was air included. Given that acetonitrile (ACN) is thermodynamically stable for iodine, I_2 was dissolved in ACN and then diluted with water before purging argon. The identical kinetic traces indicates that there was no difference obtained from the two conditions. ACN was later substituted by ethanol to evaluate the solvent effect on the reaction. As expected, no variation was detected after the replacement. All above results lead to the fact that the reaction is not oxygen sensitive.

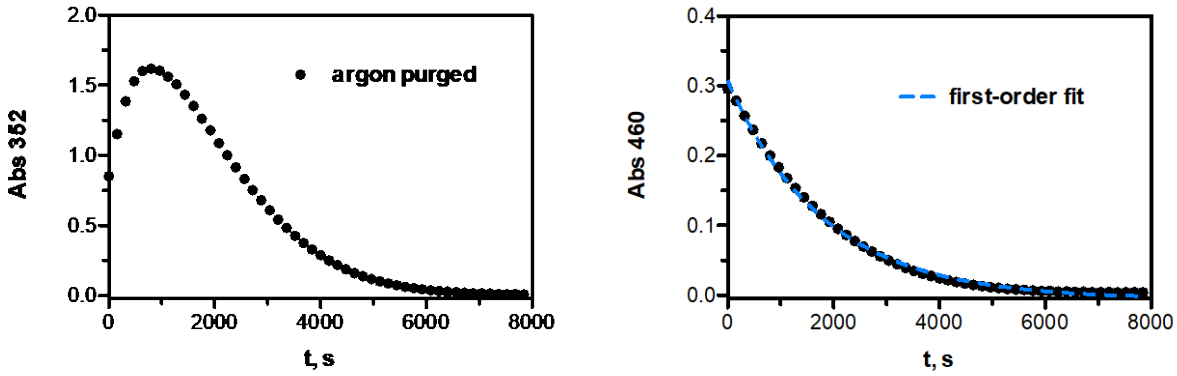

Figure 5-29. Kinetic trace of the mixture with oxygen removed.

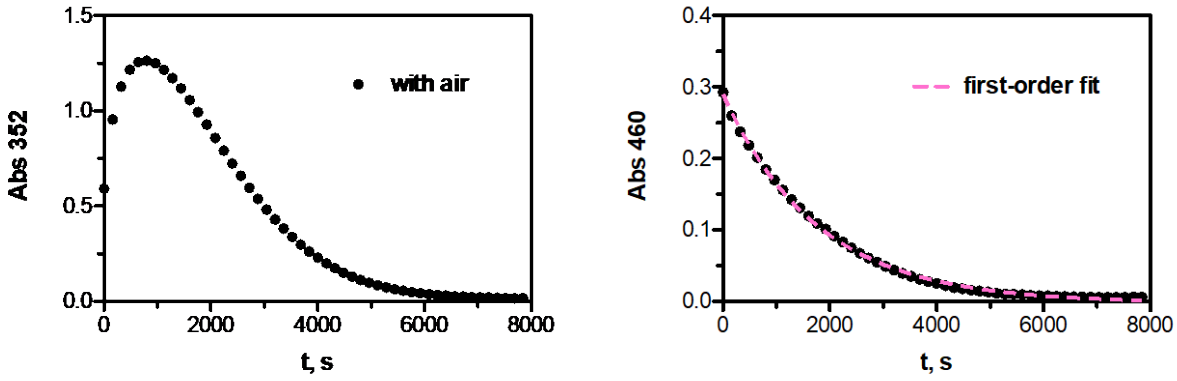

Figure 5-30. Kinetic trace of the mixture with air included.

Table 5-4. Kinetic data from the fit of the trace at 460 nm.

	Argon purged	**With air**
k_{obs}, s^{-1}	5.5×10^{-4}	5.5×10^{-4}
$t_{1/2}$, s	1259	1230

5.4.6.2 Rate dependence on [HEDS]

The kinetics of the reaction between HEDS and iodine at 460 nm was studied with $[I_2]_0 =$ 0.43 mM, $[RSSR]_0$ ranging from 8.57 mM to 45.1 mM using UV-Vis spectrophotometer. The first-order dependence of k_{obs} on [HEDS] is evident from the linear fit.

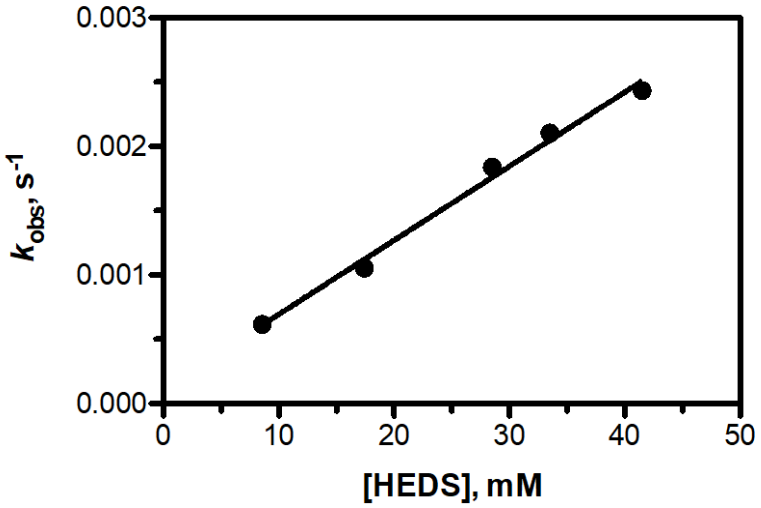

Figure 5-31. Dependence of k_{obs} on [HEDS]. Slope $= (5.76 \pm 0.31) \times 10^{-2}\ s^{-1}\ M^{-1}$, Y − intercept $= (1.18 \pm 0.88) \times 10^{-4}\ s^{-1}$.

Table 5-5. Kinetic data for determining [HEDS] dependence.

$[HEDS]_0$, mM	k_{obs}, s^{-1}	$t_{1/2}$, s
8.57	0.00062	1123
17.44	0.00105	658.4
28.50	0.00184	377.2
33.50	0.00210	329.4
41.50	0.00243	284.7

A general rate law based on the reaction is expressed as,

$$-\frac{\mathrm{d}[\mathrm{I_2}]}{\mathrm{dt}} = k[\mathrm{I_2}][\mathrm{HEDS}] \qquad \text{Eq. 5-37}$$

Given that $[\mathrm{HEDS}] \gg [\mathrm{I_2}]$, k_{obs} equals to $k[\mathrm{HEDS}]$. k is calculated to be 0.058 $s^{-1}\ M^{-1}$.

5.4.6.3 Rate dependence on $[I^-]$

$[I^-]$ dependence on k_{obs} was studied by varying I^- concentration from 0 mM to 13.1 mM and keeping the concentration of iodine and HEDS as constant. It turns out that k_{obs} decreases

when iodide concentration increases, which suggests that iodine is more reactive than triiodide under the same conditions. The experimental data is fitted with equation derived below with the consideration that both iodine and triiodide participate in the reaction and determine the rate. As a result, the solved rate constants are $k_1 = (4.98 \pm 0.35) \times 10^{-2}\ \mathrm{M^{-1}\ s^{-1}}$, $k_2 = (5.92 \pm 0.98) \times 10^{-3}\ \mathrm{M^{-1}\ s^{-1}}$.

$$[\mathrm{I_2}] + [\mathrm{I_3^-}] = [\mathrm{I_2}]_{\mathrm{total}} \quad \text{Eq. 5-38}$$

$$[\mathrm{I_3^-}] = K_{I_3^-}[\mathrm{I_2}][\mathrm{I^-}] \quad \text{Eq. 5-39}$$

$$[\mathrm{I_2}] + K_{I_3^-}[\mathrm{I_2}][\mathrm{I^-}] = [\mathrm{I_2}]_{\mathrm{total}} \quad \text{Eq. 5-40}$$

$$[\mathrm{I_2}] = \frac{[\mathrm{I_2}]_{\mathrm{total}}}{1 + K_{I_3^-}[\mathrm{I^-}]} \quad \text{Eq. 5-41}$$

$$\mathrm{Rate} = k_1[\mathrm{I_2}][\mathrm{RSSR}] + k_2[\mathrm{I_3^-}][\mathrm{RSSR}] \quad \text{Eq. 5-42}$$

$$\mathrm{Rate} = [\mathrm{RSSR}]\left(k_1[\mathrm{I_2}] + k_2K_{I_3^-}[\mathrm{I_2}][\mathrm{I^-}]\right) \quad \text{Eq. 5-43}$$

$$\mathrm{Rate} = [\mathrm{RSSR}][\mathrm{I_2}]\left(k_1 + k_2K_{I_3^-}[\mathrm{I^-}]\right) \quad \text{Eq. 5-44}$$

$$\mathrm{Rate} = [\mathrm{RSSR}]\left(\frac{[\mathrm{I_2}]_{\mathrm{total}}}{1 + K_{I_3^-}[\mathrm{I^-}]}\right)\left(k_1 + k_2K_{I_3^-}[\mathrm{I^-}]\right) \quad \text{Eq. 5-45}$$

$$\mathrm{Rate} = [\mathrm{RSSR}][\mathrm{I_2}]_{\mathrm{total}}\left(\frac{k_1 + k_2K_{I_3^-}[\mathrm{I^-}]}{1 + K_{I_3^-}[\mathrm{I^-}]}\right) \quad \text{Eq. 5-46}$$

When $[\mathrm{RSSR}] \gg [\mathrm{I_2}]$, $k_{obs} = [\mathrm{RSSR}]\left(\frac{k_1 + k_2K_{I_3^-}[\mathrm{I^-}]}{1 + K_{I_3^-}[\mathrm{I^-}]}\right)$

$$k_{obs} = \frac{k_1}{1 + \mathrm{K_{eq}}[\mathrm{I^-}]}[\mathrm{RSSR}] + \frac{k_2K_{I_3^-}}{1 + K_{I_3^-}[\mathrm{I^-}]}[\mathrm{I^-}][\mathrm{RSSR}] \quad \text{Eq. 5-47}$$

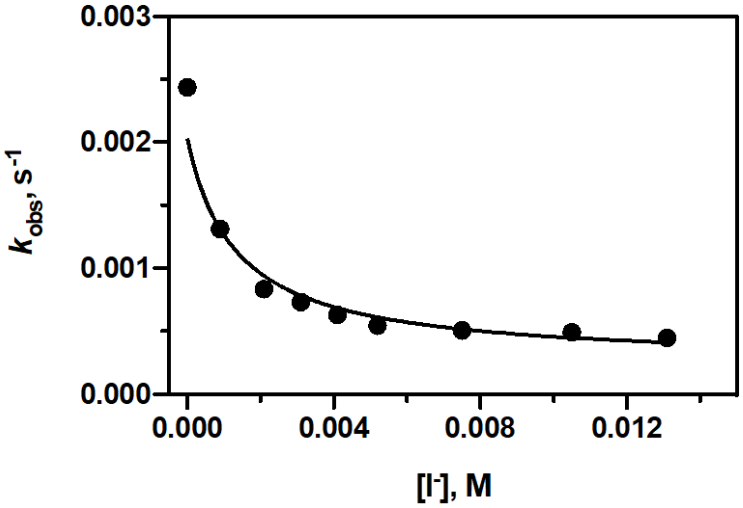

Figure 5-32. [Iodide] dependence on k_{obs}. Conditions: $[HEDS]_0 = 41.5$ mM, $[I_2]_0 = 0.48$ mM.

5.4.7 Product Characterization

5.4.7.1 ^{1}H-NMR of HEDS

^{1}H-NMR spectrum of 2-hydroxyethyldisulfide in D_2O with DSS as reference was recorded initially. A set of triplets at 2.89 ppm and 3.86 ppm from the two -CH_2 group contained in the disulfide are detected in the spectrum.

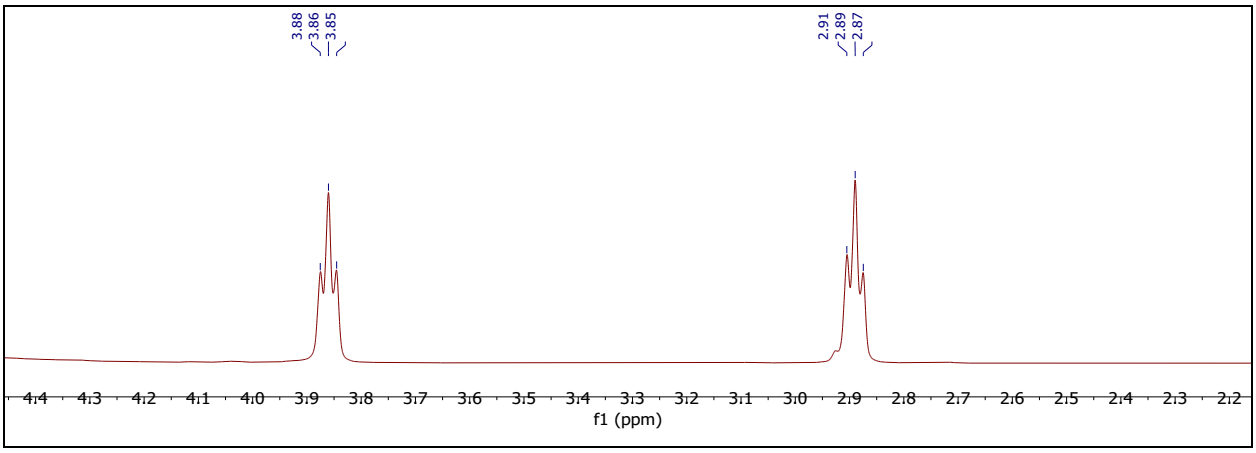

Figure 5-33. ^{1}H-NMR of HEDS in D_2O with DSS as reference.

5.4.7.2 ^{1}H-NMR of the reaction mixture

To identify the reaction product, 3.8 mM I_3^- was mixed with 12.4 mM HEDS and stirred under room temperature till the solution became colorless. The solvent was removed by rotor-evaporator. After that, ^{1}H-NMR spectrum was obtained upon dissolving the resulting solid into CD_3OD-d_4. In the spectrum, four triplets appear in the range of 3.3 ppm to 4.1 ppm. They are assigned to the reaction product that might consist of four -CH_2 groups.

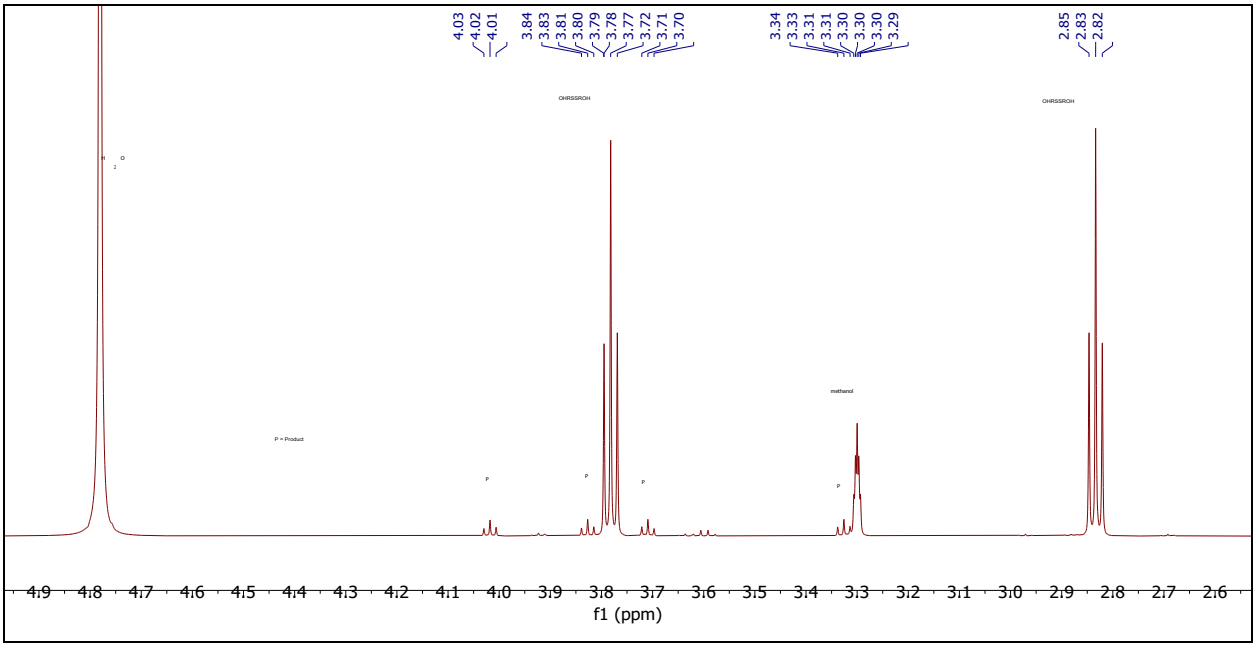

Figure 5-34. ^{1}H-NMR of the reaction product in CD_3OD-d_4.

Though the peaks are very likely to be identified as from the reaction product, there is still a chance that the signals are from other by-products or contaminants in the solution. To further identify the reaction mixture and minimize the impurities from the solvent, the reactants including 8.2 mM triiodide and 11.05 mM HEDS were mixed in D_2O and allowed to react for 7 days till the solution become colorless. After that, the ^{1}H-NMR spectrum was recorded with DSS as a reference.

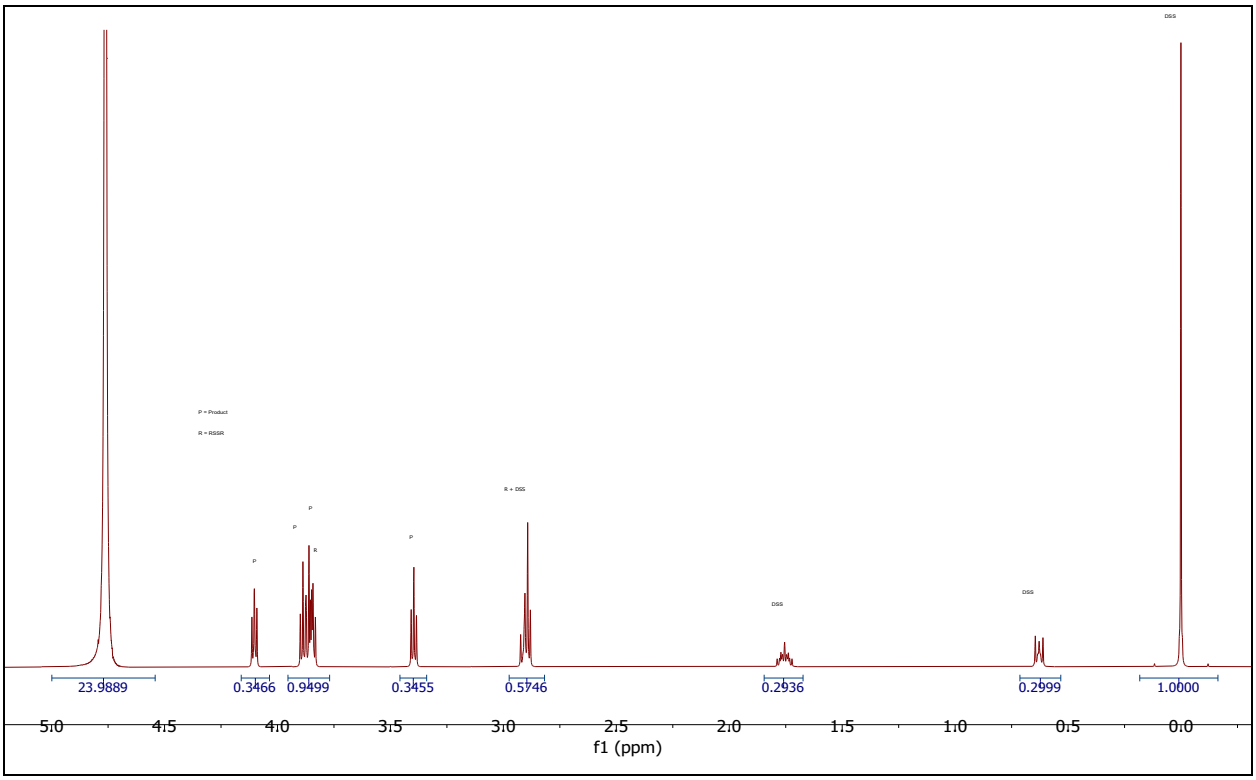

Figure 5-35. ^{1}H-NMR of the reaction mixture in D_2O with DSS as reference.

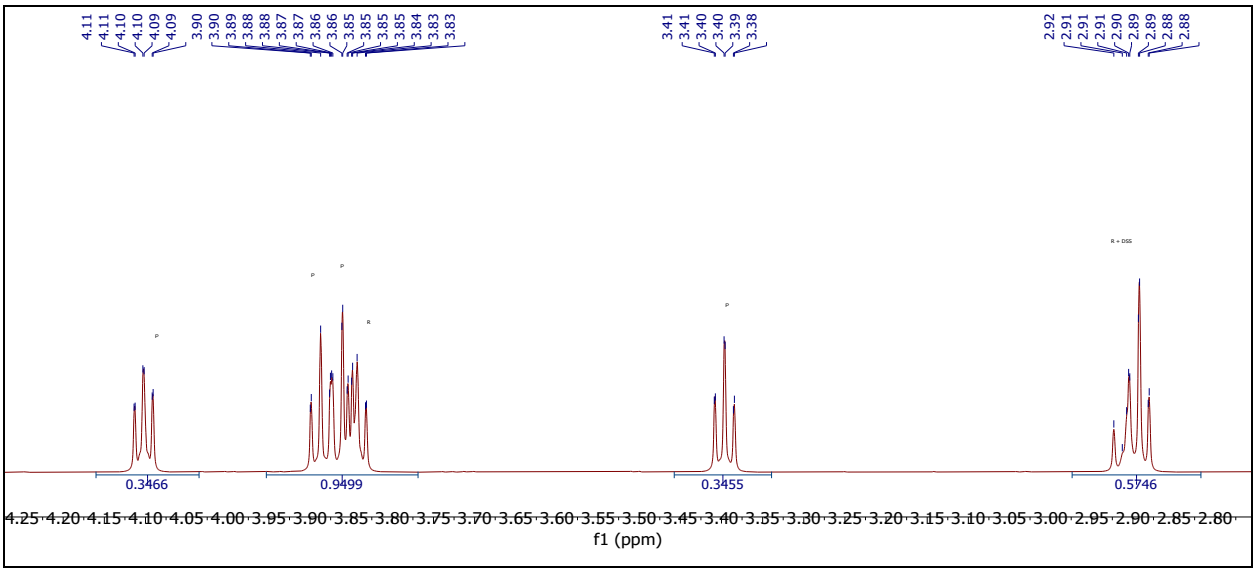

Figure 5-36. Zoom in on Figure 5-35.

It can be noticeable that a multiplet arises at 3.8-4.0 ppm. A fair guess upon that signal can be the partial overlap of the peaks from the disulfide and the reaction product. To confirm that, 2-D H-H COSY spectrum for the rection mixture was recorded. As expected, the complex pattern

was confirmed to be an overlay of the peak from HEDS and the triplet from the reaction product (at 3.85 ppm).

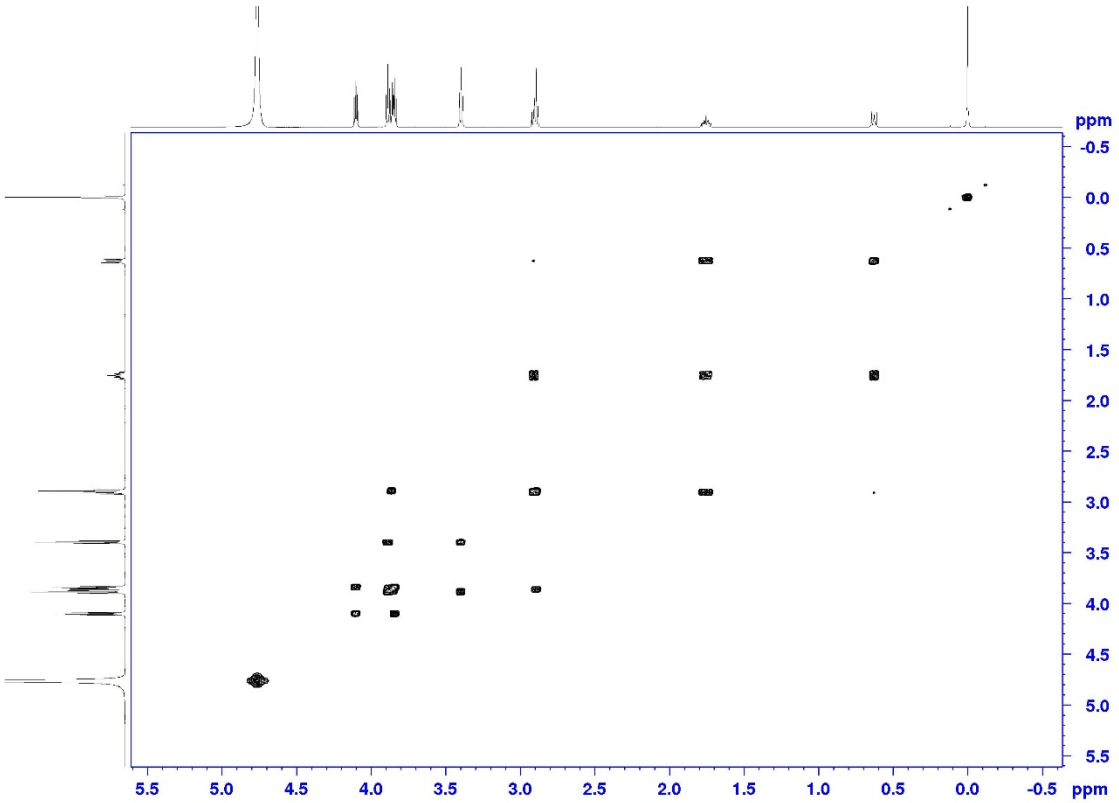

Figure 5-37. 2-D H-H COSY spectrum of the reaction mixture in D_2O with DSS as reference.

From the spectral information collected above, we regard the S-containing product of the oxidation of HEDS by iodine as thiosulfinate, $OH(CH_2)_2S(O)S(CH_2)_2OH$. To get more solid evidence, the corresponding thiosulfinate of HEDS was synthesized.

5.4.7.3 ^{1}H-NMR of the synthesized product

HEDS-thiosulfinate was synthesized by oxidation of HEDS with 30% H_2O_2. To prepare the reaction mixture, 0.830 mmol HEDS and 1.992 mmol H_2O_2 was dissolved into 2 mL water. The mixture solution was allowed to react for 23 hours at room temperature, followed by overnight drying. The resulting product was found to be an oily liquid. ^{1}H-NMR was recorded after

dissolving the liquid into D_2O with DSS as reference. In the spectrum, four triplets from 3.3 ppm to 4.2 ppm are detected from -CH_2 group of the compound.

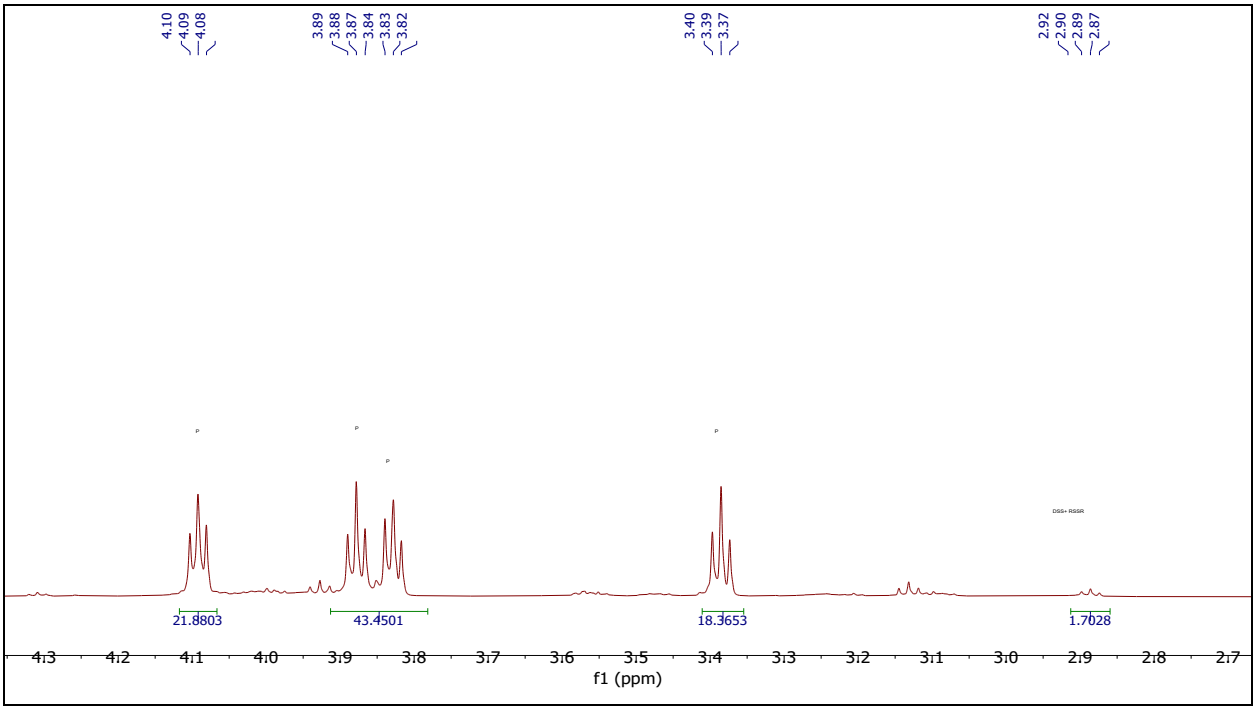

Figure 5-38. ^{1}H-NMR of the synthesized compound in D_2O with DSS as reference.

5.4.7.4 ESI-MS of the synthesized product

A mixture solution containing 4.98 mmol HEDS and 2.05 mmol 30% H_2O_2 was prepared at room temperature. After reacting for 46 hours, ESI-MS (in negative mode) of the sample was recorded and shown below. To our knowledge, it takes about 24 hours for equal-molar of disulfide and H_2O_2 to react completely and generate thiosulfinate. Plus, the by-product HEDS-thiosulfonate can be produced after a long period standing. The maximum peak with m/z = 215.0100 in the spectrum implies the formation of $(Na)_2OHC_2H_4S(O)SC_2H_4O^-$ as the main product. The peak with m/z = 231.0058 can be assigned to thiosulfonate which is converted from thiosulfinate.

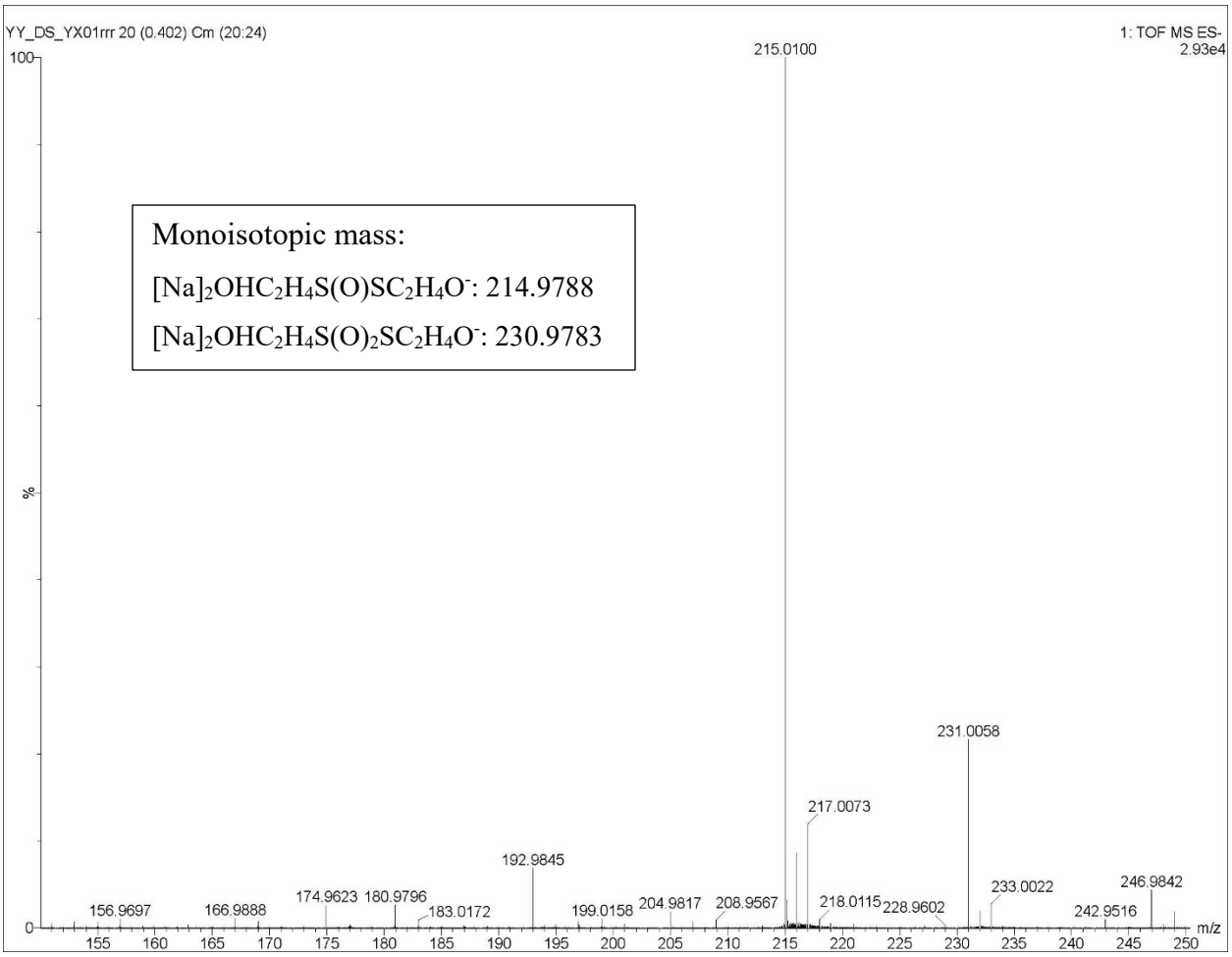

Figure 5-39. ESI-MS spectrum of the reaction mixture.

With all NMR and MS evidence collected above, the S-containing product of HEDS/iodine reaction mixture was finalized to be HEDS-thiosulfinate. The overall reaction is herein given as,

$$(\mathrm{OHCH_2CH_2S})_2 + \mathrm{I_2} + \mathrm{H_2O} \rightarrow \mathrm{OHCH_2CH_2S(O)SCH_2CH_2OH} + 2\mathrm{I^-} + 2\mathrm{H^+} \qquad \text{Eq. 5-48}$$

5.5 Part-III: Oxidation of 3,3'-Dithiodipropionic Acid (3,3-DTDP) by Iodine

5.5.1 Background

3,3'-dithiodipropionic acid (DTDP), $(COOH(CH_2)_2S)_2$, is a disulfide formed from two molecules of 3-mercaptopropionic acid. It is commercially available and generally inexpensive. DTDP has been mostly utilized for electrochemical and thermodynamic research [32] involving preparing self-assembled monolayers [29], secondary batteries [30], bacterium isolating [31], and amino acid analysis [33]. An essential function of DTDP in biological aspect reported by Steinbüchel's group is that this disulfide is capable of being a novel precursor substrate for synthesizing polythioester [34].

Despite the various reports and applications regarding its electrochemical and biochemical function, the potential of S-S group of DTDP being the reductant to generate thiosulfonate or sulfonic acid is not profoundly studied. Though the oxidative cleavage of DTDP by iodine was investigated by Doi's group previously [35], it was found that the kinetic and product analysis of the reaction is not precisely determined and discussed. For example, there is not enough data provided to confirm the rate dependence on [DTDP] and [RSSR]. As for pH and iodide effect on the reaction rate, no details are available on how the equation was derived to fit the kinetic dependence. Beyond that, it is also worthy to mention that DTDP is practically insoluble in water. Therefore, the oxidation of DTDP by iodine at pH 7 at ambient temperature should barely yield any product. In view of the limitations presented by Doi's study, plus consideration of presenting more detailed and comprehensive kinetic information of the oxidation of DTDP and comparing it with other two disulfides discussed in the previous parts to propose a more systematic mechanism scheme for $RSSR/I_2$ redox reaction, it is believed to be significant to re-investigate the reaction between DTDP and iodine in aqueous phase so that the reaction can be better understood.

5.5.2 Reaction Stoichiometry

The reaction ratio of the two reactants, DTDP and iodine, was determined via spectrophotometric titration. 0.73 mM I_2 was prepared to titrate 2 mL 0.539 mM DTDP which had been dissolved in NaOH initially. The break point is found when there is a sharp absorbance rise at 460 nm. The consumption ratio of the reaction was calculated to be $\frac{\Delta[I_2]}{\Delta[DTDP]} = 5.08$.

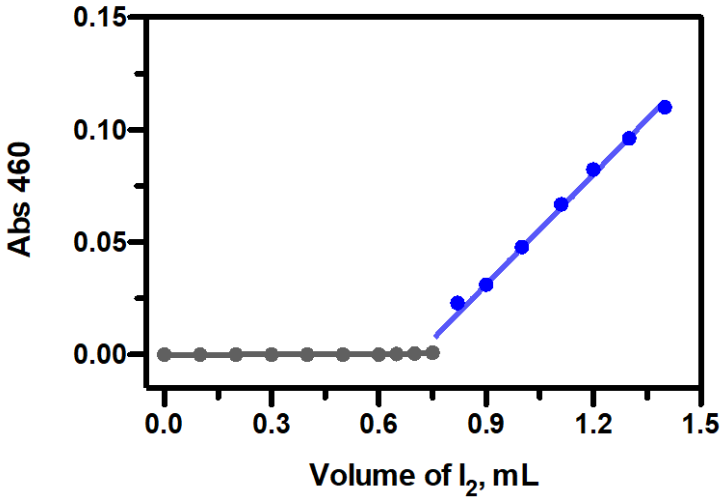

Figure 5-40. Titration curve for determining the reaction ratio.

5.5.3 Kinetic Result

Unlike the oxidation of SEDS and HEDS by iodine, the reaction between DTDP with iodine is much faster, which makes it possible to monitor the kinetic behavior using stopped-flow method. DTDP solution was prepared in hot water and then cooled down for further experiments due to its very low solubility in water at room temperature. The kinetic experiments were performed by mixing the two reactants and recording the absorbance change at 460 nm.

5.5.3.1 pH Dependence

The degradation of DTDP gives 3-mercaptopropionic acid as an intermediate [45]. This intermediate is recognized as an essential species during catabolism of the marine alga osmolyte

dimethylsulfoniopropionate [35],[36]. It is also an anaerobic degradation product of homocysteine and methionine [37],[38]. In consideration of the biological and environmental importance of DTDP, iodine and their degradation substances, plus the processes taking place over a large pH range, it is meaningful to study the pH effect on the reaction of DTDP with iodine to obtain some primary information on the regulation of the reaction kinetics. To create acidic media, $HClO_4$ was added to iodine solution to adjust pH. The kinetic trace of the reaction mixture at pH 2.59 was recorded and fitted with a second-order rate law with a rate constant of $k_{obs} = 575\ M^{-1}\ s^{-1}$.

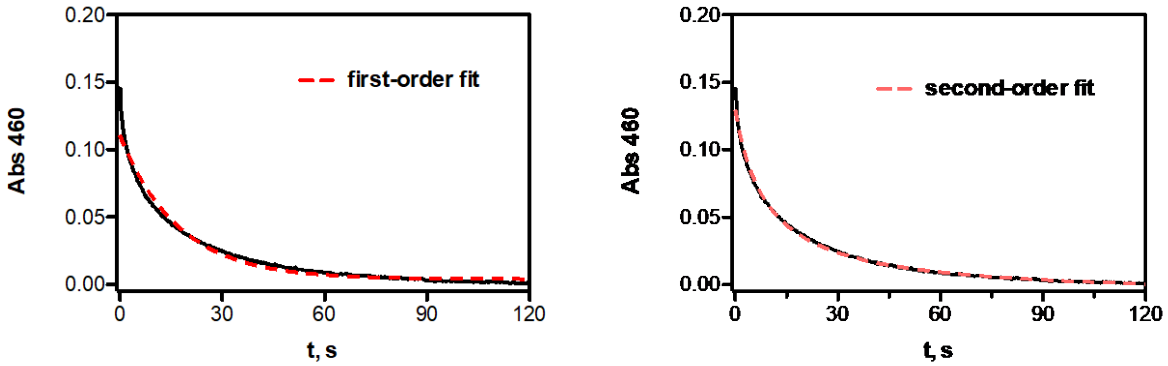

Figure 5-41. Kinetic trace and the fit of the reaction mixture with excess DTDP. Conditions: $[I_2]_0 = 0.22$ mM, $[DTDP]_0 = 1.16$ mM, pH $= 2.59$. (left) First-order fit; (right) Second-order fit.

The rate dependence on pH was studied by monitoring the kinetic traces at various pH. It can be evident from the plot of k_{obs} vs $[H^+]$ that the reaction is sensitive to pH between 2.6-5.0 and independent of pH below 2.6.

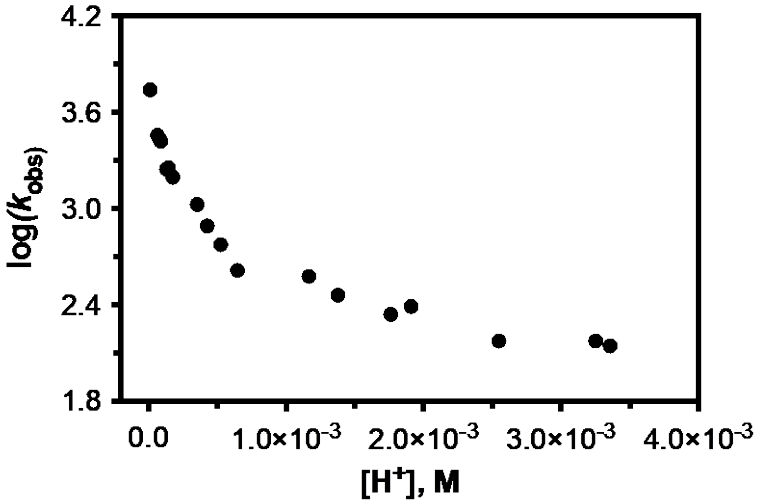

Figure 5-42. Dependence of $\log(k_{obs})$ on $[H^+]$ in the presence of excess DTDP. Conditions: $[I_2]_0 = 0.22$ mM, $[DTDP]_0 = 1.16$ mM, pH $= 2.47 - 5.0$.

Table 5-6. Kinetic data for determining pH dependence on the reaction kinetics

pH	$[H^+]$, mM	k_{obs}, s^{-1} M^{-1}
2.933	1.167	379
2.474	3.357	140
3.840	0.144	1800
2.719	1.910	246
2.488	3.251	150
2.594	2.547	168
2.754	1.762	220
2.861	1.377	290
3.150	0.645	414
3.890	0.129	1770
4.057	0.088	2638
3.451	0.354	1063
4.100	0.079	2731
3.370	0.426	782
3.281	0.523	599
4.194	0.064	2882
3.753	0.177	1576
4.994	0.010	5500

To fit the experimental data, a rate law was derived with the assumption that both acid and protonated form and the ionized form ($^{-}OOC(CH_2)_2SSCH_2COO^{-}$) of DTDP have participated in the reaction.

$$HOOC(CH_2)_2SS(CH_2)_2COOH \rightleftharpoons {}^{-}OOC(CH_2)_2SSCH_2COO^{-} + 2H^{+} \quad \text{Eq. 5-49}$$

$$A = HOOC(CH_2)_2SS(CH_2)COOH;\ B = {}^{-}OOC(CH_2)_2SSCH_2COO^{-} \quad \text{Eq. 5-50}$$

$$K_a = \frac{[B][H^+]^2}{[A]} \quad \text{Eq. 5-51}$$

$$[DTDP]_{total} = [A] + [B] \quad \text{Eq. 5-52}$$

$$[A] = [DTDP]_{total} - [B] = [DTDP]_{total} - K_a\frac{[A]}{[H^+]^2} \quad \text{Eq. 5-53}$$

$$[A] + K_a\frac{[A]}{[H^+]^2} = [DTDP]_{total};\ [A] = \frac{[DTDP]_{total}}{\left\{1 + K_a\frac{1}{[H^+]^2}\right\}} \quad \text{Eq. 5-54}$$

$$[B] = [DTDP]_{total} - [A] = [DTDP]_{total} - \frac{[DTDP]_{total}}{\left\{1 + K_a\frac{1}{[H^+]^2}\right\}} = [DTDP]_{total}\left(1 - \frac{1}{\frac{[H^+]^2 + K_a}{[H^+]^2}}\right) \quad \text{Eq. 5-55}$$

$$[B] = [DTDP]_{total}\left(1 - \frac{[H^+]^2}{[H^+]^2 + K_a}\right) \quad \text{Eq. 5-56}$$

$$k_{obs} = k_1[A] + k_2[B] \quad \text{Eq. 5-57}$$

$$k_{obs} = k_1\left(\frac{[DTDP]_{total}}{\left\{1 + K_a\frac{1}{[H^+]^2}\right\}}\right) + k_2\left([DTDP]_{total}\left\{1 - \frac{[H^+]^2}{[H^+]^2 + K_a}\right\}\right) \quad \text{Eq. 5-58}$$

$$k_{obs} = k_1[DTDP]_{total}\left(\frac{[H^+]^2}{[H^+]^2 + K_a}\right) + k_2[DTDP]_{total}\left(\frac{K_a}{[H^+]^2 + K_a}\right) \quad \text{Eq. 5-59}$$

$$k_{obs} = \frac{(k_1[H^+]^2 + k_2K_a)[DTDP]_{total}}{[H^+]^2 + K_a} \quad \text{Eq. 5-60}$$

However, this equation does not fit into the pH dependence data. Another assumption with $HOOC(CH_2)_2SSCH_2COO^{-}$ being the reactive form is applied to derive the rate law.

$$\mathrm{HOOC(CH_2)_2SS(CH_2)_2COOH} \rightleftharpoons \mathrm{HOOC(CH_2)_2SSCH_2COO^- + H^+} \quad \text{Eq. 5-61}$$

$$\mathrm{A = HOOC(CH_2)_2SS(CH_2)COOH;\ C = HOOC(CH_2)_2SS(CH_2)COO^-} \quad \text{Eq. 5-62}$$

$$K_\mathrm{a} = \frac{[\mathrm{C}][\mathrm{H^+}]}{[\mathrm{A}]} \quad \text{Eq. 5-63}$$

$$[\mathrm{DTDP}]_\mathrm{total} = [\mathrm{A}] + [\mathrm{C}] \quad \text{Eq. 5-64}$$

$$[\mathrm{A}] = [\mathrm{DTDP}]_\mathrm{total} - [\mathrm{C}] = [\mathrm{DTDP}]_\mathrm{total} - \frac{K_\mathrm{a}[\mathrm{A}]}{[\mathrm{H^+}]} \quad \text{Eq. 5-65}$$

$$[\mathrm{A}] = \frac{[\mathrm{DTDP}]_\mathrm{total}}{\left\{1 + \frac{K_\mathrm{a}}{[\mathrm{H^+}]}\right\}};\ [\mathrm{C}] = [\mathrm{DTDP}]_\mathrm{total}\left(1 - \frac{[\mathrm{H^+}]}{[\mathrm{H^+}] + K_\mathrm{a}}\right) \quad \text{Eq. 5-66}$$

$$k_{obs} = k_1[\mathrm{A}] + k_2[\mathrm{C}] \quad \text{Eq. 5-67}$$

$$k_{obs} = k_1\left(\frac{[\mathrm{DTDP}]_\mathrm{total}}{\left\{1 + \frac{K_\mathrm{a}}{[\mathrm{H^+}]}\right\}}\right) + k_2\left([\mathrm{DTDP}]_\mathrm{total}\left\{1 - \frac{[\mathrm{H^+}]}{[\mathrm{H^+}] + K_\mathrm{a}}\right\}\right) \quad \text{Eq. 5-68}$$

$$k_{obs} = [\mathrm{DTDP}]_\mathrm{total}\,\frac{k_1[\mathrm{H^+}] + k_2K_\mathrm{a}}{[\mathrm{H^+}] + K_\mathrm{a}} \quad \text{Eq. 5-69}$$

$$\log(k_{obs}) = \log([\mathrm{DTDP}]_\mathrm{total}) + \log(k_1[\mathrm{H^+}] + k_2K_\mathrm{a}) - \log([\mathrm{H^+}] + K_\mathrm{a}) \quad \text{Eq. 5-70}$$

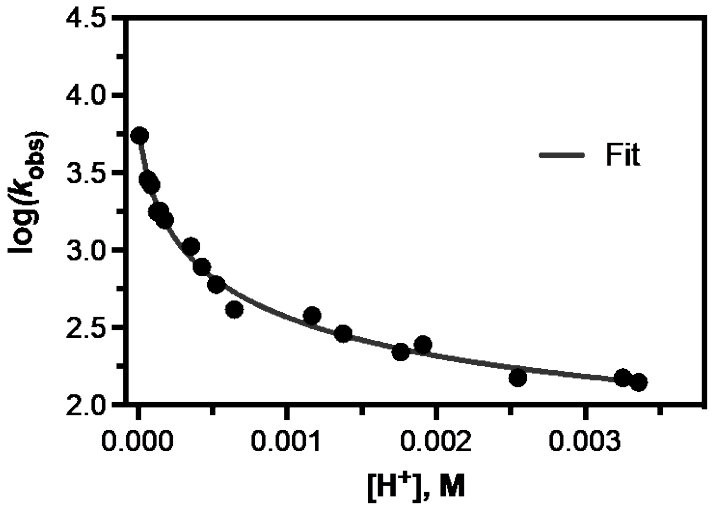

Figure 5-43. Plot of $\log(k_{obs})$ versus $[\mathrm{H^+}]$ fitted by Eq. 5-71.

The plot of $\log(k_{\mathrm{obs}})$ vs $[\mathrm{H}^+]$ is fitted with Eq. 5-72. The values of k_1, k_2 and K_a are found to be $k_1 = (3.3 \pm 1.4) \times 10^4\ \mathrm{M}^{-2}\ \mathrm{s}^{-1}, k_2 = (5.6 \pm 0.6) \times 10^6\ \mathrm{M}^{-2}\ \mathrm{s}^{-1}, K_a = (5.5 \pm 0.9) \times 10^{-5}$ M.

5.5.3.2 Rate dependence on [DTDP]

The effect of [DTDP] on the reaction rate was evaluated at pH 1.78-2.18 by varying the concentration of the disulfide from 1.16 mM to 7.55 mM and keeping the concentration of the other components as constant. The kinetic traces were fitted with second-order rate law. As a result, a first-order dependence on the disulfide concentration of the rate constant can be justified from the linear regression with a negligible intercept.

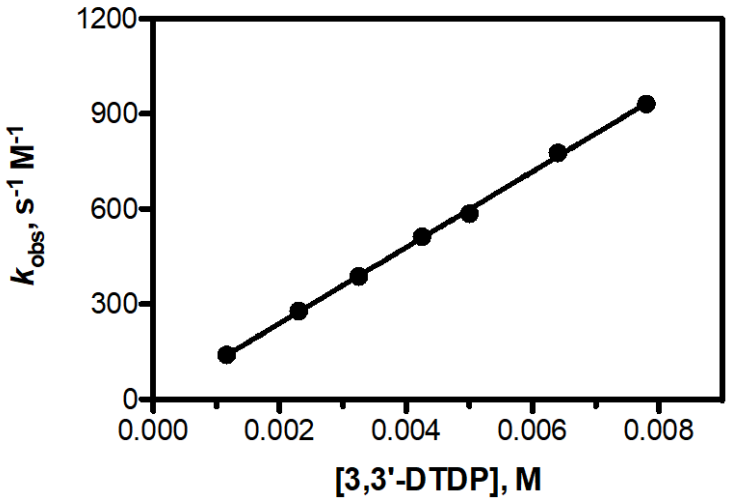

Figure 5-44. [DTDP] dependence of the rate constant k_{obs}. Conditions: $[\mathrm{I}_2]_0 = 0.2$ mM, $[\mathrm{DTDP}]_0 = 1.16 - 7.55$ mM, $\mathrm{pH} = 1.78 - 2.18$. Linear fit: $\mathrm{slope} = (1.20 \pm 0.01) \times 10^5\ \mathrm{s}^{-1}\ \mathrm{M}^{-2}$; $\mathrm{Y-intercept} = 36.05 \pm 6.92\ \mathrm{s}^{-1}\ \mathrm{M}^{-1}$.

5.5.3.3 Rate dependence on [I_2]

The rate dependence on [Iodine] with 3.25 mM DTDP was examined as a function of iodine concentration with pH adjusted to 2.42-2.50. The plot of inverse k_{obs} vs $[I_2]^2$ is shown blow. The data is well-fitted into a straight line with no intercept.

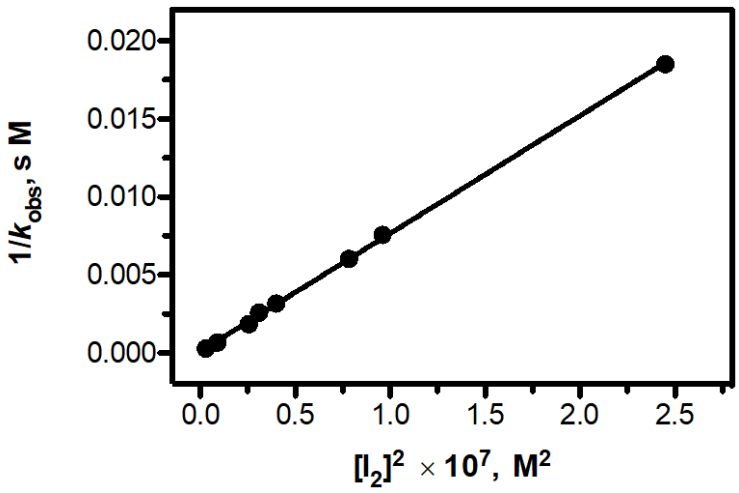

Figure 5-45. Inverse k_{obs} vs $[I_2]^2$. Linear fit with slope $= (7.55 \pm 0.07) \times 10^{-3}$ s M^{-1} ; Y − intercept = $(1.01 \pm 0.68) \times 10^{-4}$ s M).

5.5.3.4 Rate dependence on [Iodide]

Considering that the product iodide might inhibit the reaction rate, the kinetic effect of I^- on the reaction was studied using UV-Vis by varying $[I^-]$ from 2.0 mM to 19.0 mM. pH of the reaction solutions was adjusted to 1.9-2.2. I^- was added to DTDP solutions before mixing with iodine. The kinetics traces were well fitted into first-order rate law in the presence of large excess of iodide. A rate constant of 1.47×10^{-3} s^{-1} with $t_{1/2} = 472.2$ s was determined from the fit of the kinetic trace in Figure 5-46.

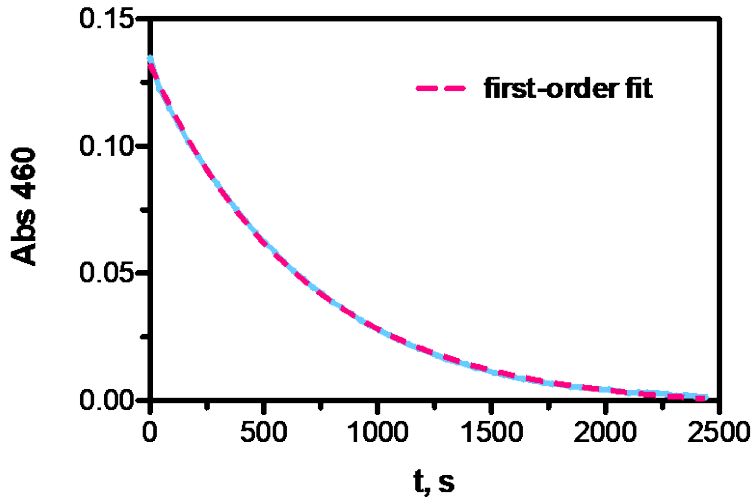

Figure 5-46. Kinetic trace of the reaction of DTDP/I_3^- with excess of I^-. Conditions: $[I_2]_0 = 0.3$ mM, $[DTDP]_0 = 7.5$ mM, $[I^-]_0 = 15.0$ mM, pH = 1.9.

To better understand [Iodide] dependence, a rate law considering iodine as the only reactive species for the oxidation is derived initially.

$$RSSR + I_2 \rightarrow \text{Product}; \quad k_1 \qquad \text{Eq. 5-73}$$

$$I_2 + I^- \rightleftharpoons I_3^-; \quad K_{I_3^-} = \frac{[I_3^-]}{[I_2][I^-]} \qquad \text{Eq. 5-74}$$

$$[I_2] + [I_3^-] = [I_2]_{\text{total}}; \; [I_2] = \frac{[I_2]_{\text{total}}}{1 + K_{I_3^-}[I^-]} \qquad \text{Eq. 5-75}$$

$$\text{Rate} = k_1[DTDP][I_2] = k_1[DTDP]\left(\frac{[I_2]_{\text{total}}}{1 + K_{I_3^-}[I^-]}\right) \qquad \text{Eq. 5-76}$$

When $[DTDP] \gg [I_2]_{\text{total}}$,

$$k_{obs} = k_1 \frac{[DTDP]}{1 + K_{I_3^-}[I^-]} \qquad \text{Eq. 5-77}$$

$$\frac{1}{k_{obs}} = \frac{1}{k_1} \times \frac{1 + K_{I_3^-}[I^-]}{[DTDP]} = \frac{1}{k_1[DTDP]} + \frac{K_{I_3^-}[I^-]}{k_1[DTDP]} \qquad \text{Eq. 5-78}$$

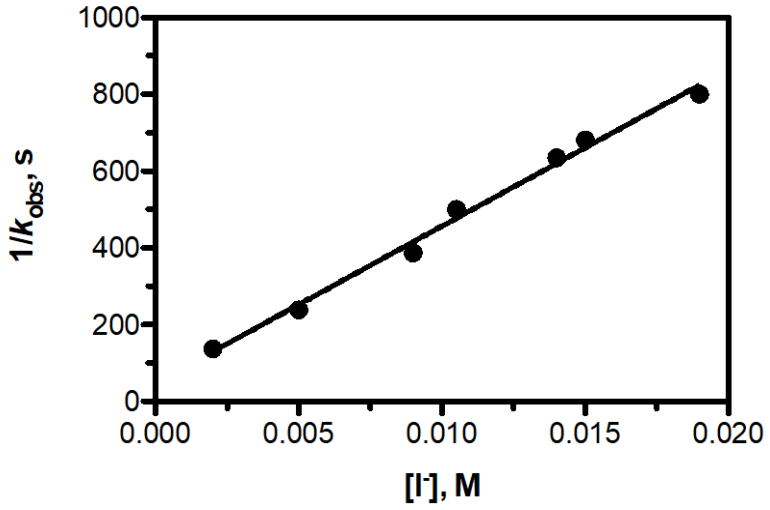

Figure 5-47. Inverse dependence k_{obs} on [I$^-$]. Conditions: $[I_2]_0 = 0.3$ mM, $[DTDP]_0 = 7.5$ mM, $[I^-]_0 = 2.0 - 19.0$ mM, pH $= 1.9 - 2.18$. Straight line fit with slope $= (4.08 \pm 0.16) \times 10^4$ s M^{-1}; Y – intercept $= 48.22 \pm 19.68$ s).

The plot of $1/k_{obs}$ vs [I$^-$] with a linear regression leads to an expression,

$$1/k_{obs} = \mathrm{A}[\mathrm{I}^-] + \mathrm{B} \qquad \text{Eq. 5-79}$$

Here, A is the slope and B is the intercept.

Comparing Eq. 5-78 and Eq. 5-79,

$$\mathrm{A} = \frac{K_{I_3^-}}{k_1[\mathrm{DTDP}]} = (4.08 \pm 0.16) \times 10^4 \ \mathrm{M}^{-1}\,\mathrm{s} \qquad \text{Eq. 5-80}$$

$$\mathrm{B} = \frac{1}{k_1[\mathrm{DTDP}]} = (48.22 \pm 19.68)\ \mathrm{s} \qquad \text{Eq. 5-81}$$

With $K_{I_3^-} = 750\ \mathrm{M}^{-1}$, k_1 was found to be $(2.45 \pm 0.3)\ \mathrm{M}^{-1}\,\mathrm{s}^{-1}$.

Even though iodine is a reactive species of the reaction, the possibility of triiodide affecting the reaction rate should not be ignored. To evaluate the importance of triiodide on the reaction kinetics, a two-term equation was obtained to fit the data.

$$\text{Rate} = k_1[\text{I}_2][\text{DTDP}] + k_2[\text{I}_3^-][\text{DTDP}] \quad \text{Eq. 5-82}$$

$$\text{Rate} = [\text{DTDP}]\left(k_1[\text{I}_2] + k_2K_{\text{I}_3^-}[\text{I}_2][\text{I}^-]\right) = [\text{DTDP}][\text{I}_2]\left(k_1 + k_2K_{\text{I}_3^-}[\text{I}^-]\right) \quad \text{Eq. 5-83}$$

$$\text{Rate} = [\text{DTDP}]\left(\frac{[\text{I}_2]_{\text{total}}}{1 + K_{\text{I}_3^-}[\text{I}^-]}\right)\left(k_1 + k_2K_{\text{I}_3^-}[\text{I}^-]\right) \quad \text{Eq. 5-84}$$

$$\text{Rate} = [\text{DTDP}][\text{I}_2]_{\text{total}}\left(\frac{k_1 + k_2K_{\text{I}_3^-}[I^-]}{1 + K_{\text{I}_3^-}[I^-]}\right) \quad \text{Eq. 5-85}$$

When $[\text{DTDP}] \gg [\text{I}_2]$,

$$k_{obs} = [\text{DTDP}]\left(\frac{k_1 + k_2K_{\text{I}_3^-}[\text{I}^-]}{1 + K_{\text{I}_3^-}[\text{I}^-]}\right) \quad \text{Eq. 5-86}$$

$$k_{obs} = \frac{k_1}{1 + K_{\text{I}_3^-}[\text{I}^-]}[\text{DTDP}] + \frac{k_2K_{\text{I}_3^-}}{1 + K_{\text{I}_3^-}[\text{I}^-]}[\text{I}^-][\text{DTDP}] \quad \text{Eq. 5-87}$$

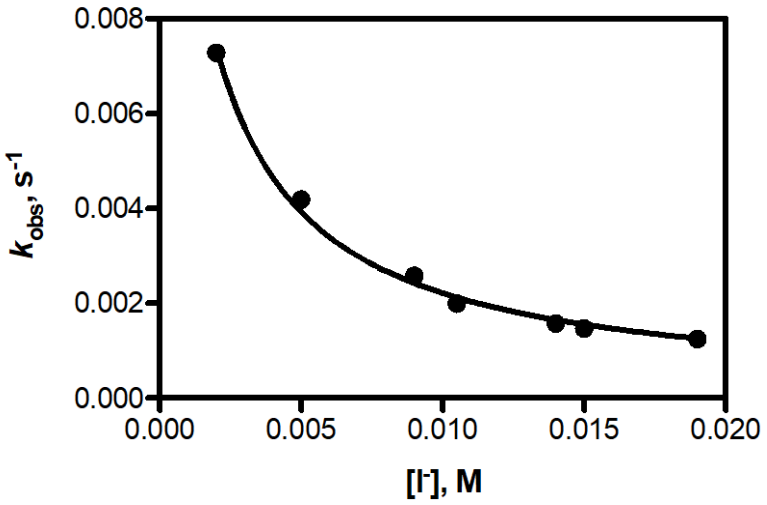

Figure 5-48. k_{obs} dependence on [I$^-$] fitted with two-term equation.

After fitting the data with Eq. 5-87, the resolved rate constants are $k_1 = 2.46 \pm 0.07\ \mathrm{M^{-1}\ s^{-1}}, k_2 = (7.54 \pm 14.7) \times 10^{-3}\ \mathrm{M^{-1}\ s^{-1}}$.

Table 5-7. Kinetic data for studying iodide dependence.

$[I^-]$, M	$1/k_{obs}$, s
0.0020	137.287
0.0050	238.549
0.0090	386.997
0.0105	500.751
0.0140	634.921
0.0150	681.199
0.0190	800.640

5.5.4 Product Analysis

^{1}H-NMR was obtained initially for the mixture of iodine with excess DTDP in D_2O with DSS as reference. The peaks of the reaction product can be detected at 2.8 ppm and 3.2 ppm.

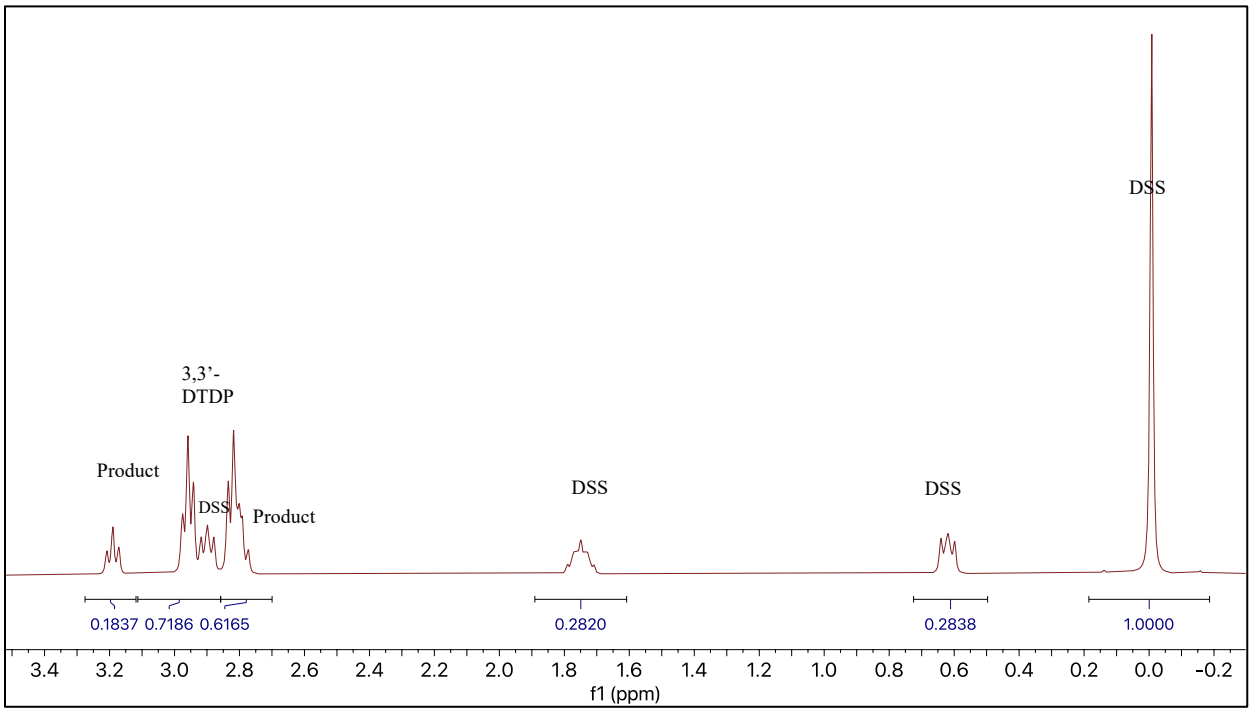

Figure 5-49. ^{1}H-NMR of the mixture of iodine with excess DTDP in D_2O.

5.5.4.1 Product synthesis

Based on the reaction stoichiometry, the speculation is made that the S-containing product might be 3-sulfopropionic acid. To verify, 3-sulfopropionic acid was synthesized according to a method described by Jariwala [39]. 0.654 mmol 3-bromopropionic acid was refluxed in an aqueous solution of 2.0 M 20 mL sodium sulfite at 110 °C for 12 hours. The pH of the reaction mixture was later adjusted with concentrated HCl to 0.8. The resulting sulfocarboxylic acid was then extracted with methanol. After that, the solvent was removed using rotor-evaporator and the compound was washed with ethanol. The final product was dried and found to be white solid with 24% yield. ^{1}H-NMR was recorded for the synthesized sulfocarboxylic acid in D_2O with DSS as reference. The spectrum shows two triplets appearing at 2.8 ppm and 3.2 ppm.

5.5.4.2 Reaction Product Characterization

Knowing that DTDP has higher solubility in alkaline solutions, the following experiments were performed by preparing the disulfide in NaOH solutions at 25 ± 0.5 °C. I_3^- was prepared by dissolving iodine into D_2O with the addition of potassium iodide. 0.8 mL triiodide solution was then injected into the NMR tube. Later, DTDP was added to the triiodide solution, followed by the addition of 0.2 mL 0.247 M NaOH in the tube. The mixture solution was allowed to react for 30 mins. ^{1}H-NMR was recorded for the colorless sample with DSS as reference.

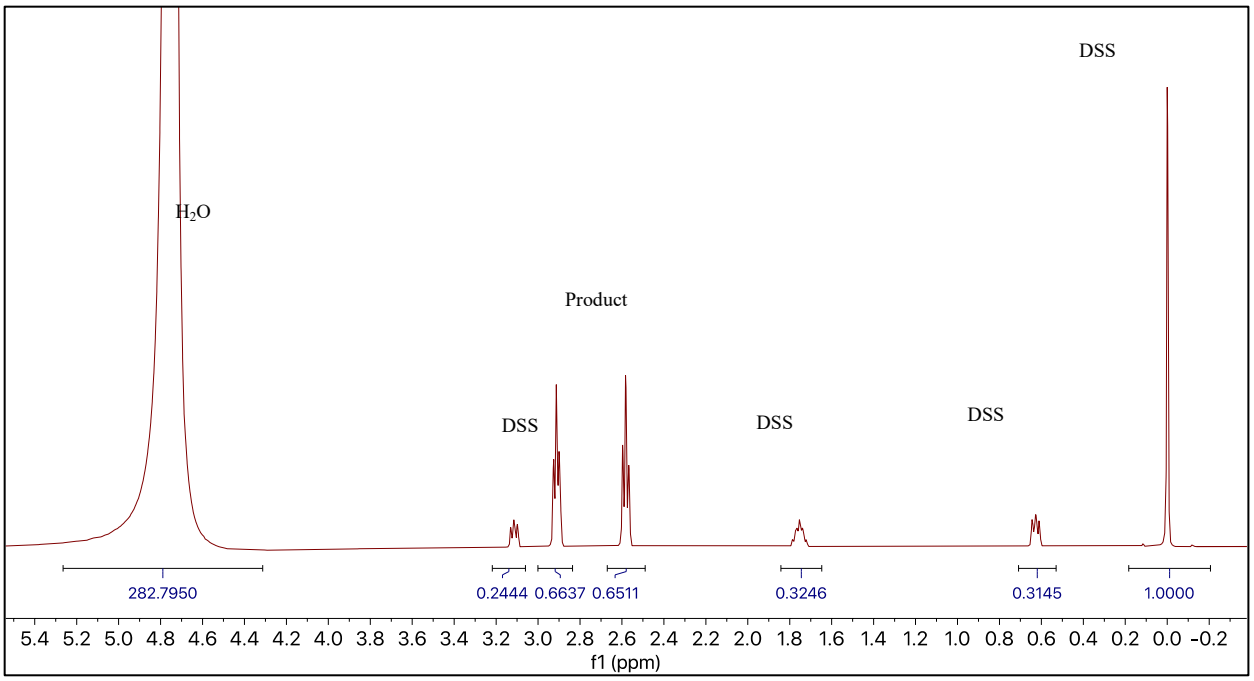

Figure 5-50. ^{1}H-NMR of the mixture of I_3^- with DTDP. Conditions: $[I_3^-] = 9.52\ \text{mM}$, $[\text{DTDP}] = 1.71\ \text{mM}$, $[\text{DSS}] = 1.74\ \text{mM}$.

Next, 12.8 mg synthesized 3-sulfopropionic acid was added to the reaction product solution. The peak at 2.59 ppm become much more intense. Notably, peaks at 2.9 ppm and 3.1 ppm can be ascribed to the proton change from the spiking of the synthesized acid. The triplets are therefore identified as from the -CH_2 group of the spiked product and the reaction product.

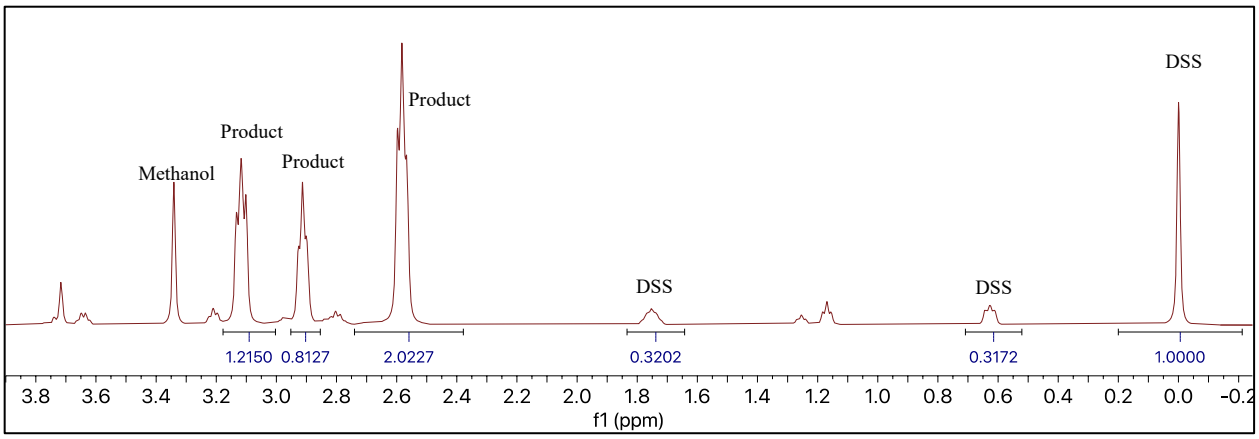

Figure 5-51. ^{1}H-NMR of 3-sulfopropionic acid spiking on the product of the reaction mixture.

With the information collected from stoichiometric titration and NMR, the overall reaction of oxidation of DTDP by iodine is determined as,

$$(COOHCH_2CH_2S)_2 + 5I_2 + 6H_2O \rightarrow 2COOHCH_2CH_2SO_3^- + 10I^- + 12H^+ \qquad \text{Eq. 5-88}$$

5.6 Discussion

The primary goal of this research is to investigate the underlying mechanism when iodine is mixed with various disulfides. The investigations are therefore conducted based on two ideas: to examine the potential of disulfide as a catalyst for iodine hydrolysis, and another to determine the kinetics and mechanism of the redox reaction between the two substances. According to published literature, the disproportionation of HOI to release iodine and iodate can be affected by buffers in both catalytical and inhibitory way. For instance, Margerum's group [40] provided information of acetic acid-acetate buffer effect on the formation of HO_2I and I_2 ($3HOI \rightarrow HO_2I + H_2O + I_2$) and pointed out that the reaction rate can be fueled up by the appearing of (acetato-O)iodine (CH_3CO_2I), which enhances the formation of the steady-state species, I_2O. With the increase in buffer concentration, the suppression from buffer on the subsequent reaction to produce IO_3^- and I_2 can be observed due to the formation of stable ion bis(acetato-O)iodate ion, $(CH_3CO_2)_2I^-$. Schmitz also mentioned that buffer has catalytic influence on the HOI disproportionation [41]. Statement was further made that the catalysis takes place on the account of the formation of a complex I_2OB^-, where B^- refers to the anion of the buffer. The formulated mechanism is

Step	Reaction
1	$2HOI \rightleftharpoons I_2O \cdot H_2O$
2	$I_2O \cdot H_2O \rightarrow$ products
3	$I_2O + B^- \rightleftharpoons I_2OB^-$
4	$I_2OB^- + I^- \rightleftharpoons IO^- + I_2 + B^-$

The rate of the decomposition of I_2OB^- is considered to be equal to the rate of the catalyzed process [41],[42]. By referring to the above reports, and our observation of non-discernable change in the reaction kinetics when iodine is mixed with MESNA-disulfide at the presence of acetate buffer, the hypothesis of RSSR serving as a catalyst for iodine hydrolysis can therefore be ruled out. Evidence collected from the stoichiometry, NMR, MS, and kinetic studies all state the fact that the disulfides investigated can be oxidized by iodine and generate different products accordingly. A summary of the overall reactions regarding the three disulfides with the same oxidant in the aqueous phase is given in Table 5-8.

Table 5-8. Reaction of three RSSR with iodine.

Disulfide	**Overall Reaction**
SEDS	$(NaSO_3CH_2CH_2S)_2 + 2I_2 + 2H_2O \rightarrow$ $NaSO_3CH_3CH_2S(O)_2SCH_2CH_2\ SO_3Na + 4I^- + 4H^+$
HEDS	$(OHCH_2CH_2S)_2 + I_2 + H_2O \rightarrow OHCH_2CH_2S(O)SCH_2CH_2OH + 2I^- + 2H^+$
3,3'-DTDP	$(COOHCH_2CH_2S)_2 + 5I_2 + 6H_2O \rightarrow 2COOHCH_2CH_2SO_3^- + 10I^- + 12H^+$

Based on the data obtained through experiments and kinetic fitting, the general mechanism of each reaction along with the corresponding kinetic parameters are discussed next. For MESNA-sulfide, the nucleophilic attack of iodine yields an intermediate, $RSSRI^+$. The process is depicted as,

$$(NaSO_3CH_2CH_2S)_2 + I_2 \rightleftharpoons (NaSO_3CH_2CH_2S)_2I^+ + I^- \quad K_{RSSRI} \qquad \text{Eq. 5-89}$$

This step is a rapid equilibrium with K_{RSSRI} of 39.3 M^{-1} from the fitted k_f, k_r values. The unstable intermediate $RSSRI^+$ slowly dissociates to form RSS(O)R with a rate constant of $4.5 \times 10^{-4}\ s^{-1}$. RSS(O)R will consume another equivalent of iodine to release MESNA-thiosulfinate and iodide ions through the process of

$$\mathrm{RSS(O)R} + \mathrm{I_2} + \mathrm{H_2O} \rightarrow \mathrm{RSS(O)_2R} + 2\mathrm{H^+} + 2\mathrm{I^-} \quad \text{Eq. 5-90}$$

The rate constant for this step cannot be determined with an equation because of the many unknown parameters with large uncertainty in the fit. Neither could the value be obtained from the experiment as the intermediate cannot be isolated. Hence, computational modeling was performed to simulate the kinetics to solve the unknowns. The mechanism used for the simulation is shown in Table 5-9**.**

Table 5-9. Proposed mechanism of SEDS/iodine reaction in the absence of extra iodide.

Step	**Reactions**	**Rate Constants**
1	$\mathrm{RSSR} + \mathrm{I_2} \rightleftharpoons \mathrm{RSSRI^+} + \mathrm{I^-}$	$k_1 = (1.2 \pm 0.1) \times 10^{-2}\ \mathrm{M^{-1}\ s^{-1}}$ $k_{-1} = 2.8 \times 10^{-4}\ \mathrm{M^{-1}\ s^{-1}}$
2	$\mathrm{RSSRI^+} + \mathrm{H_2O} \rightarrow \mathrm{RSS(O)R} + \mathrm{I^-} + 2\mathrm{H^+}$	$(4.7 \pm 0.3) \times 10^{-4}\ \mathrm{s^{-1}}$
3	$\mathrm{RSS(O)R} + \mathrm{I_2} + \mathrm{H_2O} \rightarrow \mathrm{RSS(0)_2R} + 2\mathrm{I^-} + 2\mathrm{H^+}$	$(1.9 \pm 0.1)\ \mathrm{M^{-1}\ s^{-1}}$
4	$\mathrm{I_2} + \mathrm{I^-} \rightleftharpoons \mathrm{I_3^-}$	$5.6 \times 10^9\ \mathrm{M^{-1}\ s^{-1}}; 7 \times 10^6\ \mathrm{M^{-1}\ s^{-1}}$

The kinetic traces with [SEDS] dependence in the absence of iodide are simulated with the mechanism and the rate constant for step 3 is optimized. The results are shown in the figures below.

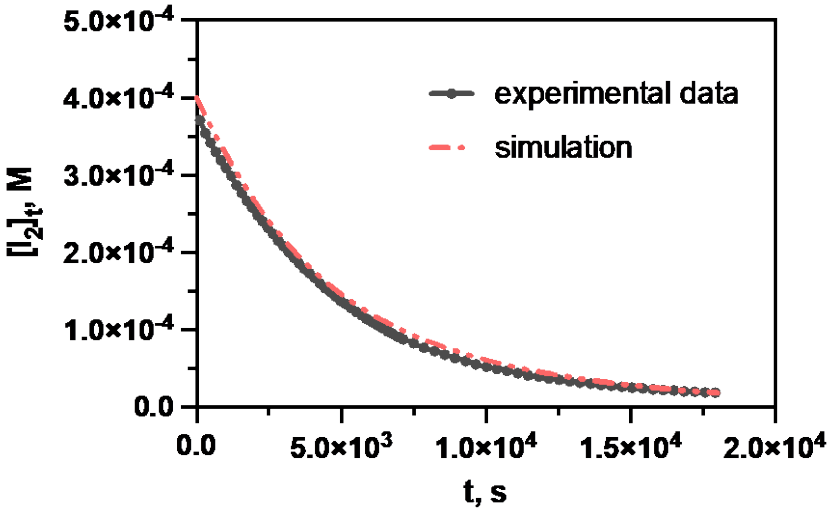

Figure 5-52. Simulation on the kinetic trace. Conditions: $[\mathrm{RSSR}]_0 = 11.9$ mM, $[\mathrm{I_2}]_0 = 0.42$ mM.

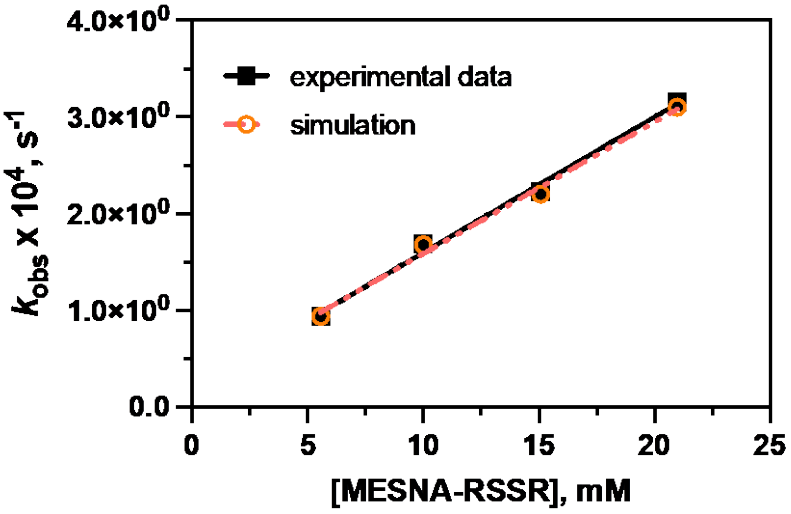

Figure 5-53. Comparison of simulated result with experimental data of [RSSR] dependence. Conditions: $[\mathrm{MESNA-RSSR}]_0 = 5.56, 10.0, 15.07, 20.98$ mM, $[\mathrm{I_2}]_0 = 0.49$ mM.

When excess of iodide is added to the reaction solution, the simulated traces of the decay of iodine show a two-phase process (a sharp drop of the concentration of iodine and a subsequent slow decrease in [iodine]) with the second phase being largely inhibited with the increase in iodide concentration. Even with one more step

Step 5 $\quad \mathbf{RSSR} + \mathbf{I_3^-} \rightleftharpoons \mathbf{RSSRI^+} + \mathbf{2I^-}$

added on top of the proposed mechanism in Table 5-9, the effect of [iodide] on the reaction kinetics could not be simulated.

For the reaction of iodine with other two RSSR: 2-hydroxyethyl disulfide (HEDS) and 3,3'-DTDP, both I_2 and I_3^- are proved to contribute to the reaction rate constant from the mathematical fit of the rate law. The general mechanism is given as

$$\text{RSSR} + I_2 + H_2O \rightarrow \text{Products} \quad k_1$$

$$\text{RSSR} + I_3^- + H_2O \rightarrow \text{Products} \quad k_2$$

It can be further confirmed that the nucleophiles attack on iodine is more effective than that on triiodide from the solved k_1, k_2 values. As expected, the inhibition by I^- on both reactions rate can be explained by the rapidly established equilibrium of RSSR with iodine to form the short-lived intermediate. The addition of iodide will shift the equilibrium to the left side, and a decreased reaction rate will be observed consequently.

$$\text{RSSR} + I_2/I_3^- \rightleftharpoons \text{intermediate} + I^-$$

Different from the slow reactions between SEDS, HEDS with iodine, the reaction of 3,3'-DTDP with iodine was turned out to be several orders of magnitude faster. Besides, I_2 was confirmed to be the predominantly reactive species in the solution instead of I_3^- as the former one reacts 100 times faster than the latter with DTDP.

According to the rate constants obtained from this work, shown in Table 5-10, it is clear that iodine can be very selective in its reactivity with these disulfides.

Table 5-10. Rate constants for reactions of I_2 with disulfides.

	Nucleophile	$k, \mathbf{M^{-1}\ s^{-1}}$
$I_2 + \text{RSSR} \rightarrow \text{product}\ (k)$	SEDS	$(1.2 \pm 0.1) \times 10^{-2}$
	HEDS	$(4.98 \pm 0.35) \times 10^{-2}$
	3,3'-DTDP	(2.45 ± 0.3)

Notably, the highest rate constant obtained was from DTDP, which might be due to the two carboxyl groups contained in the nucleophile. A possible explanation could be the interaction of carboxyl group with the sulfur atom as proposed by Doi [35]. This is most likely to happen prior to the rate limiting step, which is the dissociation of the reactive disulfide-iodine adduct, $RSSRI^+$. The cleavage of the carboxyl-bond adduct will eventually generate the corresponding sulfonic acid. This final product was reported by Doi's group and was confirmed in our study.

5.7 Conclusions

With the study, solid evidence is provided and proved that iodine/triiodide are good candidates for disulfide cleavage to generate various products. For instance, it can be used as a powerful scissor to break S-S bond in protein. Besides, it was also proved that the oxidation of disulfides takes places through the mechanism that nucleophiles approach and attack the center sulfur atom via I^+ transfer, followed by the dissociation or bond cleavage of the intermediate to give the final product. The kinetics of the process can be largely determined by the functional group of the nucleophiles, the iodide concentration, and the pH of the media.

5.8 References

[1] Schmidt, B.; Ho, L.; Hogg, P. J. *Biochem*. **2006**, *45*, 7429-7433.

[2] Hogg, P. J. *Trends Biochem. Sci.* **2003***, 28*, 210-214.

[3] Smiles, S.; Gibson, D. T. *J. Chem. Soc, Trans*. **1924**, *125*, 176-183.

[4] Sanger, F. *Nature*. **1953**, *171*, 1025.

[5] Trivedi, M. V.; Laurence, J. S.; Siahaan, T. J. *Curr. Protein Pept. Sci.* **2009**, *10*, 614–625.

[6] Chagas, R.; Laia, C. A.; Ferreira, R. B.; Ferreira, L. M. *Food Chem.* **2018**, *259*, 173.

[7] Van Sluyter, S. C.; McRae, J. M.; Falconer, R. J.; Smith, P. A.; Bacic, A.; Waters, E. J.; Marangon, M. *J. Agri. Food Chem*. **2015**, *63*, 4020–4030.

[8] Kharasch, N.; Gleason, G. I.; Buess, C. M. *J. Am. Chem. Soc*. **1950**, *72*, 1796-1798.

[9] Parker, A. J.; Kharasch, N. *Chem. Rev*. **1959**, *59*, 583-628.

[10] Liu, R. M.; McDonald, M. R.; Margerum, D. W. *Inorg. Chem.* **1995**, *34*, 6093-6099.

[11] Smith, R. H. *Aust. J. Chem.* **1970**, *23*, 431-440.

[12] Yiin, B. S.; Margerum, D. W. *Inorg. Chem.* **1990**, *29*, 1559-1564.

[13] Liu, R. M.; Margerum, D. W. *Inorg. Chem.* **1998**, *37*, 2531-2537.

[14] Otoikhian, A.; Simoyi, R. H.; Petersen, J. L. *Chem. Res. Toxicol.* **2005**, *18*, 1167-1177.

[15] Chanakira, A.; Chikwana, E.; Peyton, D. H.; Simoyi, R. H. *Can. J. Chem.* **2006**, *84*, 49-57.

[16] Chikwana, E.; Davis, B.; Morakinyo, M. K.; Simoyi, R. H. *Can. J. Chem.* **2009**, *87*, 689-697.

[17] Xu, L.; Csekö, G.; Kegl, T.; Horváth, A. K. *Inorg. Chem.* **2012**, *51*, 7837-7843.

[18] Xu, L.; Valkai, L.; Kuznetsova, A. A.; Makarov, S. V.; Horváth, A. K. *Inorg. Chem.* **2017**, *56*, 4579-4587.

[19] Stanbury, D. M. *J. Phys. Chem. A* **2018**, *122*, 3956−3957.

[20] Stanbury, D. M.; Hoffman, D. *J. Phys. Chem. A* **2019**, *123*, 5436−5445.

[21] Chipiso, K.; Mbiya, W.; Morakinyo, M. K.; Simoyi, R. H. *Aust. J. Chem.* **2014**, *67*, 626-635.

[22] Csekö, G.; Horváth, A. K. *J. Phys. Chem. A* **2010**, *114*, 6521-6526.

[23] Kerek, A.; Horváth, A. K. *J. Phys. Chem. A* **2007**, *111*, 4235-4241.

[24] Raina, S.; Missiakas, D. *Annu. Rev. Microbiol.* **1997**, *51*, 179-202.

[25] Singh, R.; Lamoureux, G.V.; Lees, W. J.; Whitesides, G. M. *Methods Enzymol.* **1995**, *251*, 167-173.

[26] S. Nagai.; Black, S. *J. Biol. Chem.* **1968**, *243*, 1942–1947.

[27] C. H. Lillig.; Berndt, C. *Antioxid. & Redox Signaling*. **2013**, *18*, 1654–1665.

[28] Begas, P.; Staudacher, V.; Deponte, M. *Chem. Sci.* **2015**, *6*, 3788–3796.

[29] Codognoto, L.; Winter, E.; Paschoal, J. A.; Suffredini, H. B.; Cabral, M. F.; Machado, S.A.; Rath, S. *Talanta*. **2007**, *72*, 427-433.

[30] Tsutsumi, H.; Okada, S.; Oishi, T. *Electrochim. Acta **1998**, 43*, 427-429.

[31] Wübbeler, J. H.; Lütke-Eversloh, T.; Van Trappen, S.; Vandamme, P.; Steinbüchel, A. *Int. J. Syst. Evol.* **2006**, *56*, 1305-1310.

[32] Wübbeler, J. H.; Bruland, N.; Kretschmer, K.; Steinbüchel, A. *Applied. Environ. Microbiol.* **2008**, *74*, 4028-4035.

[33] Tuan, Y.-H.; Phillips, R. D. *J. Agric. Food Chem. **1997**, 45*, 3535-3540.

[34] Lütke-Eversloh, T.; Steinbüchel, A. *FEMS Microbiol. Lett.* **2003**, *221*, 191-196.

[35] Doi, J. T.; Luehr, G. W.; Musker, W. K. *J. Org. Chem.* **1985**, *50*, 5716-5719.

[36] Bürgmann, H.; Howard, E. C.; Ye, W.; Sun, F.; Sun, S.; Napierala, S.; Moran, M. A. *Environ. Microbiol*. **2007**, *9*, 2742-2755.

[37] Kiene, R. P.; Malloy, K. D.; Taylor, B. F. *Appl. Environ. Microbiol.* **1990**, *56,* 156-161.

[38] Mopper, K.; Taylor, B. F. Chapter 19 of Organic marine geochemistry. American Chemical Society, Washington, DC. Ed, Sohn, M. L. **1986**, 324-339.

[39] Jariwala, F. InB.; Wood, R. E.; Nishshanka, U.; Attygalle, A. B. *J. Mass Spectrom.* **2012**, *47*, 529–538.

[40] Urbansky, E. T.; Cooper, B. T.; Margerum, D. W. *Inorg. Chem.* **1997,** *36,* 1338-1344.

[41] Schmitz, G. *Int. J. Chem. Kinet.* **2004**, *36*, 480-493.

[42] Schmitz, G. *Phys. Chem. Chem. Phys.* **2000**, ***2***, 4041-4044.

[43] Scheper, W. M.; Margerum, D. W. *Inorg. Chem.* **1992**, *31*, 5466-5473.

[44] Xu, L.; Csekő, G.; Horváth, A. K. *J. Phys. Chem.* A **2020***, 124*, 6029-6038.

[45] Turner, D. H.; Flynn, G. W.; Sutin, N.; Beitz, J. V. *J. Am. Chem. Soc.* **1972**, *94*, 1554-1559.

[46] Wübbeler, J.H.; Bruland, N.; Kretschmer, K.; Steinbüchel, A. *Appl. Environ. Microbiol*. **2008**, *74*, 4028.